Extending functionality and knowledge transfer of the Water Quality Systems Assessment Model

Report to the

Water Research Commission

by

Andrew Slaughter, David Gwapedza, Sukhmani Mantel, Denis Hughes and Neil Griffin

Institute for Water Research

Rhodes University, Grahamstown

WRC Report No 2448/1/18

ISBN 978-0-6392-0059-0

November 2018

Obtainable from

Water Research Commission

Private Bag X03

GEZINA, 0031

orders@wrc.org.za or download from www.wrc.org.za

EXECUTIVE SUMMARY

This report has been generated by the Water Research Commission (WRC)-funded project *Extending functionality and knowledge transfer of the Water Quality Systems Assessment Model* (Project No. K5/2448).

Project Aims

The WRC project (K5/2448) aims to further develop the Water Quality Systems Assessment Model (WQSAM), the development of which was initiated within a previous WRC project (K5/2237).

The aims of the project as stated in the proposal are:

1. The development and testing of a non-point source nutrient input model linked to land cover, to be integrated within WQSAM.
2. Extension of water quality variables simulated within WQSAM to include acid mine drainage and microbial water quality, and the application of WQSAM to selected catchments for historical conditions.
3. Validation of algal and hyacinth growth processes within WQSAM using remote sensing estimates of primary production for selected eutrophic reservoirs.
4. Parameterisation of a sediment transport model using remote sensing data.
5. The incorporation of a cholera prediction model within WQSAM, with application to selected catchments for historical conditions.
6. The simplification, further testing and consolidation into WQSAM of the sediment transport model, and application to selected catchments for historical conditions.
7. WQSAM model documentation and knowledge dissemination.

This is the final deliverable of the project which consolidates all previous deliverables.

Report Structure

The report is presented as follows:

Chapter 1 presents a brief introduction on the background and motivation for the project.

Chapter 2 describes the non-point nutrient input model linked to land cover.

Chapter 3 describes the extension of WQSAM to simulate microbial water quality and acid mine drainage.

Chapter 4 summarises the process of validating the algal and hyacinth growth processes in WQSAM using remote sensing estimates of primary production.

Chapter 5 outlines the regionalisation, simplification, further testing and consolidation of the WQSED model into WQSAM.

Chapter 6 describes the incorporation of a cholera prediction model into WQSAM.

Chapter 7 briefly discusses the conclusions of the project and potential for future development.

Report Summary

The current project follows on directly from a previous WRC-funded project, K5/2237. Both projects focus on the development, testing and application of the Water Quality Systems Assessment Model (WQSAM). K5/2448 has furthered development on WQSAM to: 1) include a non-point source nutrient input model linked to land cover; 2) extend water quality variables simulated to include acid mine drainage and microbial water quality; 3) validate algal and hyacinth growth processes within WQSAM using remote sensing estimates of primary production for selected eutrophic reservoirs; 4) parameterise a sediment transport model using remote sensing data; 5) incorporate a cholera prediction model within WQSAM; 6) simplify, further test and consolidate the sediment transport model; 7) implement WQSAM model documentation and knowledge dissemination.

Chapter 2 derives a formal model to link WQSAM parameters for non-point nutrient inputs to land cover. The selection of study sites was done according to biomes. The land cover categories were reduced by combining related land cover categories. The water quality of all selected sites was modelled within WQSAM. The calibrated surface water quality signatures were used within the subsequent analyses. Multiple regression within Statistica and Microsoft Excel was used to investigate the relationships between model parameters and the land cover proportions of respective study sites. The results of the regressions obtained in Excel using Solver made more conceptual sense than those obtained in Statistica. The lack of available data affected all modelling and analyses performed. It is concluded that the results of the regressions obtained in Excel should be used as a method to link parameters related to non-point source inputs with land cover, until such a time that further sites and further observed data can be identified that can improve the regression models obtained.

Chapter 3 introduces the inclusion of acid mine drainage (AMD) and microbial water quality simulations within WQSAM. Microbial water quality was simulated in a fairly simplistic manner using a first order degradation coefficient and *Escherichia coli* as the microbial indicator. Sulphates were used as a general indicator of input of acid mine drainage (AMD). The Crocodile River and Olifants River catchments were used as the study catchments. Good simulations of *E. coli* were achieved. For the simulations of sulphate in the Crocodile River Catchment, fairly high non-point- and point-source inputs had to be simulated. For the Olifants River Catchment, high non-point inputs had to be simulated to account for high variability in the observed sulphate concentrations.

Chapter 4 focused on the evaluation of chlorophyll-a using MERIS and Landsat data for two reservoirs in two catchments (Crocodile and Olifants rivers). Algal or macrophyte presence in Laing Dam (Buffalo River) was tested using near infrared to red band ratios of Landsat data that was checked against Google Earth satellite imagery. The algal simulations by WQSAM for the Loskop and Laing dams showed a strong seasonal trend with a summer maximum and a winter minimum. Using relationships between algal wet weight biomass and chl-a, the simulations of algal biomass as generated by WQSAM were converted into a minimum and maximum chl-a range so as to facilitate a comparison with the measures of chl-a for these two reservoirs derived using remote sensing data. The results showed that the measures of chl-a derived by remote sensing data fell within the same range of chl-a generated by the WQSAM model, although a strong seasonal trend was not evident within the results from the remote sensing data. The results obtained are reasonable, as the results show that WQSAM is simulating algal and hyacinth biomass and seasonal trends within the correct range.

Chapter 5 describes the conceptual basis and underlying equations of the soil erosion and sediment transport model (WQSED). The sediment yield for various catchments in South Africa was modelled. The modelled catchment is separated into runoff zones: the high, medium and low runoff zones, based on topography, with the high runoff zones generating more runoff than the low runoff zones. Soil erosion is estimated using the Modified Universal Soil Loss Equation (MUSLE). Conceptually, there are two storages in each zone: in-channel storage and catchment storage, and the model attempts to represent the dynamic movement

of sediment within and between runoff zones between the different storages. The calculation of storm duration, peak discharge for each runoff zone, and runoff depth for each runoff zone are important for calculating the runoff factor (erosivity) of the MUSLE equation, whereas the rest of the parameters are erodibility factors relate to soil, vegetation, slope and practice. The approach for simulating the suspended sediment load was adopted from Van Rijn (1984), with some simplifications. Various study sites from across South Africa were modelled, with an emphasis on sites in the Eastern Cape because of the high degree of erosion occurring in these catchments. The results of erosion and sediment transport for individual study catchments are presented and compared to previous estimates, and were found to be representative for most of the study catchments.

Chapter 6 investigated whether the instream fate of the bacterium, *Vibrio cholera*, could be represented within WQSAM using simple first-order degradation. The Olifants River Catchment was used as a case study catchment. *V. cholerae* fate was simulated by adjusting the *V. cholerae* growth rate according to the water temperature, salinity and the availability of nutrients. Although there were a lack of observed data, this study broadly showed that WQSAM could find use in investigating the risk of endemic *V. cholerae* growth due to changing climate and increasing salinity. In addition, WQSAM could be used to investigate *V. cholerae* fate instream during an epidemic, when inputs from the catchment are expected.

The outcomes of this project were successful, particularly in relation to extending the functionality of WQSAM to simulate further water quality variables, i.e. microbial water quality, sulphate and sediment. It was found that while the method of relating non-point sources of nutrients to land cover was uncertain, it was nevertheless a vast improvement compared to the uncertainty associated with calibrating non-point sources within other water quality models. Within the validation of algal growth processes in WQSAM, it is argued that the indirect correlations obtained between WQSAM estimates of primary production within reservoirs and remote sensing estimates of primary production were reasonable given the uncertainty within remote sensing data. The inclusion of *Vibrio cholerae* survival within WQSAM essentially was an exploratory exercise since the lack of data did not allow the validation of the model. Further scope for research was identified within the soil erosion and sediment transport model (WQSED), particularly related to scale-dependency issues and further validation of the main channel sediment transport implementation.

ACKNOWLEDGEMENTS

The Geography Department of Rhodes University is acknowledged for kindly providing sediment concentration data for the T35 catchments.

TABLE OF CONTENTS

ACRONYMS

ACRU	Agricultural Catchments Research Unit
AMD	Acid mine drainage
ANSWERS	Areal and Non-point Source Watershed Environmental Response Simulation
ASTER	Advanced Spaceborne Thermal Emission and Reflection Radiometer
CDOM	Carbonaceous dissolved organic matter
CREAMS	Chemicals, Runoff and Erosion from Agricultural Management Systems
CSTR	Completely stirred tank reactor
DEM	Digital elevation model
DoA	Department of Agriculture
DWA	Department of Water Affairs
DWS	Department of Water and Sanitation
EO-1	Earth Observing-1
EPA	Environmental Protection Agency
EROS	Earth Resources Observation and Science
ESA	European Space Agency
ETM	Enhanced Thematic Mapper
ETM+	Enhanced Thematic Mapper Plus
EUROSEM	European Soil Erosion Model
FDC	Flow duration curve
HRU	Hydrological response unit
HSPF	Hydrological Simulation Programme – Fortran
IWR	Institute for Water Research
KINEROS	Kinematic Runoff and Erosion model
MAP	Mean annual precipitation
MCM	Million cubic meters
MERIS	Medium Resolution Imaging Spectrometer
MODIS	MODerate resolution Imaging Spectrometer)
MPH	Maximum peak-height algorithm
MUSLE	Modified USLE
NASA	National Aeronautics and Space Administration
NEMP	National Eutrophication Monitoring Programme
NIR	Near InfraRed
NLC	National Land Cover

OLI	Operational Land Imager
PCA	Principle Component Analysis
RQIS	Resource Quality Information Services
RS	Remote Sensing
RUSLE	Revised USLE
SLC	Scan line corrector
SLR	Soil loss ratio
SPATSIM	Spatial and Time Series Information Modelling
SRTM	Shuttle Radar Topography Mission
SWAT	Soil and Water Assessment Tool
TDS	Total dissolved solids
TM	Thematic Mapper
TSS	Total suspended solids
USAID	United States Agency for International Development
USGS	United States Geological Survey
USLE	Universal Soil Loss Equation
VIS	Visual (spectral range)
WQSAM	Water Quality Systems Assessment Model
WRC	Water Research Commission
WReMP	Water Resources Modelling Platform
WRYM	Water Resources Yield Model
WWTW	Waste Water Treatment Work

CHAPTER 1. INTRODUCTION

1.1 Background to the project

The current project, K5/2448 follows on directly from a previous WRC project, K5/2237. K5/2237 introduced the Water Quality Systems Assessment Model (WQSAM). The need for the development of WQSAM was realised during a WRC-funded project on climate change adaptation measures for bulk water suppliers (K5/2018). These realisations were that existing water quality models do not fulfil the management requirements for South African water resources, and there is value in the development of a new water quality decision support system. Therefore, it was decided that a new water quality model (WQSAM) be developed, with the following important attributes:

1. Be able to accept water quantity data as input generated by an existing and routinely-used yield model.
2. Simulate data at a daily time step, as water quality is typically driven by transient events.
3. Simulate important water quality variables which are of concern to management of water resources. Initially, salinity and nutrients were the focus.
4. Adopt a 'requisite simplicity' approach (Bevan, 2006), by simulating water quality in the simplest way possible without compromising the accuracy of simulations.
5. Incorporate water quality simulation modules for river nodes and reservoir nodes, with an emphasis on water quality variable fate, including processes such as chemical speciation, sedimentation, and uptake by flora.
6. Water quality simulations as duration of exceedance curves, as this information is vital in allowing for water resource managers to assess risk associated with management scenarios. Exceedance information can also be assessed in conjunction with Thresholds of Potential Concern (TPCs), allowing rapid assessment of the possible water quality risks associated with management options.

K5/2237 outlined the conceptual and technical structure of WQSAM. In addition, this project applied the model to various case study catchments for historical conditions and future development and climate change scenarios, and also investigated the use of remote sensing data within WQSAM. Subsequent to the completion of K5/2237, it was felt that WQSAM could undergo further development, particularly for inclusion of further water quality variables of management significance. The current project, K5/2448 was initiated to achieve these further developments. The specific aims of the current project are:

1. The development and testing of a non-point source nutrient input model linked to land cover, to be integrated within WQSAM.
2. Extension of water quality variables simulated within WQSAM to include acid mine drainage and microbial water quality, and the application of WQSAM to selected catchments for historical conditions.
3. Validation of algal and hyacinth growth processes within WQSAM using remote sensing estimates of primary production for selected eutrophic reservoirs.
4. Parameterisation of a sediment transport model using remote sensing data.
5. The incorporation of a cholera prediction model within WQSAM, with application to selected catchments for historical conditions.
6. The simplification, further testing and consolidation into WQSAM of the sediment transport model, and application to selected catchments for historical conditions.
7. WQSAM model documentation and knowledge dissemination.

1.2 Guidance to the use of WQSAM

WQSAM is most useful for long-term water quality management of large river basins. Importantly, WQSAM has been developed for use with flows generated from a systems model, specifically either the Water Resources Yield Model (WRYM) or the Water Resources Modelling Platform (WReMP). The data requirements for setting up an application of WQSAM can be large, depending on the target water quality constituents the model is required to simulate. Table 1.1 below provides some guidance on the data required according to the water quality variables simulated.

Table 1.1 Data required to set up an application of the Water Quality Systems Assessment Model (WQSAM) according to different modelling outputs required

Description of data required	Basic model setup for disaggregation of monthly flows to daily	Modelling of salinity	Modelling of nutrients	Modelling of microbial water quality
Systems representation of the yield model	Required	Required	Required	Required
Monthly flows from the yield model for the entire simulation period	Required	Required	Required	Required
Unbroken daily rainfall data representative of the modelled catchment	Required	Required	Required	Required
Daily air temperature for modelling water temperature	Not Required	Not Required	Required	Required
Observed salinity data for model calibration	Not Required	Required	Not Required	Not Required
Observed nutrient data for model calibration	Not Required	Not Required	Required	Not Required
Land cover data for estimating non-point source inputs of nutrients	Not Required	Not Required	Required	Not Required
Observed microbial water quality data for model calibration	Not Required	Not Required	Not Required	Required

1.3 Report structure

Chapter 2 describes the non-point nutrient input model linked to land cover.
Chapter 3 describes the extension of WQSAM to simulate microbial water quality and acid mine drainage.
Chapter 4 summarises the process of validating the algal and hyacinth growth processes in WQSAM using remote sensing estimates of primary production.
Chapter 5 outlines the regionalisation, simplification, further testing and consolidation of the WQSED model into WQSAM.
Chapter 6 describes the incorporation of a cholera prediction model into WQSAM.
Chapter 7 discusses the conclusions of the project and potential for future development.

CHAPTER 2. A NON-POINT NUTRIENT INPUT MODEL LINKED TO LAND COVER

2.1 Introduction

The conceptual understanding and technical procedures implemented within the Water Quality Systems Assessment Model (WQSAM) are outlined in the final report of K5/2237 (Slaughter *et al*., 2015a). The model as represented in Slaughter *et al*. (2015a) did not implement a rigorous method for quantifying the non-point load of water quality variable constituents into the modelled system. A short summary of the current approach used within WQSAM to quantify non-point loads follows.

Briefly, WQSAM generates a daily time series of incremental flows within each incremental catchment represented within a modelled system. WQSAM achieves this by disaggregating monthly incremental flow (obtained from an appropriate yield/systems model) to daily. This procedure has been found to be rigorous, and is outlined in the project final report of K5/2337, but has also been published in two articles in peer reviewed journals (Hughes and Slaughter, 2015; Slaughter *et al*., 2015b). The daily incremental flow is further broken down into three flow fractions, namely surface flow, incremental flow and groundwater flow, using a simple, yet nonetheless rigorous statistical baseflow separation method (Hughes *et al*., 2003). WQSAM implements the separation of incremental flow into flow fractions to facilitate the estimation of non-point loads into the modelled river. The conceptual understanding behind the approach is that overland flow, interflow and to a lesser extent, groundwater flow, are the carriers of non-point loads into a river. In addition, the concentration of a particular water quality variable is likely to show a large variation between the flow fractions for a particular catchment. For example, catchments containing a large amount of irrigated agriculture are likely to show a large nutrient concentration within the surface water flow fraction. In contrast, in certain catchments characterised by marine derived sediment geology, the groundwater flow fraction is likely to show a much higher salt concentration then that of surface water flow. This conceptual understanding is reasonable, and is therefore additionally regarded to be a rigorous part of WQSAM.

Within the water quality simulation component of WQSAM, water quality variable concentrations are assigned to the flow fractions described above. Although the concentrations assigned can be guided by the type of landcover/landuse in the catchment, the process as it stands is subjective. Where there are observed data available, it is possibly to calibrate the signatures assigned to the fractions so as to obtain water quality simulations that are representative of the observed data. However, many processes affect water quality within any part of a modelled system, including non-point and point sources, and assigning parameter values based on calibration opens up the risk of equifinality (Bevan, 2006), which can be described in a simplistic way as obtaining the same model simulation through multiple sets of parameter values. Within equifinality, one can obtain a model simulation that is a fair representation of observed data, but for the wrong reasons, usually in models that are over-parameterised.

This realisation of subjectivity within the simulation of non-point water quality loads within WQSAM led to efforts to more formally and objectively quantify possible non-point loads originating from catchments, which has in turn led to the compilation of the current chapter.

A method of objectively quantifying non-point loads from a catchment based on land cover/use offers various advantages. Including lessening the risk of equifinality, such a method would provide more confidence during the application of the model to areas where no observed data are available. In addition, future scenarios under which land cover/use is predicted to change can be modelled rigorously within the model.

2.2 Method and study areas

2.2.1 Approach used

It can be assumed that broad regional characteristics of a catchment will affect the relationships between land cover and non-point load inputs. Therefore, these characteristics should be explored on a regional spatial scale, rather than on a national scale, so as to take into account regional patterns. Since the current study investigated the relationship between land cover and non-point source load inputs, the regionalisation category chosen was the biome categorisation by Low and Rebelo (1996) (see Figure 2.1).

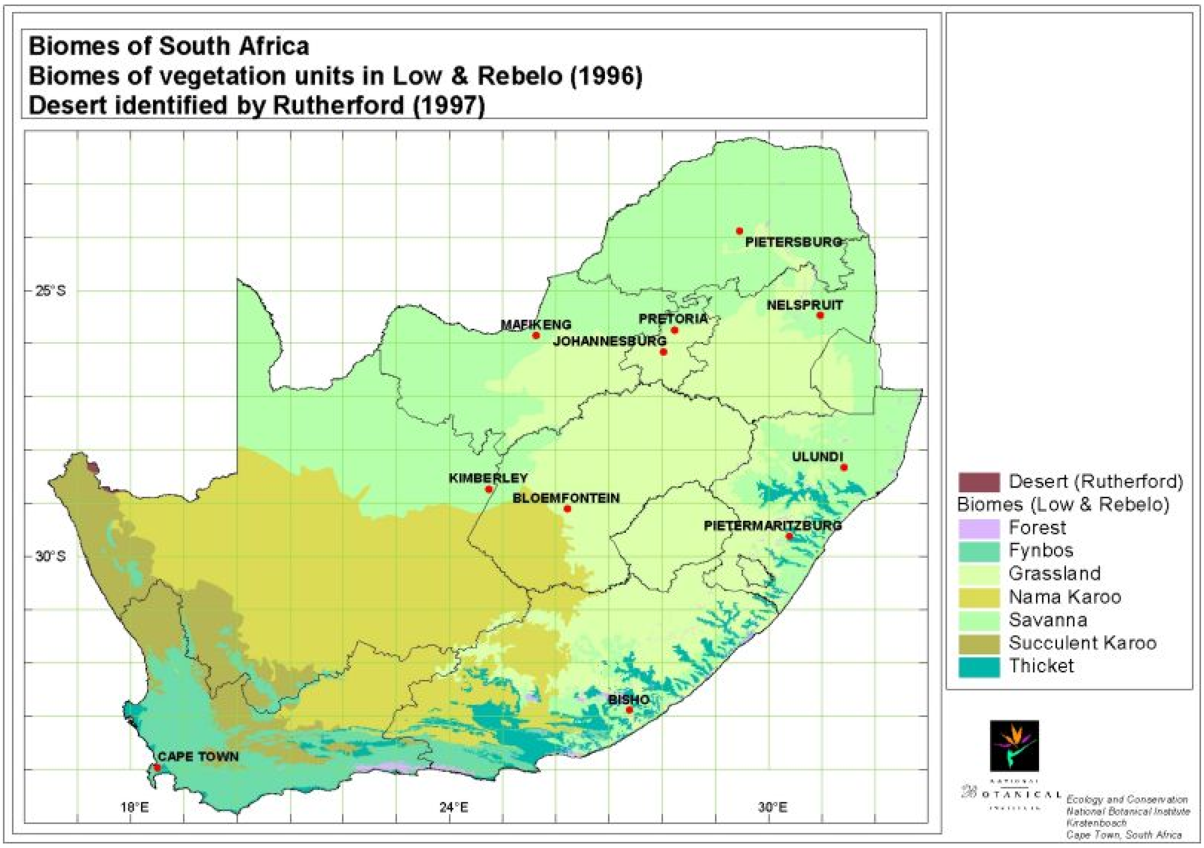

Figure 2.1 Biome categorisation of Low and Rebelo (1996), taken from Low and Rebelo (1996)

The approach taken in choosing study sites within the current study was to choose tributary catchments receiving incremental flow, and catchments with the following characteristics were chosen:

1) catchments not containing large dams;
2) catchments not containing large informal settlements, town or cities (as this would be a reasonable indication of possible point source influences);
3) catchments consisting of at most two quaternary catchments, and;
4) catchments for which there are an adequate (unbroken) amount of observed flow data as well the presence of a reasonable amount of water quality data.

2.2.2 Study areas used

Unfortunately, finding suitable study catchments with the characteristics as listed above was difficult. In total, suitable catchments within only four biomes could be identified, namely the fynbos, grassland, savannah and thicket biomes. The gauges used are listed in Table 2.1 below. Figures 2.2-2.5 show the location of gauged catchments and land cover for the fynbos, grassland, savannah and thicket sites, respectively.

Table 2.1 Gauged catchments used, specifying gauge names, quaternary catchment(s), biome and temporal period of data availability

Gauge name	**Quaternary catchment**	**Biome**	**Observed data**	
			from	to
G1H010	G10E	Fynbos	1983	2003
G1H028	G10G	Fynbos	1982	2015
G1H034	G10J	Fynbos	1985	2007
G2H037	G22F	Fynbos	1991	2015
H2H008	H20C	Fynbos	1979	1995
J1H016	J12A	Fynbos	1979	2001
C2H005	C22H/C22J	Grassland	2001	2015
C5H007	C52F	Grassland	1988	2015
C5H056	C52A	Grassland	2002	2015
C8H006	C81H	Grassland	1977	1985
A2H032	A22C	Savannah	1979	2004
A2H034	A21G	Savannah	1971	2003
A6H010	A61C	Savannah	1999	2007
B1H018	B11A	Savannah	1993	1998
B4H009	B41G	Savannah	1980	1992
B9H002	B90F	Savannah	1991	2002
X2H012	X21F	Savannah	1986	2015
X3H003	X31C	Savannah	1979	2010
X3H015	X33B	Savannah	1995	1996
P3H001	P30B	Thicket	2002	2010
P4H001	P40C	Thicket	2000	2010
R2H009	R20D	Thicket	1971	1998
R2H012	R20C	Thicket	1971	1999
U8H001	U80G	Thicket	1992	2010

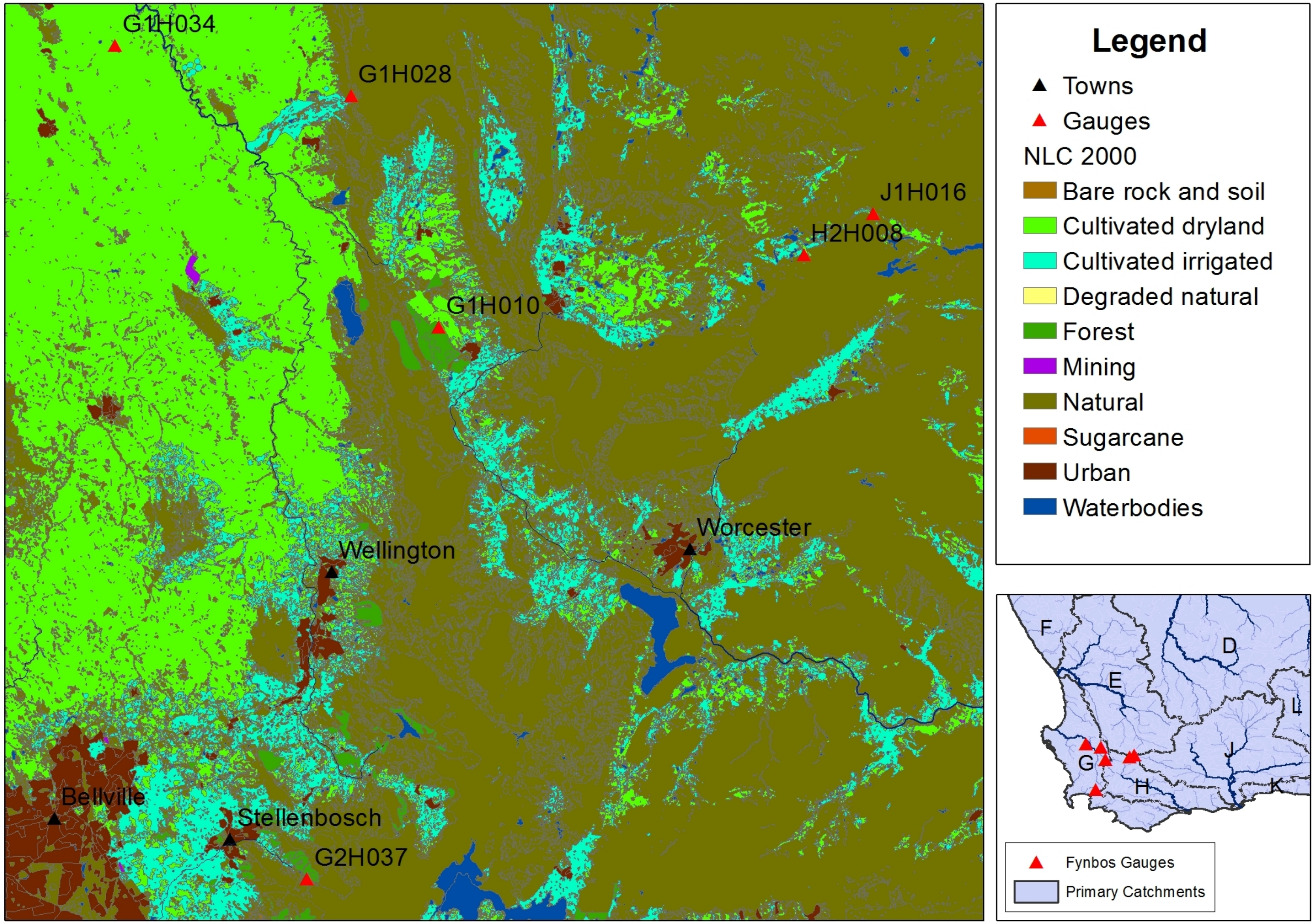

Figure 2.2 Map of the gauged tributary catchments chosen within the fynbos biomes

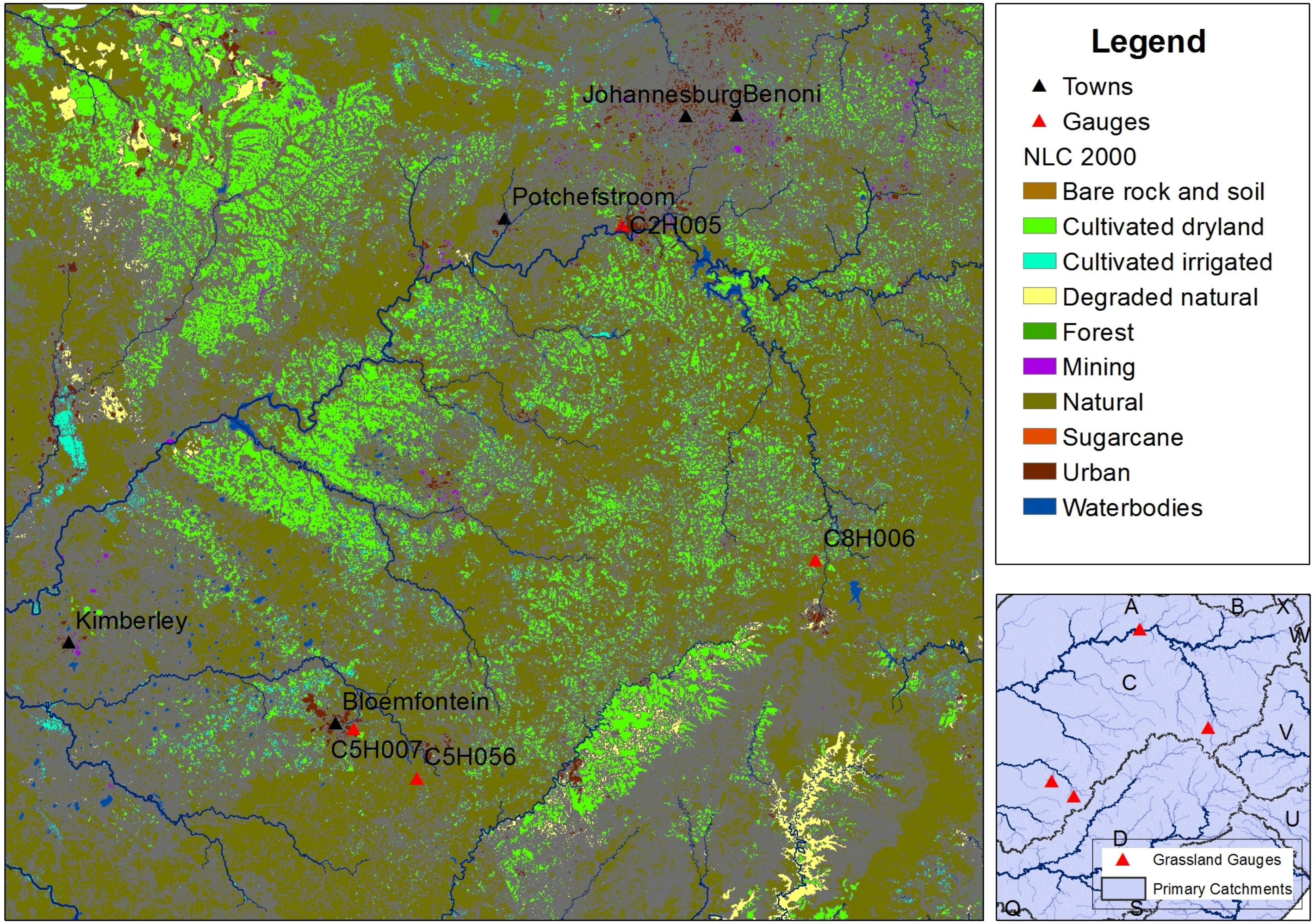

Figure 2.3 Map of the gauged tributary catchments chosen within the grassland biome

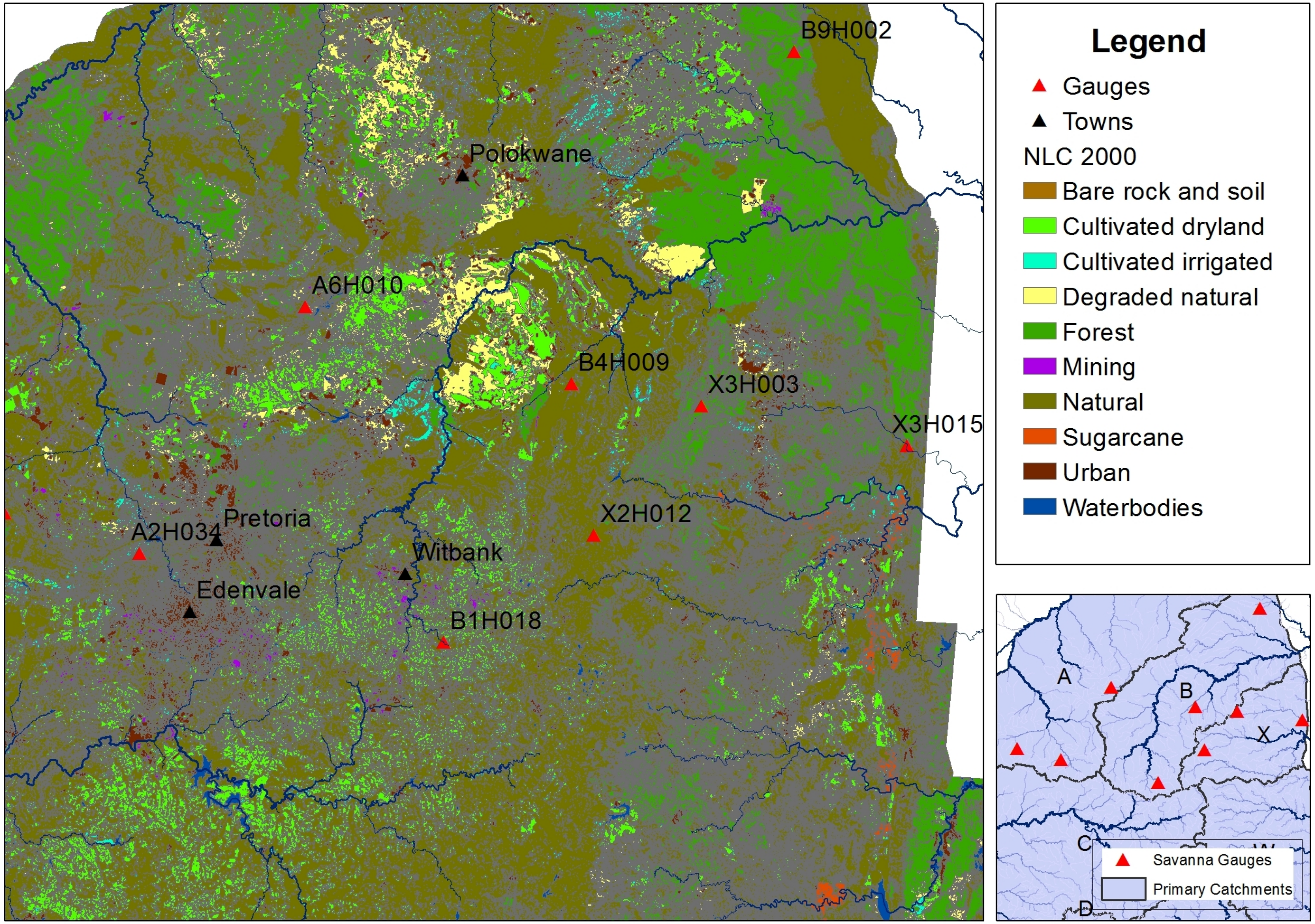

Figure 2.4 Map of the gauged tributary catchments chosen within the savannah biome

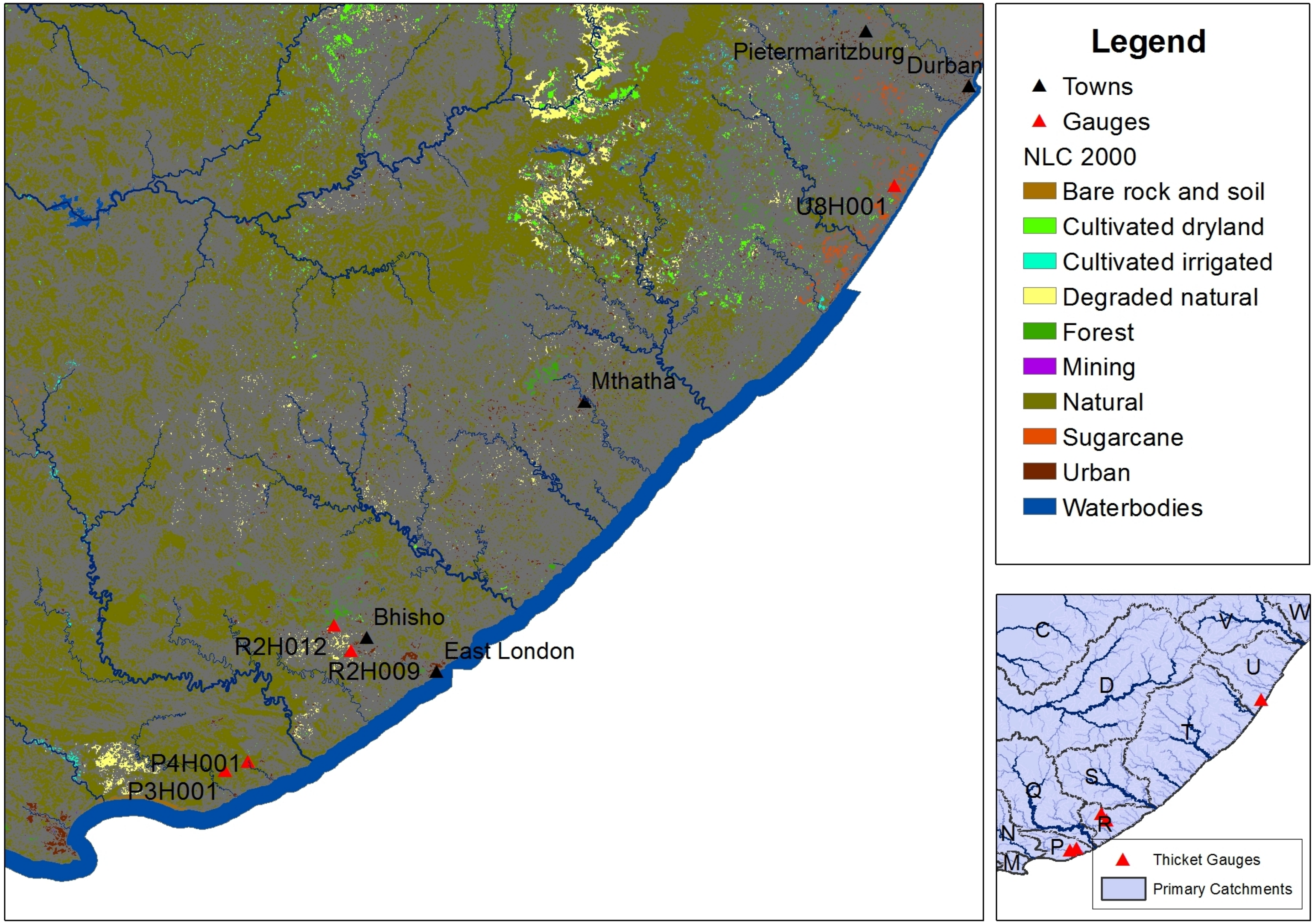

Figure 2.5 Map of the gauged tributary catchments chosen within the thicket biome

2.2.3 Methods

A period of unbroken daily observed flow was obtained for each selected study site from the Department of Water and Sanitation (DWS) Resource Quality Information Services (RQIS) website (https://www.dwa.gov.za/iwqs/report.aspx, accessed August 2015). Water quality data within the same temporal period as the flow data were in addition sourced from the same abovementioned site. This study looked at nutrients, concentrating specifically on nitrite plus nitrate nitrogen (NO_2-N + NO_3-N), ammonium nitrogen (NH_4-N) and phosphate phosphorus (PO_4-P). More information on the data chosen is available in Table 2.1.

The land cover data were obtained from the South African National Land-Cover Dataset (Van den Berg *et al*., 2008). The catchment area was delineated for each water quality monitoring point by referring to 1:50,000 river and relief shapefiles in ArcMap 10.3 (ESRI, Inc.). The land cover spatial dataset was then clipped by the monitoring point catchment and ArcMap 10.3 functions (calculate geometry, summarise) were used to calculate the total areas under each land cover class in the catchment. The original dataset contains 45 land cover classes which were combined into ten categories for this study. This was done because the low number of suitable sites identified in combination with a large number of categories decreases the power or even excludes certain statistical analyses, such as multiple regression. In addition, working with so many categories within a water quality model would be a challenge as each would require a dedicated parameter. The grouping of original land cover categories into the more general categories are listed below.

Bare rock and soil: Bare Rock and Soil (erosion: dongas / gullies); Bare Rock and Soil (erosion: sheet); Bare Rock and Soil (natural).

Cultivated dryland: Cultivated, permanent, commercial, dryland; Cultivated, temporary, commercial, dryland; Cultivated, temporary, subsistence, dryland.

Cultivated irrigated: Cultivated, permanent, commercial, irrigated; Cultivated, temporary, commercial, irrigated; Cultivated, temporary, subsistence, irrigated.

Sugarcane: Cultivated, permanent, commercial, sugarcane.

Degraded natural: Degraded Forest & Woodland; Degraded Thicket, Bushland, etc.; Degraded Unimproved (natural) Grassland.

Forest: Forest (indigenous); Forest Plantations (Acacia spp); Forest Plantations (clearfelled); Forest Plantations (Eucalyptus spp); Forest Plantations (Other / mixed spp); Forest Plantations (Pine spp); Woodland (previously termed Forest and Woodland).

Natural: Improved Grassland; Shrubland and Low Fynbos; Thicket, Bushland, Bush Clumps, High Fynbos; Unimproved (natural) Grassland.

Mining: Mines & Quarries (mine tailings, waste dumps); Mines & Quarries (surface-based mining); Mines & Quarries (underground / subsurface mining)

Urban: Urban / Built-up (residential); Urban / Built-up (residential, formal suburbs); Urban / Built-up (residential, formal township); Urban / Built-up (residential, hostels); Urban / Built-up (residential, informal squatter camp); Urban / Built-up (residential, informal township); Urban / Built-up (rural cluster); Urban / Built-up (smallholdings, shrubland); Urban / Built-up, (commercial, education, health, IT); Urban / Built-up, (commercial, mercantile); Urban / Built-up (smallholdings, grassland);Urban/Built-up (smallholdings, woodland); Urban / Built-up (smallholdings, thicket, bushland); Urban / Built-up, (industrial / transport: heavy); Urban / Built-up, (industrial / transport : light).

Waterbodies: Waterbodies; Wetlands.

The grouping strategy was guided by a Principle Component Analysis (PCA) (data not shown), to obtain a general indication of which land cover categories show a similar pattern. In addition, land cover categories that were obviously related were grouped together, such as all the cultivation categories, for example. Sugarcane was given its own category, as previous experience in the lower Crocodile River has indicated that sugar cane fields may act as a sink of nutrients, and may actually improve water quality.

Within the analyses performed in the current study, a link between non-point source loads and land cover within a catchment was investigated and quantified. These analyses were repeated for land cover within a 100 m buffer zone of the river reach, similar to the approaches of various studies that have made the assumption of activities closer to the river reach having a larger effect on water quality (e.g. Maillard and Santos, 2007; Rodriqueze *et al*., 2007).

Within the multiple regression equations given later in this report, the land cover categories are written using codes as the entire descriptions would be too long to represent in an equation. The codes are represented below.

A: Bare rock and soil.

B: Cultivated dryland.

C: Cultivated irrigated.

D: Sugarcane.

E: Natural areas.

F: Mining areas.

G: Water bodies.

H: Urban areas.

I: Degraded natural areas.

J: Forest

A setup of WQSAM was compiled for each study area. However, the only components of WQSAM used were the baseflow separation procedure (Hughes *et al*., 2003) and some aspects of the water quality simulation.

Within the baseflow separation, the same parameter sets were used across all studied catchments (see Slaughter *et al*., 2015a for the explanation of the parameter values). While this could be regarded as a possible source of uncertainty within the modelling of the flow fractions in these catchments, the determination of the appropriate parameter values for baseflow separation is regarded to be especially problematic within hydrological studies (see Kapangaziwiri *et al*., 2011). These difficulties and uncertainties generally revolve around a lack of observed data with which to validate baseflow separation methods and parameter values, the range of baseflow separation methods available and the conflicting results they generate, difficulties in distinguishing between the origins of surface water in regards to flow fractions, as well as the disparity in temporal scales at which the different flow fractions operate. Therefore, the determination of appropriate baseflow separation parameter values was regarded to be beyond the scope of the current study. Instead, the approach of using a constant and commonly used parameter set across all modelled catchments was taken.

Since the current study focussed on the simulation of non-point source inputs, the water quality simulations performed in WQSAM only took into account the inputs associated with the flow fractions. In other words, the only parameters that were adjusted within the model in regards to water quality simulation were the surface flow, interflow and groundwater flow concentration parameters for each catchment studied. Appropriate catchments were chosen so as to validate this approach. In other words, catchments not containing point sources or dams, and catchments in which modelling cumulative flow is not important, as the catchments are tributary catchments contributing incremental flow.

In this particular study, the relationship between surface flow concentrations and land cover was investigated. This is because the relationships between land cover and the water quality signatures of interflow and groundwater flow are less certain and less influential for surface water quality in regards to nutrients. In addition, the rates at which different nutrients penetrate the soil vary among the different nutrients types. For example, nitrates are regarded to be fairly water soluble, and therefore can find their way into interflow and groundwater. However, phosphates generally bind to sediments, and are therefore not expected to occur within interflow and groundwater in significant concentrations. In addition, from past studies using WQSAM, is has been found that the values of the surface flow signatures were the most important for calibrating water quality simulations against observed data. Therefore, it is unlikely that a strong relationship would be found between land cover in incremental catchments the water quality signatures for the interflow and groundwater flow fractions.

There is a strong relationship between groundwater salinity signatures and instream salinity; however, since salinity is a conservative variable, modelling of salinity within WQSAM is regarded to be less uncertain. In addition, groundwater salinity signatures would more likely be linked to geology rather than land cover, and can be guided by available water quality data from boreholes in a catchment.

Within the water quality modelling of each study catchment in the current study, the model simulations were calibrated to match observed data as closely as possible. Once calibration was completed, the surface flow water quality concentrations applied to achieve the calibrations for NO_2-N + NO_3-N, NH_4-N and PO_4-P were collated for further analyses.

The relationships between the surface flow water quality signatures and land cover were explored using multiple regression. The land cover coverage within each catchment was explored in terms of proportion of particular land cover types of the total area of the catchment. In addition, all analyses were repeated for land cover within a 100 m buffer zone. Multiple regression analyses were conducted within Statistica V8 (Statsoft Inc). Forward stepwise regression was used, with statistical significance set at $P \leq 0.05$. Multiple regressions were additionally implemented in Microsoft Excel 2010 using Solver. Within the regressions implemented in Excel, the regression equation took the form of:

$$SF = (\alpha \times A) + (\beta \times B) + (\gamma \times C) + (\delta \times D) + (\varepsilon \times E) + (\zeta \times F) + (\eta \times G) + (\theta \times H) + (\iota \times I) + (\kappa \times J), \qquad \text{Equation 2.1}$$

where SF represents the surface flow concentration (mg ℓ^{-1}), A-F represent the land cover category fractions mentioned in Section 2.2.3 and α-κ represent the regression parameters calibrated through Solver applied to respective land cover categories. The Chi-square statistic was used as a goodness of fit statistic for each regression. Solver was implemented to find the best values for the parameters α-κ by finding the minimum value for the sum of Chi-square. Values of α-κ were constrained to be ≥ 0. The relationship between the regression parameters α-κ and land cover categories is given in Table 2.2

2.3 Results

2.3.1 Introduction

The results are presented in the following way. First, the results of the water quality calibration within the case study catchments will be presented. After this, the results of the multiple regression will be presented, where the relationships between the model calibrated surface flow signatures and land cover categories are explored. This analysis is presented for all land cover within the catchments as well as for a 100 m buffer zone.

Table 2.2 The parameters associated with Equation 2.1 and representative land cover categories

Parameter	**Land cover category**
Α	Bare rock & Soil
Β	Cultivated Dryland
Γ	Cultivated Irrigated
Δ	Sugarcane
Ε	Natural
Ζ	Mining
Η	Waterbodies
Θ	Urban
Ι	Degraded Natural
Κ	Forest

2.3.2 *Results of model calibration*

Fynbos biome

Table 2.3 shows the goodness of fit statistics for calibration results, represented by the Nash-Sutcliffe (Nash and Sutcliffe, 1970) efficiency values. The calibrations are represented as frequency distributions. This is because WQSAM is not designed to simulate accurate time series of water quality data, but rather focuses on representing the frequency characteristics of the observed data (see Slaughter *et al*., 2015a).

The efficiency values obtained for NO_2-N + NO_3-N ranged from 0.14 to 0.35, and were therefore generally not very good. The simulations of NH_4-N were slightly better, ranging from 0.31 to 0.76. The simulations of PO_4-P obtained mixed results, ranging from −2.24 to 0.74.

Grassland biome

The efficiency values obtained for NO_2-N + NO_3-N were fairly good, ranging from 0.17 to 0.93. The simulations of NH_4-N were also fair, ranging from 0.51 to 0.60. The simulations of PO_4-P were fair, ranging from 0.52 to 0.66.

Savannah biome

The efficiency values obtained for NO_2-N + NO_3-N were fairly good, ranging from 0.29 to 0.96. The simulations of NH_4-N were also fair, with NSEs obtained ranging from 0.20 to 0.82. The simulations of PO_4-P were fair, with NSEs ranging from 0.14 to 0.98.

Thicket biome

The efficiency values obtained for NO_2-N + NO_3-N were relatively bad, ranging from −2.6 to 0.64. The simulations of NH_4-N obtained mixed results, with NSEs obtained ranging from −42.5 to 0.88. The simulations of PO_4-P were also mixed, with NSEs obtained ranging from −5.23 to 0.65.

Table 2.3 Nash-Sutcliffe (Nash and Sutcliffe, 1970) efficiency values obtained for WQSAM model calibration against observed data as frequency distributions

Gauge	**Nash-Sutcliffe Efficiency for Calibration**		
	NO_2-N + NO_3-N	NH_4-N	PO_4-P
Fynbos Biome			
G1H010	0.28	0.71	0.74
G1H028	0.35	0.31	−2.24
G1H034	0.25	0.34	0.72
G2H037	0.14	0.55	0.21
H2H008	0.27	0.60	0.37
J1H016	0.23	0.76	0.60
Grassland biome			
C5H007	0.93	0.52	0.64
C5H056	0.17	0.51	0.52
C2H005	0.64	0.60	0.58
C8H006	0.46	0.59	0.66
Savannah biome			
A2H032	0.29	0.2	0.14
A2H034	0.78	0.5	0.68
B1H018	0.63	0.51	0.66
X2H012	0.90	0.57	0.98
X3H015	0.96	0.82	0.80
A6H010	0.96	0.47	0.56
B9H002	0.32	0.6	0.47
B4H009	0.93	0.72	0.91
X3H003	0.76	0.78	0.62
Thicket biome			
P3H001	−21.6	−42.5	−5.23
P4H001	−2.49	0.91	0.27
R2H009	0.64	−4.01	0.49
R2H012	−17.93	0.68	0.63
U8H001	0.62	0.88	−0.65

The final surface water flow signatures for all study sites for NO_2-N + NO_3-N, NH_4-N and PO_4-P are summarised in Table 2.4.

Table 2.4 Summary of water quality modelling results in WQSAM for the selected study catchment

		WQ signatures (mg ℓ$^{-1}$)								
		NO_2-N + $N0_3$-N			NH_4-N			PO_4-P		
	Biome	Surface	Interflow	GW flow	Surface	Interflow	GW flow	Surface	Interflow	GW flow
G1H010	Fynbos	1.6	0.1	0	0.1	0.05	0	0.07	0.01	0.01
G1H028	Fynbos	0.05	0.01	0.02	0.06	0.03	0.01	0.03	0.01	0
G1H034	Fynbos	5	0.03	0.05	0.3	0.1	0.1	0.5	0.05	0
G2H037	Fynbos	0.07	0.03	0.02	0.07	0.02	0.02	0.05	0	0
H2H008	Fynbos	0.1	0.02	0.01	0.07	0.02	0.02	0.02	0.001	0
J1H016	Fynbos	0.1	0	0.02	0.15	0.01	0.01	0.05	0.1	0
C2H005	Grassland	10	3	3	5	0.7	0	5	2	0.1
C5H007	Grassland	40	30	0.5	5	0.5	0.1	15	10	0.2
C5H056	Grassland	0.5	0.1	0	0.4	0.1	0	0.5	0	0
C8H006	Grassland	0.3	0.1	0	0.2	0.05	0	0.1	0	0
A2H032	Savannah	1	0.5	0.1	0.2	0.05	0	0.2	0.05	0
A2H034	Savannah	3	1	0.5	0.3	0	0	0.3	0.01	0
A6H010	Savannah	12	5	0	0.3	0	0	0.1	0	0
B1H018	Savannah	0.2	0.05	0.03	0.07	0.04	0.02	0.07	0.05	0.01
B4H009	Savannah	0.45	0.06	0.02	0.1	0.01	0.01	0.05	0	0
B9H002	Savannah	9	0.1	0	0.1	0.04	0.02	0.1	0.03	0.01
X2H012	Savannah	2	0.5	0	0.5	0	0	0.4	0.01	0.02
X3H003	Savannah	1.3	0.7	0.2	1	0	0	0.2	0	0
X3H015	Savannah	0.5	0	0.04	0.2	0	0.02	0.06	0.04	0.01
P3H001	Thicket	7	0.5	0.05	0.4	0	0	0.1	0	0
P4H001	Thicket	1.5	0.1	0.03	0.2	0.03	0.02	0.5	0	0
R2H009	Thicket	1.5	0.1	0	0.15	0.05	0.02	0.1	0.05	0
R2H012	Thicket	1.7	0.3	0.02	0.3	0.02	0	0.1	0.01	0
U8H001	Thicket	1.6	0.7	0	0.07	0	0.02	0.1	0	0

2.3.3 Results of multiple regression in Statistica

The multiple regressions produced in Statistica did not show a good fit to the data; therefore, the regression equations produced are not shown here. The original equations can be seen in the previous deliverable (K5/2448/1)

2.3.4 Results of multiple regression in Excel

Table 2.5 gives the parameter values of parameters *α-κ* for the various biomes and nutrients, and considering the entire catchment or the 100 buffer zone. The parameter values were achieved by using Solver to derive estimates of surface water concentrations that were as close to the WQSAM derived parameter values (Table 2.4) as possible, using Equation 2.1. The results of parameter values can be applied to new catchments to estimate surface water concentrations by determining the land cover categories and coverage within a catchment, and applying the proportions of total area of respective land cover categories as well as the values given in Table 2.4 to Equation 2.1. Table 2.6 shows the results of applying the regression parameters given in Table 2.5 to the land cover coverage within the study catchments using the regression equation given in Section 2.2.3.

Table 2.5 Parameters derived for multiple regression in Excel using the equation format given in Section 2.2.3. Parameters were estimated using Solver.

	NO_2-N + NO_3-N		NH4-N		PO4-P	
Parameter	**Full**	**Buffer**	**Full**	**Buffer**	**Full**	**Buffer**
Fynbos Biome						
Α	0.000	0.000	0.000	0.000	0.000	0.000
Β	4.738	1.717	0.284	0.155	0.000	0.000
Γ	0.000	0.000	2.295	0.384	0.449	0.000
Δ	0.000	0.000	0.000	0.000	0.000	0.000
Ε	0.016	0.015	0.064	0.063	0.033	0.033
Ζ	0.000	0.000	0.000	0.000	0.000	0.000
Η	0.000	0.000	1.204	0.901	0.613	0.626
Θ	17.245	30.793	0.961	1.452	13.918	4.239
Ι	0.000	0.000	0.000	0.000	0.000	0.000
κ	1.622	1.600	0.101	0.100	0.071	0.070
Grassland Biome						
α	0.000	0.000	0.000	0.000	0.000	0.283
β	0.000	0.000	0.000	9.687	0.000	0.000
γ	2060.067	0.000	107.856	0.000	733.146	0.000
δ	0.000	0.000	0.000	0.000	0.000	0.000
ε	0.000	0.000	0.000	0.000	0.000	0.031
ζ	0.000	0.000	0.000	0.000	0.000	0.000
η	0.000	0.000	0.000	1.107	0.000	0.000
θ	89.985	498.141	37.021	102.480	41.886	266.912
ι	0.000	69.364	0.000	0.000	0.000	0.000
κ	0.000	2901.192	0.000	0.000	0.000	16.489

Table 2.5 Continued Parameters derived for multiple regression in Excel using the equation format given in Section 2.2.3. Parameters were estimated using Solver.

	NO_2-N + NO_3-N		NH4-N		PO4-P	
Parameter	**Full**	**Buffer**	**Full**	**Buffer**	**Full**	**Buffer**
Savannnah Biome						
α	0.000	0.000	0.000	0.000	0.000	0.000
β	0.000	0.000	0.000	0.000	0.000	0.000
γ	0.000	48.088	0.000	1.551	0.000	1.130
δ	0.000	0.000	0.000	0.000	0.000	0.000
ε	1.416	0.074	0.085	0.232	0.214	0.197
ζ	0.509	0.000	69.623	0.000	9.732	0.000
η	0.000	2.380	0.000	0.000	0.000	0.000
θ	0.000	3.463	0.000	6.216	0.000	0.940
ι	71.213	74.864	0.000	0.000	0.000	0.000
κ	0.000	0.000	0.747	0.041	0.131	0.000
Thicket Biome						
α	0.000	0.000	0.000	0.000	0.000	0.371
β	0.000	0.000	0.000	0.000	0.069	0.199
γ	0.000	0.000	0.000	1.288	28.682	7.871
δ	0.000	0.000	0.000	0.000	0.353	0.111
ε	2.881	0.288	0.288	0.035	0.000	0.091
ζ	0.000	0.000	0.000	0.000	0.000	0.000
η	710.856	1.339	1.339	9.382	0.000	0.000
θ	0.000	1.453	1.453	6.612	0.697	19.555
ι	0.000	0.000	0.000	0.000	0.062	0.000
κ	0.395	0.004	0.004	0.563	0.000	0.120

Table 2.6 Results of applying the regression parameters given in Table 2.5 to the land cover coverage within the study catchments using the regression equation format given in Section 2.2.3

		NO_2-N + NO_3-N			NH_4-N			PO_4-P		
Station	**Biome**	**Model**	**Full**	**Buffer**	**Model**	**Full**	**Buffer**	**Model**	**Full**	**Buffer**
G1H010	Fynbos	1.60	1.6	1.60	0.10	0.10	0.10	0.07	0.07	0.07
G1H028	Fynbos	0.05	0.05	0.03	0.06	0.07	0.07	0.03	0.03	0.03
G1H034	Fynbos	5.00	5	5.00	0.30	0.30	0.30	0.50	0.50	0.50
G2H037	Fynbos	0.07	0.07	0.06	0.07	0.06	0.06	0.05	0.03	0.03
H2H008	Fynbos	0.10	0.101	0.11	0.07	0.07	0.07	0.02	0.03	0.03
J1H016	Fynbos	0.10	0.099	0.12	0.15	0.15	0.15	0.05	0.05	0.05
C2H005	Grassland	10.00	14.59	15.79	5.00	5.19	5.00	5.00	6.54	8.21
C5H007	Grassland	40.00	32.18	36.32	5.00	4.68	5.00	15.00	12.36	12.96
C5H056	Grassland	0.50	13.84	6.74	0.40	0.95	0.40	0.50	5.00	0.07
C8H006	Grassland	0.30	0.57	0.00	0.20	0.24	0.20	0.10	0.27	0.03
A2H032	Savanna	1.00	1.29	2.82	0.20	0.18	0.27	0.20	0.19	0.21
A2H034	Savanna	3.00	1.24	2.73	0.30	0.14	0.26	0.30	0.20	0.21
A6H010	Savanna	12.00	10.79	8.68	0.30	0.33	0.18	0.10	0.14	0.14

Table 2.6 Continued Results of applying the regression parameters given in Table 2.5 to the land cover coverage within the study catchments using the regression equation format given in Section 2.2.3

		NO_2-N + NO_3-N			NH_4-N			PO_4-P		
Station	**Biome**	**Model**	**Full**	**Buffer**	**Model**	**Full**	**Buffer**	**Model**	**Full**	**Buffer**
B1H018	Savanna	0.20	0.74	0.15	0.07	0.21	0.20	0.07	0.13	0.17
B4H009	Savanna	0.45	1.35	0.73	0.10	0.29	0.23	0.05	0.23	0.19
B9H002	Savanna	9.00	8.34	9.85	0.10	0.45	0.13	0.10	0.10	0.08
X2H012	Savanna	2.00	1.35	0.11	0.50	0.38	0.23	0.40	0.25	0.19
X3H003	Savanna	1.30	0.31	0.52	1.00	0.64	0.97	0.20	0.15	0.18
X3H015	Savanna	0.50	4.72	4.30	0.20	0.36	0.32	0.06	0.14	0.14
P3H001	Thicket	7.00	4.85	5.44	0.40	0.29	0.33	0.10	0.14	0.11
P4H001	Thicket	1.50	3.46	2.26	0.20	0.30	0.20	0.50	0.49	0.49
R2H009	Thicket	1.50	2.77	3.44	0.15	0.18	0.23	0.10	0.10	0.10
R2H012	Thicket	1.70	1.60	1.67	0.30	0.27	0.28	0.10	0.10	0.10
U8H001	Thicket	1.60	1.77	1.67	0.07	0.13	0.13	0.10	0.10	0.10

2.4 Discussion and way forward

2.4.1 Availability of data

The current study was limited by a lack of data on various fronts. On the broadest level, the lack of suitable sites limited the power of the subsequent statistical analyses as well as the range of different biomes that could be represented. The nature of the study posed major restrictions on the types of sites that were suitable. The lack of suitable sites led to the Nama Karoo and succulent Karoo biomes not being represented within the analyses.

The observed data, both for daily flow and water quality, posed additional restrictions on the subsequent analyses. In many cases, identifying periods of unbroken daily flow within the flow gauging records was difficult, and posed serious restrictions on the temporal simulation period within the subsequent water quality modelling exercise. The low temporal resolution of water quality within the DWS historical monitoring data posed additional restrictions on both the number of suitable sites, as well as the accuracy of water quality model calibration in the subsequent water quality modelling. In general, the DWS water quality data contains a low representivity of water quality measures taken during higher flows. This is unfortunate within the context of the current study, as higher flows would be the periods in which non-point sources would predominate in affecting instream water quality. The lack of water quality measures taken at higher flows additionally poses problems for water quality modelling, as the time series record of water quality at a site affected by non-point sources will contain predominantly lower concentrations from measures taken at low flow, interspersed with a few 'spikes', where measures happened to occur during higher flows. Within a model such as WQSAM, representing the observed frequency distribution is difficult, as the model will tend to generate a frequency distribution that has too frequent concentrations of medium values as compared to the observed frequency distribution. However, it is likely that the frequency distribution of observed water quality is a product of a lack of data, and that the model in actual fact simulates a more 'realistic' frequency distribution of water quality. This problem is blatantly evident for various sites in the current study, for example, gauge C5H056 and C8H006 for NO_2-N + NO_3-N. This problem may lead to an underestimation of the surface water quality signature estimated during the water quality modelling performed in the current study.

2.4.2 Discussion of water quality modelling results

While in general, fairly good water quality simulations were obtained for many sites, (for example C5H007, A2H034 and X2H012 for NO_2-N + NO_3-N, J1H016 and X3H003 for NH_4-N, and X2H012 and B4H009 for PO_4-P), some poor results were additionally obtained (for example P3H001 and R2H012 for NO_2-N + NO_3-N, P3H001 for NH_4-N, and P3H001 and U8H001 for PO_4-P). As discussed above, the lack of observed water quality measures within the DWS historical monitoring data, especially during higher flows, could have influenced the accuracy of model calibration within WQSAM.

The accuracy of model calibrated surface water concentrations would directly affect the subsequent multiple regression analyses in investigating links between model calibrated surface water flow water quality signatures and land cover.

Within the fynbos biome, it is likely that agricultural activities or forestry influenced the water quality signatures of various sites, for example, G1H034 and G1H010. This is confirmed by the land cover data for the sites which show 94% cultivated dryland for G1H034 and 99% forestry for G1H010.

Within the grassland biome, the sites C5H007 and C2H005 showed very high spikes in water quality signatures for all three nutrients. The land cover data showed both C2H005 and C5H007 to have a mix of land cover that could potentially influence water quality, including 13% cultivated dryland, 1.2% cultivated irrigated and 1% urban for C5H007, and 25% cultivated dryland, 2% mining and 14% urban for C2H005. Relatively speaking, the water quality concentrations for C5H007 were considerably higher for all three nutrients than for C2H005, indicating perhaps that irrigated agriculture has a disproportionately large effect on water quality in comparison to other land cover types. From a conceptual perspective, this makes sense as whereas for other land cover types, nutrients become mobilised during rainfall, for irrigated agriculture, irrigation return flow provides a constant supply of mobilised nutrients to a river, even during dry periods.

Within the savannah biome, the sites A6H010 and B9H002 showed relatively high observed concentrations of predominantly NO_2-N + NO_3-N. The land cover data for these two sites show a mix of land cover categories that could potentially be a source of non-point source nutrients, including cultivated dryland, cultivated irrigated and urban areas; however, the large proportions of forestry in both areas (40% for A6H010 and 60% for B9H002) as well as the fact that the highest concentrations occur for NO_2-N + NO_3-N indicate that perhaps forestry has the greatest influence on water quality for this biome.

For the thicket biome, the single site that stands out from the rest in terms of concentrations of NO_2-N + NO_3-N is P3H001. Looking at the land cover data for this gauge, it is not immediately evident why NO_2-N + NO_3-N should be so high for this site, with land cover including a small amount of agriculture (2.2% cultivated dryland and < 1% cultivated irrigated), but predominantly consisting of natural area (96%).

2.4.3 Discussion of multiple regression results from Excel

Fynbos biome

The multiple regression results for NO_2-N + NO_3-N found urban, cultivated dryland, forest and natural land cover categories to affect water quality in the order of greatest to least effect. These categories make conceptual sense and were in addition consistent for both the entire catchment and the buffer zone.

The multiple regression results for NH_4-N for the entire catchment found cultivated irrigated, waterbodies, urban, cultivated dryland, forest and natural categories as affecting water quality in order of greatest to lowest effect. The results for the buffer zone showed urban, waterbodies, cultivated irrigated, cultivated dryland, forest and natural as affecting water quality from greatest to least effect. While the results for the most part make conceptual sense considering both the entire catchment and the buffer zone, there is a question around the plausibility of the effect of water bodies on water quality. It is known that certain surface waters are highly eutrophic, and perhaps water bodies such as farm dams could have a considerable effect on the water quality of adjacent rivers.

The regression results of PO_4-P showed urban areas to have the highest effect on water quality by far, followed by waterbodies and then cultivated irrigated, and a slight effect by natural land cover. It is interesting that the effect of cultivated irrigated was not detected within the 100 m buffer zone, but perhaps none of the fynbos study catchments used in the current study contained irrigated agricultural land within the buffer zone. The inclusion of water bodies as having an effect on instream phosphate is also debatable, and could be justified as for ammonium.

Grassland biome

The regression for NO_2-N + NO_3-N for the entire catchment found cultivated irrigated to have the greatest effect by far, followed by urban areas. The regression for the buffer zone found forest to have the greatest effect, followed by urban areas and degraded natural. The effect of cultivated irrigated was however not detected for the buffer zone. It could be that none of the investigated sites contained cultivated irrigated land within the buffer zone. The identified land cover categories make conceptual sense, as does the larger number of categories identified within the buffer zone, as it is expected that land cover within the buffer zone has more of an effect on instream water quality.

The regression for NH_4-N for the entire catchment, similar to that for NO_2-N + NO_3-N, found cultivated irrigated to have the greatest effect by far, followed by urban areas. The regression for the buffer zone found urban areas to have the greatest effect, followed by cultivated dryland and waterbodies. The identified categories for both regressions make conceptual sense. The inclusion of waterbodies could indicate the influence of eutrophic farms dams.

The regression for PO_4-P for the entire catchment showed cultivated irrigated land to have the greatest effect followed by urban areas. The regression for the buffer zone showed the influence of additional categories, namely urban, forest, bare rock and soil and natural from greatest to least effect on water quality. All identified categories make sense, with the additional categories identified for the buffer zone expected.

Savannah biome

The regression for NO_2-N + NO_3-N for the entire catchment found degraded natural, natural and mining to have an effect on water quality. The regression for the buffer zone detected additional categories and degraded natural, cultivated irrigated, urban, waterbodies, and natural areas were found to influence water quality from greatest to least effect.

The regression for NH_4-N found mining, forest and natural areas to have an effect on water quality from greatest to least effect. The regression for the buffer zone found the urban, cultivated irrigated, natural and forest categories to affect water quality from greatest to least effect. The identified categories make sense; however, it is debatable whether mining should have an effect on instream ammonia. The detection of additional land cover categories within the buffer zone is expected.

The regression for PO_4-P found mining, natural and forest to affect water quality from greatest to least effect. The regression for the buffer zone found cultivated irrigated, urban and natural to have an effect on water quality from greatest to least effect. The non-detection of urban areas as affecting water quality within the entire catchment was not expected; however, perhaps urban areas only influence phosphate if positioned close to the river reach, as phosphates are known to bind to soils, and would not be expected to travel far within overland flow, unless sediment is mobilised.

Thicket biome

The regression for NO_2-N + NO_3-N for the entire catchment found waterbodies, natural and forest land cover categories to affect water quality from greatest to least effect. The regression for the buffer zone found urban areas, waterbodies, natural and forest to affect water quality from greatest to least effect. All identified categories make conceptual sense.

The regression for NH_4-N found urban waterbodies, natural and forest to affect water quality from greatest to least effect. The regression for the buffer zone found waterbodies, urban, cultivated irrigated, forest and natural to affect water quality from greatest to least effect. These selected land cover categories similarly make conceptual sense.

The regression for PO_4-P found cultivated irrigated, urban, sugarcane, cultivated dryland and degraded forest as influencing water quality. The regression for the buffer zone found urban, cultivated irrigated, bare rock and soil, cultivated dryland, forest, sugarcane and natural as the categories affecting water quality from greatest to least effect. While the land cover categories for the most part make sense, the inclusion of sugarcane is questionable. The inclusion of a greater number of categories into the regression for the buffer zone makes conceptual sense.

2.4.4 Conclusions and way forward

The limitations of this study were lack of data. As discussed, few appropriate sites were identified. In addition, within each site, lack of observed flow and water quality data was a constraint on analysis.

The lack of observed data and appropriate sites affected the quality of the calibrations obtained within WQSAM. As mentioned before, very few water quality readings within the DWS historical monitoring data are taken within higher flows. From a logistical point of view, this is reasonable as there are safety concerns associated with rivers in flood. However, the non-point source water quality signature is strongest during higher flows, and it is unfortunate that there are a lack of date to quantify this signature.

The lack of data in addition affected the quality of the multiple regressions obtained in Statistica. This is probably the reason for the results obtained that did not make conceptual sense. The regressions obtained in Excel using Solver made more conceptual sense. That ability to constrain parameters to positive values within Solver was beneficial to obtaining results that were conceptually sound.

It is recommended that the results obtained using Solver be implemented within WQSAM (Table 2.5). However, the regressions should be revisited as further observed data becomes available, either as a more appropriate land cover database, the further identification of appropriate sites, or further observed flow and water quality data within sites.

CHAPTER 3. SIMULATING MICROBIAL WATER QUALITY AND ACID MINE DRAINAGE

3.1 Introduction

The Water Quality Systems Assessment Model (WQSAM) was originally developed to be as simple as possible while still representing major water quality processes (Slaughter *et al*., 2015). To this effect, the number of original water quality variables simulated by WQSAM was restricted to nutrients, algal growth and salinity. It is argued that including certain variables such as dissolved oxygen and metals for example, would require the representation of multiple additional complicated water quality processes that would so increase the complexity and data requirements of the model so as to make the model non-viable within specifically a South African water resources management context, and more generally within the context of the capabilities of a developing country.

However, given the water quality processes already represented within WQSAM, such as water temperature and salinity, the possibility of including two additional and highly important water quality variables was recognised, namely acid mine drainage (AMD) and microbial water quality. It has been recognised that arguably it is possible to represent these two variables fairly simply, as detailed in this report.

3.1.1 Acid mine drainage (AMD)

AMD results from the oxidation and hydrolysis of metal sulphides in water-permeable rock strata (Gray, 1996; 1997; 1998; Akcil and Koldas, 2007). While sulphides are generally stable and insoluble under reducing conditions, oxidation occurs once the minerals are exposed to oxygen (Olías, 2004). Exposure occurs within both working and abandoned mines, although abandoned mines produce more AMD as active pumping of water has ceased in these mines (Cobbing, 2008; Simate and Ndlovu, 2014). The chemistry of AMD is generally fairly straightforward, but may vary according to various factors such as geology, temperature, microorganisms, water and oxygen (Gray, 1998; Akcil and Koldas, 2007; Simate and Ndlovu, 2014). Constituent elements of AMD include sulphate, zinc, iron, magnesium, copper, lead, calcium and manganese (Gray 1996; Olías, 2004).

The effects of AMD have been rated as second only to climate change and ozone depletion in terms of ecological risk, and can result in irreversible destruction of ecosystems (Oelofse, 2008). Other effects include the erosion and damage of human infrastructure, increased seismic activity and the pollution of groundwater (INTER-MINISTERIAL COMMITTEE, 2010). More specifically, low pH often associated with AMD results in water that is unsuitable for domestic or other uses, will have long-term effects on infrastructure and will not support most aquatic life (Cobbing, 2008; INTER-MINISTERIAL COMMITTEE, 2010). The acidity of AMD also increases the bioavailable concentrations of various toxic metals and radionuclides, resulting in toxicity for both humans and the environment (INTER-MINISTERIAL COMMITTEE, 2010). High sulphates often associated with AMD, even after treatment, can render water unfit for human use and results in salinisation and the associated effect on aquatic ecosystems (INTER-MINISTERIAL COMMITTEE, 2010; Simate and Ndlovu, 2014).

AMD has been described in Spain (Olías, 2004), Ireland (Gray, 1996; 1998), the United Kingdom (Cobbing, 2008), Portugal (Candeias *et al*., 2014), Australia (INTER-MINISTERIAL COMMITTEE, 2010), Canada (INTER-MINISTERIAL COMMITTEE, 2010) and the USA (INTER-MINISTERIAL COMMITTEE, 2010).

AMD is particularly problematic within South Africa. This is because of the sheer scale of mining operations within certain regions in South Africa, the interconnectedness of mines and the general lack of planning to minimise impacts, particularly within the earlier mines that have since been abandoned (INTER-MINISTERIAL COMMITTEE, 2010). AMD associated with gold mining is particularly problematic within the Witwatersrand region in Gauteng (INTER-MINISTERIAL COMMITTEE, 2010). The Witwatersrand region can be divided into the western, eastern and central basins. Within the central basin, AMD is currently rising at a rate of 0.59 m day^{-1}, whereas AMD has already reached the surface in the central basin (INTER-MINISTERIAL COMMITTEE, 2010). Within the western basin, partial treatment of AMD takes place, with approximately half of the average 20 mega litres day^{-1} AMD partially treated and released to the upper Crocodile River (Tweelopie Spruit) (INTER-MINISTERIAL COMMITTEE, 2010). AMD produced in the western mining basin near Krugersdorp produces AMD of approximately 36,000 million m^3 day^{-1} which threatens a game reserve, ground water reserves as well as the Cradle of Humankind World Heritage Site (Hobbs and Cobbing, 2007). Within the central basin, pumping stopped in 2008, leading to the subsequent rise in AMD. Within the eastern basin, the water quality of AMD is slightly better because of the inflow of highly alkaline water, leading to higher pH and lower sulphate levels. However, substandard water continues to flow into the Blesbok Spruit from this region, contributing to salinity of the Crocodile and Vaal river systems (INTER-MINISTERIAL COMMITTEE, 2010).

AMD is additionally associated with the Witbank coalfields situated within the headwaters of the Olifants River, upstream of Loskop Dam (Oelofse, 2008; Oberholster *et al*., 2010). This region contributes approximately 50 mega litres day^{-1} of AMD to the upper Olifants (Maree *et al*., 2004).

3.1.2 Microbial water quality

It is generally recognised that microbial water quality of surface waters in South Africa poses a massive health risk to humans and livestock. Given the challenges faced by waste water treatment plants, the large number of people living within informal settlements and the problems associated with sewerage networks, microbial contamination of surface waters will most likely increase into the future. This problem has been highlighted by various studies. For example, Britz and Sigge (2012) have sent out an ominous warning of health risks associated with irrigated agriculture. Their baseline study found extremely high levels of faecal indicators exceeding all guidelines associated with river water used to irrigate crops. Their study concluded that produce irrigated with river water from many rivers in South Africa and consumed raw without further processing posed considerable risks to human health. Besides the implications for consumer health, this news was most unwelcome from an economic perspective within the agricultural sector, particularly for producers of export fruit. Their study concentrated on rivers in the Western Cape, KwaZulu-Natal, Limpopo and Mpumalanga. Le Roux *et al*. (2012) in addition found high levels of *Escherichia coli* within tributaries of the Wilge, Klein Olifants and Olifants rivers.

Challenges associated with microbial water quality within South African surface waters require urgent intervention and management. To achieve this, a good understanding of the behaviour of microorganisms is required at the ecosystem level (Venter *et al*., 2011). The modelling of microbial water quality can assist in prioritising mitigation measures by indicating the individual sources of contamination (Sokolova *et al*., 2013). Modelling of microbial water quality can also assist in the investigation of management scenarios (Hipsey *et al*., 2008). The management and mitigation of microbial loads at the catchment level would reduce human and livestock illness as well as provide financial benefits (Venter *et al*., 2011).

The general approach to the monitoring, measurement and modelling of microbial water quality has been to use certain bacterial or viral indicators as models of the behaviour of pathogens. These indicators are chosen according to the ease and cost of measurement, and may be relatively harmless, with the motivation being that these indicators are indicative of faecal contamination and the presence of associated pathogens such as *Salmonella* spp., *Shigella* spp., *Vibrio* spp., *Clostridium* spp. and *Giardia* spp (Hipsey *et al*., 2008). The most common indicator species are the enteric coliform bacteria which are Gram-negative bacilli belonging to the family Enterobacteriaceae (Hipsey *et al*., 2008). Specific coliform measurements include total coliforms, faecal coliforms *Escherichia coli,* with the latter two being the most common measures as they are abundant within the faeces of mammals (Hipsey *et al*., 2008). In particular, *E. coli* has been shown as a better indicator of microbial contamination than coliforms (Edberg *et al*., 2000), and as such, has been the preferred microbial indicator within several studies such as that of Sokolova *et al*. (2013). Studies have shown that the different classes of organisms show considerably different responses to environmental pressures; therefore, the strategy of using microbial water quality indicators is not without criticism (Hipsey *et al*., 2008). As there are some limited data of *E. coli* levels within the Department of Water and Sanitation (DWS) routine monitoring data, the current study used *E. coli* as the microbial indicator.

It is possible to model microbial water quality in a fairly simplistic way, which is the reason for inclusion within WQSAM. The dominant processes affecting the various species of microbial organisms are similar; therefore, the construction of a generic model for microbial pollutants appears viable (Hipsey *et al*., 2008).

From the available literature, the processes that would need to be considered in a model would include growth and the effect of temperature, salinity and light on mortality. Generally, the instream environment is regarded as hostile to microbial organisms originating from the mammalian gut, and is has been suggested that growth can be disregarded within a model (Hipsey *et al*., 2008). This was explicitly confirmed by Servais *et al*. (2007) who observed no growth of faecal coliforms within a batch experiment with sterile Seine River water. It has been found that there is a link between temperature and faecal coliforms, for example Britz and Sigge (2012).

Therefore, to model microbial water quality, it would appear that factors affecting the mortality rate of microbial indicators require consideration, whereas growth can be disregarded. As confirmed in other studies, for example Tian *et al*. (2002), Kashefipour *et al*. (2002), Collins and Rutherford (2004) and Menon *et al*. (2003), this mortality can be represented as a first order rate. Mancini (1978) proposed the following model:

$$\frac{dC}{dT} = -k_0 \times \emptyset_S^{Sal} \times \emptyset_I^{Int} \times \emptyset_T^{(Temp-20)} \times C \qquad \text{Equation 3.1}$$

where *t* is the time, *C* represents the *E. coli* concentration, k_0 (day^{-1}) is the decay rate at 20°C for a salinity of 0 ‰ and darkness, *Sal* (‰) is the salinity, $\emptyset_I$ is the light coefficient, Int is the light intensity integrated over depth, $\emptyset_T$ is the temperature coefficient for the decay rate and *Temp* is the water temperature.

3.2 Method and study areas

3.2.1 Study areas used

Within this study, the upper and middle Crocodile River Catchment and the Upper Olifants River Catchment were used as study areas. Sulphates as indicative of acid mine drainage were simulated for both the Crocodile and the Olifants river catchments, as these rivers are both affected by AMD (Oelofse, 2008; INTER-MINISTERIAL COMMITTEE, 2010; Oberholster *et al*., 2010). Microbial water quality was simulated for the Crocodile River Catchment as measured *E. coli* data were available for this catchment.

The Crocodile River Catchment was modelled up to X22 for both microbial water quality and AMD. This was mainly because most of the microbial water quality data were available up to this point.

This important catchment occurs in the province of Mpumalanga (Figure B3) and is an important irrigation area (Deksissa *et al*., 2004), with its source in the Highveld, draining an area of approximately 10,440 km^2 over a total distance of approximately 320 km, and joining the Komati River before entering Mozambique in the East (Deksissa *et al*., 2004; Pollard and du Toit, 2011). Annual rainfall varies from 600-1,200 mm decreasing from west to east, with a mean of 880 mm (Deksissa *et al*., 2004), with predominantly summer rainfall occurring between November and April through convection thunderstorms (Deksissa *et al*., 2004).

The geology of the region is relevant in regards to the simulations of sulphate. Fractured rock aquifers largely of igneous origin occur in the catchment. The broad geology of the catchment can be divided into Cambrian and Precambrian geology with associated TDS concentrations of < 65 mg ℓ^{-1} and ranging from 195 to 1,100 mgℓ^{-1}, respectively. Generally, the upper catchment is dominated by Cambrian geology, whereas the central and lower catchment is dominated by Precambrian geology; therefore, the salinity of the upper catchment is not influenced dramatically by the geology.

Extensive agriculture occurs within the catchment, ranging from wheat and maize farming in the western regions to cattle and sugar cane production in the eastern regions. Large areas of irrigated agriculture occur within the catchment (Roux *et al*., 1994; Deksissa *et al*., 2004).

The yield model up to the middle catchment can be seen in Figure B3. Because the Crocodile River Catchment is relatively large and the systems diagram of the catchment is fairly complex, the presented systems diagram is broken up into several sections.

The catchment is subject to various pollution sources, including industrial and domestic point sources of pollutants, with approximately 30 waste water treatment works (WWTWs) within the middle reaches alone (Deksissa *et al*., 2004). In addition, runoff and return flows from extensive areas of irrigated agriculture and mining sites act as diffuse sources of pollutants within the catchment (DWAF, 1995). Table 3.1 lists the gauges with observed water quality data used within the study.

The Olifants River is highly modified by human use and has been extensively dammed. Water from the river is utilised by the coal mining, petrochemical and other industries, as well as diverse agriculture (Heath *et al*., 2010). The Olifants River has been identified as one of the most threatened rivers in South Africa, with frequent reports of crocodile and fish kills (Balance *et al*., 2001; de Villiers and Mkwelo, 2009, Van Vuuren, 2009).

The Olifants River originates from the east of Johannesburg, with the upper Olifants extending from the catchment divide with the Vaal River to Loskop Dam down to Flag Boshielo Dam, including the Olifants, Klein Olifants, Wilge, Steenkoolspruit, Klipspruit and Elands rivers (Heath *et al*. 2010). The upper catchment includes various major dams such as Loskop, Witbank, Middleburg, Bronkhorstspruit and Premier Mine dams.

Large urban centres occur within Witbank and Middleburg, while several smaller urban areas occur within the upper catchment (Heath *et al*., 2010). Coal mining occurs within the Witbank and Highveld coalfields (Heath *et al*., 2010). Diverse agriculture occurs within the upper catchment, with maize farming dominating in the southern and central parts of the upper catchment (Heath *et al*., 2010).

Figure B2 shows the quaternary catchment structure of the upper Olifants River Catchment. The systems diagram of the Olifants River as used within the water quality modelling can be seen in Figure B1.

The major water quality problems within the Olifants have been identified to be acid water, metals and sulphates from mines, excessive nutrients from WWTWs and agriculture and microbial contamination from WWTWs (van Vuuren, 2013).

The pH levels within the upper Olifants have been identified as a point of concern. While for the most part, pH levels are near neutral to alkaline, certain tributaries such as the Klipspruit experience pH levels of near 4 and under due to constant acid mine drainage (AMD) (Heath *et al*., 2010). It has been pointed out that abandoned mines are responsible for the majority of

AMD, with operational mines contributing a relatively minor amount of AMD (van Vuuren, 2013).

Table 3.1 Observed DWA historical monitoring data for the Crocodile River Catchment.

Node	River Name	WQ Gauging Station	Latitude	Longitude	From:	To:
X21F-1	Elands	1-3214	30.260560	−25.657780	1972	2012
X21F-2	Elands	X2H011	30.277780	−25.645830	1972	2009
Kwena Dam	Kwena (Crocodile)	X2R05	30.386710	−25.359770	1984	2012
X21D-2	Crocodile	X2H033	30.480640	−25.374990	1977	1992
DDX21J-1	Elands	1-3212	30.599030	−25.592910	2006	2012
X22A-1	Blystaanspruit	X2H027	30.642480	−25.340570	1966	1981
X21H-1	Ngodwana	X2H034	30.673690	−25.661470	1972	1983
X21K-2	Elands	X2H015	30.697500	−25.487780	1972	2012
X22A-2	Houtbosloop	X2H014	30.700530	−25.379690	1966	2012
X22E-1	Kruisfonteinspruit	X2H035	30.880160	−25.185560	1984	2011
Witklip Dam	Witklip (Sand)	X2R03	30.899900	−25.235860	1975	2012
X22CTributary	Rietspruit	X2H031	30.942510	−25.472710	1966	2012
X22F-2	Nels	X2H005	30.965310	−25.427930	1969	2012
Longmere Dam	Longmere Dam (Witrivier)	X2R01	31.000770	−25.279030	1968	2011
Klipkoppie Dam	Klipkopjes (Wit)	X2R02	31.007640	−25.219250	1981	2012
X22J-1	Crocodile	1-9827	31.025720	−25.446510	2008	2011
Primkop Dam	Primkop (Wit)	X2R04	31.071150	−25.384960	1972	2012
X22H-3	Wit	X2H023	31.082780	−25.461330	1968	1992
X22J-2	Crocodile	X2H006	31.100000	−25.469440	1969	2012
X22K-2	Crocodile	X2H032	31.224930	−25.514120	1972	2012

Salinisation appears to be a problem within the upper Olifants, with elevated salinity near Middlekraal, with the salinity trend increasing from Witbank Dam to Middleburg Dam, and the Klipspruit contributing a large salt load due to mining (Heath *et al*., 2010). Loskop Dam acts as a sink for salts (Heath *et al*., 2010). Table 3.2 shows the gauges with observed water quality data used within the current study.

Table 3.2 Observed DWA historical monitoring data for the Olifants River Catchment.

Node	River Name	WQ Gauging Station	Latitude	Longitude	From:	To:
B11A	Olifants	B1H018	29.45917	−26.21667	1991	2014
B11F	Olifants	B1H005	29.25389	−26.00639	1979	2014
B11E	Steenkool Spruit	B1H021	29.27	−26.13611	1990	2014
B11C	Steenkool Spruit	B1H017	29.27417	−26.30556	1990	2014
B11H	Elands Spruit	B1H002	29.33778	−25.81833	1990	2014
B11K	Klip Spruit	B1H004	29.17111	−25.67333	1966	2014
Middleburg Dam	Klein Olifants	B1R002	29.54583	−25.775	1978	2013
Bronkhorst Dam	Bronkhorstspruit	B2R001	28.725	−25.8875	1968	2013
Loskop Dam	Olifants	B3R002	29.3599	−25.4183	1968	2013

3.2.2 Methods

Modelling approach

The approach taken within this study was to implement the functionality within WQSAM to simulate sulphates (as representative of AMD) and microbial water quality, and then to simulate these two variables within the Olifants and Crocodile river catchments for sulphates, and within the Crocodile River Catchment for microbial water quality, for historical conditions. The simulations are therefore calibrated against historical monitoring data, and the results obtained and parameter values used are discussed in terms of catchment characteristics and pollution sources. Calibrations are represented as frequency distributions as WQSAM is designed in a way so as to represent the frequency of water quality observations rather than accurate time series representations (Slaughter *et al*., 2015a).

Microbial modelling approach

The method used in the current study is based on a modified version of the equation by Mancini (1978). Sokolova *et al*. (2013) found no differences between the persistence of *E. coli* in light and dark incubations; therefore, they disregarded the effect of light in their model. In accordance with the model of Sokolova *et al*. (2013), the model used in the current study to simulate the first order degradation of *E. coli* is:

$$\frac{dC}{dT} = -k_0 \times \emptyset_S^{Sal} \times \emptyset_T^{(Temp-20)} \times C \qquad \text{Equation 3.2}$$

where *t* is the time, *C* represents the *E. coli* concentration, k_0 (day^{-1}) is the decay rate at 20°C for a salinity of 0 ‰, $\emptyset_s$ is the salinity coefficient, *Sal* (‰) is the salinity, $\emptyset_T$ is the temperature coefficient for the decay rate and *Temp* is the water temperature.

Modelling of AMD

It has been shown that sulphate is generally strongly associated with AMD (Gray, 1996; 1997; Simate and Ndlovu, 2014). While sulphate contributes to salinity, the general perception in South Africa is that sodium and chloride salts contribute to natural salinity, whereas sulphates are associated with either AMD or industrial effluent. Sulphate is a non-conservative variable, and generally remains relatively unchanged throughout transport in surface waters, whereas other variables associated with AMD, such as toxic metals and pH, undergo various chemical transformations associated with biotic and abiotic conditions. Arguably therefore, sulphate could be used as a general indicator of AMD within surface waters. Within the context of water quality modelling, the use of sulphate as an indicator of AMD is preferable as the processes affecting sulphate would be similar to those affecting total dissolved solids (TDS), such as dilution, input from incremental flow and return flow and evaporation. Therefore, the approach taken within WQSAM to model sulphates (as representative of AMD), are the same as that for TDS (see Slaughter *et al*., 2015).

3.2.3 Data

Table A1 contains a summary of the *Escherichia coli* data available for the sites on the Crocodile River whereas Table A2 contains a summary of effluent *Escherichia coli* data available for the sites on the Crocodile River.

3.3 Results

3.3.1 Model calibration for microbial water quality

As indicated in Equation 3.2, the generic model of the decay of the microbial indicator population (in this case, *E. coli*), is influenced by temperature and salinity. Therefore, to adequately simulate microbial water quality, the water temperature and salinity of the study catchment must first be adequately represented. Figure 3.1 shows the model calibration for salinity (TDS) within the study sites, whereas Figure 3.2 shows the calibration for water temperature within the study sites.

As can be seen in Figure 3.2, an adequate simulation of water temperature was obtained within the study sites within the Crocodile River Catchment. It is evident within Figure 3.1 that in most cases, an adequate representation of salinity was obtained for the study sites.

The results of calibrations of *E. coli* are represented in Figure 3.3. Because of the lack of observed data, calibrations could be performed at very few sites. In general, the simulations obtained were good representations of the observed data. The results obtained for EWR1 were relatively poor compared to the results obtained for the other sites.

Decay rates (k_0) across the catchment ranged from 0.1 to 0.4, with the simulations being very sensitive to this parameter. Within the flow signatures of surface flow, interflow and groundwater flow of incremental flow (see Slaughter *et al*., 2015), only the surface water flow parameter was adjusted during calibration, with the assumption that interflow and groundwater flow would generally not by contaminated by microbial pollution. The value of the surface water flow signature ranged from 500 to 15,000 cells 100 m ℓ^{-1}. $Ø_s$ and $Ø_T$ were kept constant at 1.05 and 1.04 respectively.

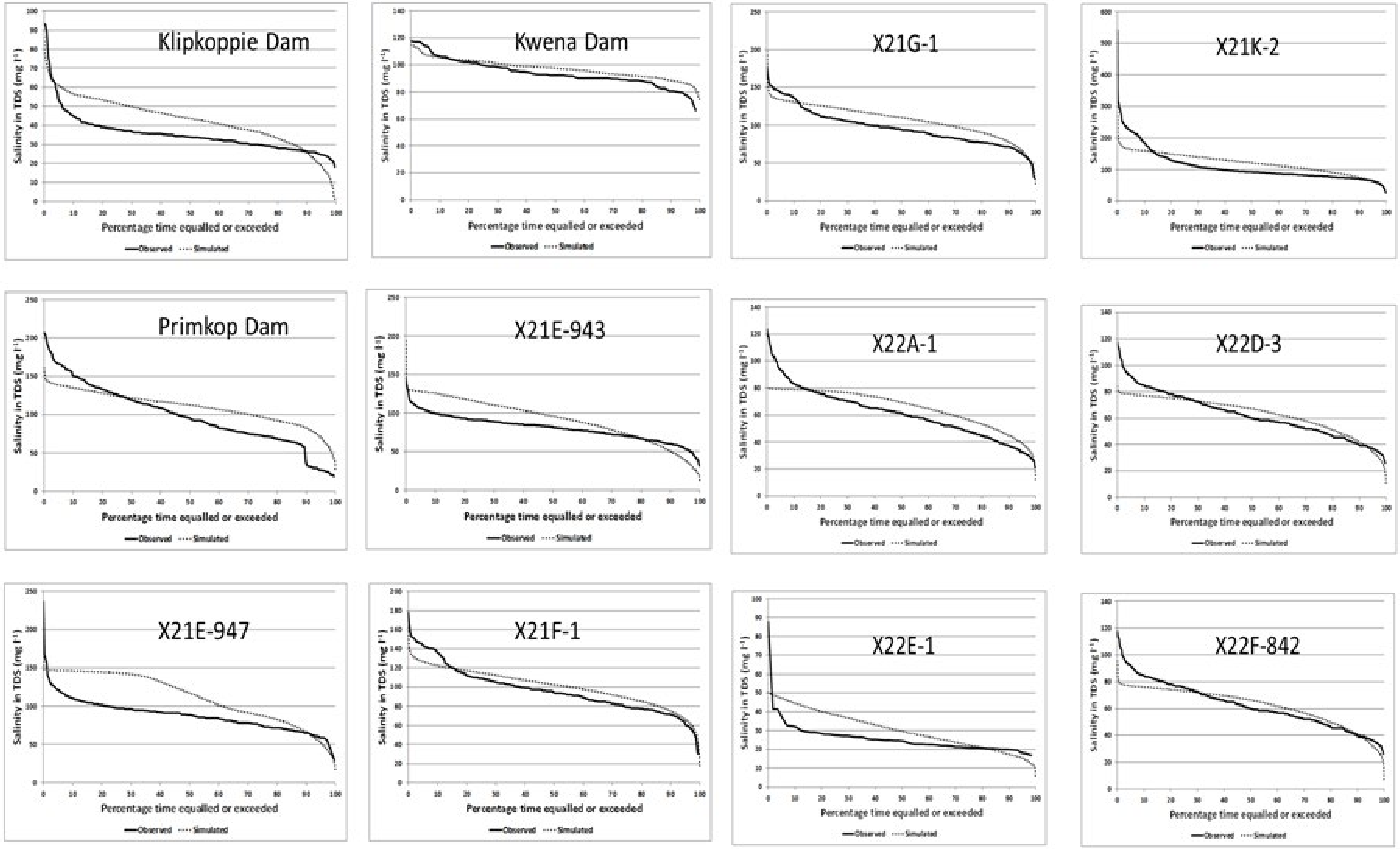

Figure 3.1 Results of calibration of salinity as total dissolved solids (TDS) within the Crocodile River Catchment study sites, represented as frequency distributions.

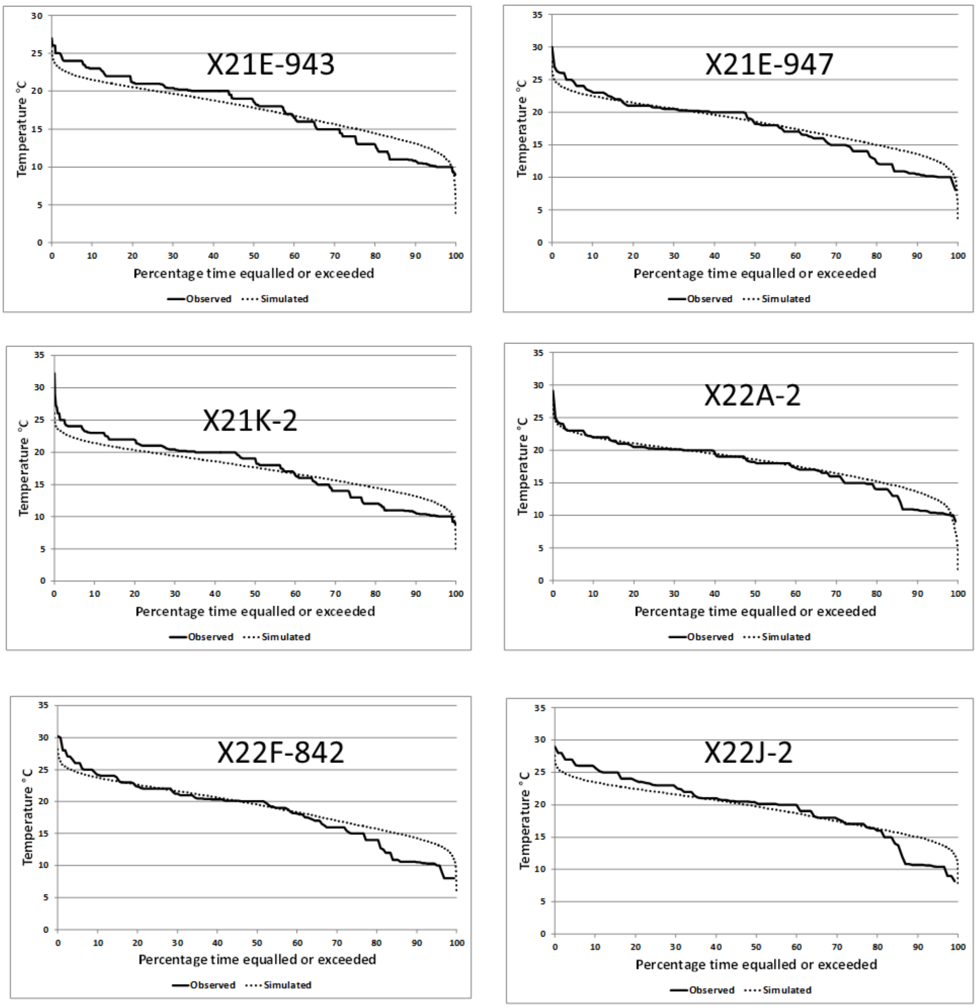

Figure 3.2 Results of calibration of water temperature simulations to observed data within the Crocodile River Catchment study sites, represented as frequency distributions.

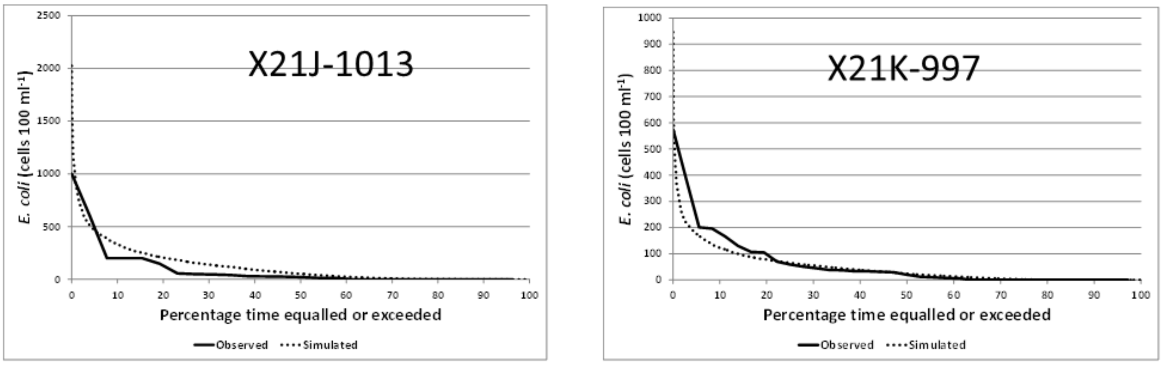

Figure 3.3 Results of *Escherichia coli* simulations calibrated to observed data within the Crocodile River Catchment study sites, represented as frequency distributions.

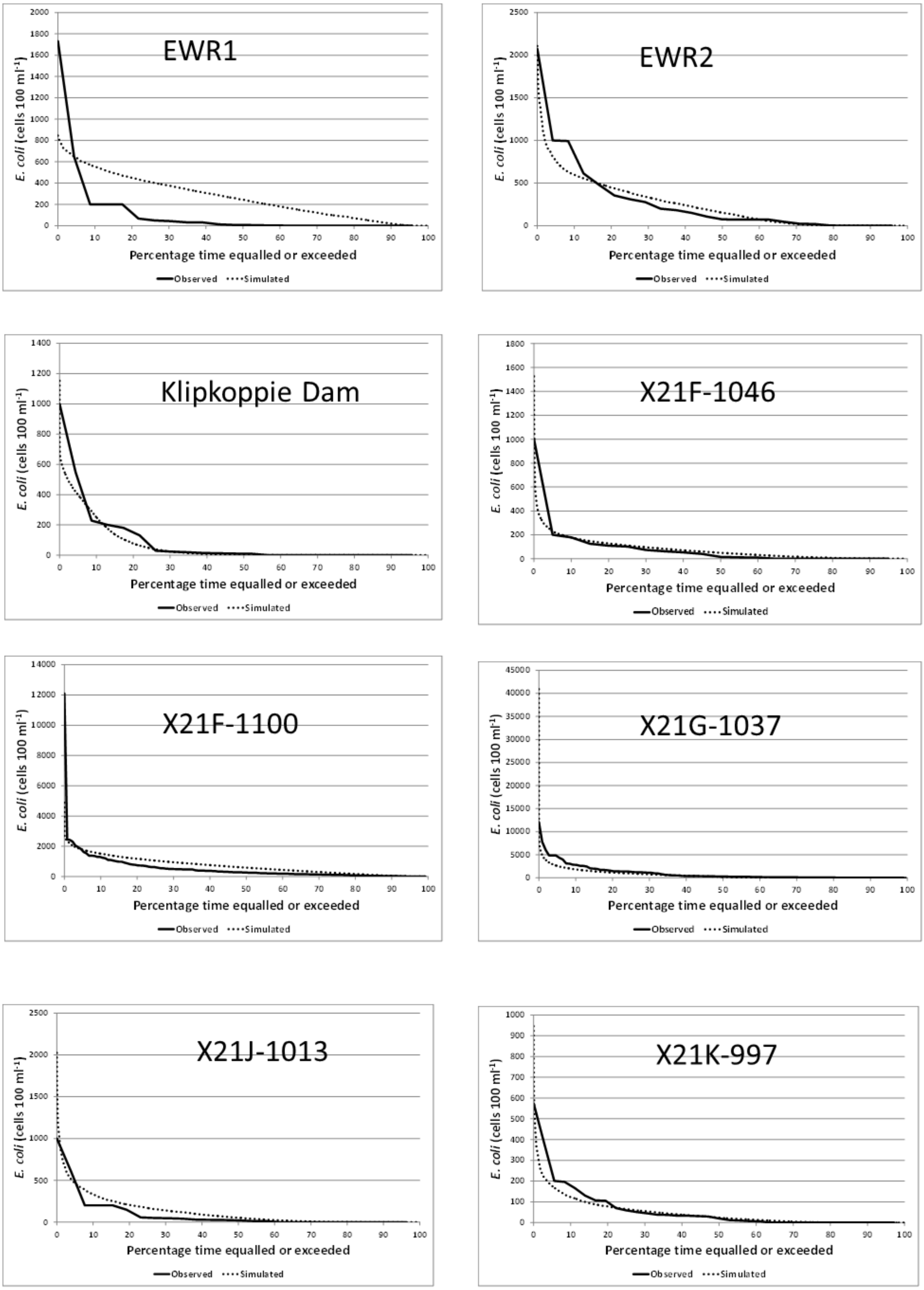

Figure 3.3 continued Results of *Escherichia coli* simulations calibrated to observed data within the Crocodile River Catchment study sites, represented as frequency distributions.

3.3.2 Model calibration for sulphates

Results for the Olifants River Catchment

Figure 3.4 shows the results of sulphate simulations for the Olifants River Catchment in WQSAM calibrated against observed data. In general, it was found that to achieve sufficient variability within the observed sulphate time series data, the surface flow signature had to be adjusted, rather than the interflow or groundwater flow signature, although the interflow and groundwater flow signatures were adjusted for some sites. Even with the adjustment of the surface flow signature, in many cases a good match to the observed data could not be achieved, for example B11A, B11C and Middelburg Dam (see Figure 3.4).

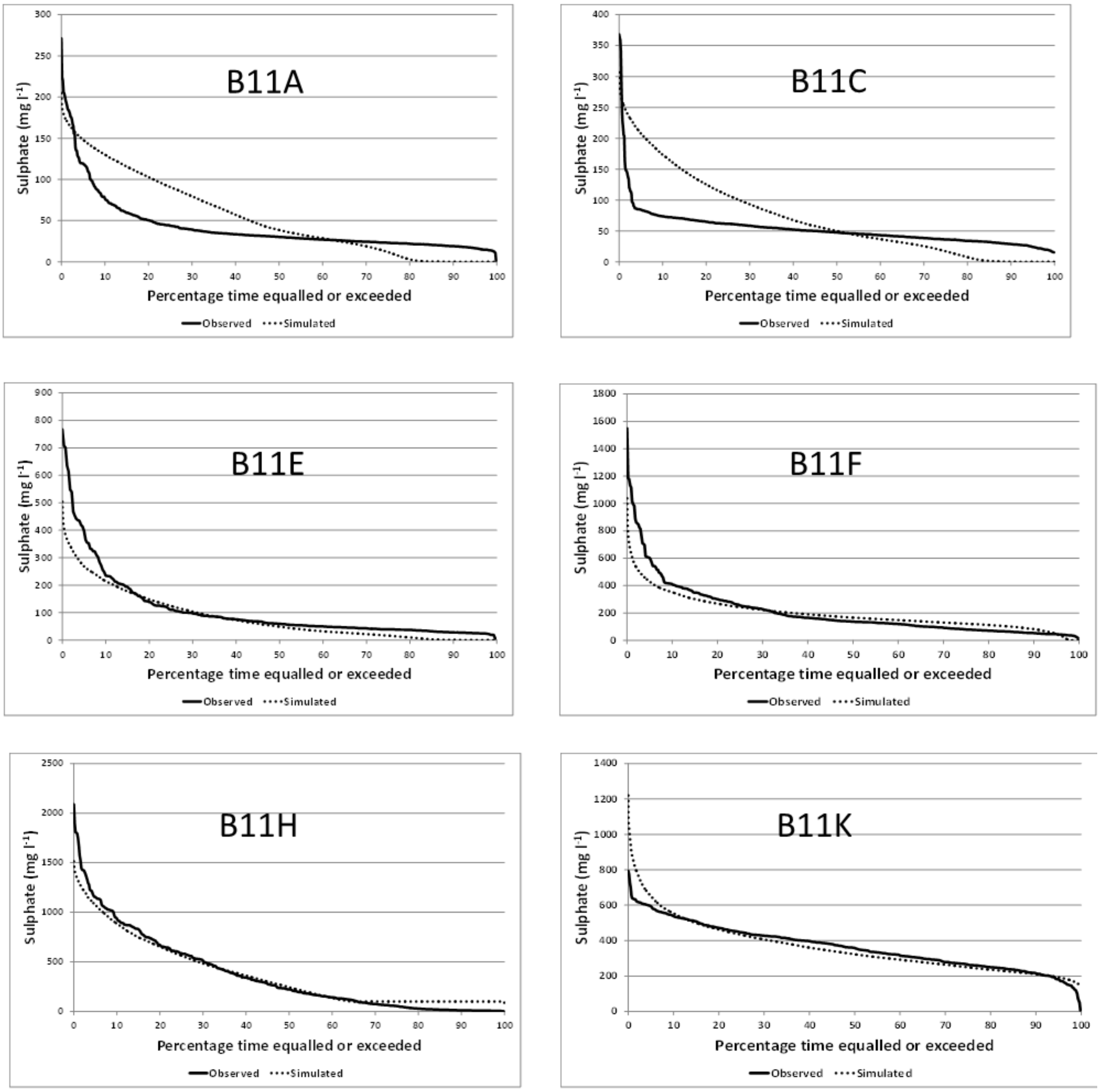

Figure 3.4 Results of sulphate simulations calibrated to observed data within the Olifants River Catchment study sites, represented as frequency distributions.

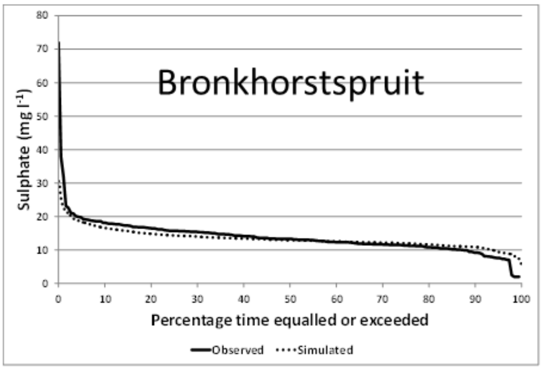

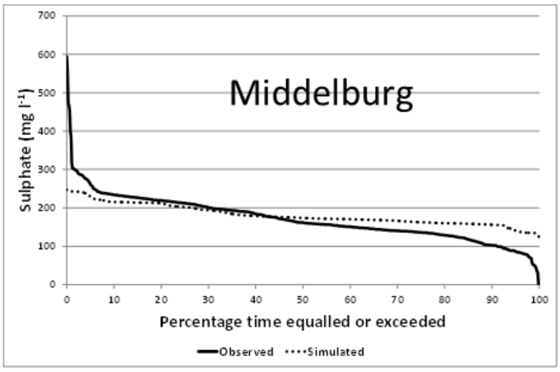

Figure 3.4 (continued) Results of sulphate simulations calibrated to observed data within the Olifants River Catchment study sites, represented as frequency distributions.

Values of the surface flow parameter ranged from 20 mg ℓ^{-1} within the B20 quaternary catchments to 200-400 mg ℓ^{-1} within the B11A-E quaternary catchments to up to 1,600 mg ℓ^{-1} within B11F and B11H, indicating that these two catchments are contributing considerable quantities of AMD to the Olifants River. It was not possible to obtain reasonable calibrations within the Loskop and Witbank dams, as there are strong increasing trends evident within the observed data (see Figures 3.5 and 3.6). WQSAM at this point is not able to simulate dynamic water quality trends.

Results for the Crocodile River Catchment

In general, the levels of sulphate within the Crocodile River sites were much lower than that in the Olifants River. Relatively high sulphate levels were evident within X21F1 and X21K2. For most sites, relatively low values ranging from 10 to 20 mg ℓ^{-1} were assigned to the surface flow signatures. For X21F1, a relatively high surface flow signature of 100 mg ℓ^{-1} was assigned to achieve a good calibration. For X21K2, a relatively high return flow concentration of 200 mg ℓ^{-1} was assigned to X21K-1035 immediately upstream.

While good simulations were achieved for many sites, the simulations could not capture the observed frequency distribution of data for a few sites, for example Kwena Dam and Witklip Dam (see Figure B3).

3.4 Discussion and way forward

3.4.1 Microbial water quality modelling

Generally, there are less microbial water quality data within the DWA historical monitoring data relative to other variables such as nutrients and salts. While there were *E. coli* data available for the Crocodile River Catchment, few sites were ultimately used within the model calibration that were sufficiently spatially proximate to allow estimation of model parameters related to microbial water quality.

The model calibration obtained simulations that were generally representative of observed data. Some uncertainties however still exist, mostly due to the lack of observed data. In most cases, calibrations were obtained by adjusting the value of the surface water flow microbial water quality signature. In other cases where possible, the microbial water quality signature of return flow was adjusted. However, the yield models are in general constructed in a way to optimise the simulation of water quantity, and return flow nodes may be assigned spatial positions within the catchment that are viable from a water quantity simulation perspective, but are however sub-optimal or inaccurate from a water quality simulation perspective. For example, while a return flow signature may be evident within the observed data, the yield model may not have assigned a return flow to the node representing that particular spatial location.

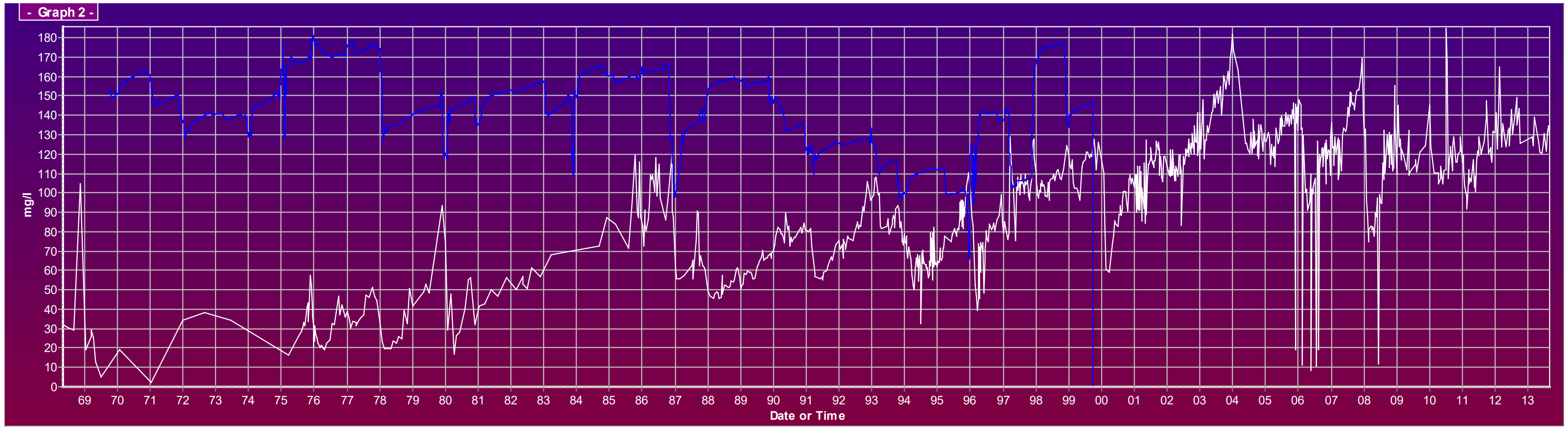

Figure 3.5 Time series results of sulphate simulations calibrated to observed data within Loskop Dam on the Olifants River. The white line represents the observed data whereas the blue line represents simulated data. A clear increasing trend is evident within the observed data.

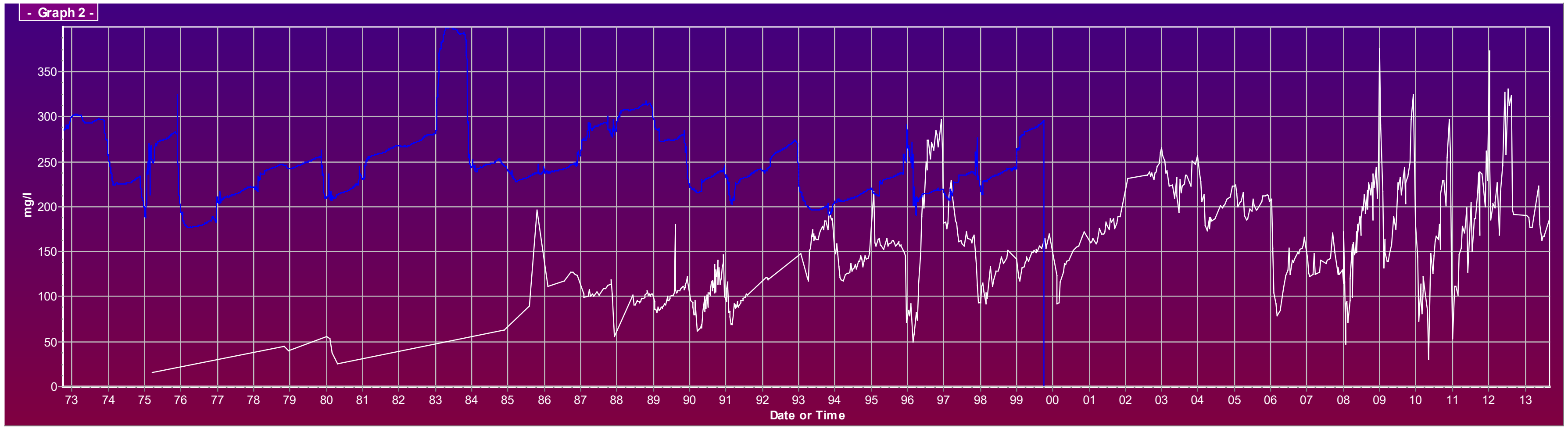

Figure 3.6 Time series results of sulphate simulations calibrated to observed data within the Witbank Dam on the Olifants River. The white line represents the observed data whereas the blue line represents simulated data. A clear increasing trend is evident within the observed data.

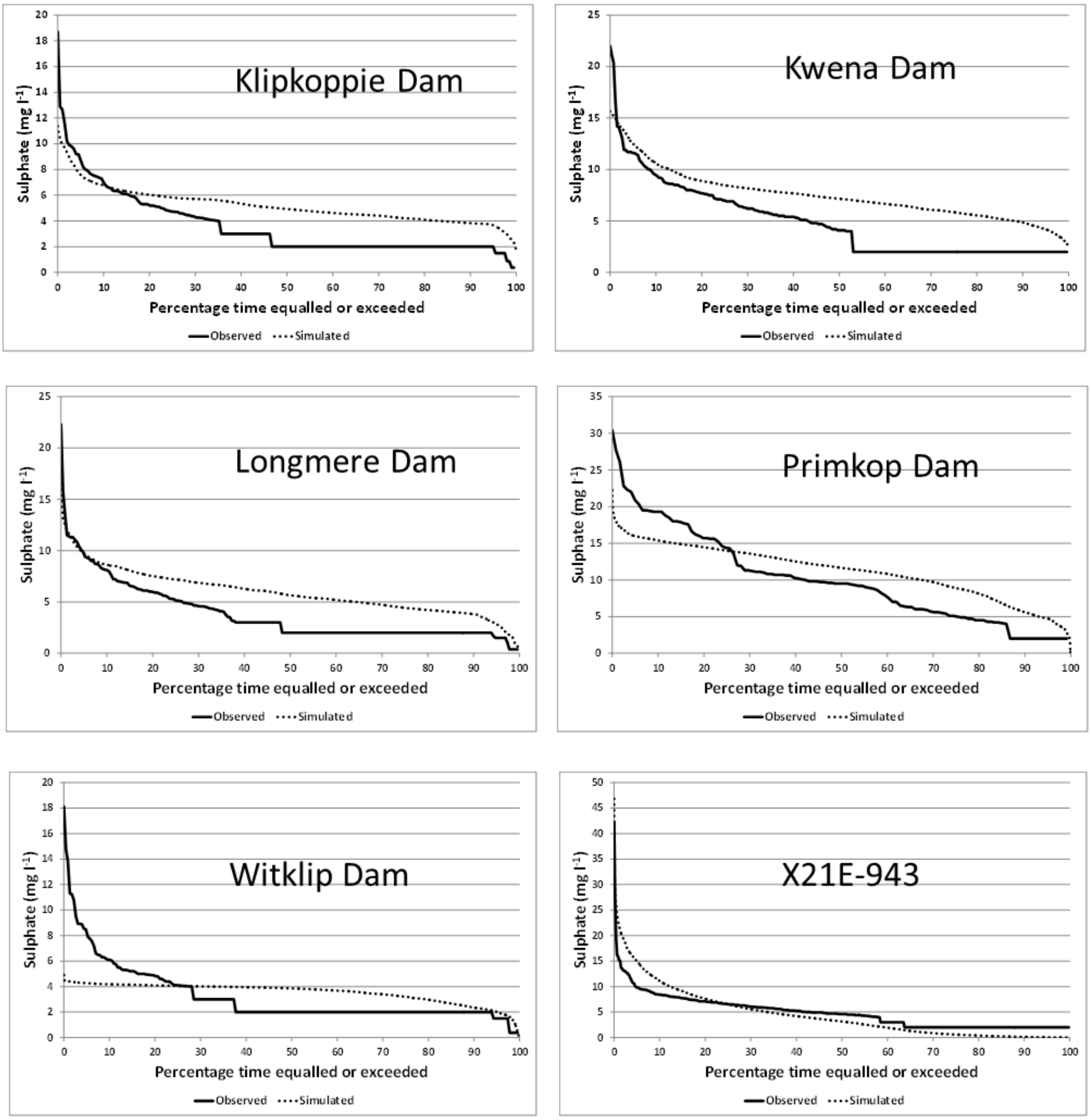

Figure 3.7 Results of sulphate simulations calibrated to observed data within the Crocodile River Catchment study sites, represented as frequency distributions.

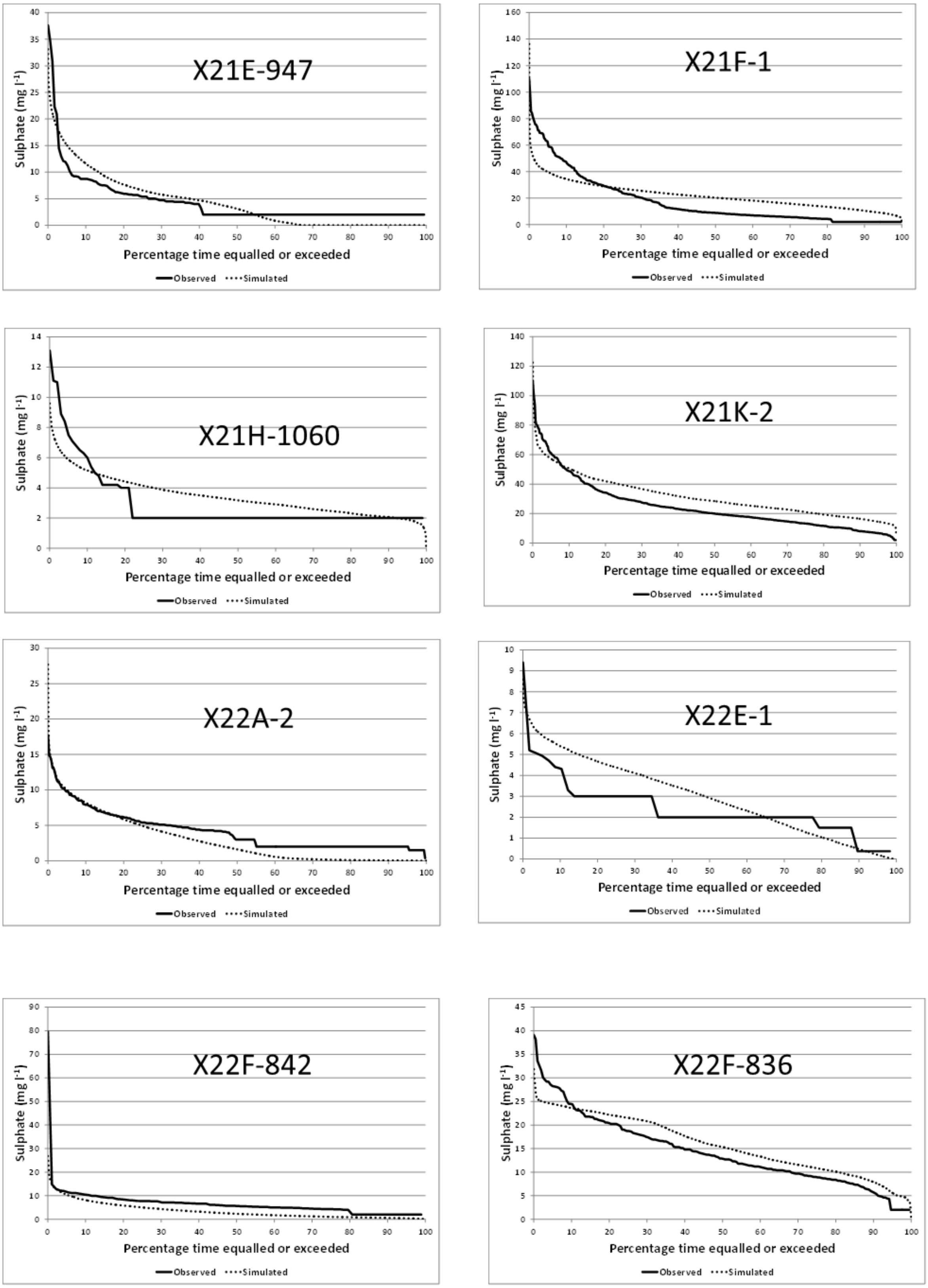

Figure 3.7 (continued) Results of sulphate simulations calibrated to observed data within the Crocodile River Catchment study sites, represented as frequency distributions.

In this case, the model simulation may be achieved by for example adjusting the incremental flow signatures for microbial water quality, and even though an adequate simulation may be obtained, the model may be achieving the simulation for the wrong reasons. In this case, it is suggested that the yield model nodal configuration be designed for optimal water quality simulation, so that nodes indicated as return flow nodes be in the correct spatial position. An additional strategy would be to link land cover/use with the incremental flow signatures using a formalised model. This would effectively eliminate an important source of uncertainty. For example, the hydro-ecological model SENEQUE/Riverstrahler assigns faecal coliform concentrations to runoff according to land use types of the catchments, with more natural areas assigned relatively low values, whereas grazed fields (1,000 cells/100 mℓ) and urban areas (5,000 cells/100 mℓ) are assigned relatively high concentrations (Servais *et al.*, 2007). While this particular example does not appear to be a rigorous formalised approach, for further implementation in WQSAM, an approach similar to that taken for nutrients (Slaughter and Mantel, 2015) could be implemented, where the relationship between model calibrated surface water flow microbial concentrations and land cover could be described within a formalised model.

The current study does indicate regions within the studied catchment where there are large inputs of faecal bacteria, and additionally provides some indication of the degradation/mortality of bacteria downstream. Therefore, while limitations and uncertainties remain, there are concrete possibilities of using WQSAM to investigate scenarios of microbial water quality management if the yield model nodal setup is designed with this objective in mind.

3.4.2 Modelling of sulphate as indicative of acid mine drainage

The use of sulphate as an indicator of AMD may be criticised as a rather simplistic representation of AMD. After all, there are many potentially toxic water quality variables associated with AMD besides sulphates such as low pH and a range of toxic metals. It is argued here however, that there are two good reasons to the approach of modelling sulphate. First of all, the broad aim of WQSAM is to represent water quality processes in as simplistic a method as possible, while still capturing the processes that explain the majority of water quality variation. The motivation behind this approach is that this strategy is reasonable given the lack of observed data available for South African catchments. In addition, complex models with many parameters are prone to problems of equifinality (Bevan, 2006), where the model may be providing an adequate simulation given observed data, but may be representing the incorrect water quality processes, which would ultimately lead to incorrect conclusions within scenario modelling. The second reason for the use of sulphate as an indication of AMD is that sulphate is generally a conservative variable, and as such is subject to a limited number of processes instream and maintains the same chemical form. As such, sulphate is much simpler to model than for example pH or the toxic metals. It is recognised that in South African catchments at least, that sulphate input generally occurs due to human activities with no significant natural input. These sources linked to human activities can either be mining or industrial effluent return flow. Sulphate as a water quality variable is additionally recognised to be serious toxicant, and contributes to the salinisation of rivers.

The modelling of sulphate within the current study provided various broad insights. First of all, the results show that it is possible to adequately represent the observed data using the WQSAM model. Secondly, it was shown that sulphate input is considerably higher in the Olifants River than in the Crocodile River.

The model showed that there is diffuse flow input of sulphates into the Crocodile River at X21F, which most probably relates to mining input. However, the model additionally shows that the Crocodile River receives some input of sulphate rich industrial effluent, such as at X21K.

The representation of sulphates within the Olifants River within the model provided various insights. First of all, the observed sulphate concentrations at most sites show a high degree of temporal variability. This could indicate that the inputs of sulphates within the Olifants River Catchment are related to catchment runoff and rainfall, as input from ground water would provide a steady and less variable signature. Generally this assumption finds support in the literature. Gray (1996) found that sources of AMD include springs and surface runoff. Oli'as (2004) found that sulphate concentrations showed an opposite pattern to flow-dilution with a high variability over the rainy season. INTER-MINISTERIAL COMMITTEE (2010) mentions sources of water to mines as including direct recharge from rainfall and surface water flow directly into mine openings, both of which would show high reactivity to rainfall. However, the modelling results within the Olifants did not obtain a very good fit to observed data in some cases, such as for B11A, B11C and Middelburg Dam, and possibly the dynamics involved within the generation of AMD cannot be completely captured by the processes represented within WQSAM currently. This possibility requires further thought and discussion with experts and those familiar with the situation within the Olifants River catchment.

Cobbing (2008) states that within the Western Mining Basin near Krugersdorp, while both surface water and groundwater can cause AMD problems, groundwater usually contributes the greater volume of AMD. Clearly, the modelling results for the Olifants appear to indicate a different situation within the Olifants River Catchment. It is generally known that coal mining proliferates within the upper Olifants River Catchment, with both open cast and underground mining, although none of the mines operate to deep levels. This is in contrast to the gold mines affecting the upper Crocodile River Catchment, which run deep underground. Within the Olifants River Catchment, surface storage of mining tailings occurs. In addition, due to the large amount of irrigated agriculture within the upper Olifants River Catchment, the groundwater levels remain fairly low, particularly at present due to the ongoing dry conditions. Within the Crocodile River Catchment, there is still active pumping of groundwater, thereby limiting the intrusion of AMD into the surface waters. Given this information, different strategies of controlling AMD within the two catchments can be recommended. Within the Crocodile River Catchment, continual pumping and treatment of the rising mine water is recommended. Within the Olifants River, the mine tailings stored at the surface need to be treated or stored in some way as to prevent contamination of surface waters, although clearly this presents a major challenge.

CHAPTER 4. VALIDATION OF ALGAL AND HYACINTH GROWTH PROCESSES WITHIN WQSAM

4.1 Introduction

Water quality of reservoirs is important to understand and model for management of South African water resources. Their water quality is linked to the landscape and morphological characteristics of the catchment and information on key variables (such as chlorophyll *a*) is essential for management agencies. The limited amount of *in-situ* data for reservoirs in addition to point location of samples makes the availability of satellite data critical for developing models for management of reservoir water quality.

Remote sensing data are being used to further our understanding of the natural variation in environmental variables, of drivers of change and as inputs to models (Politi *et al*., 2015). These data complement *in-situ* data because of the spatial and temporal (including historical data) scale of satellite data. Satellites also gather data for places that have not been sampled, and thus increase the area from which data can be gathered. However, they have the disadvantages of being at a coarser scale than *in-situ* measurements and suffer challenges such as cloud presence which might not allow evaluation during the rainy season. Once calibrated and validated, remote sensing data may be applied to similar lakes that have not been previously monitored (e.g. Hicks *et al*., 2013). This is particularly important for monitoring the resource and developing models and providing feedback for decision making and management. As an example, Servir (a collaborative project between NASA and USAID) is using remote sensing imagery to monitor development of algal blooms in lakes by relating remote sensing data (Landsat and ASTER data and hyperspectral imagery from EO-1) to chlorophyll measurements to follow development of algal blooms such as those in a Guatemalan lake (Servir Global, 2010; Servir Global, 2015).

Water quality of freshwater ecosystems (including lakes and reservoirs) are indicators of ecosystem integrity and ecosystem goods and services provided by the ecosystems (Gardiner, 2007). Satellite data are capable of detecting various water quality variables of large lakes and reservoirs (with a few recent exceptions looking at smaller lakes) in addition to catchment land use which affects the water quality. Remote sensing provides a large database of data that can supplement and complement *in-situ* data and provide useful global comparisons and trend analysis because of the periodic collection of data and comparative spatial analysis. This is particularly important for monitoring both land and water resources and developing models that provide feedback to managers for decision-making.

A deliverable on a completed WRC project (K5/2237) (see Slaughter *et al*., 2015) provided an overview of the various variables for modelling that can be extracted from remote sensing data. The present deliverable draws on that previous report to present some basic concepts.

4.1.1 Some considerations when using remote sensing data

Remote sensing data (energy wavelengths in the electromagnetic spectrum) are used for extracting information about resources (land, water, vegetation, coral reefs), people (urban), natural disasters (fire, floods) and for quantifying impacts and changes in these over space and time (e.g. ESRI, 2006; ESRI, 2008).

The spectral, spatial and temporal resolutions of the remote sensed data are important considerations in the selection of the data for use. The spectral resolution includes the number and bandwidth of the channels of spectral wavelengths generated by the sensor. A higher number of channels of finer scale (narrow bandwidth) is better for distinction between different elements on Earth.

The spatial resolution is the dimensions on Earth that each pixel in the data can be related to. A rule of thumb that the Biodiversity Informatics Facility website (http://biodiversityinformatics.amnh.org) suggests is to select data with a spatial resolution that is a factor of ten smaller than the feature to be identified. Although the spatial resolution of the sensor is important in what is visible in an image, there are other factors that can affect whether a feature is visible or not. These include the amount of contrast between features next to each other (the more the contrast, the better the visibility), the variation in the landscape (greater variation might inhibit distinguishing between a feature and this background signal as compared to if the background is homogeneous) (Horning and DuBroff, 2004).

The repeat interval or the temporal resolution defines how often the same area is imaged by the satellite. Depending on the project, there might be a need for a very frequent time series data (e.g. in the order of several days for flood mapping) or less frequent (as with land use change over a time period of years). It is not possible to implement high spectral, spatial and temporal resolution in one ideal sensor; thus, one needs to compromise based on the project requirements.

Radiometric resolution (related to the number of digital number resolution which relates to the sensitivity of the sensor to the incoming radiation, and which affects the sharpness of the image; see http://www.crisp.nus.edu.sg/~research/tutorial/image.htm) is another aspect of remote sensed imagery.

4.1.2 Satellites and sensors for water quality data

Various satellites are currently available for gathering water quality information. Water quality variables that change/modify the reflected electromagnetic signals are the ones that can be derived from satellite data such as suspended sediments, algae and plants. The spatial resolutions of satellites vary widely, and not all of them are useful for small water bodies or reservoirs.

By using satellite data, either a qualitative or quantitative estimation of water quality variables can be obtained. Qualitative estimations are relatively simple and involve visual assessment of images for presence and spatial extent of the variables of interest, e.g. hyacinth covering a lake. On the other hand, quantitative assessments are much more difficult to perform and require algorithms that draw on relationships between spectral signatures and actual on-the-ground measurements. Palmer *et al*. (2014) provide a summary of progress and challenges facing the scientific community interested in the use of remote sensing for monitoring and managing inland waters. Some of the challenges include the optical complexity of inland waters (because of independently varying water quality variables such as chlorophyll *a* and coloured dissolved organic matter), their small size, the large number of inland water bodies relative to the spatial and spectral resolution of the available data and limited coordinated research and funding for developing the science.

Table 4.1 provides a summary of some of the main satellites from which chlorophyll *a* estimations or temporal trends have been determined. Some of the satellites provide ready-to-use products which provide quantitative data on chlorophyll *a*, whereas others provide only spectral reflectance data which can be used for qualitative change / trend deriving and which can be further processed to calculate quantities using algorithms that are based on *in-situ* data.

The **Landsat** family of satellites have been around since the early 1970s and they provide data that are freely available from various platforms including Earth Explorer (http://earthexplorer.usgs.gov), GloVis (http:// http://glovis.usgs.gov) and Landsat Look Viewer (http:// landsatlook.usgs.gov). Landsat data have a high spatial resolution (30 m for many bands) making them useful for small water bodies, but their low spectral resolution (wide bands) limits their use in assessing chlorophyll *a* content. In addition, the long dataset for Landsat makes it useful for determining long-term historical trends.

MODIS (MODerate-resolution Imaging Spectroradiometer) is another sensor which is widely used because of its large number of high resolution spectral bands. But its low spatial resolution makes it primarily useful for larger water bodies.

Two satellites that are no longer operating – **SeaWiFS** and **MERIS** – have been found to be useful for looking at past data trends, understanding the extremes and changes in values and their timing and developing algorithms to relate spectral signatures to regional measurements.

Note that the data from different sensors can be available at different levels (NASA ARSET, 2015; NASA, 2011):

- Level 0 – raw data
- Level 1 – geolocated and calibrated
- Level 2 – geophysical data derived from level 1, e.g. surface reflectances
- Level 3 – composite level 2 data
- Level 4 – model-derived data product

With increasing level, the ease of use of data and comparison across time/space is simpler; however, products at higher levels are generally at a much coarser resolution than lower level data. For example, MODIS water quality products (level 3 data) are available at low spatial (4 km and 9 km) and temporal (8 day or monthly) resolution from Giovanni, while the original spectral data are at 250-1,000 m spatial resolution and are available every 1-2 days.

4.1.3 Use of satellite imagery for phytoplankton and water hyacinth

Water absorbs a significant portion of electromagnetic radiation in the ultraviolet and infrared range; thus, the optical range of the spectrum has been used to detect various water quality variables of large lakes and reservoirs (e.g. Olmanson *et al*. (2011) estimated Secchi disk transparency and chlorophyll *a* from MERIS, MODIS and Landsat ETM+ data). Researchers have used satellite data for measuring and modelling water quality for more than 30 years (e.g. Ritchie *et al*., 1976; Carpenter and Carpenter, 1983; Harrington *et al*., 1992) not just for understanding the trends, but for meeting requirements for legislation such as the Water Framework Directive of the European Commission (e.g. Bresciani *et al*., 2011). A comprehensive WRC report reviewing the use of remote sensing data for water resource management is expected to be released soon (Gibson *et al*., 2015).

For the water quality of inland and near-coastal waters, Matthews (2011) provides an extremely useful and comprehensive review of research using remote sensing for estimating water quality variables including chlorophyll *a*, total suspended solids (TSS), turbidity, carbonaceous dissolved organic matter (CDOM) and phycocyanin. A more recent review on the use of remote sensing for lake research and monitoring is provided by Dörnhöfer and Oppelt (2016). Past work assessing phytoplankton biomass and eutrophication within reservoirs using remote sensing data has used chlorophyll *a* as an indicator. There have been some studies in this regard in southern Africa, e.g. Matthews *et al*. (2010), Chawira *et al*. (2013) and Matthews and Bernard (2013). These studies used MEdium Resolution Imaging Spectrometer (MERIS), GlobColour and MODerate resolution Imaging Spectrometer (MODIS) satellite products. While Chawira *et al*. (2013) found a strong correlation between measured chlorophyll *a* and satellite predicted results, the work done by Mathews *et al*. (2010) and Matthews and Bernard (2013) struggled to separate the effects of covariant water constituents from satellite readings. Matthews *et al*. (2012) developed an algorithm to separate the effects of cyanobacterial blooms, surface scum, floating vegetation and chlorophyll *a* from within MERIS data while Gitelson *et al*. (2008) developed algorithms to separate the effects of suspended sediment from MERIS and MODIS satellite data. Hyacinth growth has been estimated using Landsat and SPOT imagery for a lake in Kenya (Onywere *et al*., 2012) and Lake Victoria (Albright *et al*., 2004).

There are trade-offs to be made when selecting imagery for use. In general, finding imagery that has high spectral, high spatial and high temporal resolution is very difficult and thus, a compromise on which criteria are more essential for a specific project are necessary. For example, high spatial resolution satellites like Landsat provide data for the same location every 8-16 days, whereas MODIS data are available almost every 1-2 days, but these data have a much lower spatial resolution. Specific to water bodies, the effect of near shore areas on the water signal needs to be considered and thus, pixels with both land and water contribution are generally ignored in analyses.

Phytoplankton

Chlorophyll *a* is an indicator of phytoplankton biomass and can be detected because of the absorption of wavelengths between 0.44-0.56 µm and near 0.67 µm (Matthews, 2011; Dörnhöfer and Oppelt, 2016). Remote sensing has been used to determine chlorophyll *a* concentrations using algorithms for the upper waters in the oceans (e.g. those shown on http://oceancolor.gsfc.nasa.gov/REPROCESSING/R2009/ocv6/, accessed on 17 November 2015). However, the use of remote sensing in shallower coastal waters is limited by interference by bottom reflection and/or turbidity (Carstensen *et al*., 2011). To estimate chlorophyll *a* in turbid waters, researchers have attempted to develop models to estimate the interactions (e.g. Gitelson *et al*., 2008). Chawira *et al*. (2013) used MERIS data for modelling chlorophyll *a* and phycocyanin (blue-green algae) concentrations of two eutrophic lakes in Zimbabwe. Their results indicated a strong correlation between measured and satellite predicted results, although a limited number of samples were used.

Matthews *et al*. (2010) studied the use of MERIS for assessing cyanobacterial-dominated algal blooms for a small hypertrophic lake in South Africa, and found that separating the signals of the covariant water constituents (including TSS and CDOM) was problematic. A novel algorithm, called the maximum peak-height algorithm (MPH), has since been developed by Matthews *et al*. (2012) for detecting cyanobacterial blooms, surface scum, floating vegetation and chlorophyll *a* by detection of the dominant peak across the red and near-infrared MERIS bands. The algorithms are applicable over a range of trophic states from oligotrophic/mesotrophic to eutrophic/hypertrophic waters. The development of these algorithms requires information on inherent optical properties of water constituents, which is what Matthews and Bernard (2013) derived for phytoplankton, gelbstoff and tripton (i.e. non-living minerals and detritus) in three South African reservoirs with different phytoplankton assemblages and concentrations. This was an important first step for calibrating remote sensing data to ground measurements. The MPH algorithm has since been improved and published by Matthews and Odermatt (2015).

Matthews assessed chlorophyll *a* values, cyanobacteria and surface scum area coverage for 50 large South African dams utilising MERIS data from 2002 to 2012 for his PhD thesis (2014) (Matthews and Bernard, 2015: Table 1). The values obtained from MERIS were compared with time series *in situ* measurements for six dams and were found to be correlated. The analysis of the 50 dams indicated that 62% are hypertrophic and 54% have presence of cyanobacterial scum. Matthews (2014), however, notes that high turbidity is an issue that complicates the evaluation conducted, particularly for dams with the highest chlorophyll *a* estimates.

Water hyacinth

Everitt *et al*. (1999) measured spectral signals from water hyacinth and hydrilla plants in the green (0.52-0.60 µm), red (0.63-0.69 µm) and near-infrared (0.76-0.90 µm) wavelengths and found that water hyacinth had higher near-infrared reflectance than water and hydrilla plants. Previous research by Everitt *et al*. (1986) noted that near infrared reflectance was strongly correlated with plant density.

Table 4.1 Summary information for some of the primary remote sensing data sources that are freely available for chlorophyll estimation (some only for research purposes). The last column indicates if a chlorophyll *a* concentration product is available (quantitative data) besides the spectral reflectances (qualitative data that require processing to extract quantitative information).

Satellite	Sensor	Dates	Spatial and temporal resolution	Chlorophyll *a* concentration product and/or spectral reflectances
Landsat	TM (Thematic Mapper), ETM+ (Enhanced Thematic Mapper), OLI (Operational Land Imaging)	1982-present	30-80 m, Pan 15 m, TIR 60-120 m; 16-17 days	Spectral reflectance
Terra	ASTER (Advanced Spaceborne Thermal Emission and Reflection Radiometer)	2000-present	15-90 m; Daily	Spectral reflectance
Terra and Aqua	MODIS (Moderate Resolution Imagine Spectroradiometer)	2000-present	250-1000 m; 1-2 days	Spectral reflectance; Chlorophyll concentration product (available through Giovanni, Ocean Color Web)
NPP (Nation Polar Orbiting Partnership)	VIIRS (Visible Infrared Imaging Radiometer Suite)	2011-present	375-750 m; 1-2 observations a day	Spectral reflectance; Chlorophyll concentration (available through Ocean Color Web)
Envisat (ESA)	MERIS (Medium-spectral Resolution Imaging Spectrometer)	2002-2012	300-100 0 m; 35 days	Spectral reflectance (available through Ocean Color Web)
SeaStar	SeaWiFS (Sea-viewing Wide Field-of-view Sensor)	1997-2010	1.1 km; 1 day	Spectral reflectance, Chlorophyll concentration (available through Giovanni, Ocean Color Web)

Onywere *et al*. (2012) used the differences in spectral signals and spectral image analysis of remote sensed data to evaluate the extent of water hyacinth in Lake Naivasha, Kenya and the landuse activities in the catchment. The authors conducted a time series analysis using Landsat (TM, ETM for 1986 and 2000) and SPOT imagery (for 2007) to link the change in water quality to catchment activities. Using similar remote sensing data providers, Albright *et al*. (2004) used unsupervised image classification to assess the time series trend for water hyacinth in Lake Victoria. These authors also used radar sensor data and identified thresholds for water hyacinth detection in these images. More recent research has used supervised classification for delineating macrophyte growth (e.g. Hunter *et al*., 2010).

4.1.4 Visualising data

There are a number of data visualisation platforms where data can be viewed without downloading. One such example is Ocean Color Web (e.g. http://oceancolor.gsfc.nasa.gov/cgi/l3) for viewing Level 3 products such as chlorophyll *a* derived from a number of sensors, although the primary focus is on providing data for oceans. An example of chlorophyll *a* concentration data from Ocean Color Web is shown in Figure 4.1 below. Since the resolution of Level 3 data is generally coarse (e.g. 4 km and 9 km resolution for MODIS), these products have limited use for the majority of reservoirs and lakes which are small.

Other visualisation platforms where data can be viewed and screened before downloading are LandsatLook Viewer (http:// landsatlook.usgs.gov) and Giovanni (http://giovanni.gsfc.nasa.gov/giovanni/). Visualising data for screening helps with assessing if there are issues such as cloud cover in the imagery from a specific date which would make the data unusable. An overview of various data products and access tools generated by NASA can be found through webinars at the following link (http://arset.gsfc.nasa.gov/airquality-disasters-ecoforecasting-water-resources/webinars/introduction-nasa-earth-science-data; accessed 13 November 2015).

Some imagery of dams is also available through Google Earth. This imagery can be useful for verifying the presence/absence of blooms, but there are disadvantages of this data. For example, Figure 4.2 shows the screen capture of Bridle Drift Dam on Buffalo River. The image shows overlap of different scenes collected by the satellite, which makes it harder to interpret the image. Also for this specific case, only one historical image is available for the dam for the year 2013 through Google Earth.

4.1.5 Band combinations for multispectral analysis

Visualising images using certain spectral band combinations can be helpful in highlighting and detecting particular objects. Specifically for water, the red, green, blue and near infrared range combinations are useful. Some algorithms have used the differential absorption of blue and green spectral wavelengths to identify low concentrations of chlorophyll *a* since blue wavelengths are absorbed more than green wavelengths which are reflected by algae (e.g. O'Reilly *et al*., 1998; http://oceancolor.gsfc.nasa.gov/REPROCESSING/R2009/ocv6/, accessed on 17 November 2015; Werdell and Bailey, 2005). On the other hand, high concentrations of chlorophyll *a* can be better estimated using the ratio of NIR and red bands (e.g. Gitelson *et al*., 2008). Table 4.2 provides the wavelengths for the relevant bands for Landsat; these will be referred to under the qualitative analysis of reservoir chlorophyll *a* later in this chapter.

4.1.6 Quantitative analysis of reservoir chlorophyll a using remote sensed imagery from MERIS data

Quantitative assessment of chlorophyll *a* was conducted using the MERIS Lakes processor for eutrophic waters (Doerffer and Schiller, 2008) in BEAM version 5.0, which is an open-source visualising and processing package designed by Brockman Consult (available through http://www.brockmann-consult.de/cms/web/beam, accessed 4 October 2015). Note that MERIS data are available from mid-2002 to 2012. The data used in this chapter are for 2002-2003, since the water quality model (presented in Chapter 2) runs until 2003, and this overlaps with Landsat 7 ETM+ data.

The Lakes processor uses MERIS radiance data provided by the European Space Agency, which is atmospherically corrected followed by calculation of water leaving reflectances in addition to chlorophyll concentration. The processor results have been validated for lakes in Finland, Spain, Germany and Africa with a training range for chlorophyll *a* of eutrophic lakes between 1 and 120 µg ℓ$^{-1}$ (Koponen *et al*., 2008).

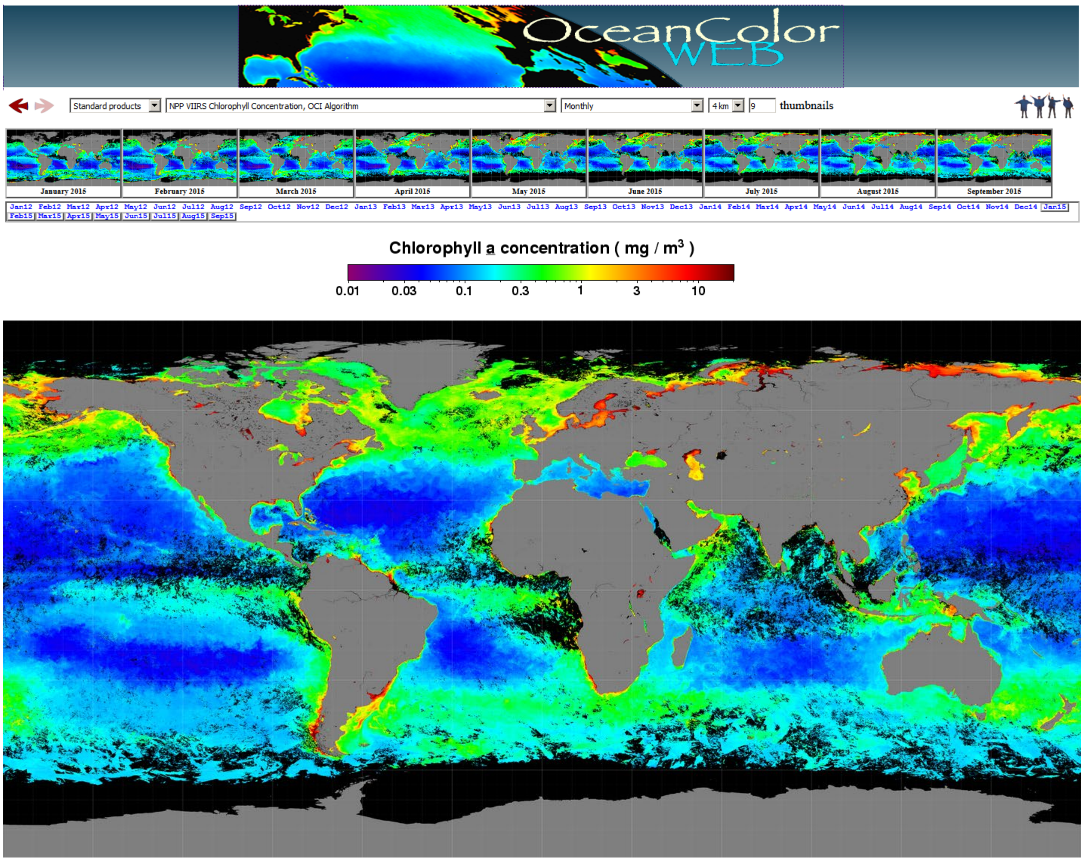

Figure 4.1 Screencapture of chlorophyll *a* concentrations using data collected by the NPP VIIRS sensor from Ocean Color Web. The top panel shows thumbnails for different dates and the lower area shows the result for September 2015.

Figure 4.2 Google Earth image of Bridle Drift Dam on 26 January 2015.

Table 4.2 Spectral bands for Landsat 7 and 8 sensors that are useful for water quality assessments (Source: USGS website http://landsat.usgs.gov/best_spectral_bands_to_use.php).

	Landsat 7 ETM+		Landsat 8 OLI		
	Band	**Wavelength (µm)**	**Band**	**Wavelength (µm)**	**Resolution (m)**
Blue	1	0.45-0.52	2	0.45-0.51	30
Green	2	0.52-0.60	3	0.53-0.59	30
Red	3	0.63-0.69	4	0.64-0.67	30
Near Infrared (NIR)	4	0.77-0.90	5	0.85-0.88	30

There were however issues with validating data for the two African lakes (Lake Victoria and Lake Manzalah) including limited validation data and overestimation for values > 10 µg ℓ^{-1}. The results of the Lakes processor for the total reservoir surface (i.e. median of all the relevant pixel values) are compared with the water quality monitoring data provided by the Department of Water and Sanitation (previously known as the Department of Water Affairs), which are available through the National Eutrophication Monitoring Programme (NEMP) website (https://www.dwaf.gov.za/iwqs/eutrophication/NEMP/). The NEMP system defines four categories of water eutrophication based on chlorophyll *a* concentration ranges:

- Oligotrophic: 0-10 µg ℓ^{-1}
- Mesotrophic: 10-20 µg ℓ^{-1}
- Eutrophic: 20-30 µg ℓ^{-1}
- Hypertrophic: >30 µg ℓ^{-1}

It must be noted that the NEMP database provides chlorophyll *a* data measured at a water quality gauge and it is not representative of the total reservoir surface; thus, this comparison has its limitations.

Loskop Dam, Olifants River

Loskop Dam is located in the upper catchment of the Olifants River (Figure 4.3). The Loskop Dam is generally regarded as the lower boundary of the upper Olifants catchment which originates from the east of Johannesburg (Heath *et al.*, 2010). The Olifants River is generally regarded as being one of the most modified rivers in South Africa, as the river is extensively dammed and is additionally highly polluted (Balance *et al.*, 2001; de Villiers and Mkwelo, 2009, Van Vuuren, 2009). Large quantities of water are extracted from the river for coal mining, petrochemical industries and diverse agriculture (Heath *et al.*, 2010), and these activities additionally affect water quality, along with the various large urban centres such as Witbank and Middleburg, as well as smaller settlements which occur in the catchment (Heath *et al.*, 2010). These impacts have resulted in various problematic water quality variables including acid mine drainage (AMD) and the associated high sulphate and metal concentrations, high nutrient concentrations from waste water treatment works (WWTWs) and agriculture and microbial contamination from incompletely-treated sewage and runoff from urban areas (van Vuuren, 2013). It is known that the water quality of Loskop Dam is problematic, as the Department of Water and Sanitation (DWS) historical monitoring data indicate that there is a clear increase in salt concentration in the dam, more specifically, sulphate concentrations. There have additionally been frequent reports of crocodile and fish kills in the dam (van Vuuren, 2009). The DWS historical monitoring data indicate that there are spikes of total dissolved solids (TDS) as high as 350 mg ℓ^{-1}, with concentrations > 250 mg ℓ^{-1} approximately 50% of the time. There are additionally high spikes in nutrients, with nitrates + nitrites as high as 3 mg ℓ$^{-1}$, with concentrations > 0.5 mg ℓ$^{-1}$ approximately 5% of the time, spikes in ammonium of up to 5.5 mg ℓ$^{-1}$, and spikes in phosphate of up to 0.6 mg ℓ$^{-1}$ (Slaughter *et al*., 2015).

The 10 year average of chlorophyll *a* values for Loskop Dam was 58.1 µg ℓ$^{-1}$ (hypertrophic status) for 2002 to 2012 as estimated by Matthews and Bernard (2015). The authors also estimated the cyanobacterial area coverage to be 0.4% and the surface scum area coverage to be 0%. Overall, this dam scored 3 on the authors' impact scale of 0 to 9 which incorporated these three measures of reservoir health. Looking at the calculations by the authors for the 2003 period, as shown in Figure 4.4, the chlorophyll a values estimated range between 5 and 30 µg ℓ$^{-1}$.

The NEMP website provides mean annual chlorophyll *a* for Loskop Dam for the year 2003 to be 2.4 µg ℓ$^{-1}$ and classifies it as an oligotrophic reservoir (https://www.dwaf.gov.za/iwqs/eutrophication/NEMP/nempdams.htm; accessed 11 November 2015). The median chlorophyll *a* concentration at the Loskop Dam wall (gauge B3R002Q01) for the winter period (April 2002 to September 2002; value for April 2003 to September 2003 is not available) was higher than during the summer period (October 2002 to March 2003) (3.5 µg ℓ$^{-1}$ versus 1.7 µg ℓ$^{-1}$; also see Figure 4.4; https://www.dwaf.gov.za/iwqs/eutrophication/NEMP/report/NEMPyears.aspx).

A time series of chlorophyll a variation in Loskop Dam was generated for November 2002 (which is the earliest date for which MERIS data are available for this area) to November 2004 using MERIS full resolution Level 1 data products downloaded from the European Space Agency website (http://merisfrs-merci-ds.eo.esa.int/merci) (see Table 4.3). The MERIS data were processed using the Lakes processor (some of the results are shown in Figure 4.5). The average chlorophyll a concentration for the surface of Loskop Dam increases in summer (Figure 4.6a), although the difference between summer and winter is not as distinct for 2003, similar to the pattern shown in Figure 4.4. Note that the standard deviation (from the pixel covering the reservoir) is extremely large (Figure 4.6b), i.e. chlorophyll *a* concentration varies hugely across the dam throughout the year. This temporal change in Loskop Dam chlorophyll *a* is similar to (although values are slightly lower) that calculated by Matthews and Bernard (2015) which is shown in Figure 4.4.

Kwena Dam, Crocodile River

Kwena Dam is located on the Crocodile River (Figure 4.7)

The Crocodile River Catchment is an economically important catchment occurring in the province of Mpumalanga, and contributes to industry, agriculture and tourism (Deksissa *et al*., 2004). Kwena Dam occurs within the upper catchment, which is within the dryer part of the catchment, with an annual rainfall of approximately 600 mm, and a predominately summer rainfall through convection thunderstorms (Deksissa *et al*., 2004). Generally, the upper catchment is dominated by Cambrian geology with an associated low salinity (< 65 mg ℓ$^{-1}$). Agriculture in the upper region includes wheat and maize farming (Roux *et al*., 1994; Deksissa *et al*., 2004). The catchment as a whole is impacted by various pollution sources, including industrial and domestic sources of pollutants and runoff and return flow from irrigated agriculture and mining sites (DWAF, 1995). As can be observed from the DWS historical monitoring data, the salinity of Kwena Dam is relatively low, with total dissolved solids (TDS) generally below 120 mg ℓ$^{-1}$. However, there are moderate spikes in nutrient concentrations, with nitrates + nitrites as high as 1 mg ℓ$^{-1}$ and > 0.2 mg ℓ$^{-1}$ approximately 40% of the time, ammonium spikes as high as 0.3 mg ℓ$^{-1}$, and > 0.1 mg ℓ$^{-1}$ approximately 5% of the time, and spikes of phosphate as high as 0.45 mg ℓ$^{-1}$, and > 0.1 mg ℓ$^{-1}$ approximately 2% of the time (see Slaughter *et al*., 2015). Therefore, there may be some potential for eutrophication in the dam.

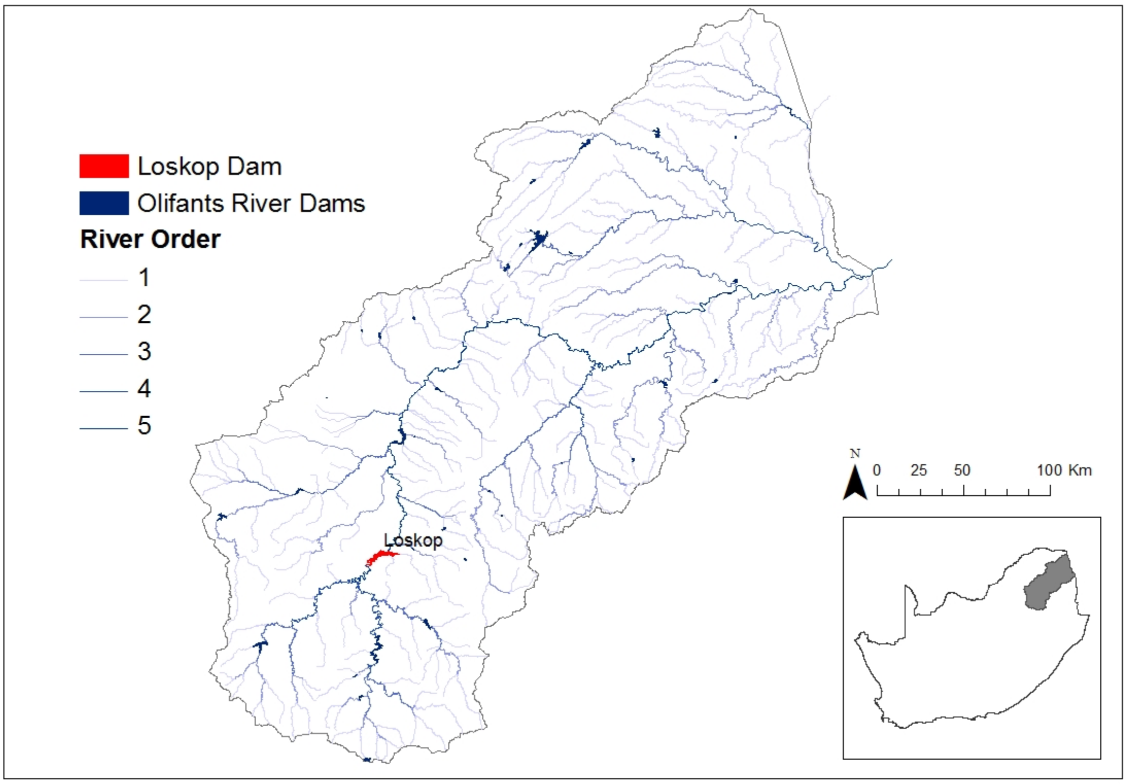

Figure 4.3 Location of Loskop Dam on the Olifants River.

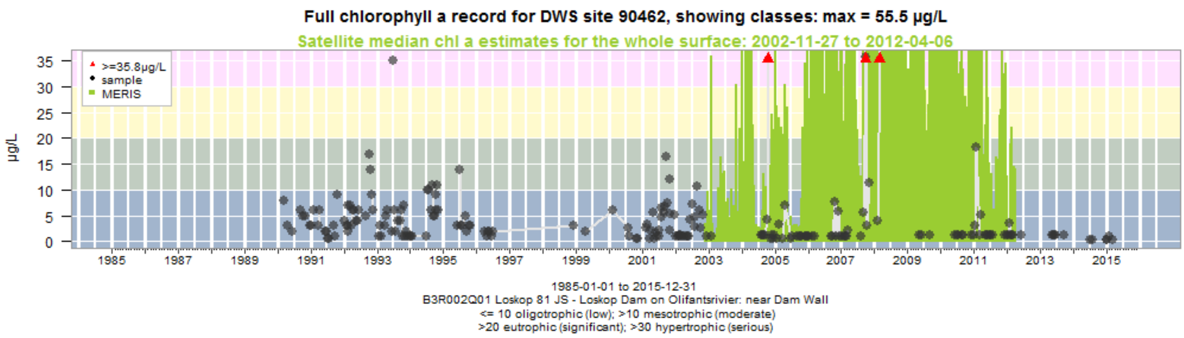

Figure 4.4 Data for Loskop Dam (gauge B3R002Q01) extracted from the Department of Water Affairs' National Eutrophication Monitoring Programme (NEMP) website: https://www.dwaf.gov.za/iwqs/eutrophication/NEMP/report/Chart_nemp_90462.png; accessed on 22 October 2015.

Table 4.3 MERIS level 1 data for 2002-2004 downloaded for the area near Loskop and Kwena Dams. Dates for data download were selected due to the requirement of the imagery being primarily cloud free particularly above the dam.

Date	Scene ID
27 Nov 2002	MER_FRS_1PPBCM20021127_072829_000000232011_00321_03882_0001
03 Dec 2002	MER_FRS_1PPBCM20021203_073948_000000232011_00407_03968_0006
22 Dec 2002	MER_FRS_1PPBCM20021222_074236_000000232012_00178_04240_0004
25 Dec 2002	MER_FRS_1PPBCM20021225_074817_000000232012_00221_04283_0002
01 Jan 2003	MER_FRS_1PPBCM20030101_072839_000000172012_00321_04383_0005
04 Jan 2003	MER_FRS_1PPBCM20030104_073419_000000172012_00364_04426_0011
07 Jan 2003	MER_FRS_1PPBCM20030107_073919_000000872012_00407_04469_0003
20 Jan 2003	MER_FRS_1PPBCM20030120_073131_000000142013_00092_04655_0001
26 Jan 2003	MER_FRS_1PPBCM20030126_074249_000000172013_00178_04741_0003
05 Feb 2003	MER_FRS_1PPBCM20030205_072839_000000172013_00321_04884_0004
02 Mar 2003	MER_FRS_1PPBCM20030302_074206_000001242014_00178_05242_0007
31 Mar 2003	MER_FRS_1PPBCM20030331_073050_000001242015_00092_05657_0001
25 Apr 2003	MER_FRS_1PPBCM20030425_074504_000001242015_00450_06015_0002
12 Jun 2003	MER_FRS_1PPBCM20030612_073655_000001012017_00135_06702_0004
14 Jul 2003	MER_FRS_1PPBCM20030714_073055_000001242018_00092_07160_0009
02 Aug 2003	MER_FRS_1PPBCM20030802_073426_000000172018_00364_07432_0001
21 Aug 2003	MER_FRS_1PPBCM20030821_073722_000000822019_00135_07704_0008
24 Aug 2003	MER_FRS_1PPBCM20030824_074221_000001242019_00178_07747_0006
03 Sep 2003	MER_FRS_1PPBCM20030903_072850_000000172019_00321_07890_0004
12 Sep 2003	MER_FRS_1PPBCM20030912_074513_000001212019_00450_08019_0010
25 Sep 2003	MER_FRS_1PPBCM20030925_073640_000001242020_00135_08205_0001

Table 4.3 (cont.)

Date	Scene ID
01 Oct 2003	MER_FRS_1PPBCM20031001_074759_000001212020_00221_08291_0004
10 Oct 2003	MER_FRS_1PPBCM20031024_072554_000000172021_00049_08620_0008
08 Nov 2003	MER_FRS_1PPBCM20031108_075335_000001242021_00264_08835_0008
21 Nov 2003	MER_FRS_1PPBCM20031121_074506_000000872021_00450_09021_0007
13 Dec 2003	MER_FRS_1PPBCM20031213_075351_000001072022_00264_09336_0005
30 Dec 2003	MER_FRS_1PPBCM20031230_072017_000000172023_00006_09579_0009
02 Jan 2004	MER_FRS_1PPBCM20040102_072558_000000172023_00049_09622_0014
08 Jan 2004	MER_FRS_1PPBCM20040108_073717_000000142023_00135_09708_0016
14 Jan 2004	MER_FRS_1PPBCM20040114_074834_000000172023_00221_09794_0013
27 Jan 2004	MER_FRS_1PPBCM20040127_074005_000000142023_00407_09980_0012
03 Feb 2004	MER_FRS_1PPBCM20040203_072014_000000172024_00006_10080_0011
18 Feb 2004	MER_FRS_1PPBCM20040218_074835_000000142024_00221_10295_0007
22 Feb 2004	MER_FRS_1PPBCM20040222_072304_000000172024_00278_10352_0002
02 Mar 2004	MER_FRS_1PPBCM20040302_074004_000000172024_00407_10481_0006
09 Apr 2004	MER_FRS_1PPBCM20040409_074544_000000172025_00450_11025_0005
19 Apr 2004	MER_FRS_1PPBCM20040419_073134_000000172026_00092_11168_0015
25 Apr 2004	MER_FRS_1PPBCM20040425_074254_000000172026_00178_11254_0003
05 May 2004	MER_FRS_1PPBCM20040505_072844_000000172026_00321_11397_0002
24 May 2004	MER_FRS_1PPBCM20040524_073140_000000142027_00092_11669_0004
02 Jun 2004	MER_FRS_1PPBCM20040602_074839_000000172027_00221_11798_0010
12 Jun 2004	MER_FRS_1PPBCM20040612_073429_000000172027_00364_11941_0011

Table 4.3 (cont.)

Date	Scene ID
01 Jul 2004	MER_FRS_1PPBCM20040701_073718_000000142028_00135_12213_0009
23 Jul 2004	MER_FRS_1PPBCM20040723_074551_000000172028_00450_12528_0008
08 Aug 2004	MER_FRS_1PPBCM20040808_074259_000000172029_00178_12757_0005
15 Sep 2004	MER_FRS_1PPBCM20040915_074837_000000172030_00221_13301_0010
17 Oct 2004	MER_FRS_1PPBCM20041017_074300_000000172031_00178_13759_0009
18 Nov 2004	MER_FRS_1PPBCM20041118_073718_000000172032_00135_14217_0013

The 10 year average of chlorophyll *a* values for Kwena Dam was lower than that of Loskop Dam at 30.2 µg ℓ^{-1} (just above the hypertrophic lower limit) for 2002 to 2012 (Matthews and Bernard, 2015). The cyanobacterial area coverage was estimated to be 1.1% and the surface scum area coverage as 0%. Overall, this dam scored 4 on the authors' reservoir health impact scale of 0 to 9, which is higher than the score for Loskop Dam because of the higher cyanobacterial area coverage.

Chlorophyll values for Kwena Dam are not listed on the NEMP website (https://www.dwaf.gov.za/iwqs/eutrophication/NEMP/nempdams.htm; accessed 11 November 2015); thus, the MERIS results presented below cannot be compared with those values.

A time series of chlorophyll *a* variation in Kwena Dam was generated for 2002-2004 using MERIS full resolution Level 1 data products downloaded from the European Space Agency website (http://merisfrs-merci-ds.eo.esa.int/merci). MERIS data for Kwena Dam were available in the same scenes from which Loskop Dam data were extracted (see Table 4.3). These data were processed using the Lakes processor (some of the resulting images are shown in Figure 4.8). The summarised average chlorophyll *a* concentration is high during summer 2004 for Kwena Dam, similar to Loskop Dam, and there is an unexpected peak in winter 2003 (Figure 4.9a). Note the relatively smaller standard deviation error bars compared to Loskop Dam, with a couple of exceptions in June and December (Figure 4.9b versus 4.6b).

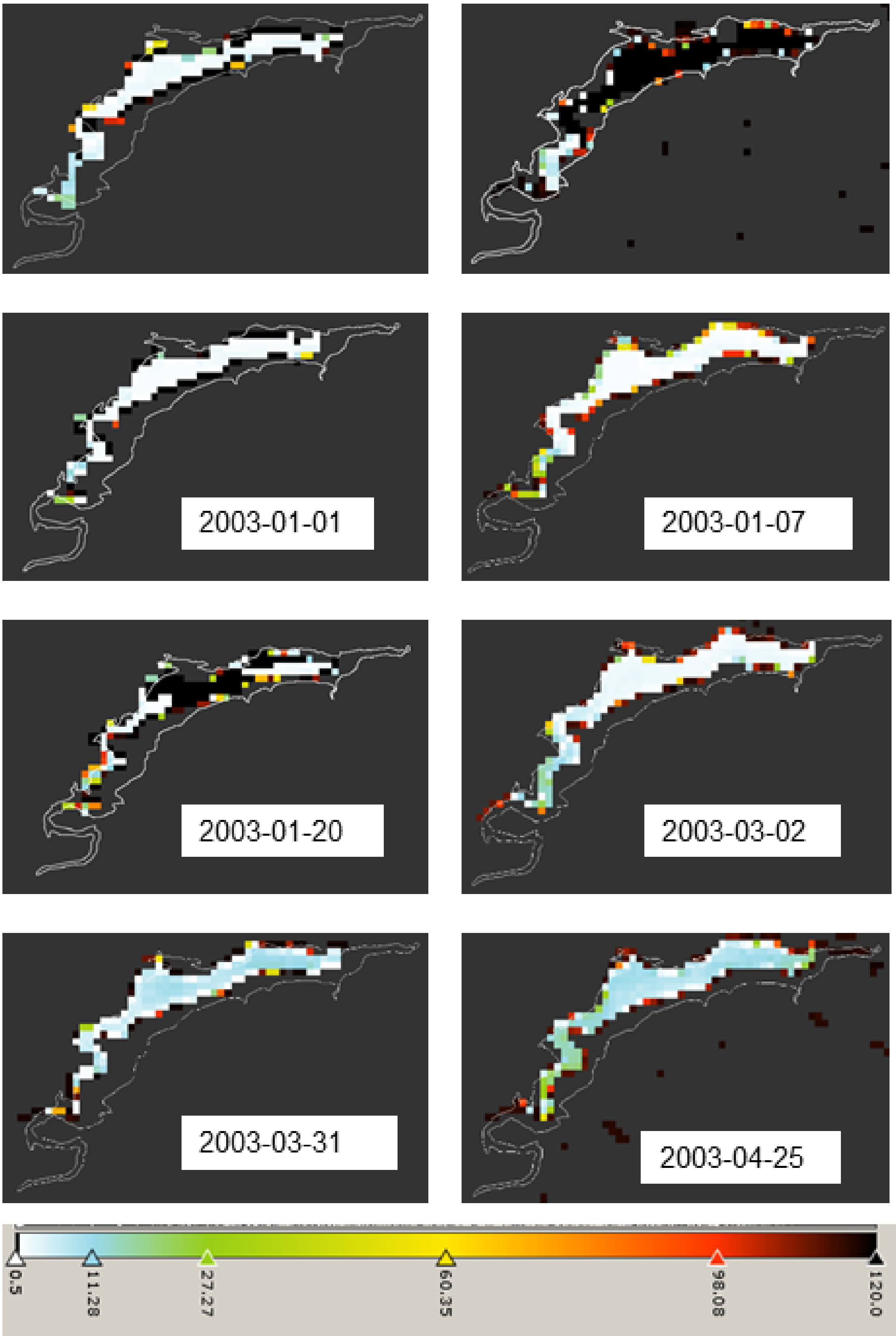

Figure 4.5 Chlorophyll a concentration (µg ℓ^{-1}) for Loskop Dam derived from MERIS data for using the MERIS Lakes processor in BEAM.

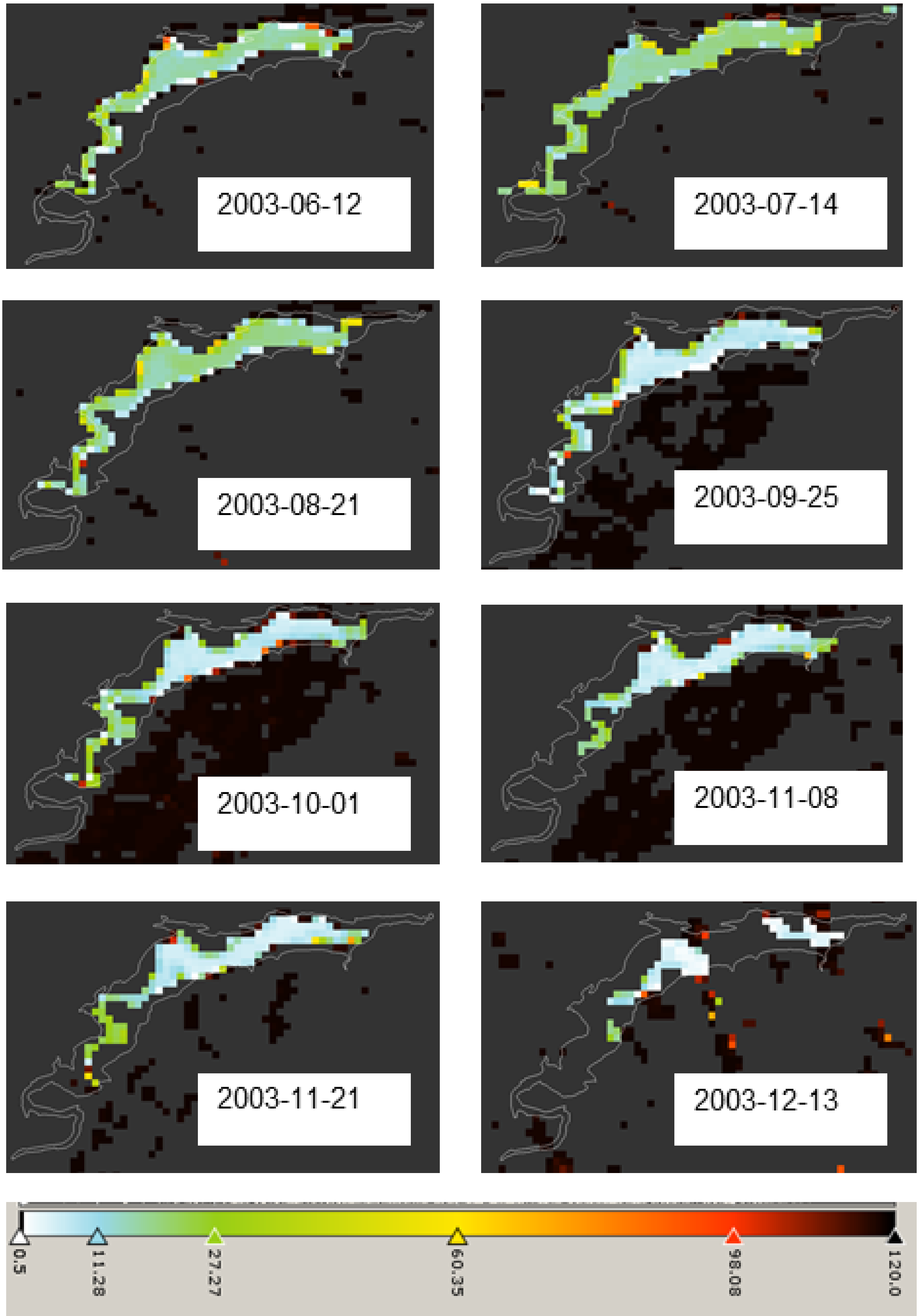

Figure 4.5 continued

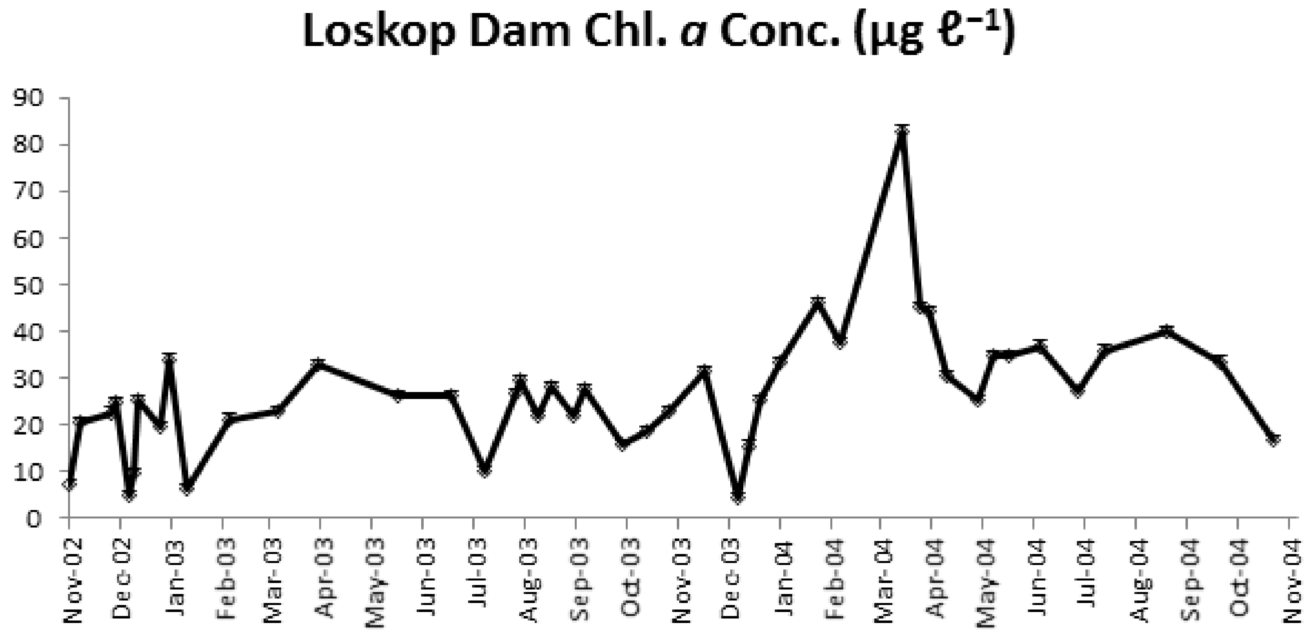

Figure 4.6a Temporal variation in average chlorophyll *a* concentration of Loskop Dam derived from MERIS data using the Lakes processor in BEAM.

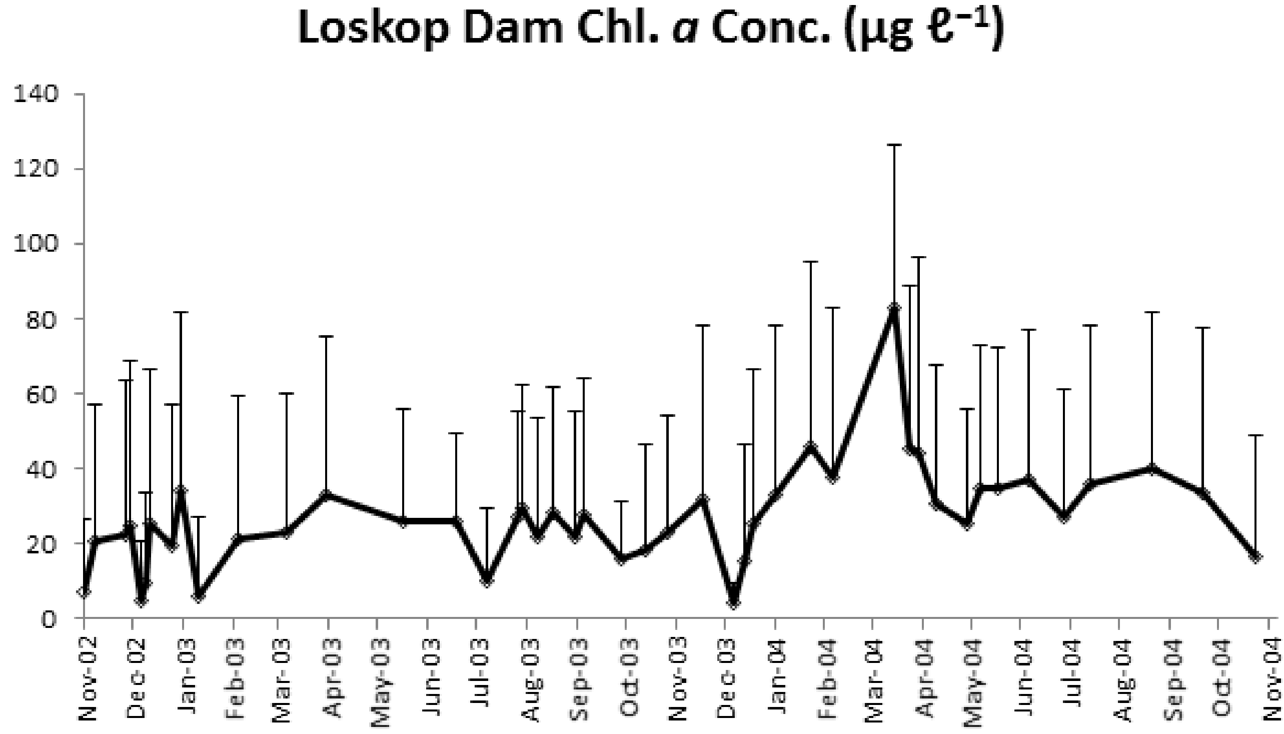

Figure 4.6b Temporal variation in average chlorophyll *a* concentration of Loskop Dam shown with standard deviation error bars.

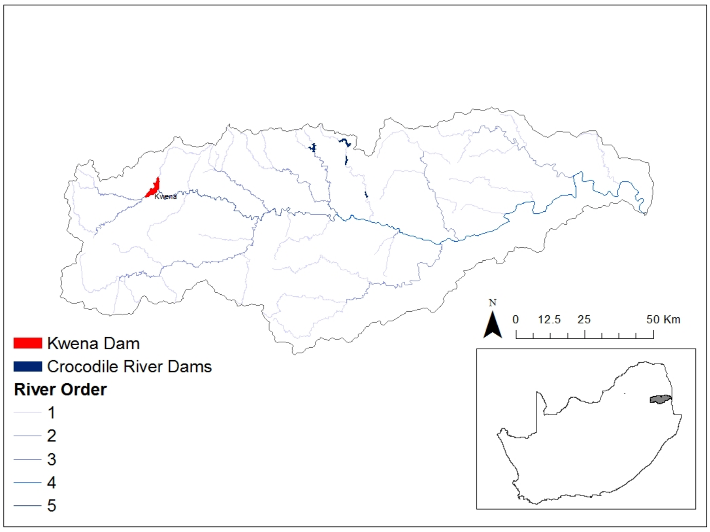

Figure 4.7 Location of Kwena Dam on the Crocodile River.

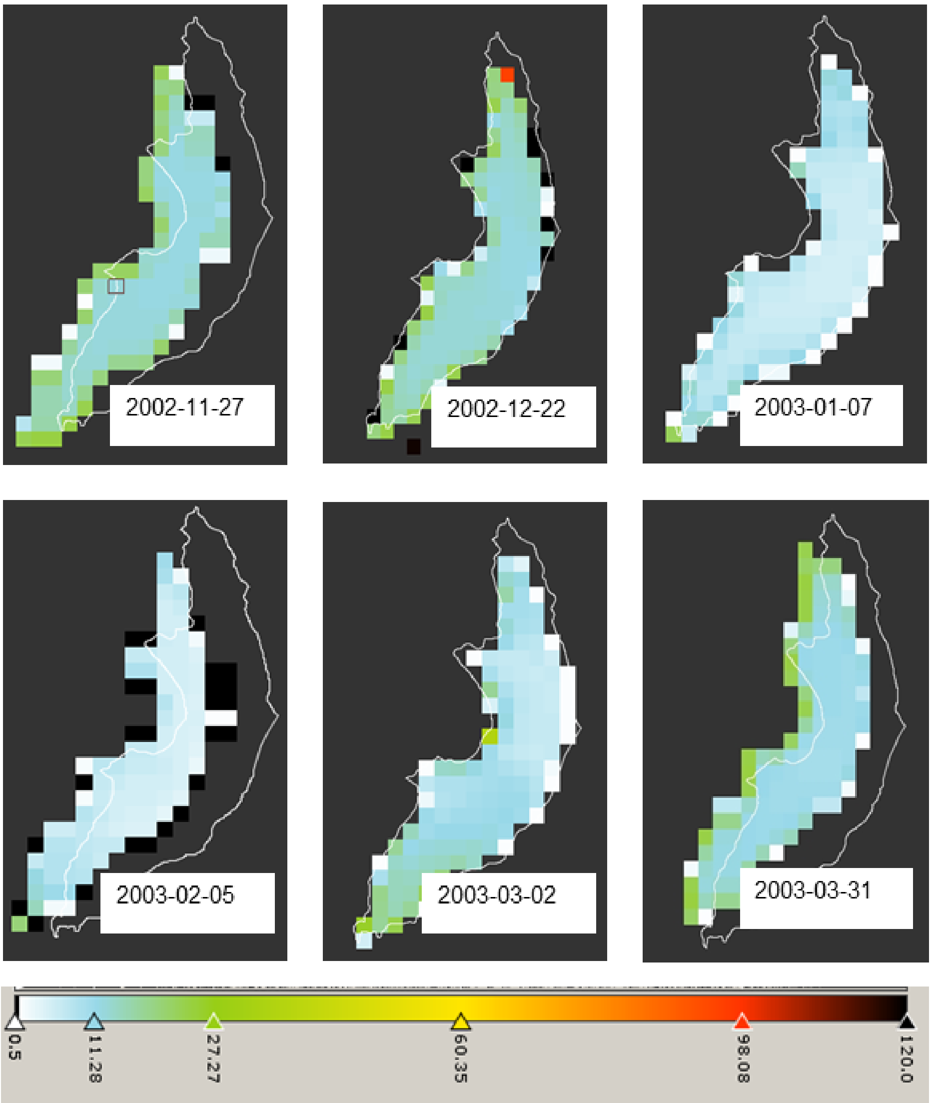

Figure 4.8 Chlorophyll *a* concentration (µg ℓ^{-1}) for Kwena Dam derived from MERIS data using the MERIS Lakes processor in BEAM.

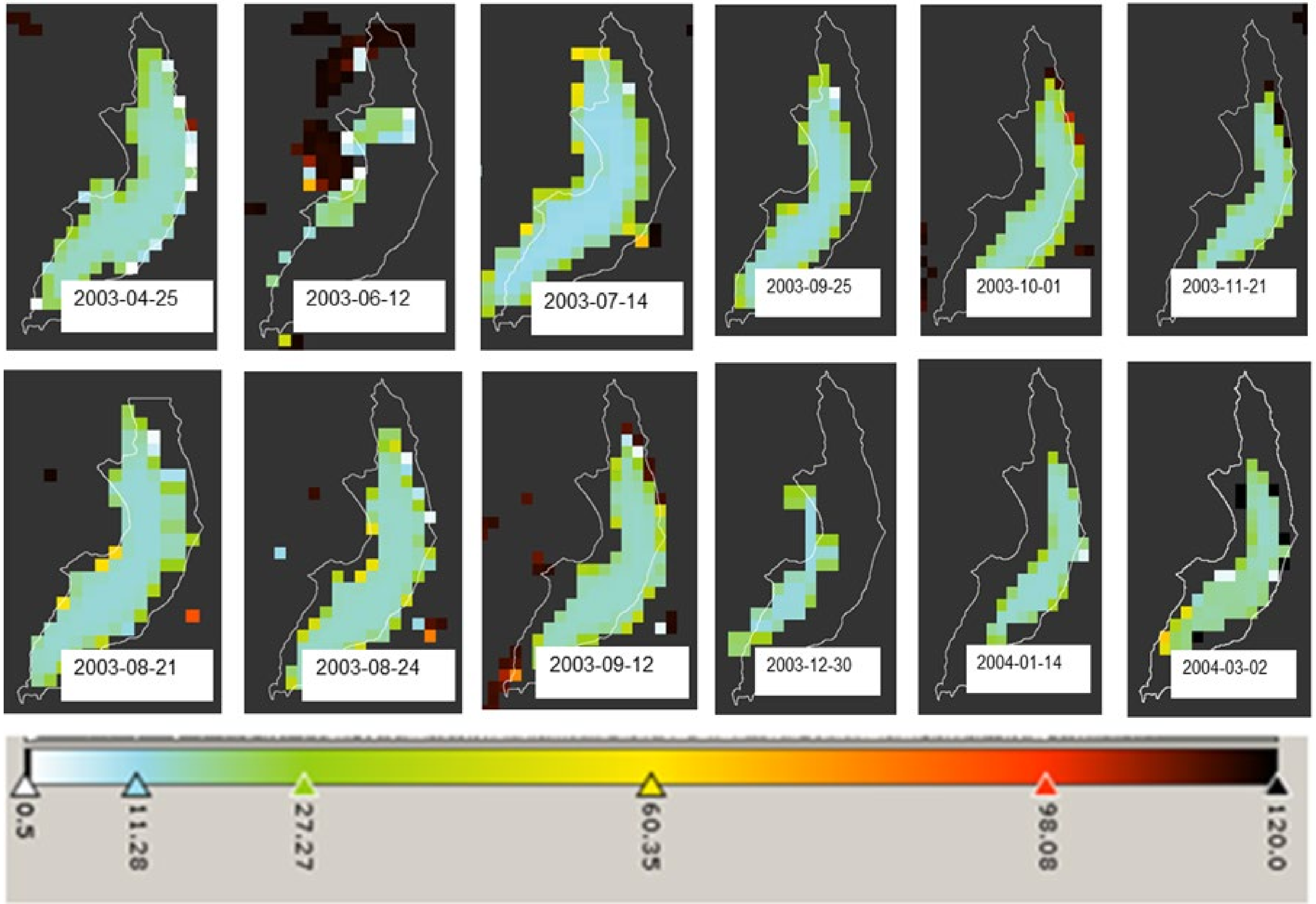

Figure 4.8 Continued

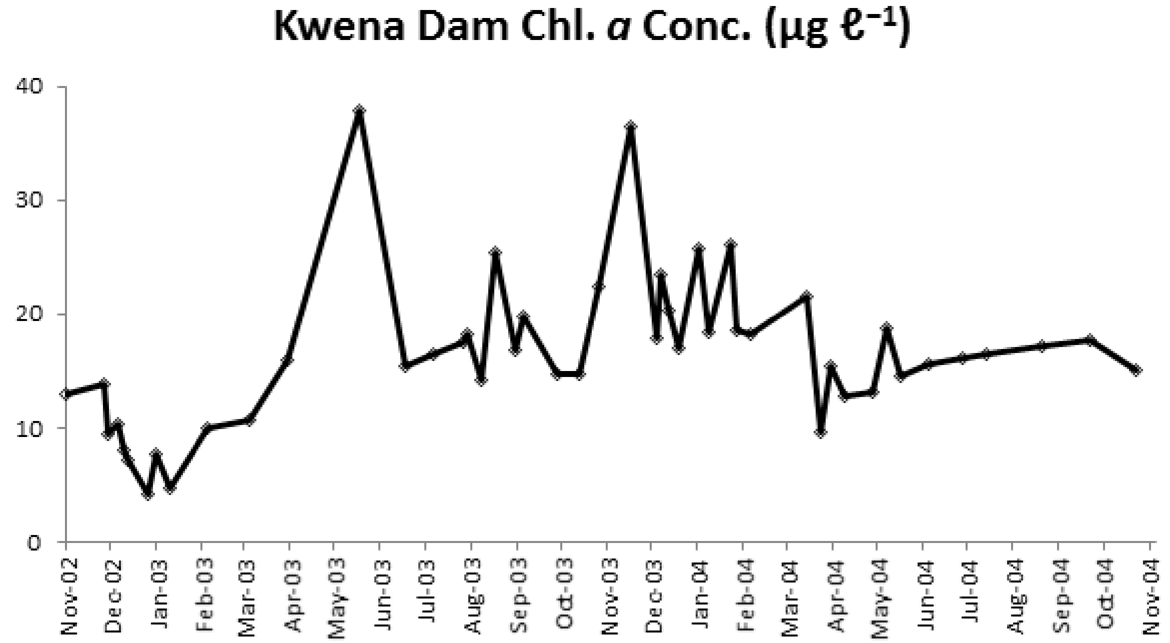

Figure 4.9a Temporal variation in average chlorophyll *a* concentration of Kwena Dam derived from MERIS data using the Lakes processor in BEAM.

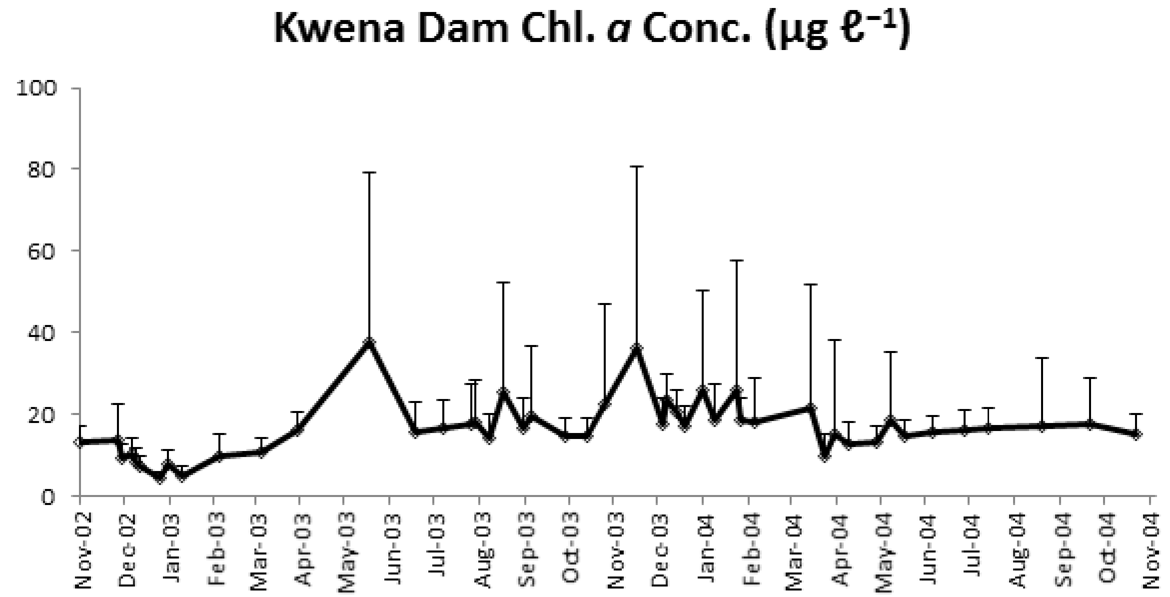

Figure 4.9b Temporal variation in average chlorophyll *a* concentration of Kwena Dam shown with standard deviation error bars derived from MERIS data.

Laing Dam, Buffalo River

Laing Dam is located on the Buffalo River (Figure 4.10).

The Buffalo River Catchment is situated on the east coast of South Africa in the Eastern Cape, with the estuary entering the Indian Ocean at the city of East London. The headwaters of the river are in the Amatole Mountains, after which the river flows in a south-easterly direction for a relatively short total length of 125 km through a catchment area of 1,276 km^2 before reaching the sea. Most runoff occurs within the upper catchment, with annual rainfall averaging 1,500-2,000 mm and 500-625 mm for the upper and middle catchment, respectively. There are two reservoirs in the upper catchment, the Maden and Rooikrants dams, resulting in very little flow being released to the middle catchment. Due to WWTW return flow, the flows in the river are increased through King Williams Town. Laing Dam is positioned in the middle Buffalo River Catchment just below King Williams Town.

Although the water quality of the upper catchment is relatively unimpacted, water quality problems have been a continual challenge within the middle and lower catchment. The flow within the middle catchment is dominated by return flow from inefficiently managed WWTWs; therefore, high nutrient concentrations and eutrophication is problematic. The Laing Dam acts as a nutrient trap, and this problem is compounded by water being extracted for domestic use from the dam and released upstream as WWTW effluent, thereby creating a ‘closed loop’. Hyacinth (*Eichhornia crassipes*) blooms have been a continual problem in the dam (O’Keefe *et al*., 1996). The dam acts as a nutrient sink, and also results in an artificial decrease of water temperature of the water released downstream (O’Keefe *et al*., 1996). In addition to eutrophication problems, the Buffalo River Catchment is underlain by marine derived geology, and is therefore naturally saline (O’Keefe *et al*., 1996; River Health Programme, 2004).

The DWS historical monitoring data indicate spikes in TDS of as much as 750 mg ℓ^{-1}, with concentrations of > 330 mg ℓ^{-1} approximately 50% of the time. In regards to nutrients, spikes of nitrate + nitrite of up to 3 mg ℓ^{-1} occur, with concentrations of > 1 mg ℓ^{-1} approximately 50% of the time, spikes of ammonium of up to 1.6 1 mg ℓ^{-1}, and spikes of phosphate of up to 0.3 mg ℓ^{-1}.

The result of the Lakes processor for MERIS data for Laing Dam is shown in Figure 4.12. Note that the pixel size/resolution (260 m) is generally larger than the width of the dam, and due to the error generated by overlap of land and water areas for the pixels, quantitative analysis for Laing Dam was abandoned.

4.1.7 Qualitative analysis of reservoir chlorophyll a using remote sensed imagery from Landsat

Landsat satellites provide a long series of remote sensed imagery that is useful to qualitatively monitor change in reservoir water quality over time and space due to frequent repeated measurements. Landsat 7 and 8 surface reflectance data with no cloud cover in the area of interest was downloaded from the US Geological Survey's (USGS) Earth Resources Observation and Science (EROS) Data Center (using the EarthExplorer website; http://earthexplorer.usgs.gov/).

Loskop Dam, Olifants River

The ratio of Landsat 7 ETM+ surface reflectance bands 1 and 2 (blue and green wavelengths) was used to generate maps of Loskop Dam using ArcMap 10.3 (Figures 4.13 and 4.14). The Scan Line Corrector (SLC) in the ETM+ instrument resulted in signal drop banding visible in the images after May 2003.

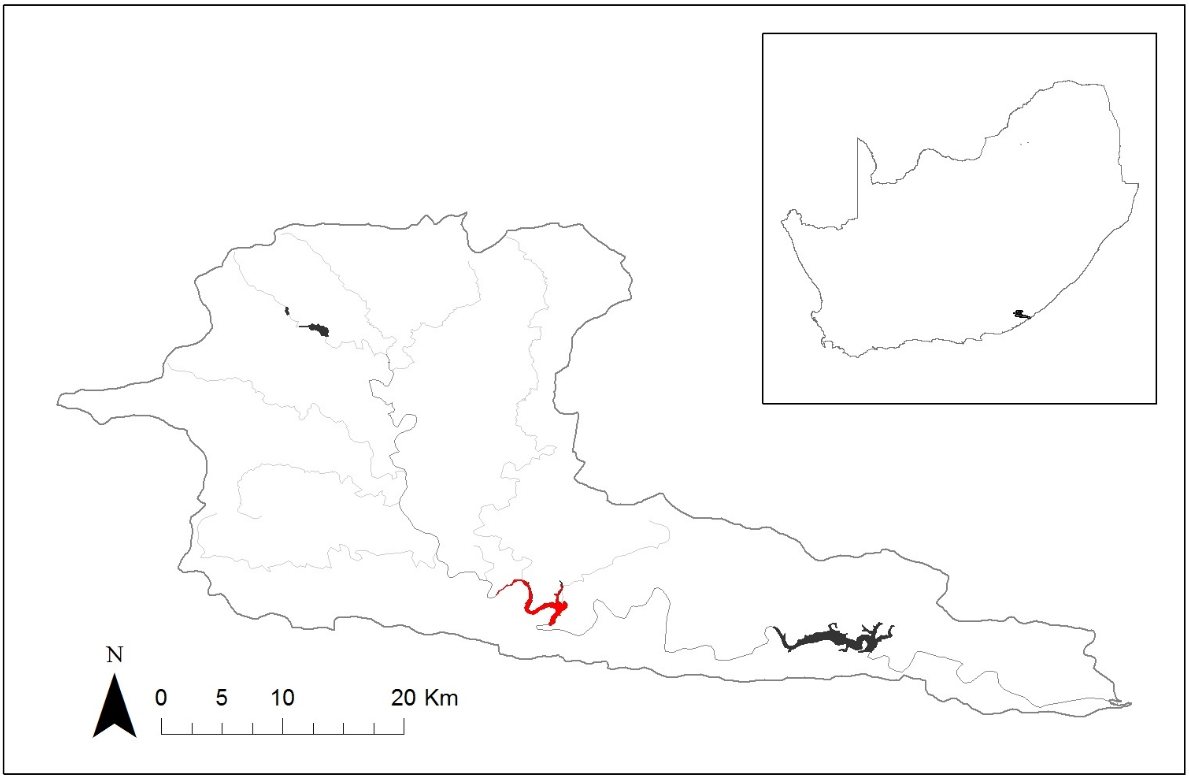

Figure 4.10 Location of Laing Dam on the Buffalo River.

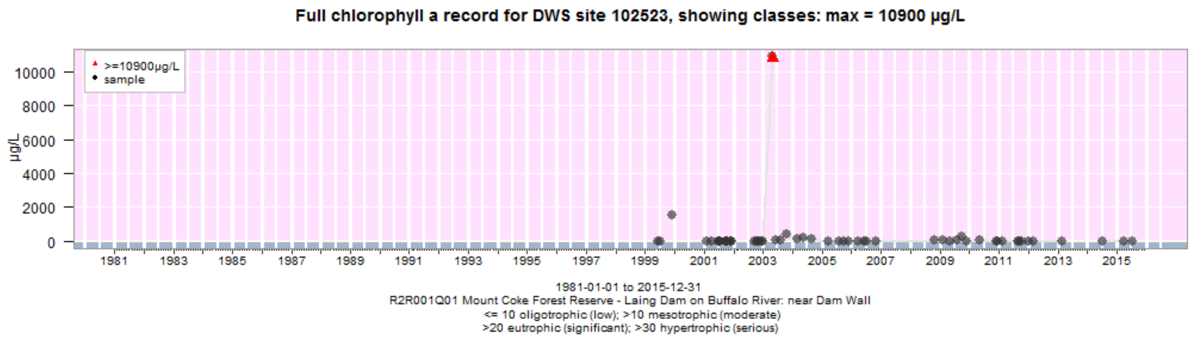

Figure 4.11 Data for Laing Dam (gauge R2R001Q01) extracted from the Department of Water Affairs' National Eutrophication Monitoring Programme (NEMP) website: https://www.dwaf.gov.za/iwqs/eutrophication/NEMP/report/Chart_nemp_102523.png; accessed on 11 January 2016.

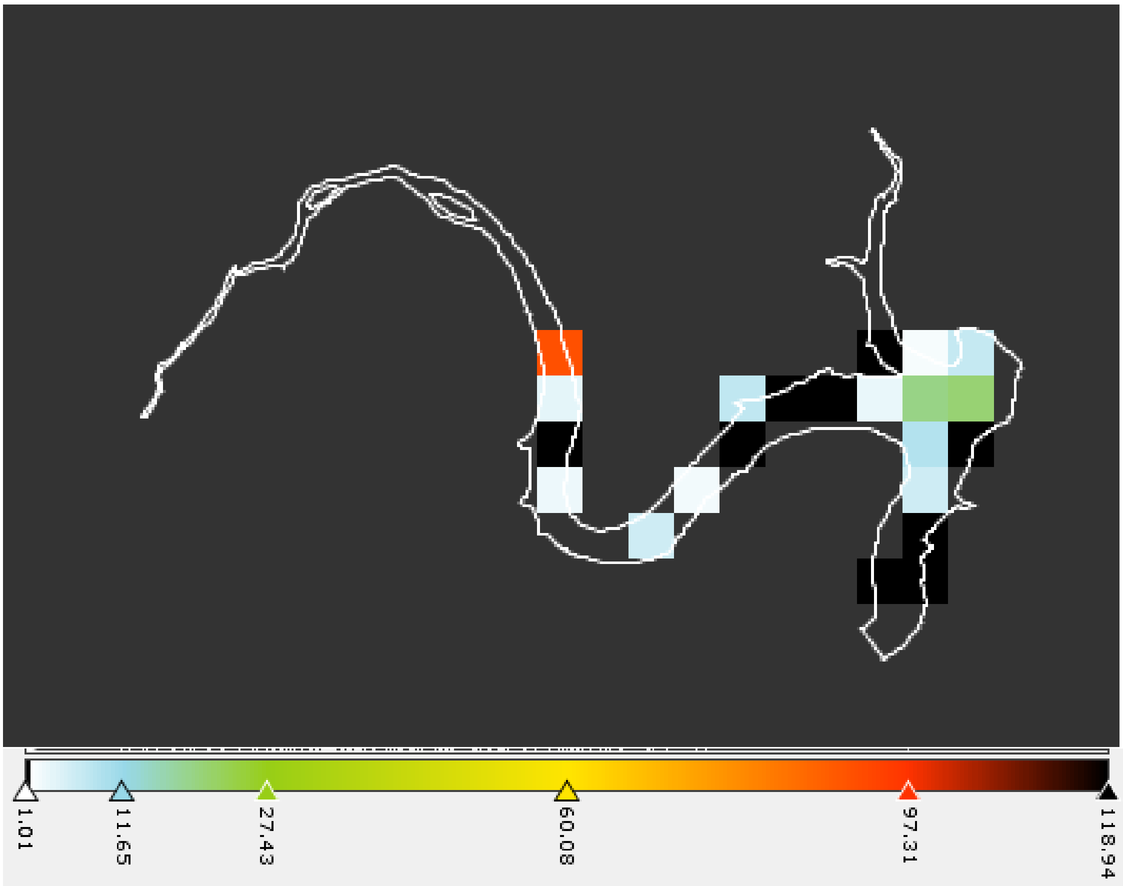

Figure 4.12 Chlorophyll *a* concentration (µg ℓ$^{-1}$) for Laing Dam derived from MERIS data for 2 March 2003 using the MERIS Lakes processor in BEAM.

An example of such a result is shown for 22 August 2003, but other images after this date are not shown. Note that low values are coded as shades of green (present towards the edges of the dam) relative to purple pixels in the centre of the reservoir. They are symbolised thus since algae absorbs blue and reflects green bandwidth, it is expected that where algae is present, the values of blue/green ratio will be lower. However, one cannot assign chlorophyll *a* values and this is a qualitative assessment since Landsat bands are relatively broad in the bandwidth that they cover and narrow bandwidth is recommended for extracting water quality signatures. Comparison of these results with those obtained from the Lakes processor (Figure 4.5) shows that there is general correspondence in the spatial variation for 2003 (Figure 4.14). The images in Figures 4.13 and 4.14 have been symbolised over the same range, and thus in terms of temporal trend, a worsening of water quality in the centre of the reservoir can be seen with the change in colour from dark blue to blue-green pixels between January and March 2003 (similar to Figure 4.5). The value of these Landsat images is primarily for assessing the coverage of algae as can be seen in the lower section of the western side of Loskop Dam in Figure 4.15.

Kwena Dam, Crocodile River

As above for Loskop Dam, the ratio of Landsat 7 ETM+ surface reflectance bands 1 and 2 (blue and green wavelengths) was used to generate maps of Kwena Dam using ArcMap 10.3 (Figures 4.16 and 4.17). The same Landsat scenes as those for Loskop Dam (listed in Table 4.4) were used since the scenes were large enough to cover both the dams. The imagery for 16 January 2002 had clouds over Kwena Dam and was not analysed. The images have been symbolised over the same data range to allow comparison.

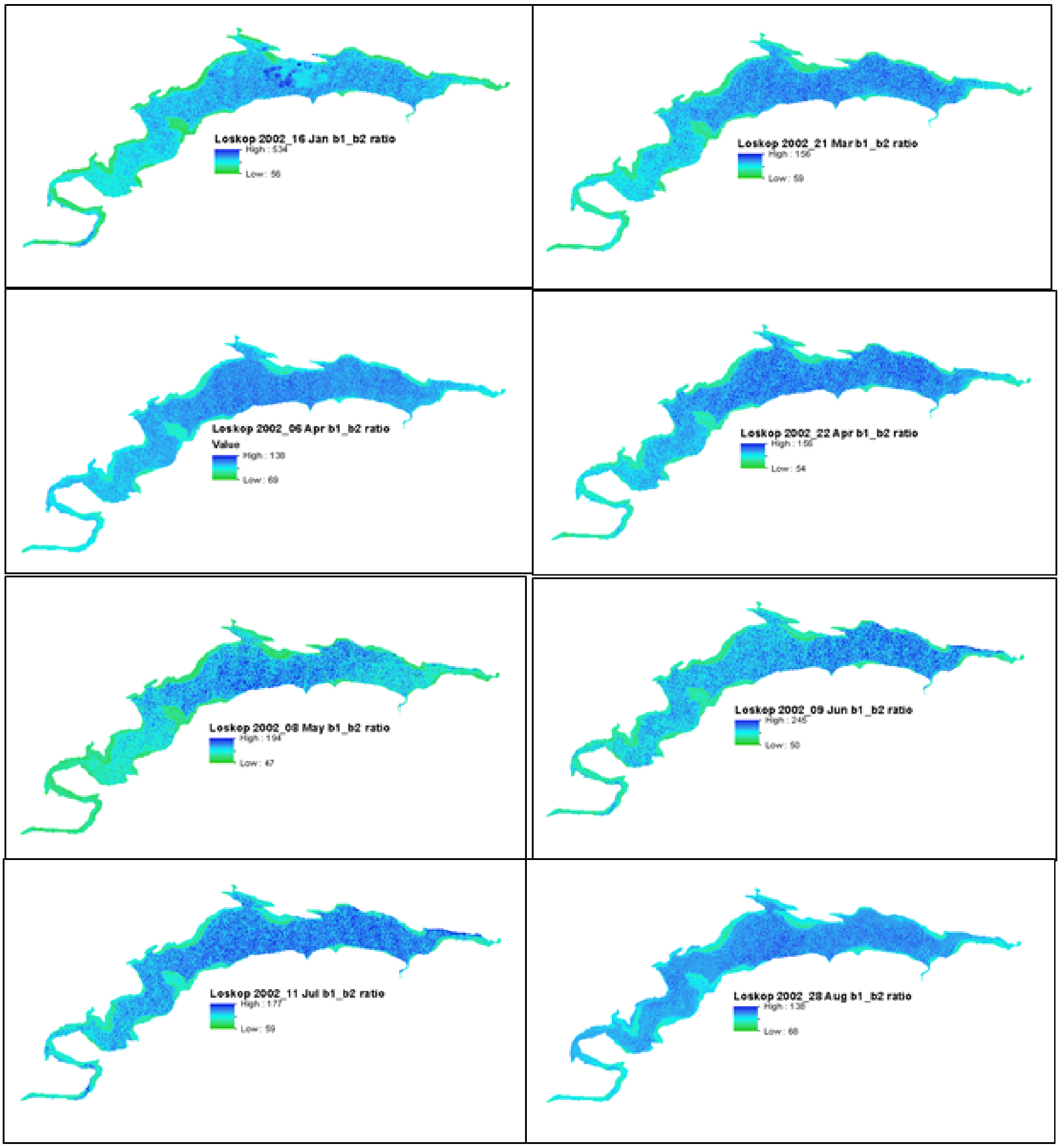

Figure 4.13 Ratio of blue and green wavelengths (bands 1 and 2; mutlitplied by 100) for Loskop Dam derived from Landsat 7 surface reflectance data for January to October 2002.

The ratio of blue to green bands shows the development of algal growth in the middle and end of 2002 and 2003, comparable to the pattern seen using MERIS data (Figure 4.8).

Laing Dam, Buffalo River

To conduct a qualitative analysis using Landsat analysis which can be in some manner verified, available Google Earth imagery without cloud cover was assessed for the area around Laing Dam to assess when hyacinth growth or surface scum is present.

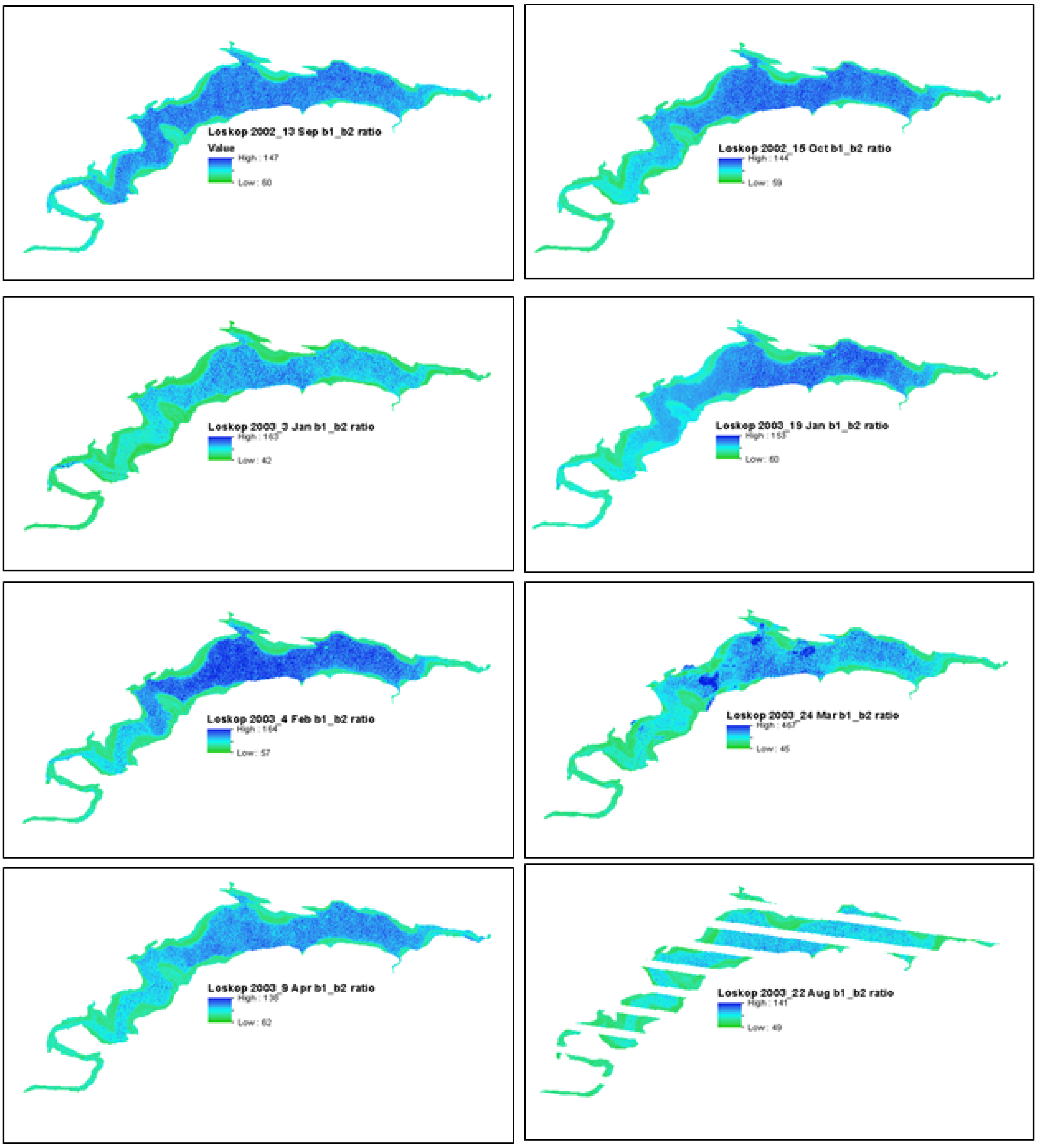

Figure 4.14 Ratio of blue and green wavelengths (bands 1 and 2; mutlitplied by 100) for Loskop Dam derived from Landsat 7 surface reflectance data for January to August 2003. Due to the failure of the SLC in the ETM+ instrument, images after May 2003 show signal drop banding, an example of which is shown for 22 August 2003.

Three Google Earth images of the Laing Dam area with visible growth were chosen for 2013 and 2014. Landsat 8 data closest to the 2013 and 2014 dates (shown in Table 4.5) were downloaded to assess which band ratios can better distinguish the presence of hyacinth or surface scum. As noted previously in this chapter, water hyacinth reflects higher amount of near infrared wavelengths compared to water. Two band ratios were assessed for their performance: blue to green ratio (band 2 / band 3 for Landsat 8) which has been used above to identify presence of algae and NIR to red (band 5 / band 4 for Landsat 8) since NIR wavelengths are expected to be affected by hyacinth. The results are shown in Figures 4.18 to 4.23.

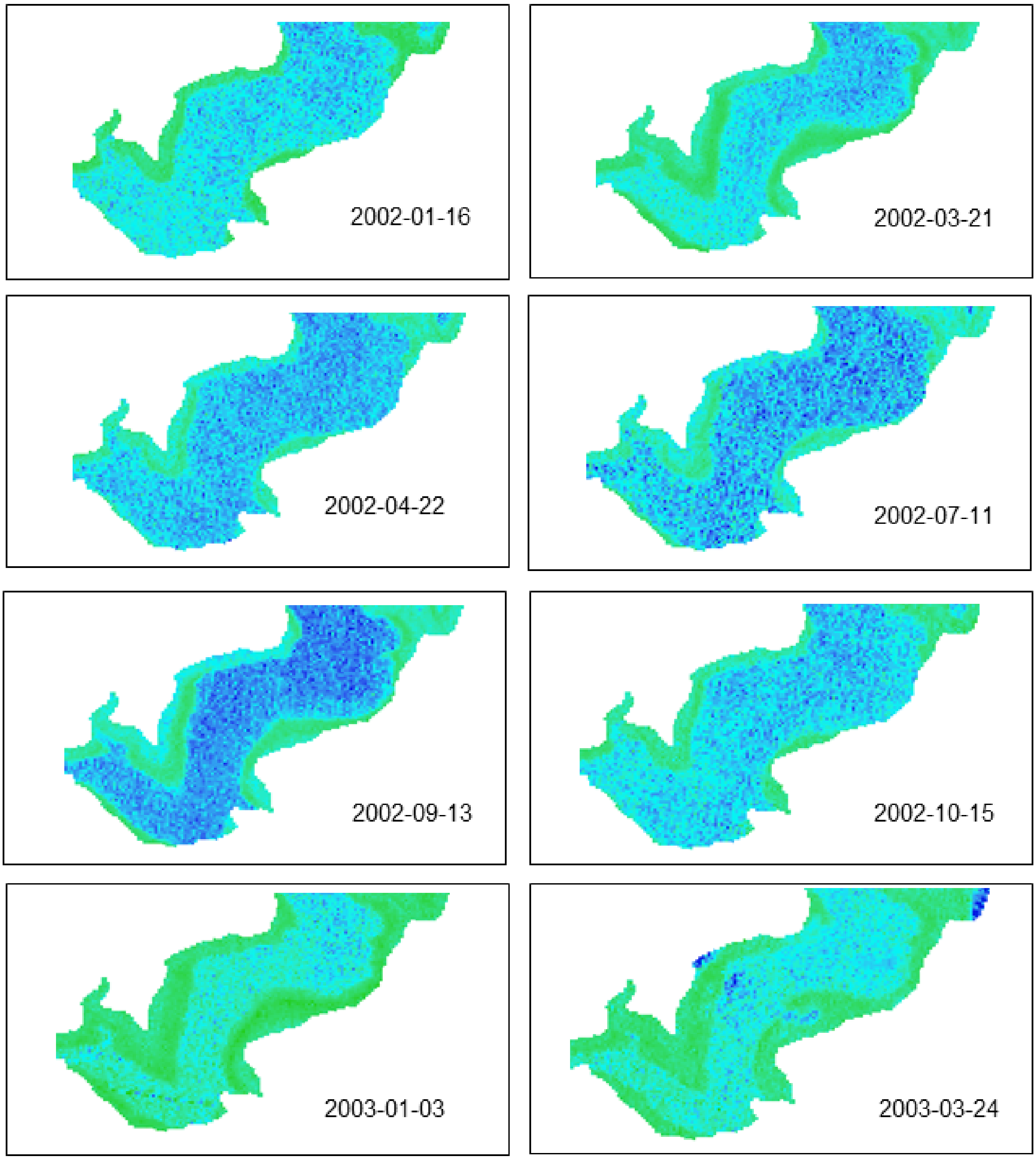

Figure 4.15 Detail of western section of Loskop Dam showing the variation in algal coverage from 16 January 2002 to 24 march 2003 (surface reflectance data derived from Landsat 7 ETM+ as noted in the legend for Figure 4.13).

The Landsat results are symbolised based on the expected changes in the band ratios over the same data range. The presence of algae is expected to result in lower blue/green ratio values, and hyacinth growth is expected to increase NIR/red ratio because of greater reflection of NIR signal.

Table 4.4 Imagery downloaded from Landsat 7 satellite for area near Loskop Dam for qualitative assessment of chlorophyll *a* from the US Geological Survey's (USGS) Earth Resources Observation and Science (EROS) Data Center. Dates for data download were selected due to the requirement of the imagery being primarily cloud free.

Date of Landsat imagery	Scene ID
16 January 2002	LE71690782002016SGS01
21 March 2002	LE71690782002080SGS00
06 April 2002	LE71690782002096JSA00
22 April 2002	LE71690782002112JSA00
08 May 2002	LE71690782002128JSA00
09 June 2002	LE71690782002160EDC00
11 July 2002	LE71690782002192JSA00
28 August 2002	LE71690782002240JSA00
13 September 2002	LE71690782002256EDC00
15 October 2002	LE71690782002288JSA00
03 January 2003	LE71690782003003SGS00
19 January 2003	LE71690782003019SGS00
04 February 2003	LE71690782003035SGS00
24 March 2003	LE71690782003083JSA00
09 April 2003	LE71690782003099SGS00
22 August 2003	LE71690782003243ASN01

Table 4.5 Landsat 8 OLI/TIRS Land Surface Reflectances downloaded from USGS website for area near Buffalo River, Eastern Cape for assessment of water quality.

Date of Google Earth image	Date of Landsat imagery	Scene ID
20 August 2013	18 August 2013	LC81690832013230LGN00
31 March 2014	21 March 2014	LC81700832014080LGN00
20 July 2014	20 July 2014	LC81690832014201LGN00

Comparison of Landsat band ratios with Google Earth imagery suggests that the NIR to red band ratio performs better than the blue to green ratio (see Figures 4.18 to 4.23) in identifying areas with high growth in the north (in all three images) and the east side (August 2013 and July 2014) of the dam. Thus, for the time series imagery for 2002 (see below), only the NIR to red band ratio is provided and inferences about hyacinth growth are drawn from it.

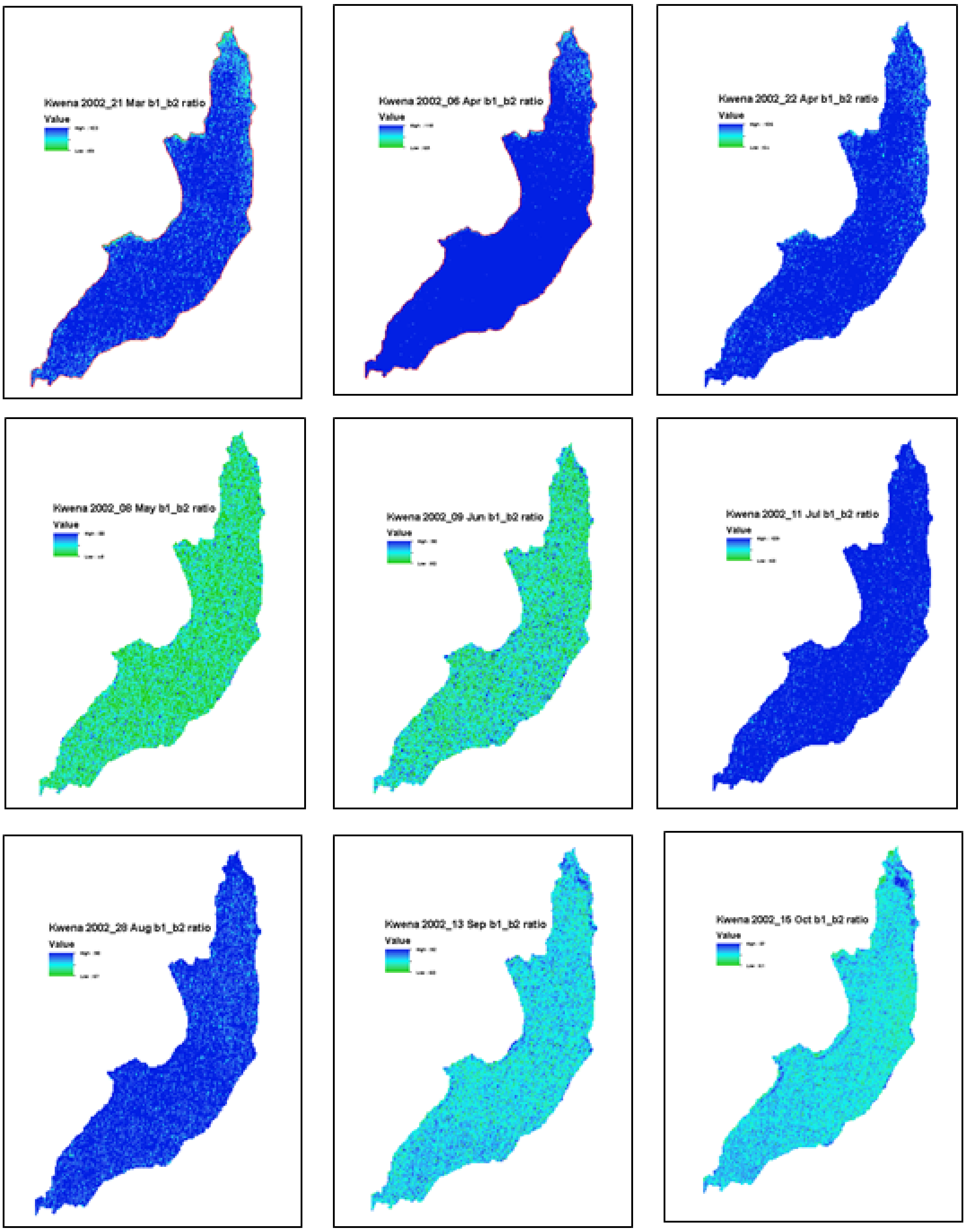

Figure 4.16 Ratio of blue and green wavelengths (bands 1 and 2; mutlitplied by 100) for Kwena Dam derived from Landsat 7 surface reflectance data for 2002.

The ratio of Landsat 7 ETM+ surface reflectance bands 4 and 3 (NIR to red wavelengths) was used to generate a time series of changes in Laing Dam water quality during 2002. The six surface reflectance data products that were used are shown in Table 4.6 and the resulting band ratio (Figure 4.24) shows a high value for the north of the dam in March/April that reduces slightly over the rest of the year. For the east side of the dam, the highest band ratio value is in June 2002.

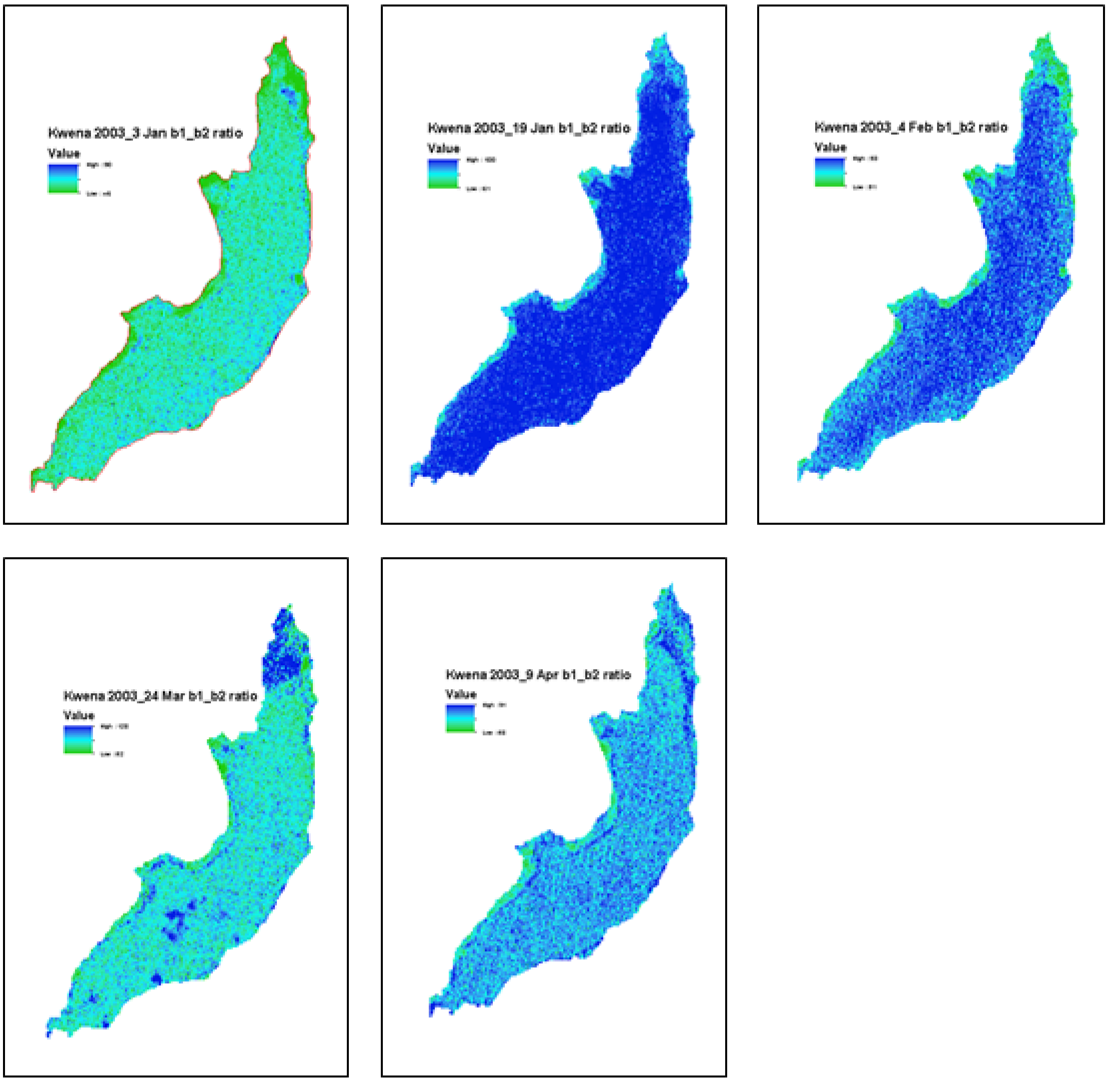

Figure 4.17 Ratio of blue and green wavelengths (bands 1 and 2; mutlitplied by 100) for Kwena Dam derived from Landsat 7 surface reflectance data for January to April 2003. Due to the failure of the SLC in the ETM+ instrument, images after May 2003 show signal drop banding and are therefore not shown.

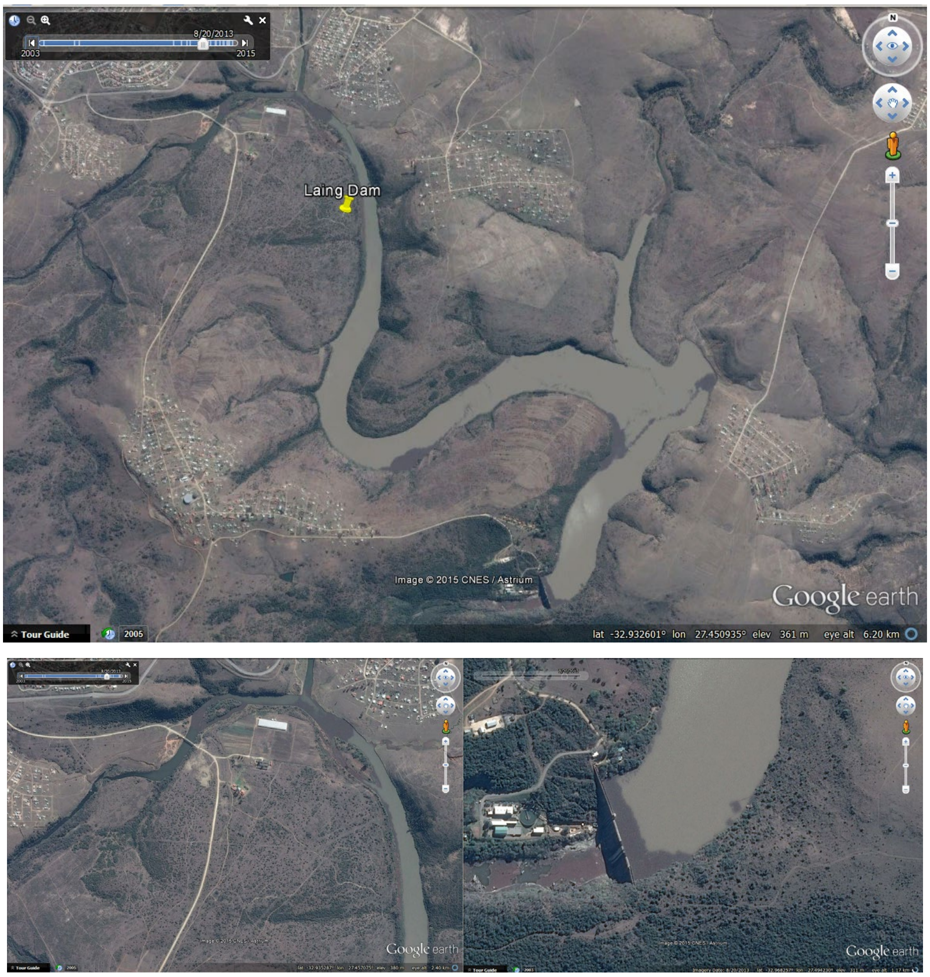

Figure 4.18 Google Earth images of Laing Dam for 20 August 2013 with bottom images showing detailed views.

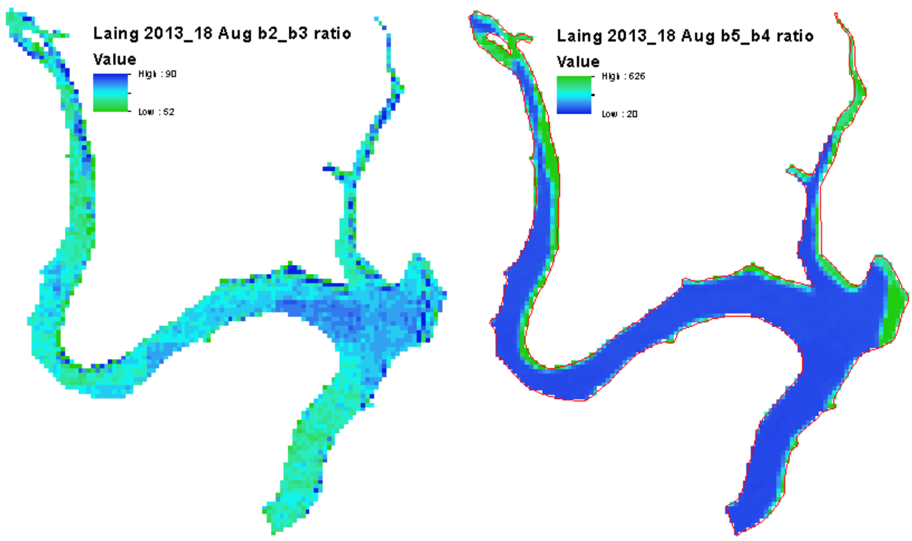

Figure 4.19 Landsat 8 surface relfectance band ratio (mutlitplied by 100) results for 18 August 2013: blue to green (left) and NIR to red (right image).

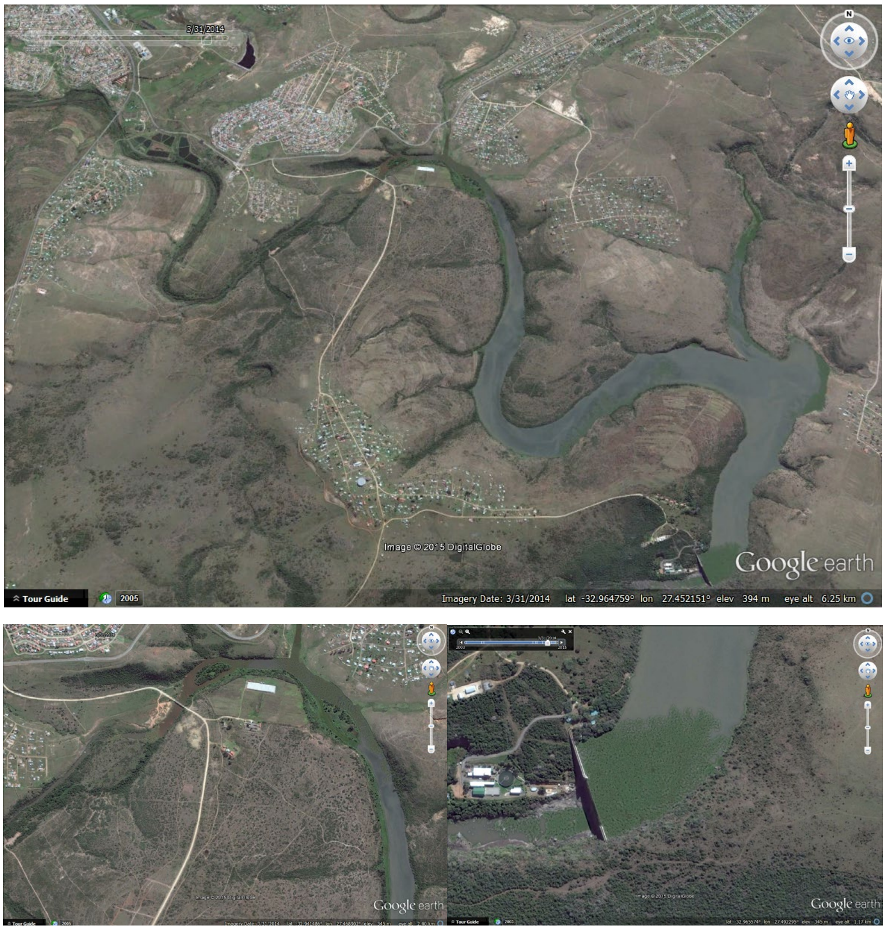

Figure 4.20 Google Earth imagery for Laing Dam for 31 March 2014 with bottom images showing detailed views.

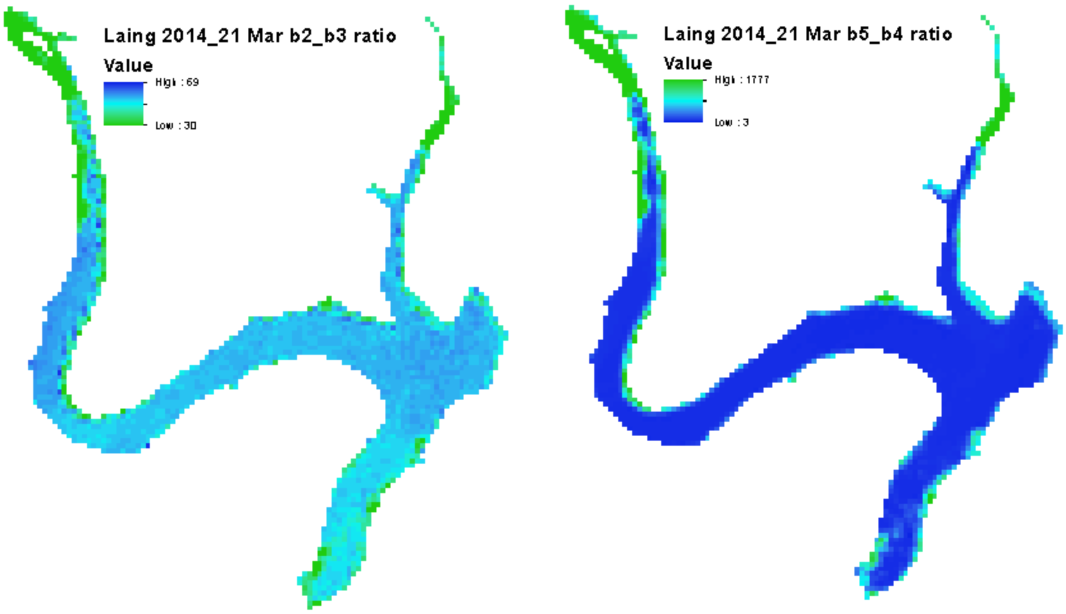

Figure 4.21 Landsat 8 surface relfectance band ratio (mutlitplied by 100) results for 21 March 2014: blue to green (left) and NIR to red (right image).

Figure 4.22 Google Earth imagery for Laing Dam for 20 July 2014 with bottom images showing detailed views.

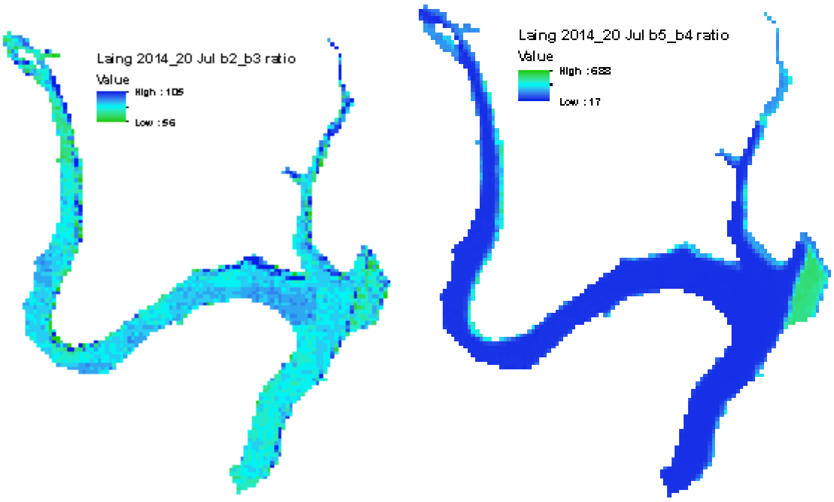

Figure 4.23 Landsat 8 surface relfectance band ratio (mutlitplied by 100) results for 20 July 2014: blue to green (left) and NIR to red (right image).

Table 4.6 Landsat 7 ETM Land Surface Reflectance downloaded from USGS website for area near Buffalo River, Eastern Cape for assessment of water quality.

Date of Landsat imagery	Scene ID
05 March 2002	LE71690832002064SGS00
22 April 2002	LE71690832002112SGS00
09 June 2002	LE71690832002160JSA00
27 July 2002	LE71690832002208JSA00
28 August 2002	LE71690832002240JSA00
31 October 2002	LE71690832002304SGS00

4.1.8 Discussion

The use of satellite imagery for gathering environmental data (both temporal and spatial) is a growing field of research that is expected to provide greater understanding of temporal changes and spatial comparisons to better manage the water resources for the future when water is expected to be even more limited in availability (both quantity and quality).

The pros and cons of remote sensing data for water quality monitoring need to be considered when using this information. Some of the advantages include provision of data in areas with no information, periodically available data which is for the full surface of the lake or dam instead of point measurements (as seen with the MERIS results), and the possibility of comparison of dams in a region. However, the available spatial and temporal resolution of the imagery itself can be limiting in its application to some waters, e.g. small reservoirs (as was the case for the use of MERIS for Laing Dam). Additionally, the presence of clouds, edge effects near land / water boundaries and limitations of algorithms for atmospheric correction can be issues when using remote sensing data.

This report has shown the use of remote sensing data from MERIS and Landsat satellites from 2002 and 2003 to assess chlorophyll levels and algal presence, including temporal variation, for three reservoirs in South Africa. MERIS data were processed through an ESA algorithm to provide a quantitative evaluation of two reservoirs (Loskop and Kwena) that were large enough relative to the MERIS pixel resolution. Although the MERIS satellite is no longer functioning, there are upcoming sensors including Sentinel-3 that are expected to provide similar data for water quality evaluation in the near future. Landsat data on the other hand is currently available and despite its broad bandwidth, it provides the possibility of assessing spatial changes over time. The smaller pixel resolution of Landsat, compared to MERIS, also makes its data useful for small reservoirs like Laing Dam.

Monitoring networks for reservoirs in South Africa at present are primarily based on ground data. While this practice needs to continue, Dörnhöfer and Oppelt (2016) suggest that water quality monitoring networks need to consider integrating remote sensing data as part of their operation. Recent research by Matthews and Bernard (2015) clearly indicated through their analysis of 50 large South African reservoirs that satellite imagery can be useful for assessing the status of chlorophyll *a*, cyanobacterial blooms and cyanobacterial surface scum.

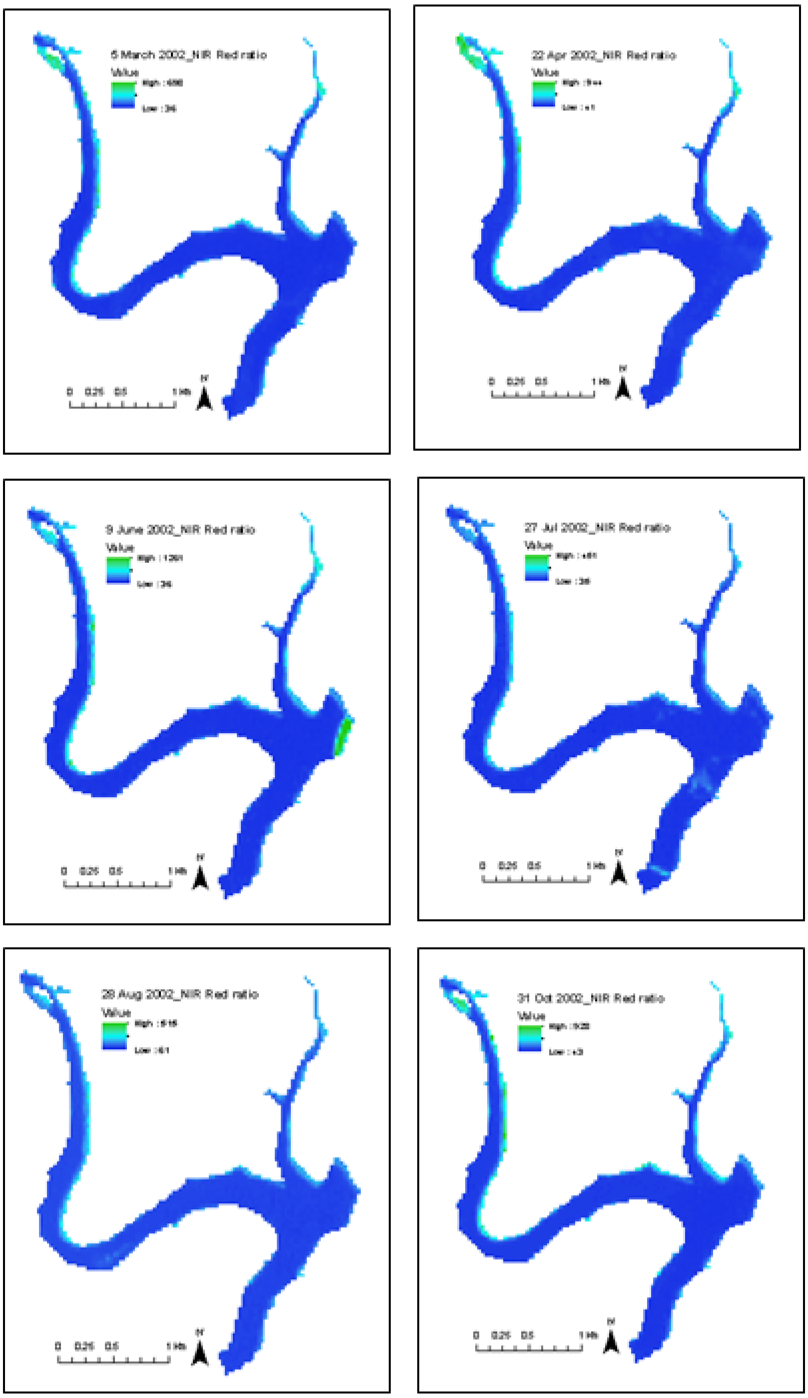

Figure 4.24 Ratio of NIR to red wavelengths (bands 4 and 3; mutlitplied by 100) for Laing Dam derived from Landsat 7 surface reflectance data for March to October 2002.

4.2 Validation of simulations of primary production using WQSAM within the case study catchments

4.2.1 Introduction

The Water Quality Systems Assessment Model (WQSAM) is a water quality decision support system designed specifically for use within water quality management in South Africa.

In that regard, the model development has been guided by the principle of requisite simplicity to keep model data requirements at a minimum. More information on the model development is available within Slaughter *et al*. (2015a). The model takes as input flow data generated by a routinely-used systems model, either the Water Resources Modelling Platform (WReMP; Mallory *et al*., 2011) or the Water Resources Yield Model (WRYM).

WQSAM originally concentrated on modelling nutrients and salinity (Slaughter *et al*., 2015), and has recently been updated to additionally model sulphates as an indication of acid mine drainage, as well as microbial water quality (see Deliverable 2 of the current WRC project) (Slaughter, 2017). In regards to the modelling of nutrients, the model has incorporated various processes affecting nutrients, which have been adopted and simplified from other more established models, such as the CE-QUAL-W2 model (Cole and Wells, 2008). These include nutrient speciation, organic matter decomposition and the uptake of nutrients by aquatic flora, which are all processes that are regulated by water temperature. WQSAM has adopted the algal growth processes from the CE-QUAL-W2 model, except that WQSAM currently clumps all algae into one group, whereas CE-QUAL-W2 adopts a more sophisticated approach. WQSAM has additionally specifically focussed on modelling hyacinth, as this floating invasive macrophyte is regarded as a huge water quality problem in reservoirs in South Africa, with considerable impacts within the Crocodile River and Buffalo River catchments (Deksissa *et al*., 2004; O'Keefe *et al*., 1996). WQSAM has adopted the process for simulating aquatic macrophyte growth from the CE-QUAL-W2 model, with adaptations regarding the assumption of predominantly floating plants and the uptake of both ammonia/ammonium and nitrate + nitrite in regards to nitrogen species.

Past water quality studies using WQSAM have modelled historical water quality as well as future scenarios, with calibration of the model performed against Department of Water and Sanitation (DWS) historical monitoring data. These data are generally restricted to measurements of nutrients and salinity. To obtain simulated nutrient concentrations, WQSAM was required to model algal and hyacinth growth. Although the processes adopted within WQSAM for growth of aquatic flora are based on an established model and best science, the simulations of algal and hyacinth growth have not been validated against observed data, mainly because these data in terms of traditional historical monitoring data do not exist. However, the validation of these processes is imperative as there is a danger of equifinality within the WQSAM model if the model is producing correct historical simulations of nutrients, but using incorrect processes. This would result in incorrect simulations when the model is applied to future scenario modelling.

The availability of remote sensing data provides the opportunity to validate the processes for algal and hyacinth growth used within WQSAM, even if merely at a qualitative level, but hopefully at a quantitative level as well.

4.2.2 Simulations of primary production within study reservoirs

Loskop Dam

Loskop Dam forms the boundary of the upper Olifants River Catchment. Figure B2 shows the quaternary catchments and major dams of the upper Olifants River Catchment. Figure B1 shows the systems diagram structure of the upper Olifants River Catchment.

As can be seen from Figure B2, the Loskop Dam occurs at the lower end of the upper catchment; therefore there are many catchments above the dam that would affect the water quality of the dam. The modelling strategy would therefore require that the model simulations be calibrated against observed data for all catchments above the dam before the dam water quality can be simulated. However, water quality simulations such as salinity and nutrients have been reported for this catchment in a previous report (Slaughter *et al*., 2015), and the current report will therefore only report on simulations of primary production within the studied reservoir.

Figure 4.25 shows the seasonal distribution of simulate algae within the Loskop Dam within the calibrated application of the WQSAM model. The simulations show a max algae wet weight biomass of approximately 10 mg ℓ^{-1} which occurs over summer, and a minimum biomass of approximately 1 mg ℓ^{-1} that occurs around august. The results show a strong seasonal trend.

Figure 4.26 shows the observed versus simulated water temperature in the reservoir, as water temperature drives the rate of algal growth. It is evident that the simulated temperatures, although in the correct range, are not in sync with the seasonal trend of the observed water temperature.

Kwena Dam

Figure B3 shows the location of quaternary catchments, rivers and DWS gauging stations within the Crocodile River Catchment. The Kwena Dam is located within the upper reaches, and can be observed within the top left of Figure B3.

Figure B4 shows the systems diagram for the upper Crocodile River Catchment. Kwena Dam is evident at approximately the middle of this part of the catchment.

Figure 4.27 shows the seasonal distribution of simulated algae for this dam, as generated by WQSAM. The results indicate a noticeable seasonal algal biomass trend, with a minimum algal biomass over August. The algal biomass for this reservoir is evidently lower than that for the Loskop Dam, with a maximum of approximately 5 mg ℓ^{-1} obtained.

There were no observed water temperature data available to compare to simulated water temperature (Figure 4.28). Evident within the simulations of water temperature was a strong seasonal trend with a maximum during summer and a minimum during winter.

Laing Dam

Laing Dam occurs within the middle catchment of the Buffalo River. Figure B4 shows the quaternary catchments, dams and DWS flow gauges.

Figure B4 shows the systems diagram for the catchment.

Figure 4.29 shows the seasonal distribution of hyacinth wet weight biomass within Laing Dam as simulated by WQSAM. The model shows a strong seasonal trend within the hyacinth biomass with a maximum of approximately 3 kg m^{-2} over January and March/April, and a minimum of 2.4 kg m^{-2} over October. Evident is that hyacinth growth appears to persist throughout the year.

Figure 4.30 shows the seasonal distribution of algal wet weight biomass within Laing Dam as simulated by WQSAM. As with the simulations of hyacinth, the seasonal trend is slightly different from that simulated within the Kwena and Loskop Dams, with a peak in March/April of approximately 3.5 mg ℓ^{-1} and a minimum of approximately 0.5 mg ℓ^{-1} during October.

Figure 4.31 shows the monthly average water temperature simulation by WQSAM along with the observed data within Laing Dam.

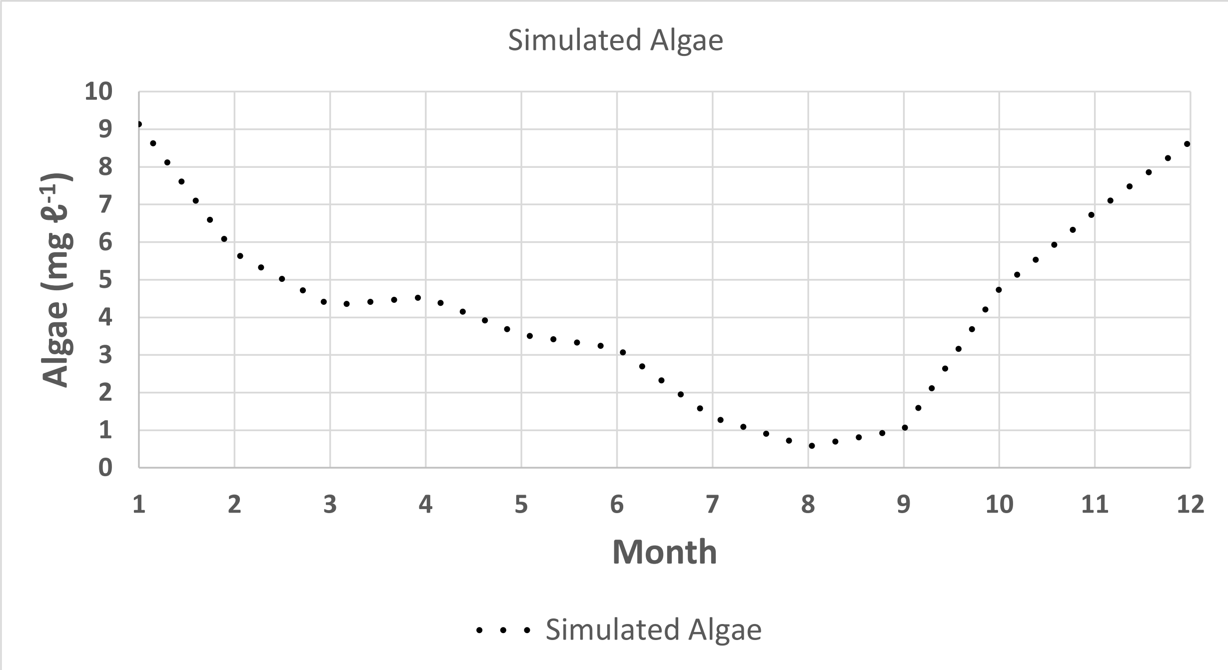

Figure 4.25 Monthly average (seasonal) algae simulation for Loskop Dam on the Olifants River from 1923 to 2003

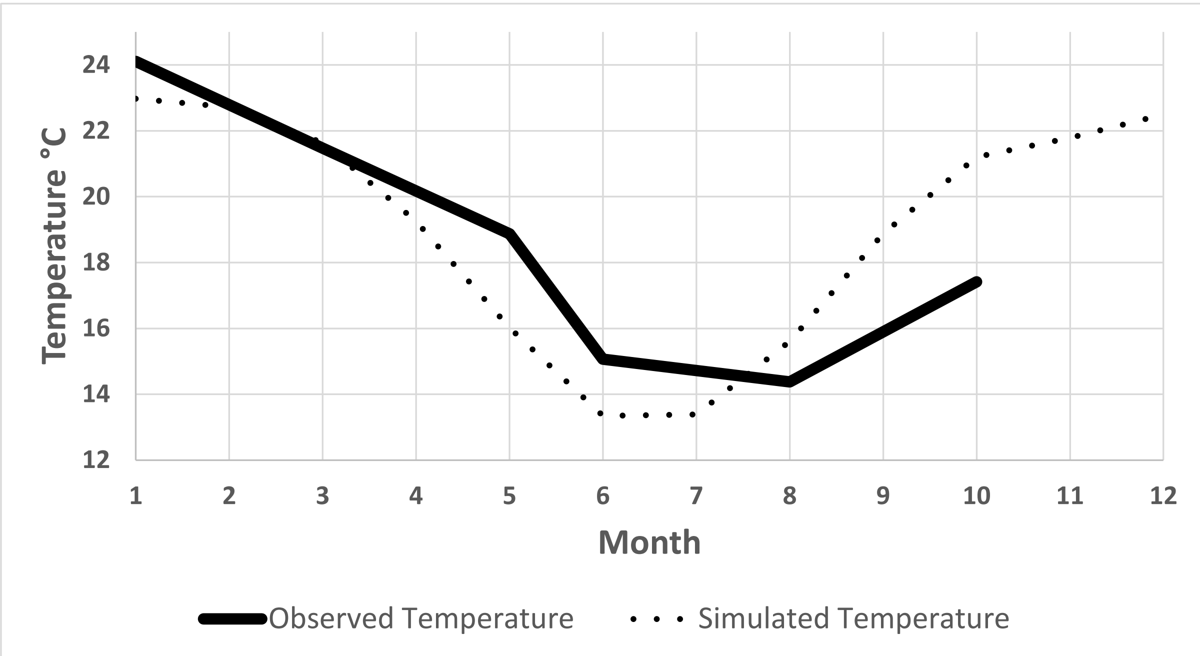

Figure 4.26 Monthly average (seasonal) water temperature simulation for Loskop Dam on the Olifants River from 1923 to 2003

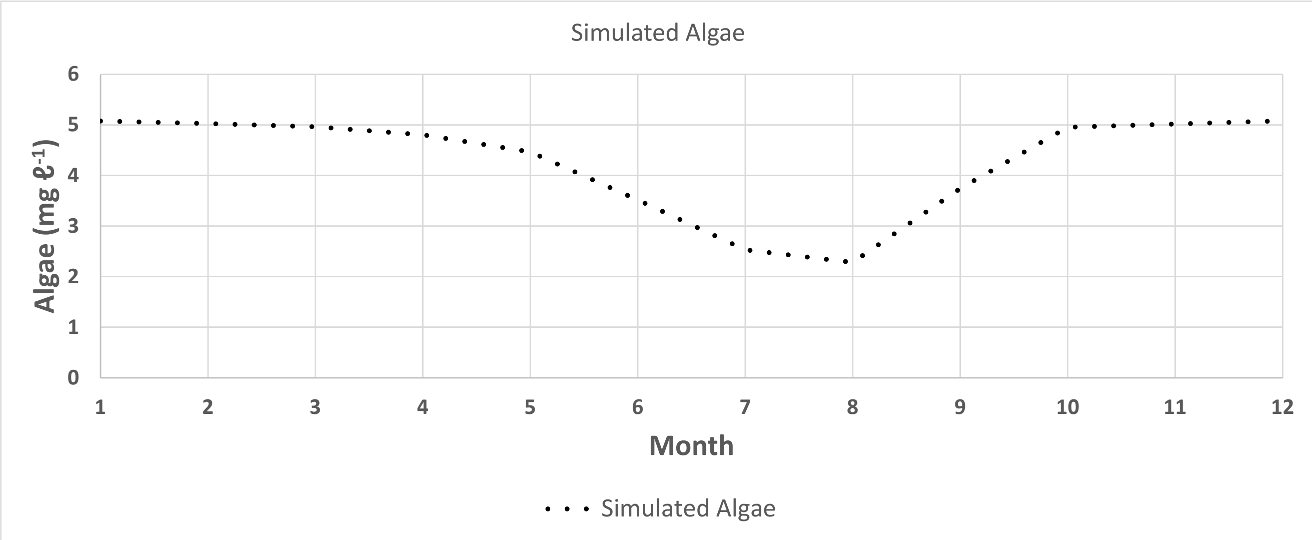

Figure 4.27 Monthly average (seasonal) algae simulation for Kwena Dam on the Crocodile River from 1955 to 2003

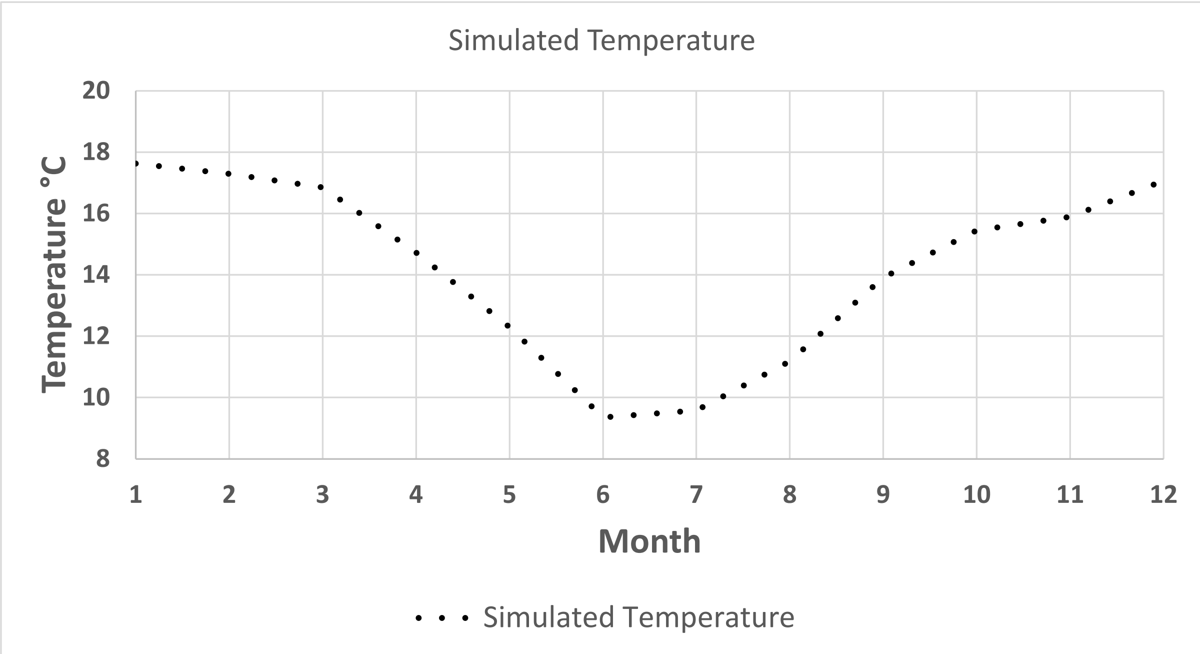

Figure 4.28 Monthly average (seasonal) water temperature simulation for Kwena Dam on the Crocodile River from 1955 to 2003

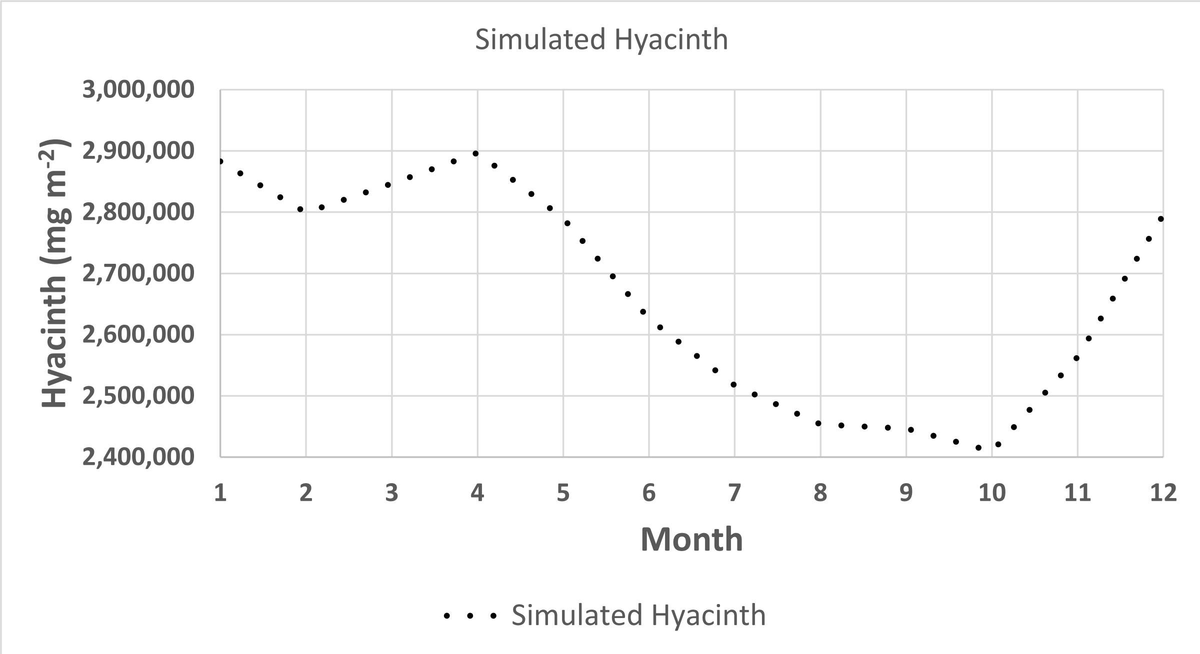

Figure 4.29 Monthly average (seasonal) hyacinth simulation for Laing Dam on the Buffalo River from 1920 to 2003

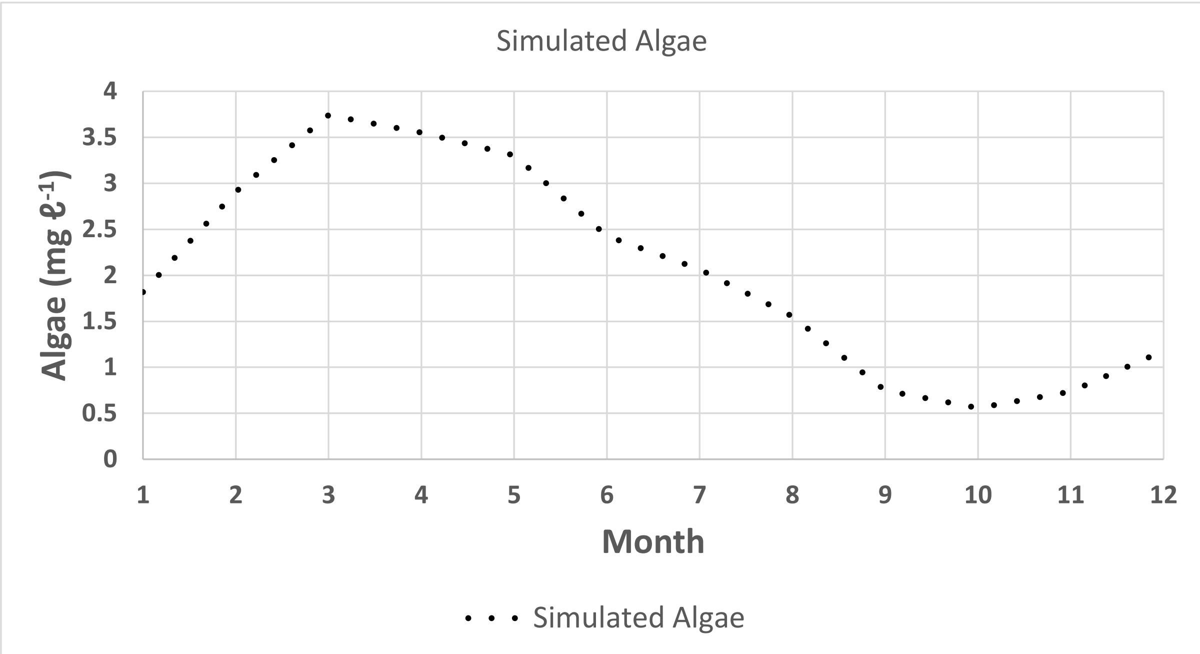

Figure 4.30 Monthly average (seasonal) algae simulation for Laing Dam on the Buffalo River from 1920 to 2003

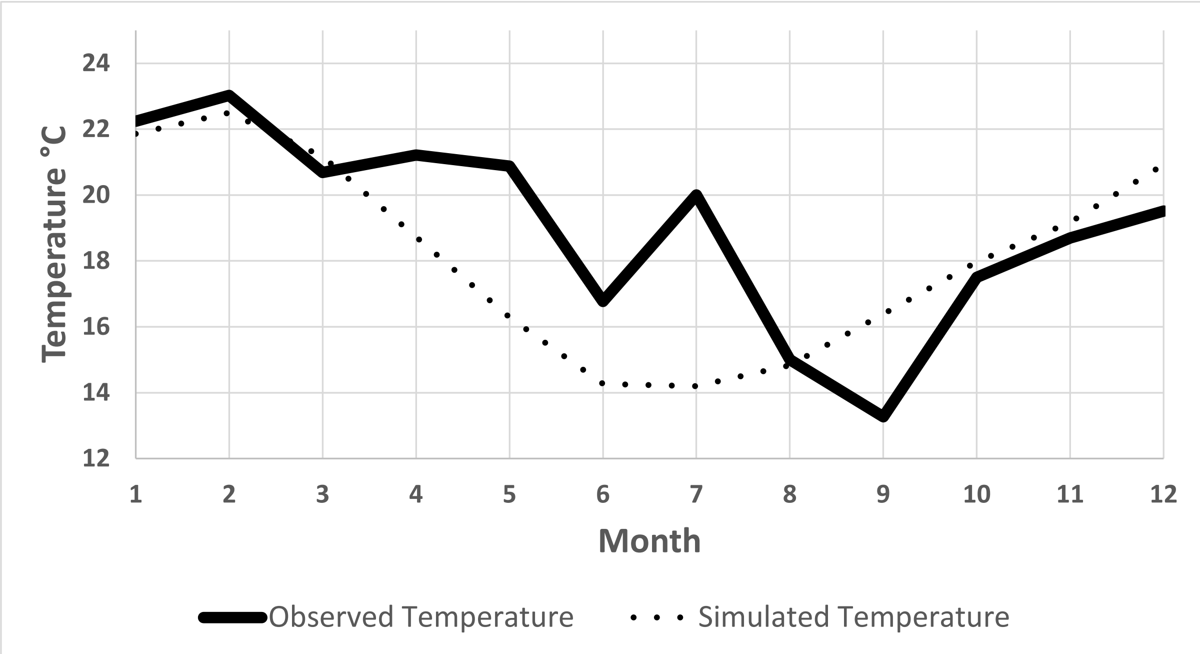

Figure 4.31 Monthly average (seasonal) water temperature simulation for Laing Dam on the Buffalo River from 1920 to 2003

4.2.3 Validation of simulations of primary production by WQSAM using remote sensing estimates of chlorophyll a

Introduction

WQSAM simulates algal biomass as a wet weight mass. The model assigns a nitrogen and phosphorus content to algae as a proportion of wet weight, commonly around 10% for nitrogen and 7% for phosphorus. In this way, decomposition of 1 g of algae will release 0.1 g of nitrogen and 0.07 g of phosphorus. Likewise, an increase in the biomass of algae due to growth will capture the same values of these nutrients. The model allows users to change these values. Within WQSAM, organic sediment as well as dissolved and particulate organic matter resulting from algal death and respiration contains the same proportions of nitrogen and phosphorus, to ensure mass-balance within the model. Although there are typically no observed data for algal biomass available, the calibration process within WQSAM will typically calibrate simulated values of nitrate +nitrite, ammonium and phosphate against observed data. Simulations of algal growth therefore are part of the process to obtain model simulations of the aforementioned nutrients that are within the same range as the observed nutrient data. It could be argued therefore, that the model can simulate a reasonable estimate of algal biomass, providing that the nitrogen and phosphorus composition of algae used in the model are sensible, and that the algal processes simulated in the model are reasonable.

One approach of validating the simulations of algal growth within WQSAM could be to determine the relationship between algal biomass in wet weight, and the associated chlorophyll *a* (chl-a) concentrations in water bodies. In this way, model simulations of algal biomass could be converted to chl-a concentrations and compared to remote sensing estimates of chl-a. This relationship has in fact been of interest in past limnology and oceanography studies, as estimates of algal biomass are very useful within ecological studies. It is however evident that this relationship is by no means constant or easy to determine, and varies according to trophic status of the lake/impoundment, season, the taxonomic composition of algae within the community and the size frequency distribution of algal cells (Felip and Catalan, 2000; Kasprzak *et al*., 2008). Kasprzak *et al*. (2008) noted that chl-a content per unit biomass decreases as standing stocks increase, and using the literature, determined that the proportion of chl-a within the wet weight biomass of algae within the range of 0.1-50 g m^{-3} ranges from 2.5% to 0.18%. Although this relationship is associated with many large uncertainties, it does at least provide a way in which the simulations of algal biomass by WQSAM can be validated within a very general way: if the simulations of algal biomass converted to chl-a fall within the same general range as the values of chl-a determined through the remote sensing products, we can at least assert that WQSAM provides reasonably sensible estimates of algal growth processes.

Approach used for validating simulations of algae within WQSAM

The values of mean chl-a concentrations determined through the BEAM remote sensing product for the period 2004 were averaged into a seasonal distribution for the Loskop and the Kwena dams, using the results given earlier in this chapter (see Figures 4.6 and 4.9). The year 2004 was used as the data associated with the previous years (2002 and 2003) contained uncertainties associated with the quality of the data. Using the relationship by Kasprzak *et al*. (2008), the seasonal distribution of algal biomass as simulated by WQSAM was converted to estimates of chl-a within an uncertainty band, with the lower estimate using the 0.18% value and the upper estimate using the 2.5% value. The entire data period of simulations by WQSAM was used in this process (1920-2003 for the Laing and Loskop dams and 1954-2003 for the Kwena Dam), as the simulations by WQSAM do not extend into 2004, and we decided compare the overall trend of algal simulation in WQSAM with the remote sensing results from 2004. By plotting the BEAM estimate of seasonal distribution of chl-a on the same graph as the WQSAM estimate of algal biomass converted to an uncertainty band of chlorophyll-a concentration, it can at least be judged whether WQSAM is simulating algal biomass within the correct range.

Results for the Loskop and Kwena dams

Figure 3.32 is taken from Matthews (2014), with the top graph showing a time series of chl-a within the Loskop Dam as estimated through the BEAM product for the years 2003-2012. It is evident that a strong seasonal trend is present in the data from approximately 2008-2012, whereas prior to this, the seasonal trend is less pronounced.

Figure 4.33 shows the results of the analysis for Loskop Dam. From the graph it is evident that the BEAM measures of chl-a fall within the uncertainty band of chl-a concentrations produced by converting simulations of algal biomass produced by WQSAM into chl-a, although the BEAM measures are positioned near the chl-a minimum generated by WQSAM. It is additionally evident that the chl-a range obtained from WQSAM shows a much more pronounced seasonal distribution as compared to the BEAM estimates, which are relatively constant throughout the season. The relatively drastic drop in algal biomass as simulated by WQSAM over the winter season results in a very short period in which the BEAM measures of chl-a fall outside of the band of chl-a simulated by WQSAM.

Figure 4.34 shows the results of the analysis for Kwena Dam. It is first of all evident that algal biomass and corresponding chl-a concentrations are lower in this dam as compared to the Loskop Dam. The remote sensing estimates of chl-a by BEAM once again fall within the uncertainty band of chl-a produced by WQSAM by converting simulations of algal biomass into chl-a concentrations. Similar to the case of the Loskop Dam, the season trend of chl-a produced by WQSAM is much more pronounced as compared to that by the BEAM measures, with a sharp drop in chl-a over winter as generated by WQSAM not replicated by the BEAM measures.

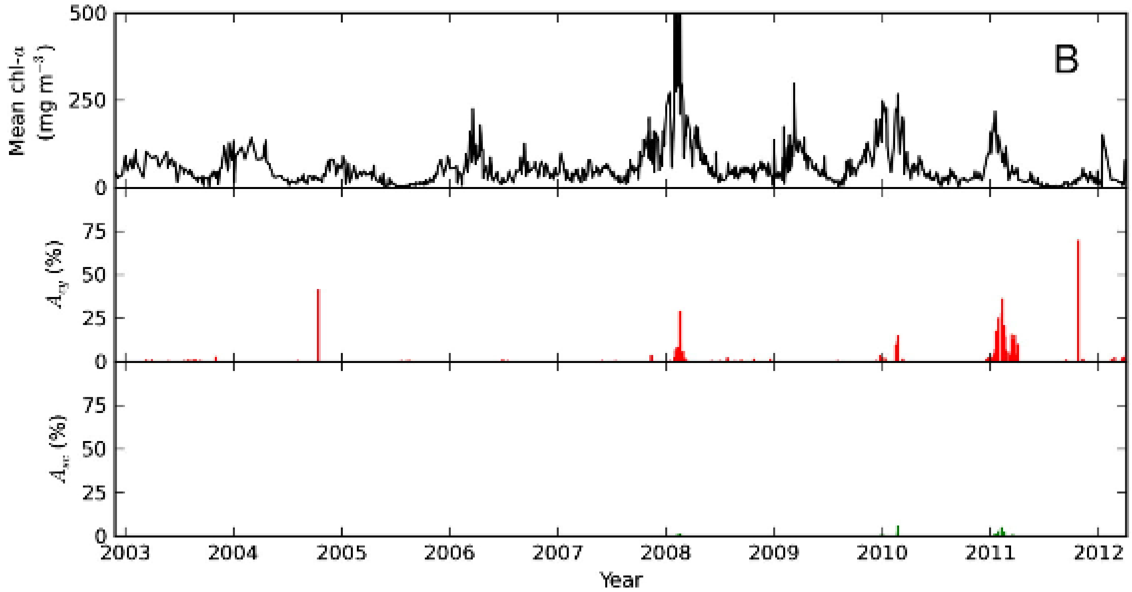

Figure 4.32 Figure 2 from Matthews (2014). Only the top graph is of relevance to this chapter.

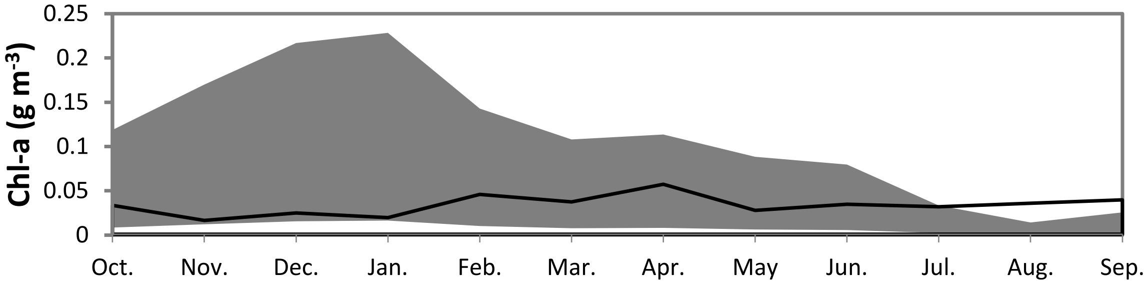

Figure 4.33 Seasonal distribution of chl-a within Loskop Dam. Solid line – chl-a for 2004 as measured by the BEAM remote sensing technology; grey band – estimates of chl-a by converting simulations of the seasonal distribution of algal biomass by the Water Quality Systems Assessment Model (WQSAM) for the years 1920-2003 to estimates of chl-a concentration using the relationships by Kasprzak *et al*. (2008), with the lower bounds equating to 0.18% chl-a: algal biomass and the upper bounds equating to 2.5% chl-a: algal biomass.

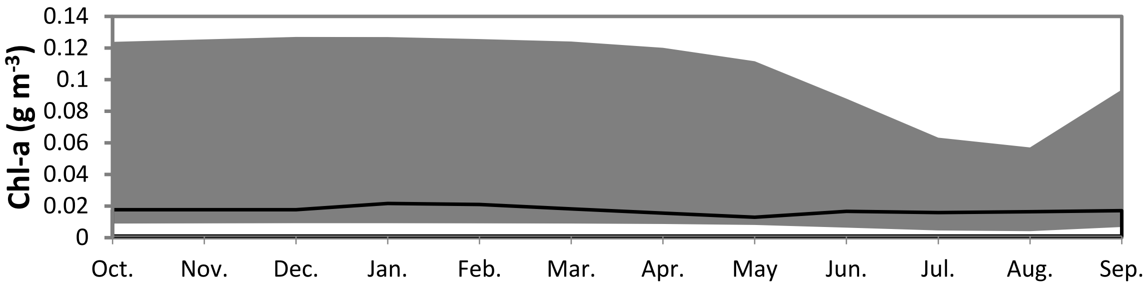

Figure 4.34 Seasonal distribution of chl-a within Kwena Dam. Solid line – chl-a for 2004 as measured by the BEAM remote sensing technology; grey band – simulations of chl-a by converting estimates of the seasonal distribution of algal biomass by the Water Quality Systems Assessment Model (WQSAM) for the years 1954-2003 to estimates of chl-a concentration using the relationships by Kasprzak *et al.* (2008) with the lower bounds equating to 0.18% chl-a: algal biomass and the upper bounds equating to 2.5% chl-a: algal biomass.

Discussion of the results for the Loskop and Kwena dams

The results show that WQSAM is producing simulations of algal biomass that are within the correct range for the equivalent measures of chl-a measured by the BEAM remote sensing product. However, WQSAM estimates of algal biomass show a much more pronounced seasonal signature as compared to the remote sensing estimates of chl-a. The estimates of chl-a for Loskop Dam using the BEAM product do however show a strong seasonal trend that is more similar to the results of WQSAM from approximately 2008, and it can only be surmised that the remote sensing data prior to 2008 did not allow the seasonal trend to be distinguished.

If the overall strategy of WQSAM is considered, the results obtained within this analysis are in fact reasonable. WQSAM aims to adhere to the principle of requisite simplicity. This is because WQSAM is designed for use within water quality management for South African water resources, for which there are typically very little observed data available. WQSAM has adopted the strategy of modelling the water quality processes that explain the majority of the variation of water quality. The model also aims to simulate the frequency distribution of water quality (which can be related to the risk of exceedance by water resource managers), rather that accurate time series results of water quality. The various water quality processes adopted within WQSAM are therefore relatively simplified as compared to those of more complex water quality models, which could arguably be motivated as necessary so as to use the available observed water quality data, to limit the complexity of the model and the number of parameters, and to avoid equifinality.

In relation to the simulation of algal and hyacinth processes, there are various simplifications within the WQSAM model that are of relevance. First of all, WQSAM simulates all algal taxonomic groups as one generic group, so as to limit the number of parameters in the model as well as the complexity of the model. If is fairly obvious that this simplification is a trade-off on some of the model accuracy. It is generally accepted that different taxonomic groups of algae will show varying growth processes, different nutrient requirements for growth, and different proportions of chl-a. Some of the processes that may differ between algal taxonomic groups that can be directly related to parameters controlling processes modelled in WQSAM include:

1. Parameters specifying the proportions of nitrogen and phosphorus within algal biomass.

2. The temperature parameters related to algal growth: the minimum, maximum and optimal temperatures for growth (see Slaughter *et al*., 2015a).
3. The parameters directly related to growth: the respiration, growth and mortality rates.
4. The parameters related to algal size, such as the algal settling rate.
5. The parameters related to nutrient uptake, such as the algal ammonium preference rate (some algae absorb ammonium in preference to nitrate/nitrite).

The other major simplification of WQSAM that is of relevance to algal growth simulations is that stratification of reservoirs is not simulated within WQSAM. This means that some of the more complex associations between water temperature and nutrient turnover within reservoirs associated with the breakdown of stratification are not considered within WQSAM. Instead, WQSAM models reservoirs as completely stirred tank reactors (CSTRs), and water temperature is modelled according to a simple multiple linear regression relationship with air temperature (see Slaughter *et al*., 2015). The effect of complex stratification can in fact be seen in the comparison of model simulated water temperatures with observed water temperatures, for example for Laing Dam, where the observed data appear to show a spike in water temperature during winter, possibly related to reservoir turnover with the breakdown of stratification. The observed seasonal distribution of water temperature in Laing Dam also shows a temperature minimum that is not in step with that of the simulated water temperature, occurring approximately three months later than that of the simulated water temperature. This discrepancy between the model and observed data could affect the growth processes of algae, with the model algal minimum (associated with water temperature) slightly out of sync with that of the actual algal growth. Reservoir turnover may also have pronounced effects on algal growth, with reservoir turnover causing a breakdown of stratification, which may introduce bottom nutrients into the surface layers which may be beneficial to algal growth, whereas this may be disadvantageous for heavy algae which may sink.

Although the WQSAM model adopts various simplifications that may affect model accuracy within the simulations of algal biomass, the relationship between algal biomass and chl-a is also variable and uncertain, as mentioned previously, and depends on the trophic status of the lake/impoundment, the season, the taxonomic composition of the algal community and the size frequency distribution of the algal cells (Felip and Catalan, 2000; Kasprzak *et al*., 2008). In addition, it has also been noted that the chl-a content per unit biomass of algae decreases as algal biomass increases. There are also uncertainties related to the remote sensing measures of chl-a. The analysis adopted in this chapter show that the BEAM remote sensing measures of chl-a show very little seasonal effect on chl-a as compared to the WQSAM estimates of algal biomass, with the model showing a very pronounced summer peak and a winter minimum, whereas the chl-a measures by BEAM are relatively constant. It generally makes sense that the algal maximum would occur during summer, given the generally accepted relationship between water temperature and algal growth. Therefore, one could assume that the seasonal pattern of algal growth is reasonable. The fact that the remote sensing measures of chl-a do not pick up a similar seasonal distribution may be due to inaccuracies in the remote sensing measures, or it could be due to the variable relationship between algal biomass and chl-a mentioned earlier. The measurement of chl-a by Matthews (2014) using the BEAM product do in fact show a strong seasonal trend from approximately 2008.

Validation of simulations of hyacinth growth by WQSAM using remote sensing estimates of hyacinth coverage

As mentioned in previously in this chapter, Landsat 8 data closest to 2013 and 2014 were compared to Google Earth images of Laing Dam so as to assess which band ratios in Landsat 8 could better distinguish the presence of hyacinth. It was found that the NIR to red band ratio performs better than the blue to green ratio. The NIR to red band ratio showed hyacinth coverage to the north and east sides of the dam. The coverage to the north of the dam appears to be high over March and April and slightly reduced over the rest of the year.

It is impossible to attempt a quantitative validation of WQSAM simulations of hyacinth growth using these data, whereas the qualitative validation of WQSAM possible using these data is limited. The model simulations of hyacinth growth by WQSAM show hyacinth coverage throughout the year, with a peak in January and April, and a minimum in October. The results by WQSAM are validated by the Landsat remote sensing data on two limited fronts: 1) both the remote sensing data and the WQSAM simulations show hyacinth coverage throughout the year and; 2) both the landsat data and the WQSAM simulations show a peak over March/April. The seasonal distribution of hyacinth coverage is most likely related to nutrient availability in the reservoir. Laing Dam is known as a nutrient sink, and it appears that a decreasing input of nutrients between April and October that may be related to decreasing flow may cause a decreasing coverage of hyacinth.

4.2.4 Conclusions

The validation of algal and hyacinth growth simulated by WQSAM by remote sensing measures achieved within this chapter was limited. However, given the uncertainties within WQSAM (which are as a consequence of the requisite simplicity approach taken), within the remote sensing data and within the relationship between algal biomass and chl-a, the validation results obtained can be argued to be reasonable. It can be argued that given the uncertainties, a direct and accurate correlation between WQSAM estimates of primary production within reservoirs and remote sensing estimates of primary production was never going to be possible. However, this chapter has shown that the estimates of algal biomass by WQSAM are within the right range. This chapter has also shown that the simulations of hyacinth coverage over the entire year are reasonable, and show that the seasonality of maximum hyacinth growth is correct.

Given that WQSAM was not designed to accurate simulate algal and hyacinth growth (these processes were only included in relation to their effect on nutrient concentrations), and the focus of the model on requisite simplicity, it can be argued that WQSAM has achieved simulations of algal and hyacinth growth that are of sufficient accuracy for water quality management of nutrients in South Africa. More specific water quality management that would require estimates of the taxonomic composition of the algal community (for example, in the case of toxic algae), or a scientific study requiring accurate estimates of hyacinth biomass and coverage within a reservoir may require a more complex model, such as the CE-QUAL-W2 model (Cole and Wells, 2008). Further validation of the primary production processes simulated within the WQSAM model may become possible as further observed data become available.

CHAPTER 5. DEVELOPMENT AND TESTING OF THE WQSED MODEL

5.1 Introduction

Soil erosion is one of the most critical environmental issues globally and in southern Africa. In the context of the present study, erosion is the term used to describe the loss of topsoil, which in turn often affects the productivity of agricultural lands, resulting in a decline of crop yields, and depending on sediment transport, can result in the deposition of sediment in reservoirs, thereby decreasing reservoir volumes (Kusimi *et al*., 2008). Soil erosion is essentially a process of detachment and transportation of soil materials by wind or water. The process of raindrops making impact with soil loosens the soil particles, and even on a 2% slope, this can initiate the movement of soil downhill. The impact of soil erosion is increased on slopes, where there is a positive relationship between the degree of slope and the amount of topsoil transported as water flows downhill into valleys and streams (Pimentel and Burgess, 2013). Topography is one of the most important drivers of erosion as it accelerates the rate of erosion and sediment transport. Although 25% of SA is susceptible to wind erosion (Hoffman & Todd, 2000), water is the dominant agent causing erosion in southern Africa. Water erosion occurs mostly through detachment of soil by rain-splash, sheet erosion as well as rill and gully erosion where concentrated flows incise through the soil surface. During water erosion, outcomes such as the amount of soil eroded, transported and delivered at the outlet of channels depends on a combination of factors such as rainfall erosivity, soil erodibility, slope steepness and slope length, crop management and support practice factor (Le Roux *et al*., 2008).

Among water erosion processes, gully erosion contributes more to sedimentation than related water erosion processes (Zhu, 2012). Gullied systems are characterised by unstable walls and unconsolidated soils which readily erode and wash away when exposed to rainfall. Catchments containing gulley systems are therefore likely to produce more sediments (Wasson, 1994; Zhu, 2012). According to Poesen *et al*. (2002), sediment yield data collected in different parts of the world show that soil loss caused by gully erosion ranges between 10-94% of total sediment yield caused by water erosion. Wasson (1994) found that there is a positive relationship between high sediment yield and steep gullied upland basins. Gullies can therefore be referred to as sediment production zones as they contribute a lot of sediment to streams. According to Poesen *et al*. (2005), the former Transkei region was faced by a dramatic increase in livestock during the 20th century as a result of the Apartheid system. This development led to a drastic loss of vegetation cover as land use patterns changed as a result of the growing human and livestock populations. This resulted in the concentration of cattle and human activities along footpaths and animal tracks, with rainwater increasingly filtering deep into the soil layers, and subsequent sub-surface erosion increased the rates of gully formation (Poesen *et al*., 2005). This is evidenced by the heavily gullied catchments in the former Transkei such as the Umzimvubu River Catchment. Field-based evidence by Poesen *et al*. (2002) suggest that sheet and rill erosion processes as measured on runoff plots are not realistic indicators of total catchment erosion, nor do they satisfactorily indicate the redistribution of eroded soil within a field. It is through gully erosion that a large fraction of soil eroded within a catchment is redistributed and delivered to watercourses (Le Roux *et al*., 2014).

The repeated loss of fertile topsoil negatively affects the long-term sustainability of natural systems. Much of the agricultural land across the world has either been lost or is rapidly experiencing degradation as a result of soil erosion. According to Arekhi *et al*. (2012), close to 40% of the world's agricultural land is degraded, including 65% in Africa and 74% and 45% for North and South America, respectively. Notable is that soil loss by erosion is an ongoing process; it was earlier reported by Dudal (1981) that globally, approximately 6,000,000 ha of fertile topsoil is lost every year as a result of soil erosion and related factors (Arekhi *et al*., 2012). A major concern lies in that most of the soil being lost from agricultural land is transported into rivers and reservoirs. According to Kusimi *et al*. (2008), soil erosion in southern Africa is associated with reservoir sedimentation.

The problem of reservoir sedimentation is not only a contemporary issue, but has evolved over the years. According to Rooseboom and Lotriet (1992), reservoir sedimentation was first identified as a serious problem in South Africa during 1901 when the Camperdown Dam rapidly suffered a loss in storage capacity as a result of sedimentation. This led to many studies being conducted to understand and quantify reservoir sedimentation as a step towards sustainable catchment management, and consequently these studies have contributed to erosion data in the form of erosion risk maps and reservoir sedimentation rates (Rooseboom and Lotriet, 1992). According to Msadala *et al*. (2010a), the mean loss of storage in reservoirs in SA due to sedimentation is 0.4%, which is half of the global average; however, 25% of the assessed reservoirs lost between 10-30% of their initial storage. A major challenge exists in connecting these sediment yields in reservoirs to catchment erosion and sediment delivery data (Boardman, 2012), as a large amount of variability over both temporal and spatial scales exists. Erosion rates may vary with soil type, slope angle and vegetation cover, with connectivity complicating the association of sediment yield observed at the outlet with erosion rates within the entire catchment (Bryson, 2015; Le Roux *et al*., 2008).

5.2 Literature review

5.2.1 Factors influencing soil erosion

Soil loss through erosion is influenced by a variety of factors, with the most important being erosivity of the eroding agent, the erodibility of the soil, the slope of the land and the nature of the plant cover (Morgan, 2005). The eroding agent essentially refers to eroding forces such as water and wind. However, the current study focuses only on erosion by water, even though wind erosion is also significant. The above factors are also highlighted by Wischmeier and Smith (1978) and incorporated into the Universal Soil Loss Equation (USLE):

$$A = RKLSCP, \qquad \text{(Equation 5.1)}$$

where A represents the computed soil loss per unit area, R is rainfall, K is soil erodibility, LS is slope length, C is vegetation cover and P is the support practice factor (Wischmeier and Smith, 1978). A comprehensive discussion on the effect of these factors on erosion is presented by Morgan (2005) and Renard *et al*. (1997).

Rainfall

Soil loss is closely related to rainfall, partly through raindrops striking the soil surface and detaching soil and mostly through the contribution of precipitation to runoff (Pimentel and Burgess, 2013). This applies particularly to erosion by overland flow and rills, where rainfall intensity is generally the most important characteristic driving erosion. A study conducted in Ohio between 1934 and1942 showed that average soil loss per precipitation event increases with the intensity of the storm (Morgan, 2005). This promoted the initial theory that significant erosion is solely a function of peak intensities. However, through 30 years of measurements by Wischmeier (1962) in several states in the United States of America (USA), it was shown that the rainfall factor used to estimate average annual soil loss must include cumulative effects of the many moderate sized storms, as well as the sporadic severe storms (Renard *et al*., 1997). This justifies the use of a complete rainfall time series in an erosion estimation model.

However, a need to highlight the threshold flow for erosion remains. Hudson (1981) provides a figure based on his studies in Zimbabwe of 25 mm h^{-1}, a value that has also been found appropriate in Tanzania and Malaysia, and applicable to semi-arid catchments that characterise Sub-Saharan Africa (Morgan, 1974). However, this value is too high for applicability to Western Europe, where it is rarely exceeded. This illustrates that models developed for use in a different climatic and geographical setting may not be appropriate for universal application. Arbitrary thresholds of 10, 6 and even 1.0 mm h^{-1} have been used in England, Germany and Belgium, respectively (Renard *et al*., 1997).

Erodibility

According to Renard *et al*. (1997), soil erodibility is the average long-term soil and soil profile response to the erosive power of rainstorms. Soil erodibility is therefore a lumped parameter that represents an integrated average annual value of the total soil and soil profile reaction to a large number of erosion and hydrologic processes (Tingting *et al*., 2008). Erodibility defines the resistance of the soil to both detachment and transport. Although the resistance of soil to erosion depends in part on topographic position, slope steepness and the amount of physical disturbance, such as during tillage, the properties of the soil are the most important determinants (Tya & Oluwaseye, 2015). Erodibility varies with soil texture, aggregate stability, shear strength, infiltration capacity and organic and chemical content (Renard *et al*., 1997). Large particles are resistant to transport because of the greater force required for entrainment and fine particles are resistant to detachment because of their cohesiveness (Renard *et al*., 1997). The least resistant particles are silt and fine sands. Thus, soils with silt content above 40% are highly erodible (Richter and Negendank, 1977). Evans (1980) examined erodibility in terms of clay content, and found that soils with clay content between 9-30% are the most susceptible to erosion. High soil erodibility is usually observed at lower elevations where soil structure profiles are more defined and soils are much deeper. This also assumes that catchments located in gentle plateau areas have higher erodibility.

Vegetation cover

Vegetation acts as a protective layer or buffer against the force of raindrops between the atmosphere and the soil. The leaves and stems of plants absorb some of the energy of falling raindrops and running water, resulting in less force directed at the soil, whereas the root system contributes to the mechanical strength of the soil (Morgan, 2005). Interdependency is therefore established between the vegetation cover and soil erodibility, where the cover increases the soil's resistance to erosion, termed erodibility.

An experiment demonstrating the effect of vegetation cover known as the mosquito gauze experiment was conducted by Hudson and Jackson (1959). Soil loss was measured from two identical bare plots on a clay loam soil. Over one plot, a fine wire gauze was suspended, which had the effect of breaking up the force of the raindrops, absorbing their impact and allowing the water to fall to the ground from a low height as a fine spray; the mean annual soil loss over a ten-year period was 126.6 t ha^{-1} for the open plot and 0.9 t ha^{-1} for the plot covered by gauze (Morgan, 2005). There is therefore a very significant effect of vegetation on lowering erosion rates. Figure 5.1 demonstrates the relationship between the soil loss ratio (SLR) and vegetation cover:

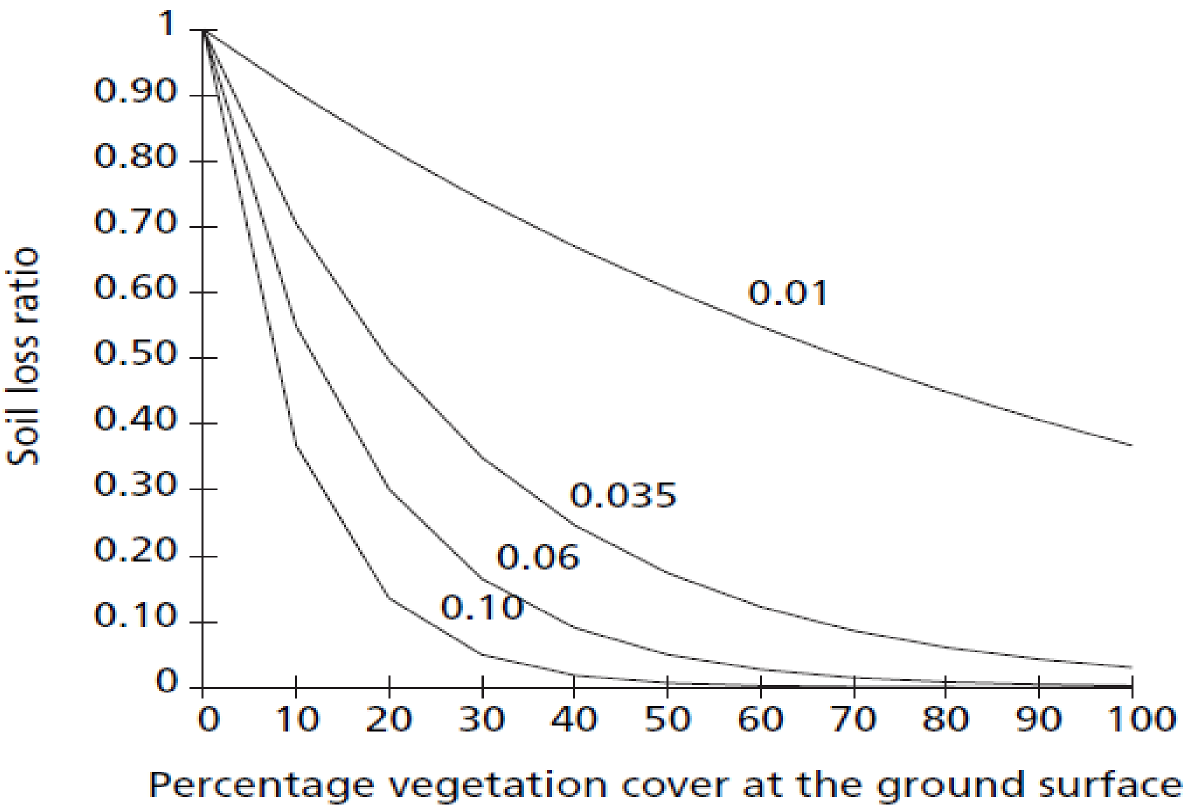

Figure 5.1 Relationship between soil loss ratio (SLR) and percentage vegetation cover at the ground surface. Taken from Morgan (2005).

Figure 5.1, taken from Morgan (2005), illustrates that a lower percentage ground cover is associated with high rates of soil loss, whereas in contrast, a higher percentage of cover is associated with lower rates of soil loss. Overall, it is generally recognised that for adequate protection, at least 70% of the ground surface must be covered (Elwell and Stocking, 1976), although reasonable protection can sometimes be achieved with between 30-40% cover (Morgan, 2005). However, Morgan (2005) also warns that the effects of vegetation are far from straightforward, and under certain conditions, plant cover can exacerbate erosion, depending on how cover interacts with the erosion processes. Therefore, the vegetation canopy can potentially protect the soil from rain splash, whereas plant roots bind the soil together to prevent soil from being washed away. Notable is that there is a high level of interaction between all the erosion factors.

Topography

According to Renard *et al*. (1997), erosion increases as slope increases, and is considered as the *LS* factor in the Modified USLE (MUSLE). Slope length *L* is defined as the horizontal distance from the origin of overland flow to the point where either: 1) the slope gradient decreases to a sufficient extent to initiate deposition or; 2) runoff becomes concentrated in a defined channel (Wischmeier and Smith, 1978). Slope steepness *S* reflects the influence of slope gradient on erosion (Renard *et al*., 1997). Slope has been estimated in the field using an inclinometer and other related devices, as well as using contour intervals. Digital Elevation Model (DEM) and GIS techniques are now popularly used to obtain both slope gradient (*S*) and slope length (*L*) (Wolka *et al*., 2015).

Morgan (2005) stressed that erosion would normally be expected to increase with increases in slope steepness and slope length as a result of respective increases in velocity and volume of surface runoff. The combined interactive effects of erosion factors act to erode a given land surface (Bryson, 2015). Vegetation and soil erodibility increase downslope whereas orographic rainfall increases with elevation (Bryson, 2015). Furthermore, although raindrops splash soil particles randomly in all directions on a flat surface, on sloping ground, more soil is splashed downslope than upslope, and the proportion increases as the slope steepens. Slope length and steepness therefore contribute to soil erosion by increasing the velocity of runoff; thus the erosive and transport capacity of surface runoff is subsequently enhanced.

5.2.2 Erosion and sediment yield model

Erosion models have evolved as important tools to measure and predict catchment erosion. According to Xu (2002), most hydrologic systems are extremely complex, and we cannot hope to understand all their detail. Therefore, is important to use models to simplify, explain and investigate complex natural processes, as this facilitates the investigation of management scenarios. Soil erosion models are essential for catchment management; not only do they increase our understanding of complex natural systems, but they also facilitate the development of sound catchment management principles. Models are used to simulate natural systems, thereby saving time and cost, as at times it is not feasible or practical to conduct field measurements over a large spatial extent or fine temporal resolution (Nearing *et al*., 2005).

Numerical models are very useful tools for the estimation of erosion and sediment yield from a watershed, as well as for the analysis of land use impacts on sediment generation (Schmidt *et al*., 2008). The ability to model soil erosion and sediment yield is essential for facilitating management to reduce sedimentation rates of reservoirs, as models provide simulations of erosion and sediments yields that can be used to control the rates of sedimentation. According to Msadala *et al*. (2010), this is mostly achieved using spatially distributed models to provide spatially distributed information on erosion and sediment yield at a catchment scale. This information is used by water managers to not only determine control measures, but also to prioritise problems areas so as to effectively allocate scarce financial resources, characteristic of most countries in southern Africa. However, the effectiveness of soil erosion modelling is hindered by various problems such as data variability, over-parameterisation, unrealistic input requirements and unsuitability of model assumptions or misleading parameter values in a local context, and the lack of verification data (Le Roux *et al*., 2007). According to Le Roux *et al*. (2007), recent assessments on the quality of erosion models have demonstrated that the available models are not effectively predicting the spatiality of erosion. Therefore, the quantity of erosion predicted by models cannot be regarded as absolute erosion figures due to the high degree of uncertainty. However, it is essential to note that patterns of erosion quantities predicted by models are useful to provide direction in management scenarios. This requires the continuous development of models through improvement in parameter estimation, comprehensive testing and validation of new models.

At the catchment scale, a significant amount of sediment that is produced originates from the higher slopes. The proportion of sediment load in streams is therefore determined by the erosion on the slopes and the availability of rain for energy to deliver the sediment into streams (Gao, 2008). The emergence of computers and related software has made it possible to successfully estimate sediment yield. Notable also is that the increased storage and processing capability of computers has made it possible to describe erosion processes using mathematical equations and to simulate the dynamic nature of natural systems at the catchment scale (Parsons, 2012). Models are differentiated based on the level of complexity represented in soil erosion processes, as well as the spatial and temporal resolution of the model (Le Roux *et al*., 2007).

Historically, models representing soil erosion by water have been either physically-based, empirically-based or a mix of empirically and physically based (Randle *et al*., 2006). The first soil erosion models were empirically-based. The prime example of the empirically-based model is the USLE (Nearing *et al*., 2005; Wischmeier and Smith, 1978). Models can also be classified as conceptual (Le Roux *et al*., 2007). Models are classified based on the hydrological processes that are represented. Parameters used in the physically-based models are determined using field data and should be representative of conditions and physical characteristics of the catchment (Msadala *et al*., 2010).

Physically-based models can represent the catchment as either lumped or distributed. Empirically-based models are developed using physical catchment properties that are determined from field data collected or from other spatial data sources such as aerial and satellite imagery. These data are collected for particular and specific geographic areas; therefore, for the achievement of optimum results, the equations developed should be limited to areas for which the data were collected (Randle *et al*., 2006). Conceptual models are differentiated from empirical models in that they lump or aggregate representative processes over the scale at which outputs are simulated (Wheater *et al*., 1993); however, they incorporate important transfer mechanisms of sediment and runoff generation in their structure (Merritt *et al*., 2003). Conceptual models primarily use simplified deterministic representations of the processes governing soil erosion and sediment delivery, including a hydrological module and an empirical sediment module (Van Zyl, 2007).

Physically-based models

Physically-based models are characterised by a much more sophisticated model structure than either empirical or conceptual models, and are based on the solution of physical equations describing mass and momentum of flow and sediment transport in a catchment (Merritt *et al*., 2003). According to Le Roux (2008), physically-based models are usually spatially distributed and event-based so as to simulate the response of a given area to a rainfall event. Physically-based models are based on the interrelationships of factors governing both erosion and sediment yield; therefore, the physical and theoretical processes that control erosion and sediment yield are both represented in physically-based models (Msadala *et al*., 2010). Physically-based models are able to simulate erosion and sediment yield at various spatial and temporal scales (Msadala *et al*., 2010). These models provide a detailed description of the flow and transport processes that are involved in erosion and sediment yield at various spatial and temporal scales. Some physically-based models include:

- The Areal Non-point Source Watershed Environmental Response Simulation (ANSWERS) (Beasley *et al*., 1980).
- The Hydrological Simulation Programme – Fortran (HSPF) (Bicknell *et al*., 1997).
- Chemicals, Runoff, and Erosion from Agricultural Management Systems (CREAMS) (Kinsel, 1980).
- The European Soil Erosion Model (EUROSEM) (Morgan *et al*., 1998).
- The Kinematic Runoff and Erosion model (KINEROS) (Woolhiser *et al*., 1990).

Mhangara (2011) outlines how physically-based models represent a combination of the individual components and mechanisms controlling soil erosion; they take account of complex interactions between several factors and the associated spatial and temporal variability. The application of these models is limited because of their large data and computation requirements (Mhangara, 2011).

Empirically-based models

Empirical models are based on observations and inductive logic, and are generally statistical in nature (Msadala *et al*., 2010). The parameters for empirical models require calibration, and examples include the USLE. The USLE method computes annual soil loss resulting from sheet and rill erosion from a specified area. The USLE model has been the most commonly used model and method of estimating soil erosion since the 1960s (Kinnell, 2000).

Figure 5.2 represents the conceptual structure of the USLE and is taken from Wischmeier and Smith (1978).

Other examples of empirical models are the Revised USLE (RUSLE) and the Modified USLE (MUSLE), which are improvements of the USLE model. The RUSLE computes annual soil loss, and MUSLE proposed in 1972 computes sediment yield for a single storm event (Williams, 1975).

Conceptual models

Conceptual models are typically based on the representation of a catchment as a series of internal storages (Merritt *et al*., 2003). Conceptual models can represent the catchment as a series of grids, with a series of internal storages represented within each grid. Transfer mechanisms of runoff generation and sediment transport are incorporated within the structure to represent flows paths as a series of storages, and the dynamic behaviour of these mechanisms has to be characterised within the model (Merritt *et al*., 2003). Conceptual models usually include a generalised description of catchment processes because detailed catchment processes would require detailed information regarding the catchment, which may not be readily available or may be very difficult to access (Wheater *et al*., 1993). However, generalised descriptions allow the models to estimate the qualitative and quantitative effects of factors such as land use change with minimal data. Traditionally, conceptual models lump representative processes over the scale at which outputs are simulated (Wheater *et al*., 1993). According to Merritt *et al*. (2003), recently developed conceptual models have provided outputs in a spatially-distributed manner, making it easier to identify areas that are more impacted by erosion.

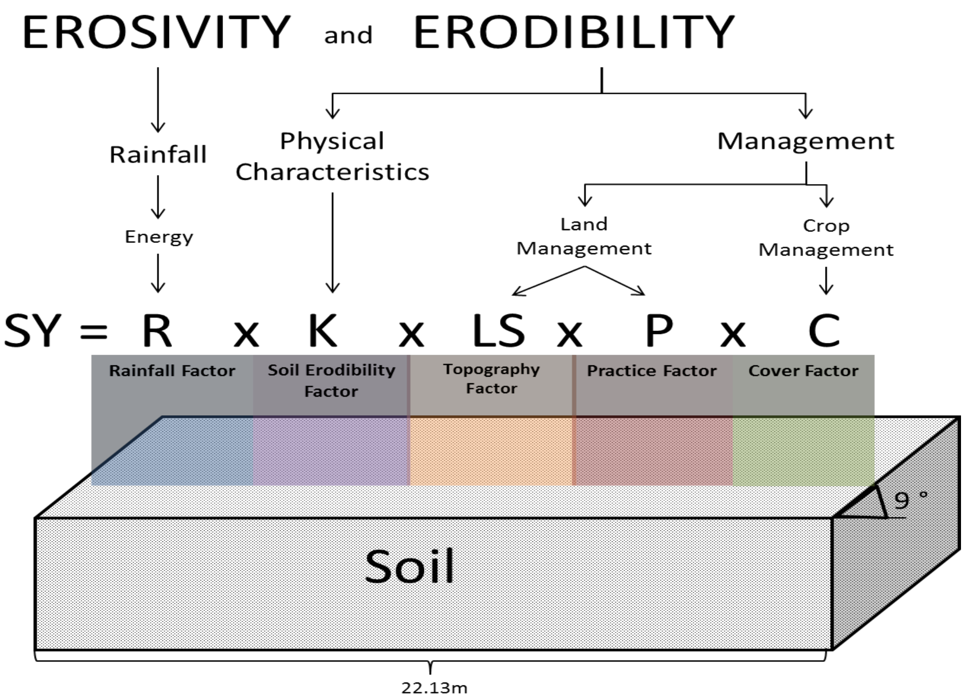

Figure 5.2 The Universal Soil Loss Equation (USLE) accompanied by a conceptualisation of a standard unit plot description adapted from Wischmeier and Smith (1978), and taken from Bryson (2015).

Parameter values for conceptual models are commonly estimated through calibration to observed data such as sediment concentrations and stream discharge data (Merritt *et al*., 2003). The application of conceptual models is often hindered by problems of parameter identification because calibration is required to be performed against observed data, which may not be available; a common problem within southern African catchments (Jakeman and

Hornberger, 1993). Therefore, most forms of calibration techniques used for conceptual models are only able to identify the local optimal parameter values. Problems associated with model identification can be reduced by limiting the number of parameters that are meant to be estimated through calibration (Merritt *et al.*, 2003).

5.2.3 Erosion and sediment yield modelling in South Africa

As erosion is a major environmental issue, information relating to erosion rates, yields and impacts is widely sought after by water managers in South Africa. Bryson (2015) indicates that sediment has long been recognised as one of South Africa's significant water quality problems. For this reason, the Department of Agriculture (DoA) and the Water Research Commission (WRC) have funded many regional-based research projects in the country, as the spatial extent of the problem requires identification. A review of the methodology for monitoring soil erosion in South Africa at a regional scale is presented by Le Roux *et al*. (2007). The authors identified that some of the challenges facing SA with regards to soil erosion research are limited data availability and the fact that not all erosion types occurring in SA are accounted for. This can be seen by the fact that the main approach adopted by researchers in South Africa has been to develop sediment yield maps. Although these maps have provided an important tool in sediment yield prediction, they are not effective at a catchment scale; the scale at which land and resource management is usually required (Bryson, 2015).

Agricultural Catchments Research Unit (ACRU)

The Agricultural Catchments Research Unit (ACRU) hydrological model was originally developed to study catchment evapotranspiration in the then Natal Province during the early 1970s (Schulze, 1989). The ACRU model was developed by the Agricultural Catchments Research Unit within the Department of Agricultural Engineering of the University of Natal in Pietermaritzburg, South Africa (Schulze, 1995). The agrohydrological component of ACRU, which was subsequently added, resulted in the ability of the model to simulate the integration and inter linkage of agrohydrological and hydrological processes related to applied engineering, scientific hydrology and water resources (Schulze, 1995). Sediment yields are modelled using MUSLE in sub-catchments. The rainfall-runoff model then routes the flow and sediment through the catchment. However, the model does not include important sediment storage processes. Problems such as over-parameterisation are significant as parameters may be difficult to determine in data-poor environments. The model user must also prepare a certain amount of data and information before operating the model. The ACRU model is therefore not considered to be an effective sediment delivery model for catchments in SA (Bryson, 2015). Figure 5.3 is a conceptual representation of the components of ACRU.

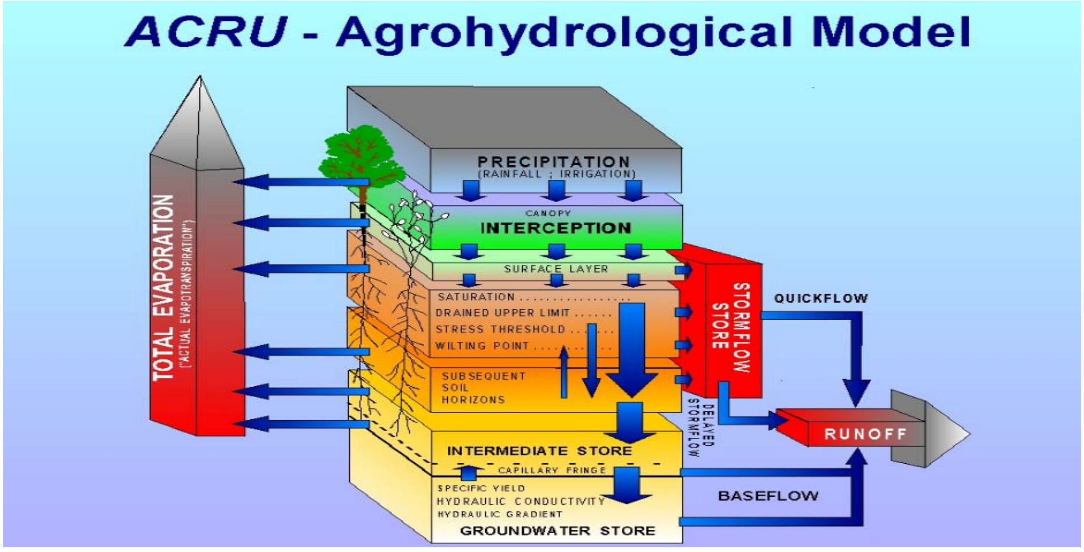

Figure 5.3 The agrohydrological concepts of the Agricultural Catchments Research Unit (ACRU) model (taken from Schulze (1995).

Soil and Water Assessment Tool (SWAT)

An additional model that has been used recently in a study in South Africa is the Soil and Water Assessment Tool (SWAT) (Neitsch *et al*., 2005). SWAT was recently used in a study to determine gully connectivity in a catchment in SA with identified source and sink zones (Le Roux *et al*., 2013). According to Le Roux *et al*. (2013), the model was designed to simulate water, sediment and chemical fluxes in watersheds and large catchments with varying erosion factors such as slope, rainfall, soils and vegetation cover. SWAT is a continuous time-scale model which uses readily-available inputs on soils, land use, topography, drainage and climate to provide outputs on a sub-basin scale. The catchment is divided into sub-basins and hydrological response units (HRUs) are used, which are considered areas within the sub-basin that have a high homogeneity in terms of factors such as land cover, soil and support practice (Le Roux *et al*., 2013). Calculations for the HRUs are conducted separately whereas the outputs are channelled to the catchment outlet so as to quantify total basin loads. A major weakness identified in the SWAT model was that it does not consider that sediment is deposited along the way during transport from slopes to the channels (Le Roux *et al*., 2013).

SHETRAN

An additional model that has been used recently in a study in South Africa is SHETRAN. This is a very effective model for modelling subsurface flow and transport (Ewen *et al*., 2000). SHETRAN was used to estimate sediment yield for the Polihali Dam catchment by Msadala *et al*. (2010). The SHETRAN model uses a grid network to describe the catchment areas and links as river networks. It is a three dimensional model that possesses a column of horizontal layers underlying each grid square in the vertical direction within each soil layer representing soil thickness, and the upper layer represents the overland surface. Flow is routed from the surface, subsurface and up to the channel or gullies (Ewen *et al*., 2000). The overall assessment of SHETRAN is that the user must be able to prepare and generate a certain amount of data independently before applying it in the modelling system; the authors required approximately five months to determine how to use the modelling system and how to set up and run the model (Msadala *et al*. 2010). The extensive data requirements of the model result in the unsuitability of the model for data-scarce environments, whereas the time required for professional researchers to sufficiently learn how to use the model results in the model being less applicable for water managers in SA.

The Pitman model

The Pitman model has been the most widely applied hydrological model within the southern African region (Hughes *et al*., 2006). This model was developed in the 1970s

(Pitman, 1973) as an explicit soil moisture accounting model, representing interception, soil moisture and groundwater storages, with functions to represent the inflows and outflows (Hughes, 2008). The Institute for Water Research (IWR) at Rhodes University has added a number of refinements based on assessments of the southern African Flow Regimes by the International Experimental and Network Data (FRIEND) programme (Hughes, 1995), and subsequently have also added more explicit groundwater recharge and discharge functions. An advantage of the Pitman Model is the availability of guidelines for parameter estimation provided by the WR90 study (Midgley *et al*., 1994). The guidelines can be used to establish initial parameter values for almost any climatic region of southern Africa, which can then be refined through local calibration (Hughes, 2008). Linking the sediment delivery model with the Pitman Model would be useful, as the Pitman Model represents a hydrological model that has proven to be effective and widely applied in semi-arid South African catchments.

In the current study, the Pitman Model was used to derive the surface flow component of the Erosion and Sediment Delivery Model, because of its wide popularity in southern Africa. Using existing and established hydrological models increases the likelihood of use by water resource managers and ensures that already established routines would not need to be redeveloped (Slaughter *et al*., 2011). The modelled sediment delivery results are therefore partly dependent upon the accuracy (or representativeness) of the flow simulations generated by the Pitman Model and the daily disaggregation model (Bryson, 2015). Figure 5.4 shows the conceptual structure of the Pitman Model as contained in the SPATSIM modelling framework.

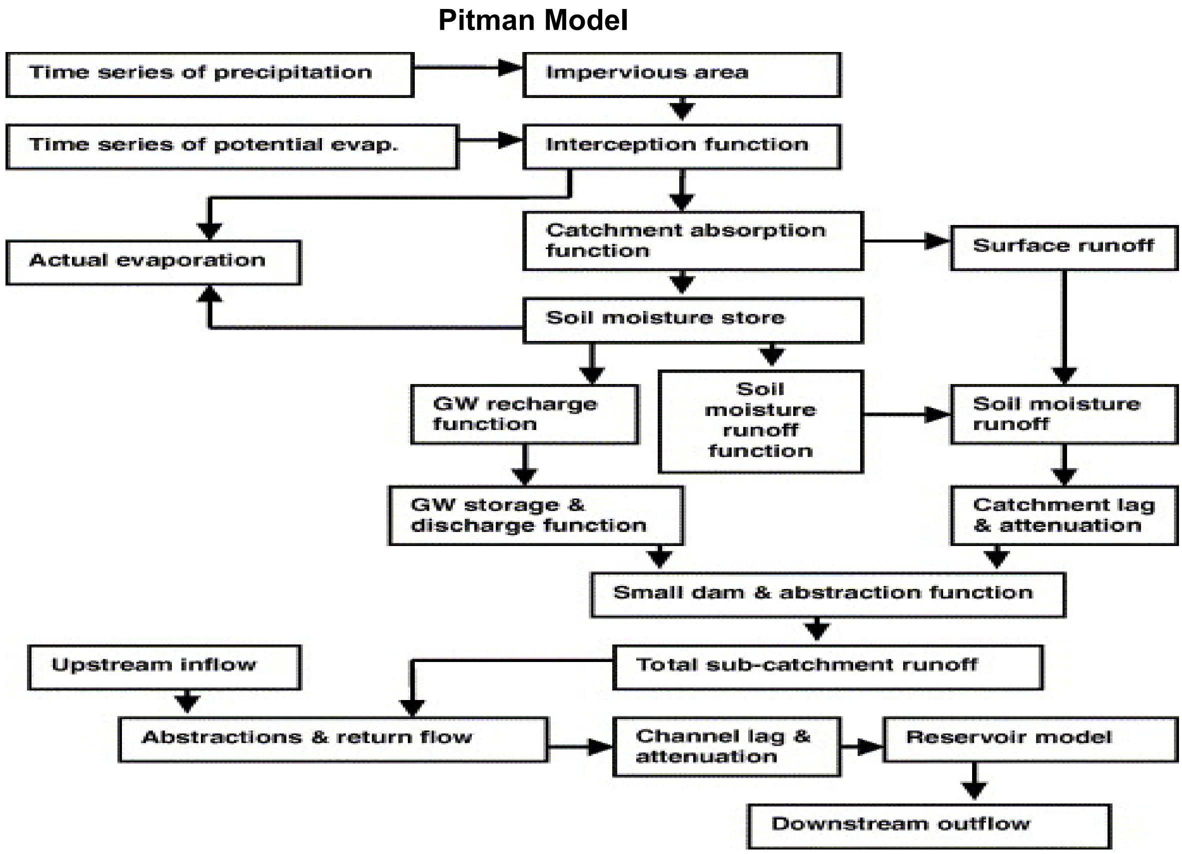

Figure 5.4 Flow diagram showing the main components of the Spatial and Time Series Information Modelling (SPATSIM) version of the Pitman Model (Hughes *et al*., 2006)

According to Bryson (2015), established hydrological models, such as the Pitman Rainfall Runoff Model, act on a monthly time step; however, rainfall events in semi-arid areas are generally in the form of high-intensity, short-duration storms. The output of the Pitman Model is disaggregated to a daily time step to represent surface runoff in semi-arid catchments. This process has already been developed as part of a water quality model that has been linked to existing water resources estimation methods (Hughes and Slaughter, 2015; Slaughter *et al.*, 2011; Slaughter *et al.*, 2015a). The method followed the principles established by Smakhtin and Masse (2000) and includes an approach that separates total daily flow into surface, interflow and groundwater components. These are important for the overall water quality model and are also highly relevant for the sediment model, as quantification of these flow components is important to distinguish between surface flow that could generate slope sediment delivery and other flows that might be more important for within-channel sediment transport (Bryson, 2015).

The MUSLE model

The MUSLE is an improvement of the USLE developed by Wischmeier and Smith (1978). The USLE and the revised versions (RUSLE and MUSLE) are among the most widely used erosion and sediment models, used to compute potential erosion and sediment yield in hydrology and environmental engineering fields (Mishra *et al.*, 2006). The USLE was originally conceived to estimate the rate of soil loss from small plots. Subsequently, when applied to larger spatial scales, the USLE gave large errors (Kinnell, 2005). The USLE does not take into account runoff, although the erosion process involves sediment being discharged with flow; runoff is an important determinant of both erosion and transport (Kinnell, 2005). It has been observed that delivery ratios to determine sediment yield from the soil loss equation can be predicted accurately; however, these ratios vary considerably (Arekhi *et al.*, 2012). As a result of uncertainty surrounding the delivery ratio, Williams and Berndt (1977) proposed the MUSLE with the replacement of the rainfall factor with a runoff factor. The MUSLE increases the accuracy of sediment yield prediction by incorporating flows, and also eliminates the requirement for delivery ratios (Arekhi *et al.*, 2012).

According to Sadeghi *et al.* (2013), combining the sediment delivery ratio (SDR) with gross erosion to determine sediment yield is tedious if one is interested in particular rainfall events. The rainfall factor of the USLE does not effectively account for the effective rainfall that generates sufficient runoff to mobilise sediment, which is an important factor in erosion and sediment delivery (Sadeghi *et al.*, 2014). Williams (1975) used 778 storm-runoff events collected from 18 small watersheds, with areas varying from 15 to 1,500 ha, slopes from 0.9 to 5.9% and slope lengths of 78.64 to 173.74 m (Williams and Berndt, 1977). The Modified USLE (MUSLE) model was given in the general form of:

$Sy = a\ (Qqp)\ LSCP$, (Equation 5.2)

where *Sy* is sediment yield (in tonnes) on a storm basis for the entire catchment, *Q* is volume of runoff (in m^3), *qp* is the peak flow rate (in $m^3\ s^{-1}$) and *K*, *L*, *S* and *P* are the soil erodibility (in t ha h $MJ^{-1}\ mm^{-1}$), slope length, slope steepness, crop management and soil erosion control practice factors, respectively, similar to the USLE model, and *a* and *b* are location coefficients. For the area where the equation was developed, the *a* and *b* coefficients were 11.8 and 0.56, respectively (Williams and Berndt, 1977).

A review of the international application of the MUSLE model has been presented by Sadeghi *et al.* (2014) to evaluate the applicable conditions and methods used to determine the MUSLE model parameters. The trends in the methodology to determine the factors in the MUSLE model indicated that for the erodibility factor, most values were obtained by using the Wischmeier and Smith (1978) diagrams, with the erodibility estimation methodology not affecting the accuracy of results. The topography factor was estimated by the direct use of a topographic map at a scale of 1:50,000 in most studies, with the use of GIS providing an improved performance of model estimates. Crop management and control practice factors were mainly estimated by using existing data, with the incorporation of temporal variation of these factors resulting in significant improvements in performance. Sadeghi *et al.* (2014) concluded that application of the MUSLE model may provide reasonable results when applied under appropriate conditions similar to those of the original model, or when the model factors are calibrated accordingly.

According to Nearing and Hairsine (2011), the popularity of the MUSLE model emanates from its ease of use in a GIS, in particular the ease of deriving the topography (*LS*) factor from a DEM. In addition, the availability of remote sensing images for determining vegetation cover has added to the popularity of the MUSLE. The MUSLE has been previously and recently used in many studies (Arekhi *et al*., 2012; Bryson, 2015; Jang *et al*., 2015; Sadeghi and Mizuyama, 2007). Notable also is that Tripathi *et al*. (2001) used the MUSLE and GIS in India, and obtained estimated values close to observed values. Meanwhile, Bryson (2015) has applied the MUSLE in South Africa and reported that the model had managed to characterise the dynamics of erosion and sediment for arid catchments in SA. From the literature, it is evident that the MUSLE is a rationally efficient model for estimating sediment yield.

A central model for the current study is the erosion and sediment delivery model for semi-arid catchments developed and used by Bryson (2015) under the Institute of Water Research (IWR) at Rhodes University. The author attempted to avoid problems of over-prediction of sediment yield typically associated with empirical models. This was conducted by linking the empirical erosion model to the Pitman Hydrological Model. The MUSLE model was linked to the Pitman Model for the purpose of avoiding over prediction. The model was tested on the Ganora (2.7 km^2), Cranemere (57 km^2) and the Nqweba (3 667.7 km^2) catchments. The results for the two small and one large catchments were as according to Bryson (2015): 'an effective representation of sediment dynamics in semi-arid catchments'. This current study will however further test and validate Bryson's model within catchments with a variety of conditions including soils, climate and vegetation cover. A considerable reduction in the number of parameters required to be parameterised will be achieved through the use of GIS and readily available spatial datasets to estimate the values of these parameters.

5.2.4 Sediment transport modelling

Sediment transport is the movement of organic and inorganic particles by water (Czuba *et al*., 2011). These particles are dislodged from their original surfaces by erosional forces. The amount of sediment transported is dependent on the power of flow (Southard, 2006). Therefore, a channel with a greater velocity is likely to move a greater amount of sediment. The total load that is transported includes bedload, suspended load and washload.

Bedload is the sediment that rolls, slides or bounces along the bed of the channel (EPA, 2012). Some of this sediment may not maintain constant contact with the river bed, but it does not move in suspension either. Its movement is neither uniform nor continuous (Southard, 2006). According to EPA (2012), bedload transport occurs when the force of the water is sufficiently strong to overcome the weight and cohesion of the sediment. The particles are dragged along and move slower than the water around them, as the flow rate is too weak to suspend the sediment. This process occurs at low and high flows for smaller and larger particles, respectively. Up to 20% of sediment that is transported is bedload (Czuba *et al*., 2011).

Suspended load refers to the amount of sediment that is carried downstream within a water column (Southard, 2006). The turbulence that is created by moving water keeps sediment particles suspended above the streambed (Hickin, 1995). The amount and size of particles that can be carried as suspended load is dependent on the rate of flow (Southard, 2006). Czuba *et al*. (2011) state that larger particles will fall to the stream bed unless the flow rate increases turbulence on the streambed.

Washload is generally regarded as part of suspended load (Hickin, 1995). This load is comprised of the fine sediment of sizes less than 0.00195 mm. This load is different from suspended load because it does not settle on the channel bed during periods of low to no flows (Southard, 2006), as the particles remain suspended and bounce off water molecules to remain afloat (Southard, 2006). However wash and suspended loads are barely distinguishable when there is flow. Turbidity in waterbodies is an important indicator of washload (Fink, 2005). However, although turbidity can be used to approximate suspended sediment concentration, it cannot be used to estimate sediment transport of river channels (Fink, 2005).

Sediment transport is a dynamic process that is subject to constant change. Geological formation, geomorphology and organic elements affect the volume and nature of sediment output. However, sediment transport may also be altered by external forces such as changes in water flow, water level, weather elements and anthropogenic controls.

Discharge is identified as the single most important factor/element of sediment transport. Flow is essential for setting sediment in motion and without it, sediment will either settle on the stream bed or remain in suspension (McNally & Mehta, 2004) and not move downstream. Two basic methods to calculate water flow are shown in Equations 5.3 and 5.4:

$$\text{Flow (m}^3\text{ s}^{-1}\text{)} = \text{Area (m}^2\text{)} \times \text{Velocity (m s}^{-1}\text{)} \quad \text{(Equation 5.3)}$$

Or

$$\text{Flow (m3 s}^{-1}\text{)} = \text{Volume (m}^3\text{)} / \text{Time (s)} \quad \text{(Equation 5.4)}$$

The calculations of the relationship between sediment transport and water flow are more complex because of the large number of variables requiring consideration, which include bed geometry, particle size and concentration (Southard, 2006). Multiple forces are active on the sediment, including relative inertia, turbulence and velocity. Although most of these variables will be unknown or not simple to ascertain, they are required as input to the equations describing the relationship between erosion and sediment transport (Southard, 2006). Southard (2006) also states that methods of measurement inevitably alter the reading because they disturb the flow. This makes sediment transport difficult to measure. This challenge has been dealt with by using equations to simplify flow rate and sediment transport scenarios. This method ignores some geomorphological variables and non-uniformity in flows (Southard, 2006).

According to Crone (2004), the two main factors to consider in sediment transport are settling rate and shear stress on the boundary layer. The Stokes settling rate is the rate at which sediment within a liquid settles on the bottom (Crone, 2004), and is controlled by the drag force which maintains the particles in suspension and the gravitational force. This is an important relationship in the determination of forces that have to be overcome for sediment of various particle sizes to be moved. The Stoke settling rate is defined by Equation 5.5:

$$V_s = (g \times (\rho_p - \rho_f) \times D_p^2) / 18\mu \quad \text{(Equation 5.5)}$$

where V_s is the settling velocity, g is the gravitational constant, ρ_p is the particle density, ρ_f is the fluid density, D_p is the particle diameter and μ is the fluid viscosity.

The shear stress explains how much force is required for flow to overcome relative inertia and initiate sediment transport (Crone, 2004), and is defined by Equation 5.6:

$$\tau = \rho_f \times u \times 2, \quad \text{(Equation 5.6)}$$

where τ is shear stress, ρ_f is fluid density and u is the characteristic velocity of turbulent flow (shear velocity).

The characteristic velocity of turbulent flow (u) for river systems is calculated using Equation 5.7 (Crone, 2004):

$$u = \text{Sqrt}\ (g \times h \times s), \quad \text{(Equation 5.7)}$$

where u is shear velocity, g is the gravitational constant, h is the river depth and s is the river slope.

The above equations are important for understanding and identifying the forces that act on sediment in water (Crone, 2004). However, the Shields stress equation can be used to further understand the conditions required for sediment transport. According to Crone (2004), the Shields stress equation and the particle Reynolds number can be used estimate how much flow is required to transport the sediment. The Reynolds particle number essentially expresses particle resistance to viscous force, which is the ability of flow to overcome relative inertia of sediment particles (Benson, 2014). However, the critical point at which water flow begins to move sediment is the Shields shear stress defined by Equation 5.8:

$$\tau_* = \tau / (g \times (\rho_p - \rho_f) \times D_p), \qquad \text{(Equation 5.8)}$$

where τ_* is Shields stress, τ is shear stress, g is the gravitational constant, ρ_p is the particle density, ρ_f is the density of the fluid and D_p is the particle diameter.

The Shields shear stress equation creates an empirical curve, which can be used to determine the size of sediment that can be moved by a particular flow rate (Crone, 2004).

The aforementioned equations (5.3-5.8) are essential for defining minimum flow rates for sediment transport. However, they do not determine actual sediment load and transport rates. Van Rijn developed a sediment transport rate equation for bedload and suspended transport rates (McNally & Mehta, 2004). Suspended load transport rate is defined by Equation 5.9:

$$q_s = u \times h \times ca \times [((a / h)\ Z - (a / h)\ 1.2) / ((1 - a/h)\ Z \times (1.2 - Z))], \qquad \text{(Equation 5.9)}$$

where qs is the suspended load transport rate, u is the average flow velocity, h is the average flow depth, ca is the reference concentration, a is the height above the stream bed, relative to particle size and Z is the suspension number.

The construction of dams and land cover/use changes affect the nature and quantity of sediment load as well as the river's ability to transport sediment (Czuba *et al*., 2011). Dams affect water flow by completely holding up or restricting river channels (Missouri DNR, 2009). The restricted channel will result in sediment being deposited behind the dam wall and the downstream river ecosystem being starved of sediment (Zaimes & Emanuel, 2006). Notably, instream erosion processes are also affected by low flows. Czuba *et al*. (2011) states that dam releases dramatically increase flows downstream. Although controlled releases can restore habitats for benthic organisms, uncontrolled releases can result in flooding of the river, scouring of the channel and the transport of sediment further downstream (Czuba *et al*., 2011).

Anthropogenic factors such as land use have an impact on sediment load but not transport rate (Czuba *et al*., 2011). An increase in flow power is therefore necessary to move the sediment. Zaimes & Emanuel (2006) identified anthropogenic land use as a leading cause of excessive sedimentation. This occurs when activities such as logging, mining and construction remove vegetation and expose the topsoil to erosion by rainfall and runoff (Murphy, 2007).

5.3 Erosion and sediment delivery model

5.3.1 Introduction

The sediment transport model was developed using geomorphological principles by Bryson (2015) with supervision by Prof. Denis Hughes. A conceptualisation of catchment processes was used to develop the model, following which equations and linkages were incorporated into the model structure. The Modified Universal Soil Loss Equation (MUSLE) was linked to the Pitman hydrological model for this purpose. Distribution function theory was used to represent the stochastic nature of erosion. Erosional processes were accounted for by using a probability distribution of conceptual sediment stores (Bryson, 2015). This simplifies the distribution of catchment processes within the sediment transport model. The erosion part of the model estimates the amount of soil loss within the catchment and the hydrological model provides the flows. The flow component is the driving force behind the model as it moves sediment between storages and to the catchment outlet. The model is categorised into the flow estimation, erosion estimation and the storage and delivery estimation components.

5.3.2 Flow estimation

Source of flows

The flow component is an important part of the erosion transport model. Flows constitute the energy that drives the model; therefore, the accuracy of the simulated output is dependent on the accuracy of the flow data used within the model. Observed flow data are available from the Department of Water and Sanitation (DWS) website. Flows can also be simulated using the Pitman hydrological model. The simulation of flows is useful for catchments where there are no observed flow data, or for investigating management scenarios.

Disaggregation of monthly flows to daily

Since the Pitman Model simulates monthly flows, and the sediment model requires daily flows, the approach taken was to disaggregate monthly flows to daily. This disaggregation method was first implemented for use in WQSAM, which also requires daily flows, but the method is applicable within any hydrological application where daily flows are required, such as in the sediment model. The detailed approach within the disaggregation model is presented in Slaughter *et al*. (2015b); however, a summary is presented here. The conceptual approach taken within the disaggregation model is also shown in Figure 5.5.

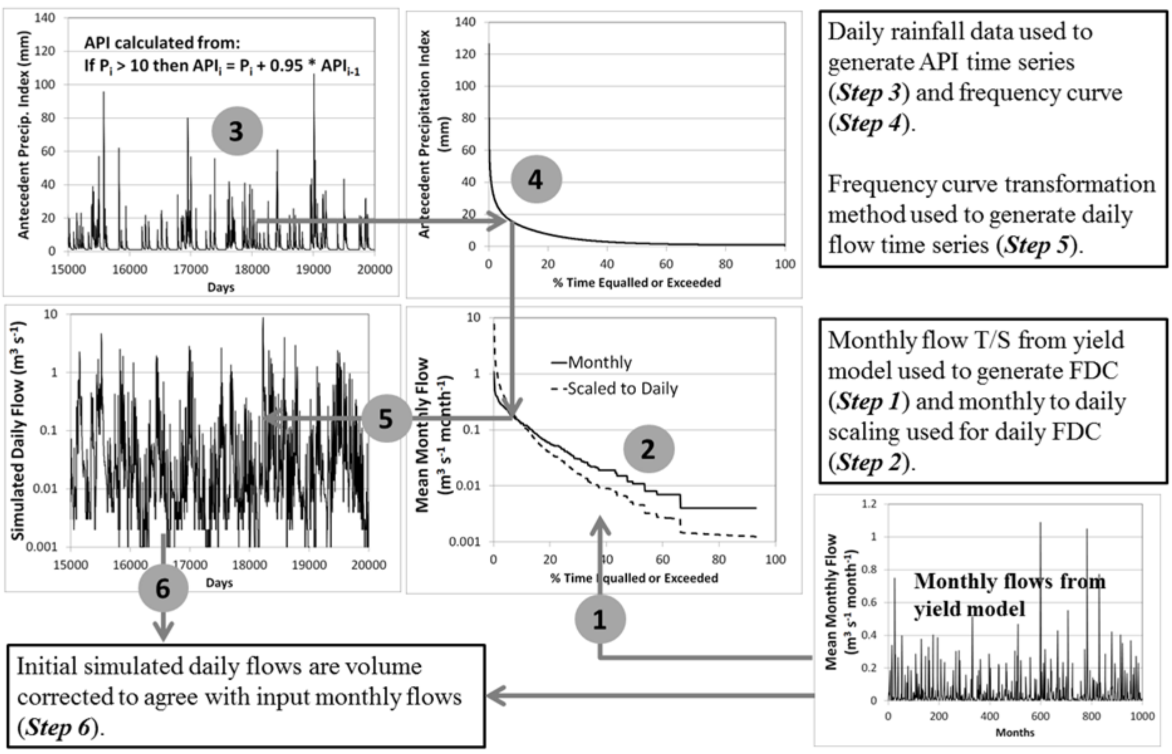

Figure 5.5 The conceptual framework of the monthly-to-daily flow disaggregation method. Taken from Slaughter *et al*. (2015b).

First, monthly simulated flows are used to generate a monthly flow duration curve (FDC) of mean monthly flows. A scaling equation is then use to scale the monthly FDC as close as possible to a daily FDC, which is derived from any available daily flow data, either observed or simulated, for the catchment of concern or from a catchment of representative conditions. A minimum of one but as many as three time series of antecedent rainfall representative of the catchment of interest and time period of simulation are then collated to derive a single time series of daily antecedent rainfall. Antecedent in this context refers to daily rainfall that takes into account rainfall within the recent past, as soil moisture conditions affect the degree of runoff associated with single rainfall events. Therefore, the calculation of antecedent rainfall takes into account the fact that there is a threshold of rainfall above which runoff will be expected, and that the storage characteristics of the catchment will affect runoff, with these processes being dependent on catchment conditions. Daily rainfall for this process is typically derived from ground-based weather stations; however, Hughes and Slaughter (2015) found that the use of global rainfall datasets, such as remote sensing estimates of rainfall, could successfully be used within the disaggregation model. The collated time series of daily antecedent rainfall is then used to generate a daily antecedent rainfall frequency distribution. The disaggregation model then steps through the time series of daily antecedent rainfall, and for each day:

- Determines the frequency of the rainfall from the antecedent rainfall frequency distribution.
- Identifies the equivalent daily flow for the frequency derived from (1) from the daily flow FDC, thereby producing a time series of daily flow.
- The time series of daily flows produced in (2) is volume corrected against the original monthly flows.

The study by Slaughter *et al.* (2015b) found that the volume correction (3), ensuring that daily sums of flows are equal to the monthly flows, reduces the sensitivity of the model to some of the parameters, thereby preventing the generation of drastically incorrect disaggregated flows.

Separation of daily flows into flow fractions

Subsequent the disaggregation, daily incremental flows are separated into surface flow, interflow and groundwater, using a simple statistical baseflow separation method by Hughes *et al*. (2003). This approach requires the setting of two parameter values, whereas the value of a third parameter remains constant as recommended by Hughes *et al*. (2003), and the approach taken in setting these values is to usually use default values determined during previous hydrological modelling studies in similar catchments. This may introduce a source of uncertainty; however, it can be argued that a rigorous determination of appropriate parameter values for the flow separation method is problematic (see Kapangaziwiri *et al*., 2011) due to the general lack of observed data with which to validate flow separation methods, the range of baseflow separation methods available and the conflicting results they generate, the difficulties in distinguishing between the origins of surface water in regards to flow fractions as well as the disparity in temporal scales at which the different flow fractions operate.

5.3.3 Erosion estimation

The MUSLE model was used to estimate erosion. The MUSLE was developed by Williams (1975) and is defined by Equation 5.10:

$$SA = R \times LS \times K \times C \times P \qquad \text{(Equation 5.10)}$$

Where SA is the daily sediment availability (in t ha^{-1}), R is the runoff factor, C is the cover factor, LS is the topography factor, K is the soil erodibility factor and P is the practice factor.

The MUSLE is an improvement of the Universal Soil Loss Equation (USLE) developed by Wischmeier and Smith (1978). The USLE was later revised into the Revised Universal Soil Loss Equation (RUSLE) and then modified into the MUSLE. The MUSLE is used in this study because of its ability to estimate soil loss on a single storm basis. It can therefore be used with a flow time series to provide temporal distributions of erosion yield. In the erosion and transport model, estimates of sediment availability (SA) are made according to the inputs of the MUSLE model. These inputs are made for 100 sub grids that are assumed to represent the total catchment. The sub grids are distributed according to the high, medium and low slope zones.

Thus, if the proportions for the high, moderate and low runoff zones are 0.2, 0.6 and 0.2 respectively, 20, 60 and 20 sub-grids will be used for the three zones (Bryson, 2015).

5.3.4 Determining parameters associated with erodibility

Topography (*LS*) Factor

The topography factor is an important parameter as it is closely related to the runoff factor. A catchment with high topography is a high energy catchment that has lower storage capacity and high erosion and sediment yield (Bryson, 2015). Erosion would normally be expected to increase with increases in slope steepness which corresponds in increases in velocity and volume of surface runoff (Morgan, 2005). The *S* sub-factor represents the effect of slope gradient on erosion, and it has more effect on soil loss as compared to slope length (Wischmeier and Smith, 1978). Slopes that are convex increase downslope and have high erosion rates. Because of such interaction, the effect of *L* and *S* is usually considered together. It has been demonstrated that increases in slope length and slope steepness can marginally increase the velocity of flow and thereby also increase erosion and sediment delivery rates (Yang *et al*., 2015).

According to Yang *et al.* (2015), the *LS* factor may be determined accurately from a DEM using GIS methods. The precision with which the *LS* factor can be estimated depends on the resolution of the DEM. A DEM contains cells that store spatial data from which elevation values can be determined. A DEM is generically described as a spatially geo-referenced dataset that is a popular method of encoding the topography for environmental modelling purposes (Sulebak, 2000). GIS-based methods for calculating the *LS* factor are presented in Zhang *et al*. (2013).

The DEM provides input necessary to extract slope and flow accumulation using ArcGIS (version 10.3.1). The first stage is to acquire the DEM, preferably the Shuttle Radar Topography Mission (SRTM) with a 30 m spatial resolution; because of its high resolution, it contains more data per pixel and is expected to improve the estimation significantly (Gallant *et al*., 2011). The DEM may be further processed for use, for example, if there are two or more DEMs covering the catchment, there is a need to combine all the DEMs using the mosaic tool in Arc Toolbox.

The DEM is further processed to fit dimensions of the catchment using a mask extraction tool from the Arc toolbox. This is achieved by laying a shapefile of the catchment boundary onto the DEM, and then extracting only the portion of the DEM that is contained within the catchment boundary. The DEM is then conditioned to be depressionless using the 'fill sink' command to determine the maximum downhill slope and the flow direction (e.g. Jain *et al*., 2010). The slope (*S*) factor and flow accumulation are derived from the depressionless DEM. The *LS* factor map is generated in ArcGIS using the raster calculator (Jain *et al*., 2010), by using the *LS* equation given by Moore & Burch (1986):

(Power ((("FlowAcc" × cell size) / 22.13), 0.4)) × (Power ((Sin
("Slope_Degree" × 0.01745 / 0.0896)), 1.3)) (Equation 5.11)

The flow diagram to determine *LS* is shown in Figure 5.6.

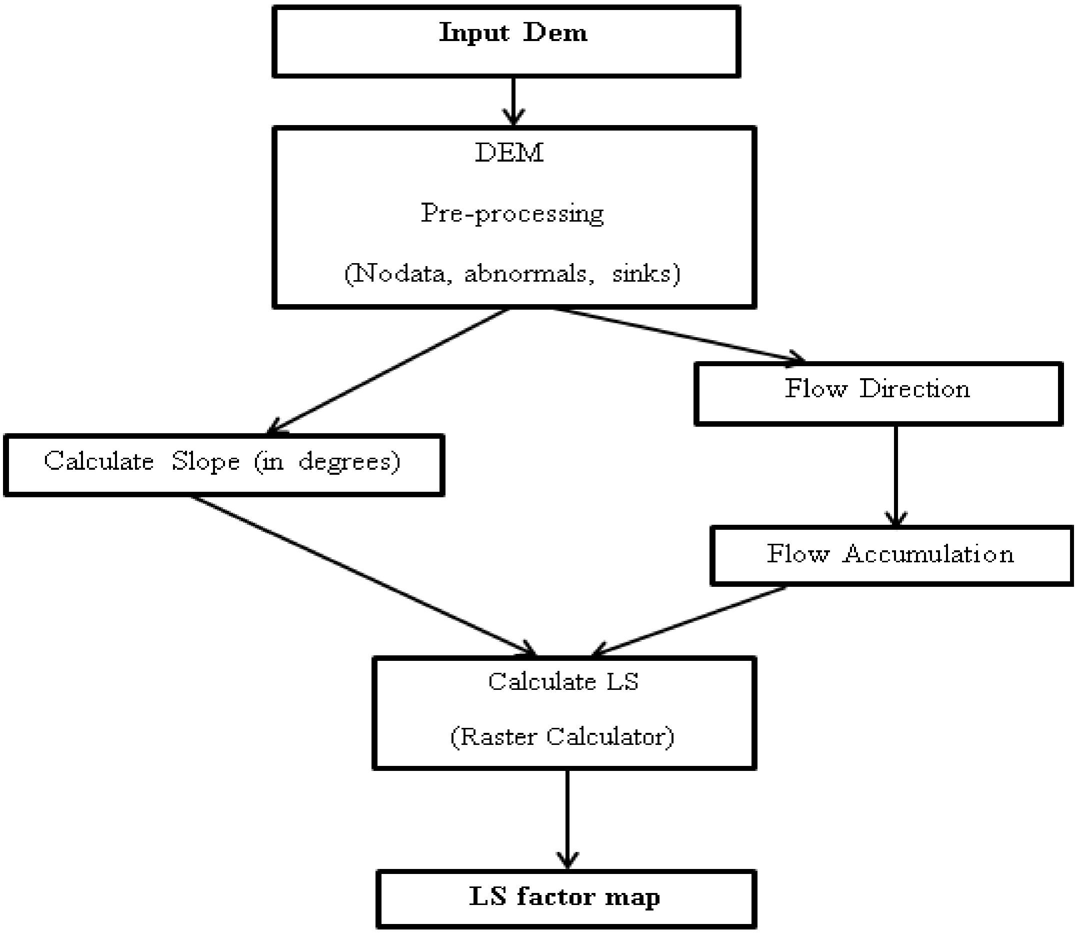

Figure 5.6 Flowchart illustrating the process of determining the Modified Universal Soil Loss Equation (MUSLE) topography (*LS*) factor.

Cover (*C*) factor

According to Sadeghi *et al*. (2014), it is essential to consider variations in vegetation cover when considering the *C* factor for the MUSLE model. The *C* factor is a value between 0 and 0.5 that relates to the extent of vegetation cover which protects the soil from soil erosion in a given catchment. The cover factor was determined for each land cover type using guidelines by Ayalew *et al*. (2015). Table 5.1 shows the *C* factor values assigned for SA land cover types.

The cover management factor (*C*) is determined using the national land cover data (NLC, 2014). The NLC (2014) is a national-scale shapefile showing land cover and land use across South Africa. Catchment-specific cover properties can be extracted from the readily-available shapefile by using the Geoprocessing tools in ArcMap to clip out catchment-specific data from the national land cover map.

The attribute containing land cover categories is exported to Microsoft Excel where *C* factor values suggested by Wischmeier and Smith (1978) are used to assign *C* values to respective land cover classes. Assigned *C* values are weighted according to the proportion of the catchment covered by particular land cover classes. The mean of the *C* factor values assigned to the land cover categories represented in the study catchment and weighted by proportional area is then used as an input to the model. It is essential to note that *C* values for particular land cover categories can also be obtained and/or verified using *C* values from recent erosion modelling studies, including that by Jang *et al*. (2015) and Shinde *et al*. (2011). The process to determine the cover factor is shown in Figure 5.7.

Table 5.1 Cover factor (*C*) for SA land cover/use categories

Land Cover Type	*C*
Forest, bush ,thicket	0.009
Grasslands	0.12
cultivated lands	0.37
low shrub	0.013
open bush	0.012
bare/degraded land	0.45
Plantations / Woodlots	0.012
Waterbodies	0.01
Wetlands	0.038
Settlements	0.1

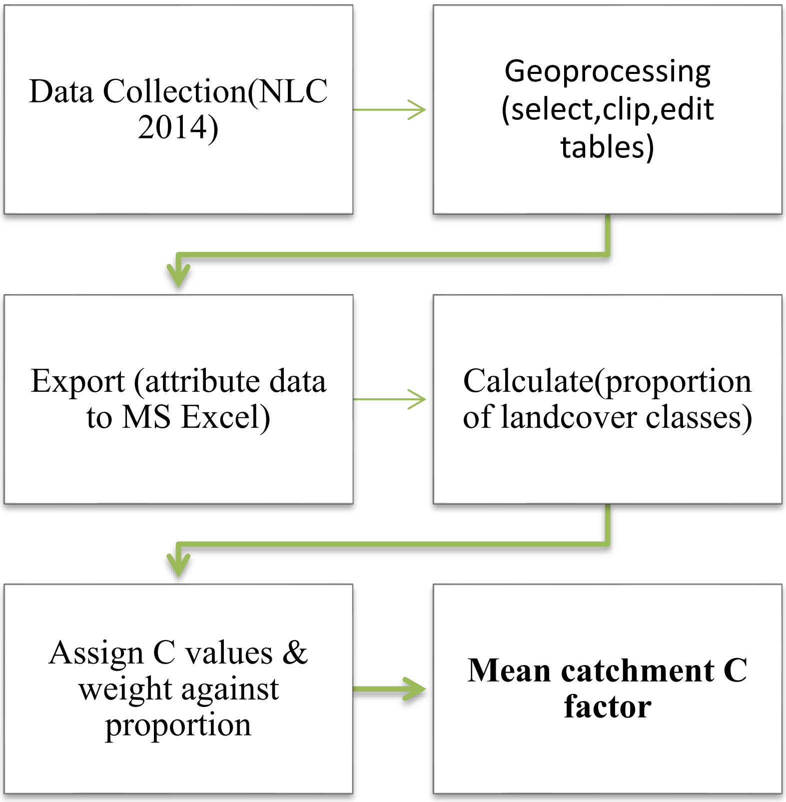

Figure 5.7 Flowchart illustrating the process of determining the Modified Universal Soil Loss Equation (MUSLE) cover management (C) factor.

Soil erodibility (*K*) factor

Soil erodibility refers to the susceptibility of the soil to erosional processes, and involves soil characteristics such as structure, organic content and texture which are important determinants of the aggregate soil strength and water infiltration capacity. The *K* factor is rated on a scale from 0 to 1, with 0 indicating soils with the least susceptibility to erosion whereas 1 indicates soils which are highly susceptible to soil erosion by water (Mhangara, 2011).

The soil type distribution for South Africa is obtained from readily-available shapefiles from the SA Atlas of Climatology and Agro-hydrology. These data contain the distribution of soil types and related *K* values for the soils. Catchment-specific soil data will be extracted from shapefile and attribute data exported to Excel to weight the *K* factor against the proportion of the catchment covered by each *K* class. The Schulze and Lorentz (1995) *K* values classification table (Table 5:2) will be used to classify the *K* values of respective catchments.

Table 5.2 Erodibility factors for various soil erodibility classes (Schulze and Lorentz, 1995).

***K*-Factor**	**Soil Erodibility Class**
> 0.70	Very High
0.50-0.70	High
0.25-0.50	Moderate
0.13-0.25	Low
< 0.13	Very Low

Schulze and Lorentz (1995) grouped *K* factor ranges and assigned descriptive classes. This makes it easier to attach *K* factor values to their impact on catchment soil erosion. Figure 5.8 below is a simplified flowchart of how soil erodibility is determined.

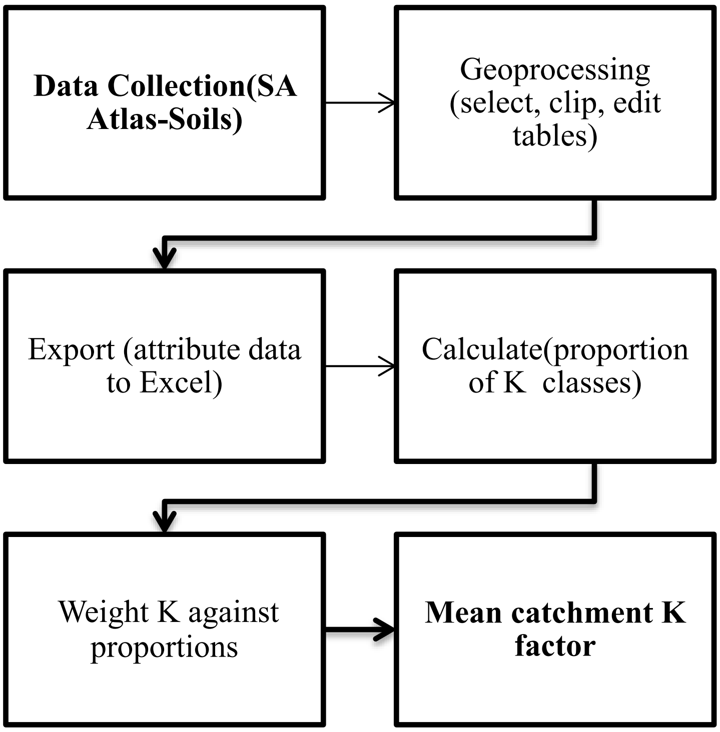

Figure 5.8 Flowchart illustrating the process of determining the Modified Universal Soil Loss Equation (MUSLE) soil erodibility (*K*) factor.

Management practice (*P*) factor

The management practice factor relates to conservation methods that are implemented to reduce the rate of soil loss from agricultural lands. These practices include contour and strip farming. The *P* factor refers to management practices that relate to agricultural lands. The Wischmeier & Smith (1978) values are used to determine the *P* factor for cultivated land and plantations. However, a value of 1 is assigned as the *P* factor for non-agricultural lands (Jang *et al*., 2015; Luo *et al*., 2016). Table 5.3 shows the *P* factor for SA land cover/use types.

Table 5.3 Practice factor (*P*) for cultivation on various slope categories (Wischmeier & Smith, 1978)

Land slope percent (%)	*P* factor
1 to 2	0.60
3 to 5	0.50
6 to 8	0.50
9 to 12	0.60
13 to 16	0.70
17 to 20	0.80
21 to 35	0.90

The quantification of the *P* factor requires mapping of agricultural areas and related conservation practices using high resolution imagery. Using land cover/use maps is a relatively easier and efficient method of determining the *P* factor (Jang *et al*., 2015; Luo *et al*., 2016). The *P* factor for the current study was determined by using land use/land cover maps. The method by Wischmeier and Smith (1978) is used to determine *P* values. The proportion of cultivated land in each runoff zone is used to weight the *P* factor and this provides the mean catchment *P*, which is an input to the model. Figure 5.9 is a flowchart showing how P factor is derived.

5.4 Sediment storage and delivery model

5.4.1 Introduction

This section describes the conceptual basis of the sediment storage and transport part of WQSED as well as the underlying mathematical equations for both the sediment yield and transport components of WQSED. The description of the WQSED model within this chapter is restricted to sediment transport to the outlet of a single quaternary catchment. Integration of WQSED into WQSAM will be implemented to describe routing of sediment through multiple quaternary catchments, and is the subject of a later section of this chapter.

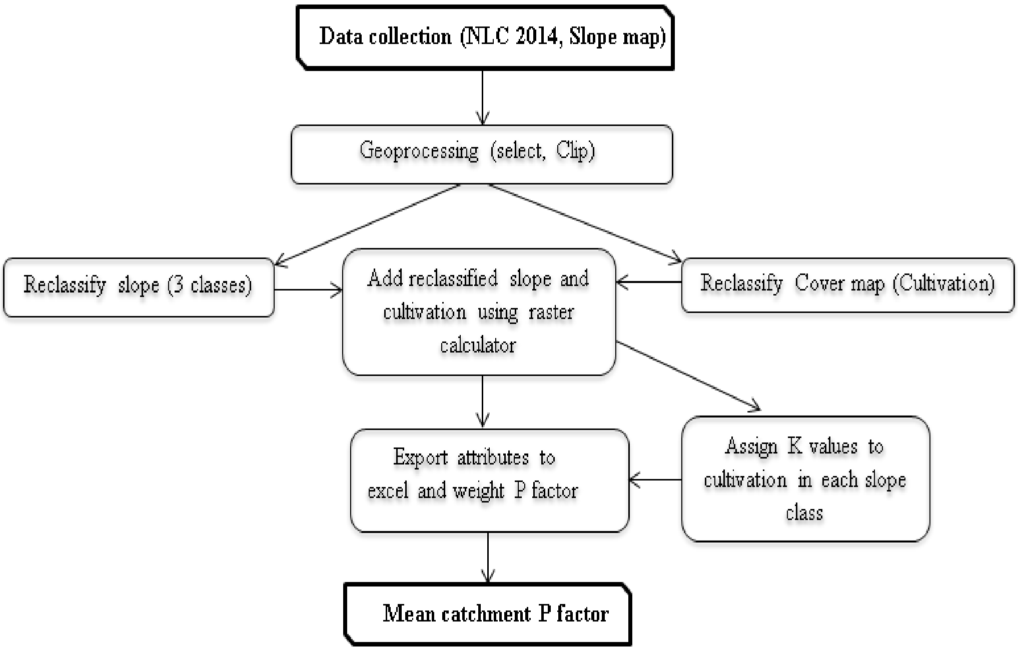

Figure 5.9 Flowchart illustrating the process of determining Modified Universal Soil Loss Equation (MUSLE) management practice (*P*) factor.

5.4.2 Conceptual model of WQSED sediment storage and transport

Separation of the study catchment into zones

The catchment is divided into three runoff zones. These divisions are based on the topography factor. The three slope categories are high, medium and low which represent high, medium and low runoff zones, respectively. It is assumed within the sediment transport model that runoff is related to slope gradient, with higher slopes producing higher flow and greater erosion. The high runoff zone is assumed to generate more flow than the medium runoff zone, whereas the medium runoff zone generates more flow than the low runoff zone. The zone with the higher slope/flow produces more erosion and sediment delivery relative to other slope zones (Pimentel and Burgess, 2013).

In the original sediment transport model, Bryson (2015) dealt with the issue of scale in sediment delivery modelling by focusing on the sediment cascade, incorporating an analysis of connectivity within the catchment which involves features that act as sediment sources, sinks and conduits to transfer sediment. Geomorphologic features that act as sources of sediment include badlands, gullies and the rest of the catchment area from which sediment is derived. Sediment sink features include flood outs, alluvial fans and reservoirs. Gulley systems and channels transfer sediment from slope storage to channel storage. Gullies (that are connected) are considered to be a part of drainage features as they are formed by streams eroding head-ward into hill slopes.

Landscape units can however act as buffers that absorb the sediment flux within the catchment (Bryson, 2015). The sediment flux in such scenarios is reflected by the re-organisation of storage as sediment moves across storages. High upstream erosion and sediment transport in such instances will not correspond with the low delivery at the outlet. A lumped model does not sufficiently reflect this behaviour, whereas a distributed catchment model can reflect responses of various spatial units across the catchment (Bryson, 2015).

The erosion model (MUSLE) makes sediment available for various storages within the catchment. Without the energy factor from flow, this sediment settles into the storage. Sediment movement across storages and to the outlet is initiated when flow energy is available. The division of the catchment into zones characterises both the runoff and the spatial distribution of topography within a catchment. Each runoff zone is characterised by two storages. These are the slope storage and channel storage, which includes all drainage features and gullies. Sediment moves from the high runoff zone to the low runoff zone, into the channel and out of the catchment. The model attempts to represent the stochastic nature of erosion by accounting for the dynamic movement of sediment between and within storages.

Figure 5.10 illustrates the storage and delivery components of the model. In Figure 5.10a, the three storage and runoff zones are depicted with the main channel cutting through all the zones. The (C_{prop}) represents other channel storages and gulley systems through which sediment is routed to the main channel. In Figure 5.10b, SA_0, SA_1 and SA_2 are inputs from the erosion model and these are placed into the three slope zones S_0, S_1 and S_2, respectively. A proportion of the sediment placed within the storages is removed through the channel storages $C_{prop}0$, $C_{prop}1$ and $C_{prop}2$, depending on the transport energy of the runoff (Bryson, 2015). Sediment can be moved across storages, where it settles until a strong runoff event flushes stored sediment to the catchment outlet. The illustration in Figure 5.10 captures the robust sediment storage and delivery process.

5.4.3 Mathematical description of WQSED

Please refer to Appendix C.

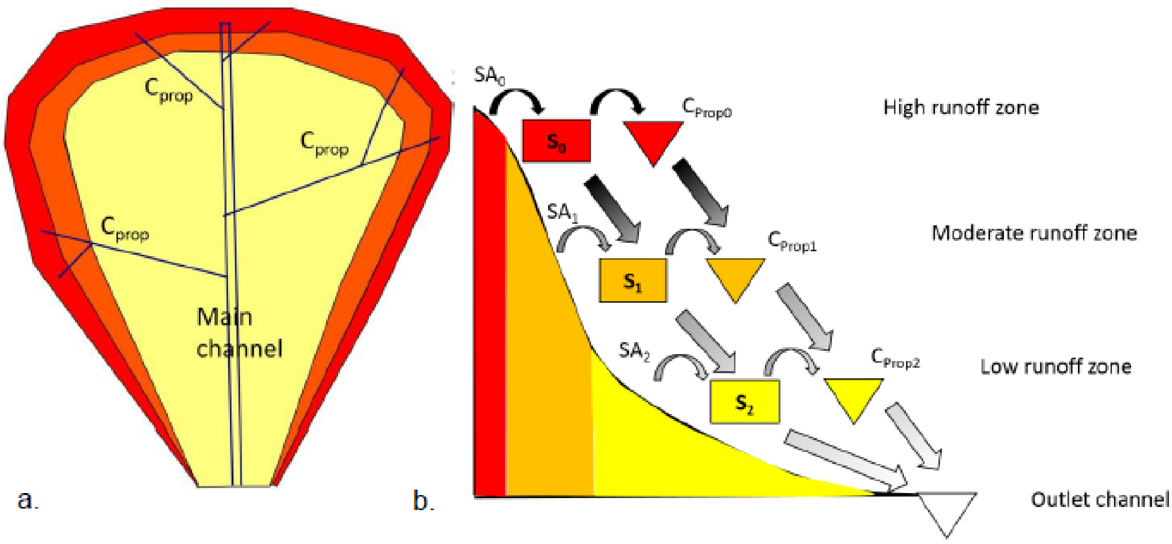

Figure 5.10 The sediment storage and delivery component of the model. Sourced from Bryson (2015)

5.5 Study sites and data

5.5.1 T35A-E

The Tsitsa River Catchment (T35A-E) is part of the larger Umzimvubu River Catchment. It is located between −16.453928 (Lat.) and 32.888327 (Lon.), in the Eastern Cape, with well-known towns within the catchment including Maclear and Mount Fletcher. Although the Umzimvubu River is noted as the largest undeveloped water resource in South Africa, plans are underway to construct a dam in quaternary T35E at Ntabelanga on the Tsitsa River. The river has a flow length of approximately 200 km before it joins the Tina River. Tributaries to the Tsitsa River include the Inxu River. The Tsitsa River Catchment lies in a very mountainous region and varies considerably in elevation. The catchment has complex topography characterised by steep mountain slopes (Figure 5.11), gentle undulating foot slopes and almost flat valley floors (Le Roux *et al.,* 2014).

The catchment also varies considerably in geology, with high areas around the escarpment consisting of basaltic lava from the Drakensberg formation (Jurassic). This is underlain by a strata of Triassic sand stones and mudstones (Le Roux *et al.,* 2014). The most dominant geological formation is the fine sandstones from the Clarens formation, followed by mudstones from the Elliot formation and sandstones of the Molteno formation (Le Roux *et al.,* 2014). There is also a small presence of quaternary alluvium, whereas dolerite occurs in thin bands.

Soil depth is limited on the steep slopes and gradually deepens towards the foot slopes and floodplain areas due to colluvium and alluvial deposits. The thin soils on steeper slopes become highly erodible when vegetation is removed (Dollar and Rowntree, 1995), and this situation gradually worsens as livestock graze on the slopes .The soil erodibility index of the catchment is according to Schulze (2007) moderate to highly erodible. These conditions have resulted in massive gullying (Figure 5.12, 5.13) within the catchment.

The climate is characterised by a distinct seasonality in rainfalls and temperatures within the catchment. Most of the rain (around 80%) falls during the summer (October to March), whereas winters are generally dry. Mean annual rainfall ranges from 625 mm in the low lying areas to 1,415 mm in the mountainous regions (Climatology Staff, 1978-2012). Mean temperatures range from 7°C in winter to 19°C in summer, with high variation during the day.

The Tsitsa River Catchment is dominated by the grassland biome, whereas Eastern valley bushveld thrives along river channels in the lower catchment (Mucina and Rutherford, 2006). The natural vegetation is largely influenced by altitude and burning (Le Roux *et al.,* 2014); therefore, small pockets of Afromontane forest occur along drainage lines and ravines where fire has minimal effect. The National Land Cover (NLC, 2014) shows that over 60% of the catchment area is covered by grassland. Patches of natural forest also occur alongside forest plantations. Other minority land cover/ uses include commercial and subsistence agriculture, waterbodies, mines, bare/degraded land and both urban and rural settlements (NLC, 2014).

5.5.2 Duiwenhoks Dam catchment

The Duiwenhoks Dam catchment (quaternary H80A) (Figure 5.14) is located at coordinate Lat. −33.98° and Lon. 20.98° in the Western Cape. The quaternary covers an area of 150 km^2. The main towns within the catchment include Heidelberg and Vermaaklikheid. The Duiwenhoks River drains the Langeberg Mountains and flows towards the coast, entering the sea west of Mossel Bay.

The topography of the catchment varies considerably (Figure 5.15), with the northern and southern parts of the catchment characterised by steep slopes with altitudes of around 600 m and 1,200 m, respectively. The area between the escarpments comprises a relatively flat to gentle valley with an altitude of around 300 m. The geology of the area consists of the Peninsula formation that dominates the northern escarpment and the Ceres formation that dominates the southern areas. The formation consists of sandstones, shales and tillites of the Cape Supergroup. The area is according to Schulze (2007) is characterised as highly erodible, which means that the soils are very susceptible to erosion. The catchment experiences a temperate climate, with rainfall occurring during both summer and winter. The mean annual precipitation is less than 500 mm and mean annual runoff is 212 MCM. Average daily temperature (ºC) ranges from 0 to more than 32 (Climatology Staff, 1978-2012).

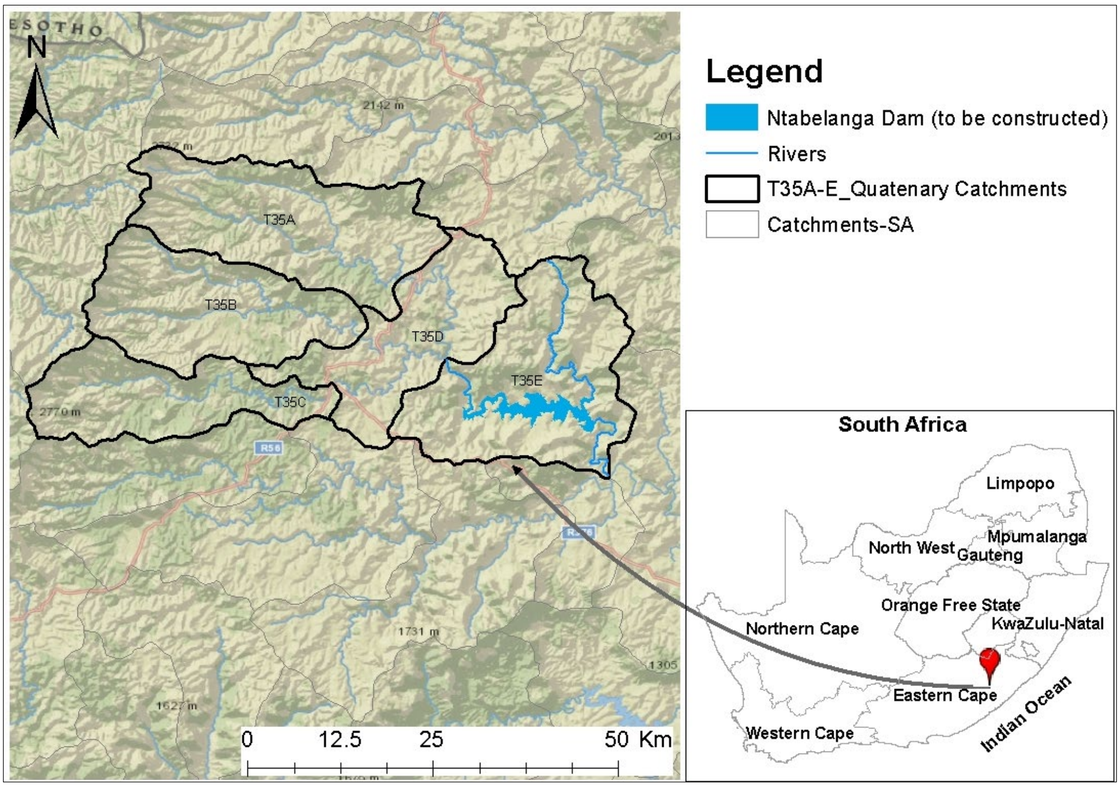

Figure 5.11 Map showing location of the study area T35A–E.

Figure 5.12 Steep gullied slopes in quaternary T35E

Figure 5.13 Gulley erosion and sediment transport in quaternary T35E

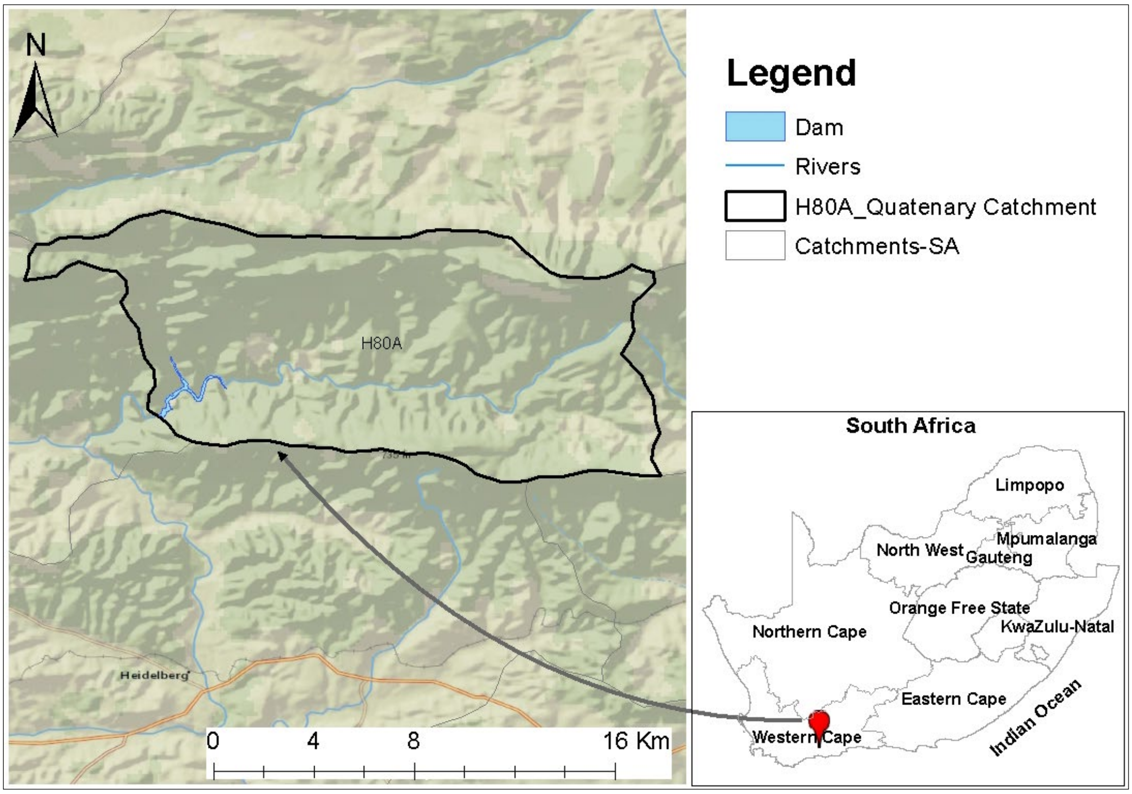

Figure 5.14 Map showing location of the study area of the Duiwenhoks Dam catchment (H80A).

Figure 5.15 The Duiwenhoks Dam and topography and vegetation of part of the catchment.

The vegetation is mainly a mixture of temperate, transitional forest and scrub. The dominant vegetation is fynbos which covers approximately 60% of the catchment (NLC, 2014). The natural vegetation is modified by a few forest plantations situated on the slopes of the southern edge of the catchment. The dominant land use type is cultivation, comprising approximately 15% of the entire catchment. Notable is that most of the cultivation within the catchment is commercial (dryland and irrigated agriculture). Other land uses include mining and sheep and ostrich farming in the more arid areas. Settlements are not a very significant land use as the catchment has a low population of around 30,000.

5.5.3 Prinsriver Dam catchment

The Prinsriver Dam catchment (quaternary J12G) (Figure 5.16) is located at the coordinates 20.812 (Lon.), −33.468 (Lat.) southwest of Laingsburg in the Western Cape. The catchment has an area of 768 km^2.The landscape within the catchment consists of moderate to high relief mountains and hills with a mean altitude of 300-1,900 m (Figure 5.17). Slope varies widely across the catchment as this is a region containing folded mountains. The geology also varies widely with geological formations including Nardouw, Ceres, Bidouw and Waltevrede, with the latter being the most dominant in the catchment (Schulze, 2007). The formations are overlain by shales and sandstones; however, it is essential to note that sandstone dominates the study area. The soils are moderately erodible (Schulze, 2007). The area is semi-arid and characterised by a hot and dry climate. Rain falls in the very late summer to winter. The mean annual precipitation (MAP) ranges from 200-500 mm, whereas mean annual runoff is approximately 6 mm. The daily average temperature is 10-32ºC (Climatology Staff, 1978-2012).

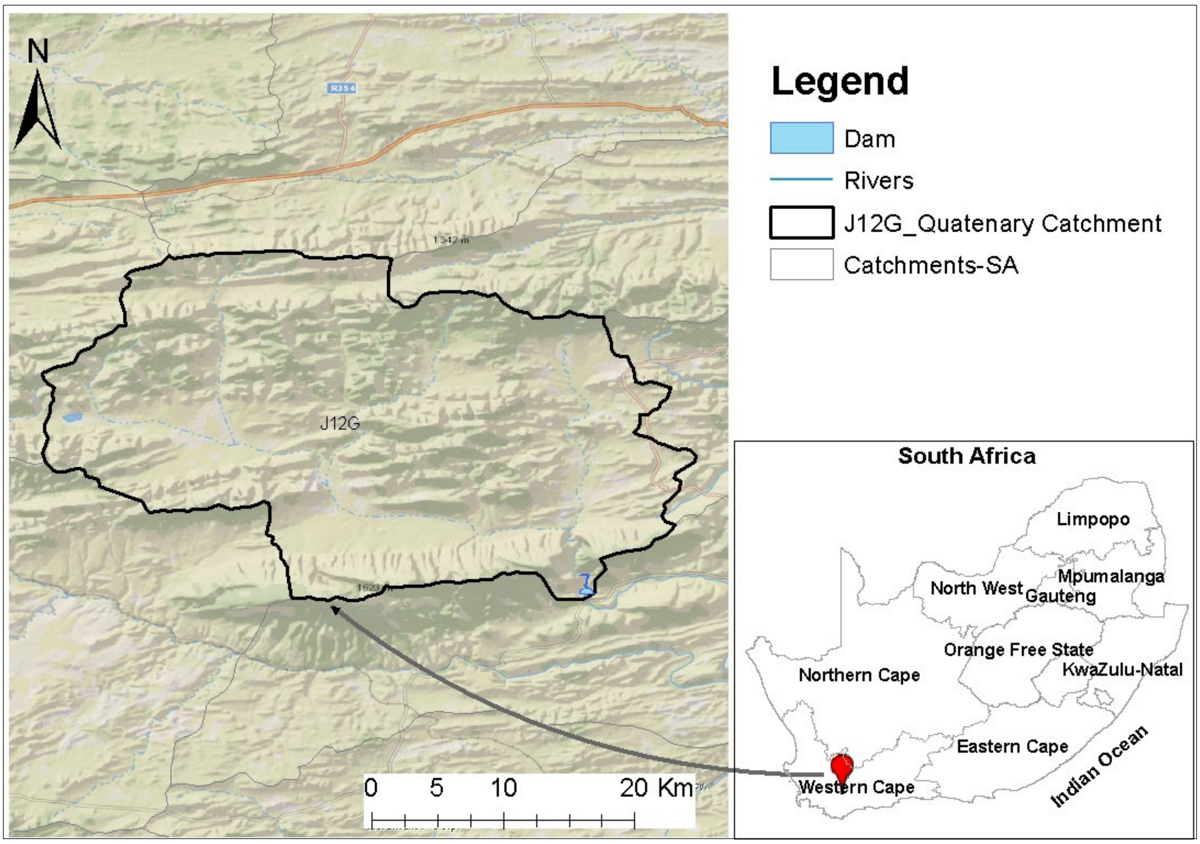

Figure 5.16 Map showing location of the study area of the Prinsriver Dam catchment (J12G).

Figure 5.17 The Prinsriver Dam and topography and vegetation of part of the catchment. Source (DWS)

The vegetation consists mainly of sandstone fynbos and succulent Karoo. Fynbos covers close to 70% of the study area, whereas succulent Karoo covers 15% (NLC, 2014). Notable also is that 11% of the catchment comprises bare ground; this kind of ground cover together with steep slopes is likely to exacerbate erosion (NLC, 2014). Land uses within the catchment consist of nature reserves such as the Anysberg and Witterberg, which are private nature reserves. Mining activity is carried out within the catchment, whereas human settlements are very limited.

5.5.4 Churchill Dam catchment

The Churchill Dam Catchment (Quaternaries K90A-B) (Figure 5.18) is located in the Eastern Cape at the coordinates 24.488 (Lon.), −33.994 (Lat.) in a ravine between the Suuranysberge and Tsitsikama mountains near the southern coast.

The geology of the area is defined by sandstone and quartzite, leading to the formation of grey sandy soils and Table Mountain Sandstone. Podzolic and litholic soils are dominant in the catchment. The lower slopes are characterised by dark structured soils with fine sand, whereas the steep slopes contain nutrient deficient, acidic lithosols (Mucina and Rutherford 2010). The valley bottoms consist of permanent and seasonally saturated hydric soils. These conditions are suitable for the formation of valley bottom peat which characterises the catchment.

The catchment is drained by the Kromme River, which flows for approximately 100 km before entering the Churchill Dam. Tributaries drain from the escarpment in a trellised pattern (Figure 5.19). The mean annual rainfall (MAR) is 700 mm, with a wide temporal variation, with yearly averages ranging from 300-700 mm.

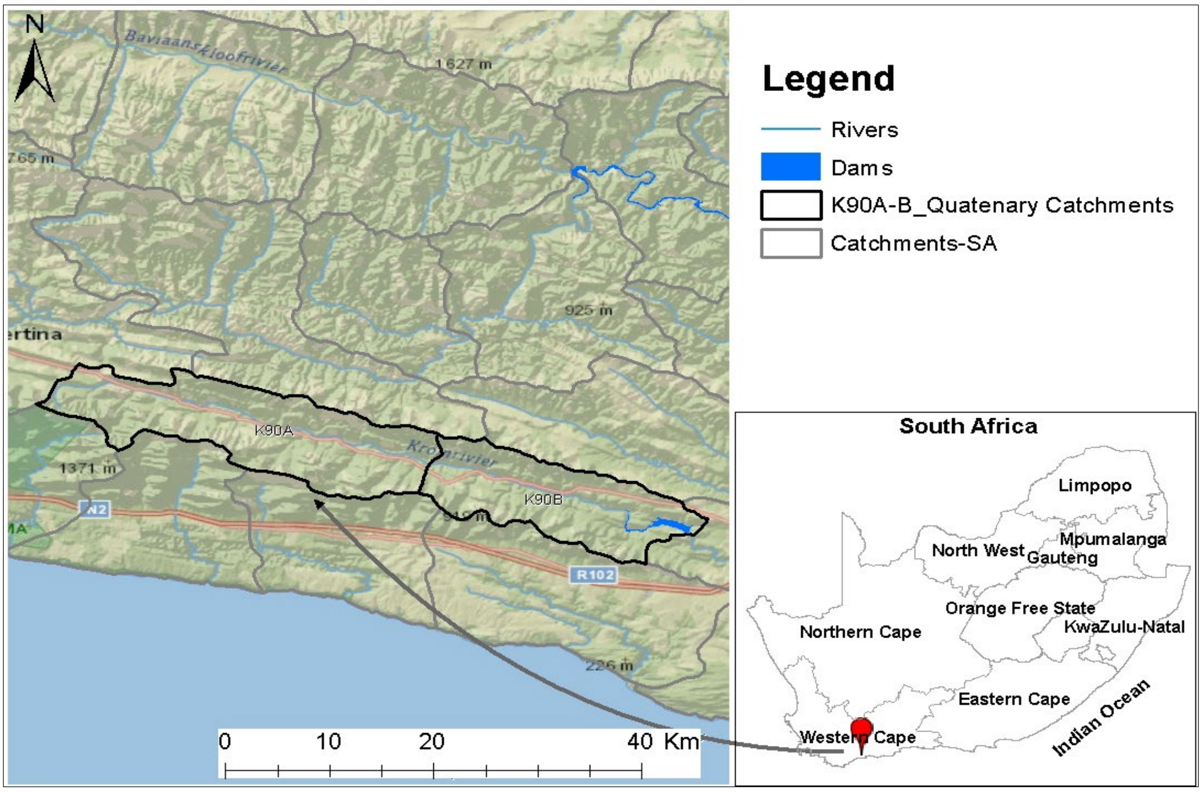

Figure 5.18 Map showing location of the study area of the Churchill Dam catchment (Quaternaries K90A-B).

Figure 5.19 Google Earth image showing the topography and vegetation of part of the Churchill Dam catchment.

The natural vegetation (Figure 5.19) of the area is dominated by fynbos, with other cover types including grassland, thicket and forest (Mucina and Rutherford, 2006). The valley bottom peatland is dominated by Palmiet (*Prionium seratum*), ferns, grasses and reeds, which are also found on the peatland. The considerable portion of the catchment consists of degraded vegetation comprising invasive alien species.

Land uses in the catchment include nature reserves, orchards, livestock farms and vegetable farming. Much of the agriculture is large-scale commercial farming. Other land uses include mines and human settlements.

5.5.5 Maden Dam catchment

The Maden Dam catchment is a small catchment located in the Upper Buffalo River Catchment (quaternary catchment R20A). It is located between co-ordinates −32.672957 (Lat.) and 27.310065 (Lon.), near King Williams Town in the Eastern Cape province of South Africa. The catchment has an area of 30 km^2 and is located in the steep upper reaches of the Amatola Mountains with an altitude ranging between 600-1,400 m above sea level. The catchment is characterised by steep slopes as shown in Figure 5.20.

The catchment is well vegetated, with > 50% of the catchment covered in thicket, bushland and bush clumps. Indigenous forest and forest plantations cover the rest of the catchment (NLC, 2014). The geology of the catchment is dominated by the Karoo dolerite subgroup, whereas a small proportion lies in the Adelaide subgroup (Middleton and Bailey, 2008). Soils in the mountainous areas (Karoo dolerite group) which characterise the Maden Dam Catchment are thin, shallow and poorly drained as compared to the deep well-drained soils of the foothills (Adelaide group), which are prone to erosion because of reduced vegetation cover. Figure 5.20 show that soils in the catchment have low erodibility.

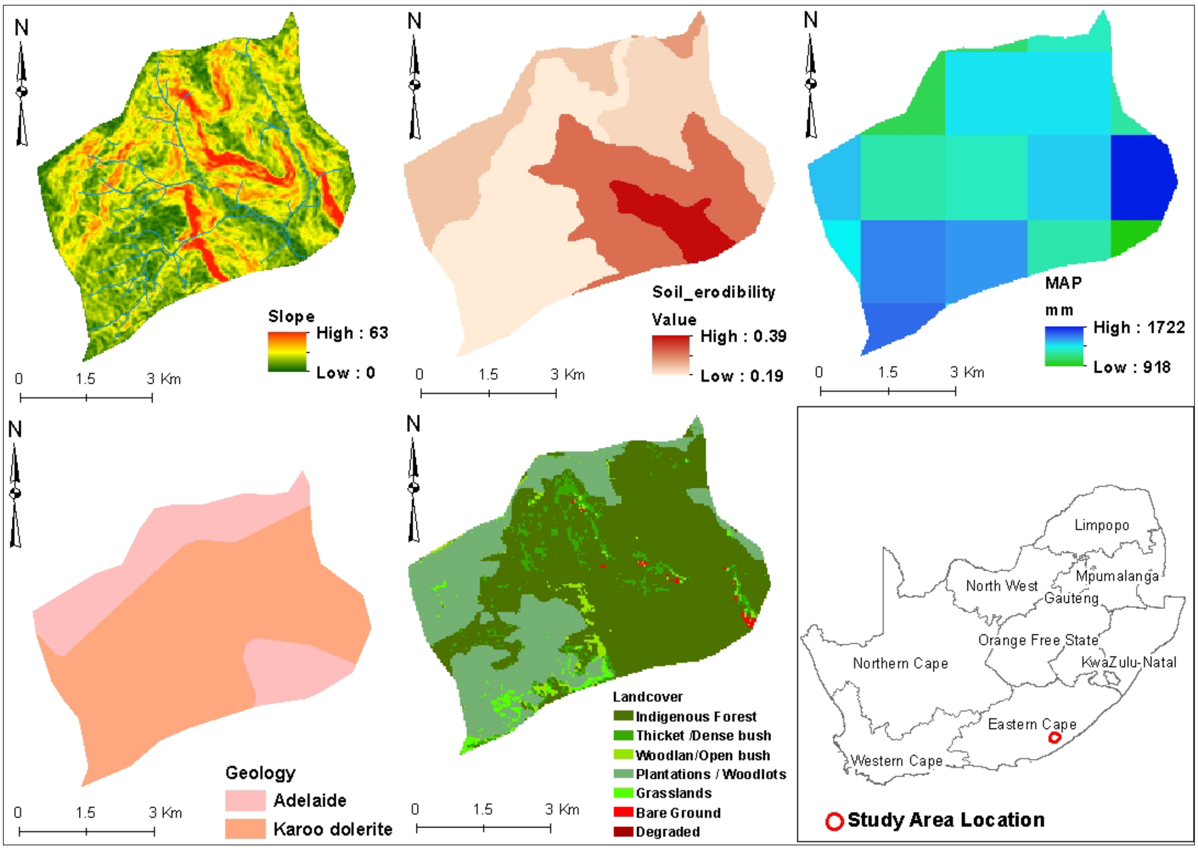

Figure 5.20 Map showing slope, soil erodibility, mean annual precipitation, simplified geology, vegetation types and location of the Maden Dam catchment in the Eastern Cape of South Africa.

The climate of the catchment is warm to temperate with a mean annual temperature of 21°C. The rainfall of the Buffalo River Catchment ranges from 400 mm to > 1,000 mm per year, with a mean annual rainfall of 700 mm; however, the segment of the Buffalo River Catchment upstream of the Maden Dam receives rainfall in the higher end of this range (1,500-2,000 mm) as this area represents the headwaters of the catchment, and generates approximately 42% of the runoff of the entire catchment (O'Keefe *et al*., 1996).

5.5.6 Klaserie Dam catchment

The Klaserie (Jan Wessenar) Dam catchment (Figure 5.21) is located in the Klaserie River Catchment (quaternary catchment B73A). It is located between co-ordinates −24.659418 (Lat.) and 31.085407 (Lon.) in Mpumalanga Province, South Africa. The catchment has an area of 136 km^2. The catchment is located in a Lowveld region with a mean altitude of between 300-600 m. Figure 5.21 shows that the area west of the catchment is characterised by steep slopes, whereas the rest of the catchment lies in the lower slope zone.

The area generally has a dry climate, with temperatures averaging 22°C. Precipitation ranges between 400-800 mm year^{-1} (DWAF, 2004). However, rainfall on the escarpment is generally higher, ranging between 600-1,200 mm year^{-1}, with mean annual temperatures varying between 10-22°C. Although the lower lying areas are warmer, they are also much drier, with an average rainfall of between 400-600 mm year^{-1} (DWAF, 2004).

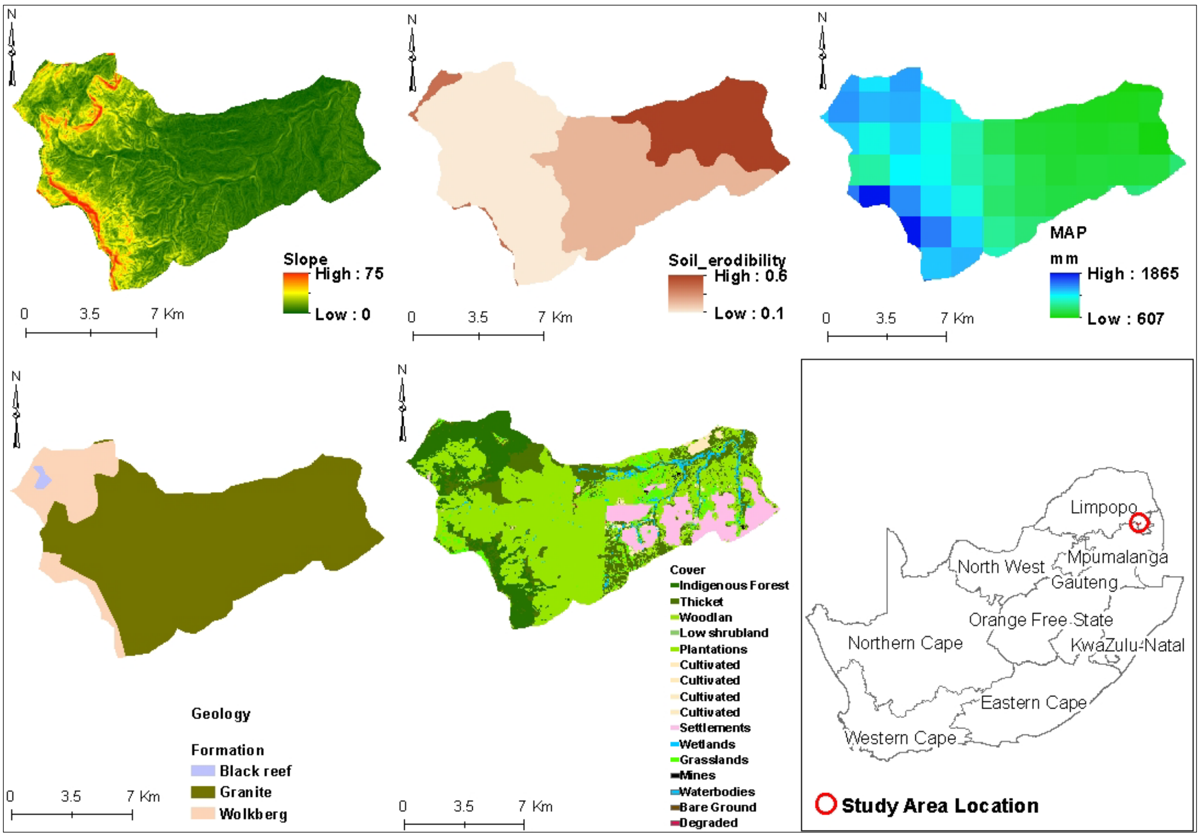

Figure 5.21 Map showing slope, soil erodibility, mean annual precipitation, simplified geology, vegetation types and location of the Klaserie Dam catchment.

The upper catchment is characterised by steep mountain slopes that are well vegetated, comprising Afromontane forests in the moist gorges of the Drakensberg escarpment. The vegetation comprises dense indigenous forest and timber plantations (NLC, 2014). The lower catchment is dominated by human settlements (high density suburbs) occupying the south eastern part of the area, whereas the north eastern part is dominated by commercial farming activities. Even though the lower catchment is sparsely vegetated, satellite imagery (Google Earth, 2016) does not show evidence of extensive land degradation. The geology of the area is mainly composed of granite rock, covering > 75% of the area and all of the lower catchment (Middleton and Bailey, 2008). The rest of the catchment is covered in quartzite and shales. The catchment is dominated by lowly erodible soils which reduce the rate of soil loss.

5.5.7 Xonxa Dam catchment

The Xonxa Dam catchment (Figure 5.22) is located on the White-Kei River. The dam receives water from rivers in quaternaries S10A-E. The catchment is located between coordinates −30.793738 (Lat.) and 28.748414 (Lon.), and is situated north of Queenstown in the Eastern Cape, South Africa. The total catchment area is 1,476 km^2.

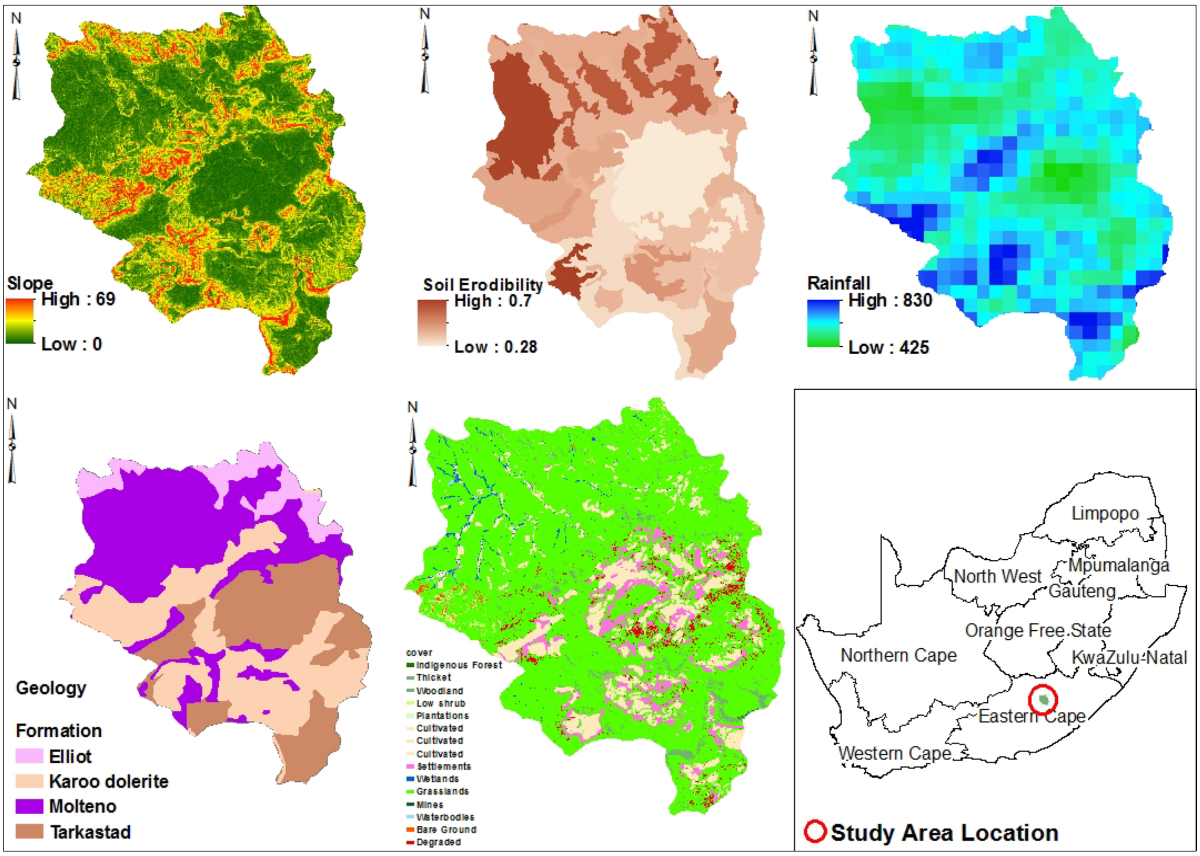

Figure 5.22 Map showing slope, soil erodibility, mean annual precipitation, simplified geology, vegetation types, and location of the Xonxa Dam catchment.

The geology of the area is largely comprised of the Karoo supergroup which includes shales, mudstones and sandstones (Figure 5.22). The Tarkastad and Adelaide supergroups also characterise the area, consisting of sandstones and mudstones. The catchment also contains patches of Elliot, Clarens and Molteno formations, comprised of shales, siltstones, mudstones and sandstones. The soils of the catchment are largely deep clayey loams, rocky shallow soils and alluvial soils in the valleys. The soils have a high erodibility, ranging between 0.2-0.7 (Figure 5.22).

The catchment is located in one of the driest parts of the country. The vegetation is mainly comprised of grassland (> 70% of the total area), with patches of acacia Karoo thornveld as well as Afromontane forest and sub-arid thorn bushveld (NLC, 2014). The lower reaches of the catchment are characterised by valley thicket. Alien invasive species dominated by black wattle have a significant presence in the catchment, particularly along the riparian zones (DWAF, 2009). Land use within the catchment comprises livestock farming, subsistence and commercial farming, as well as forest plantations. Game farming is also being practised, whereas mining activities occur at a lesser scale. Human settlements comprise a major land use in the catchment, comprised of both urban and rural settlements (DWAF, 2009).

5.5.8 Koster Dam catchment

The Koster Dam is located in the Koster River Catchment (quaternary catchment A22B) (Figure 5.23). It is located between coordinates (decimal degrees) −25.713371 (Lat.) and 26.768959 (Lon.) in the North West Province of South Africa. The catchment has an area of 187 km^2.

The geology of the catchment comprises of the Silverton, Daspoort and Strubenkop formations (Figure 5.23). The erodibility of the catchment ranges between 0.26-0.33, falling within the low to moderate erodibility class (Schulze and Lorentz, 1995). The vegetation of the catchment comprises mostly grassland, indigenous forest and thicket bush.

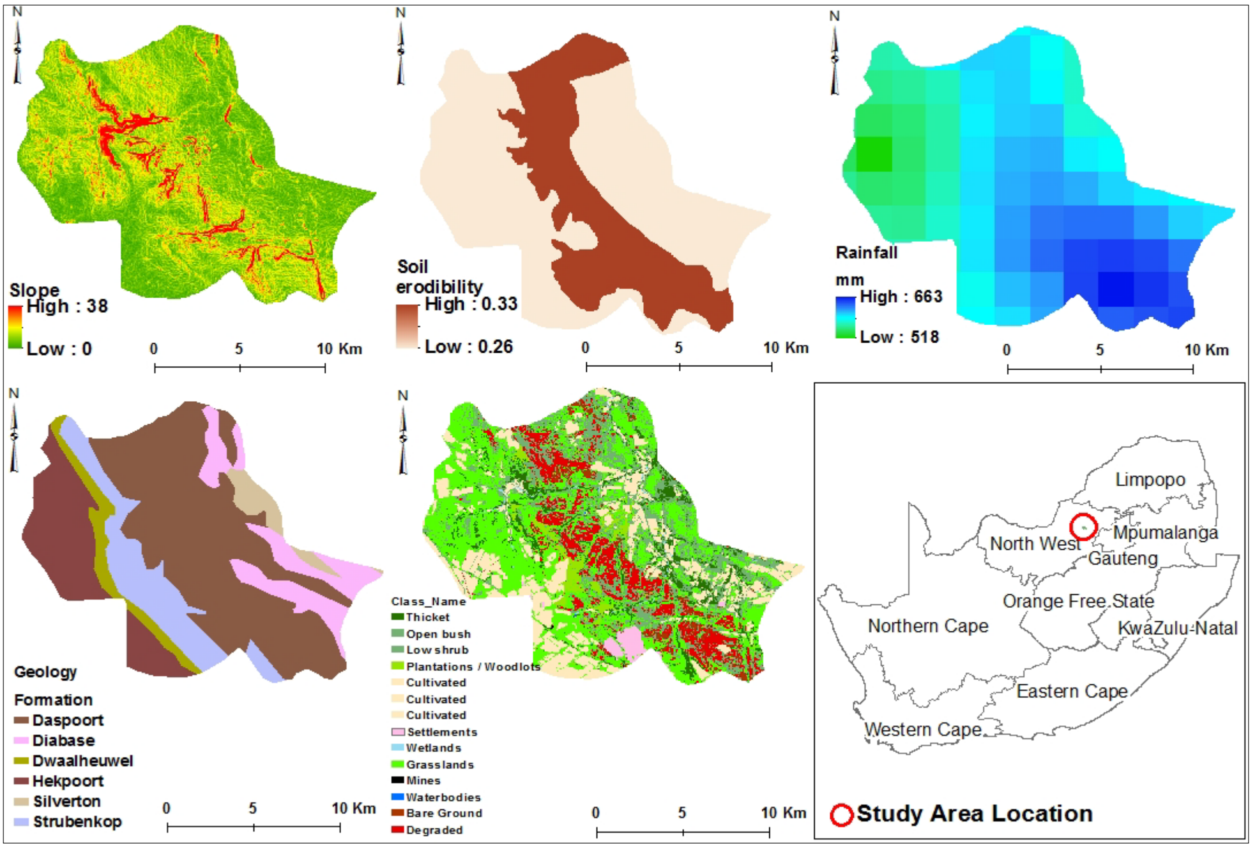

Figure 5.23 Map showing slope, soil erodibility, mean annual precipitation, simplified geology, vegetation types, and location of the Koster Dam catchment

A significant proportion of the catchment is covered by degraded land (NLC, 2014) which is susceptible to erosion. Cultivation is the dominant land use, comprising both subsistence and commercial agriculture. The mean annual rainfall ranges between 500-700 mm.

5.6 Results and discussion

5.6.1 Catchment parameters

Topography (*LS*) factor

The *LS* factor varied considerably across the study catchments, with a mean and median of 6.3 and 6.6, respectively. The *LS* factor used for the Duiwenhoks Dam catchment has the highest value at 9.7 followed by that of the K90A quaternary of 8. Both these catchments are located in the Western Cape. Figure 5.24 shows the distribution of the *LS* factor values across the study sites. The lowest value of *LS* of 1 was used in quaternary A22B, which is > 75% lower than those used for the other selected catchments. This quaternary is located in the Northern Cape. Values of *LS* > 6 were used for the T35A-C group of quaternaries, much higher than those of the T35D and T35E catchments that have values of *LS* of 4.6 and 5.6, respectively, which is attributed to T35A-C being steep headwater catchments.

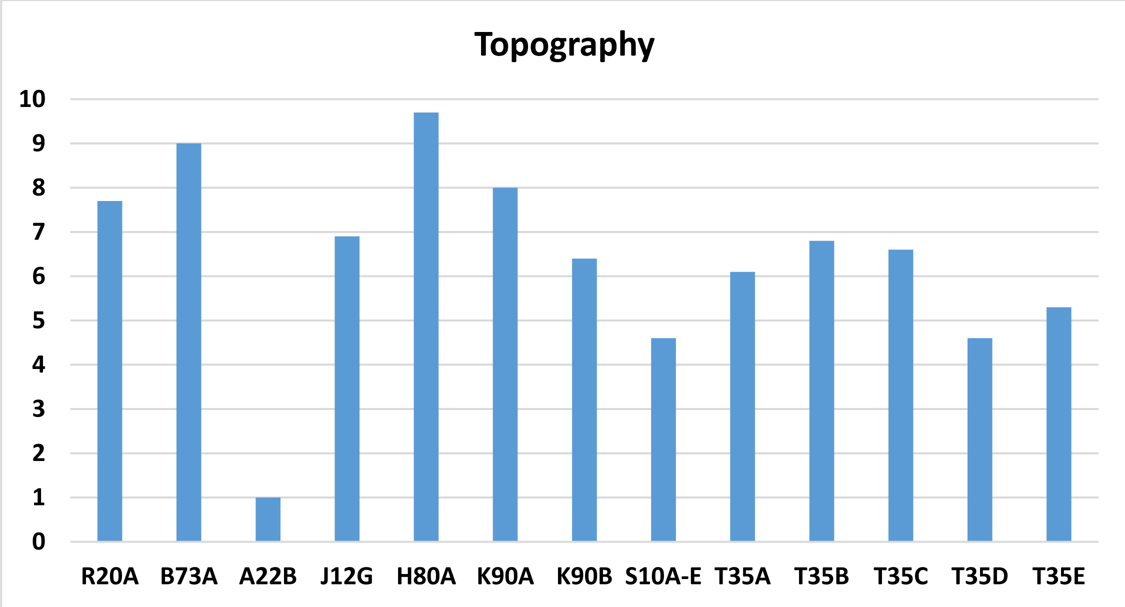

Figure 5.24 Distribution of the values of the topography (*LS*) factor in the selected study sites

Vegetation cover (*C*) factor

The *C* factor indicates the state of vegetation cover in a particular catchment. Values closer to 0 indicate good vegetation cover whereas values closer to 0.5 indicate poor cover. A distinct variation between catchments in the southeastern part of the country and the rest of the country is evident. Quaternaries such as R20A, H80A and K90A-B that are located in the southeast have low cover factors of 0.01, 0.05 and 0.03 respectively (Figure 5.25).

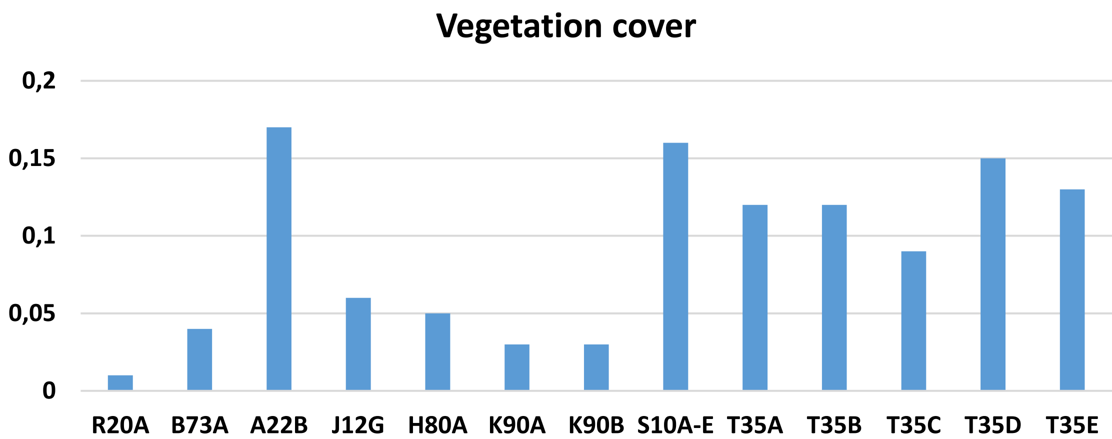

Figure 5.25 Distribution of the vegetation cover (*C*) factor in the selected study sites

The rest of the selected catchments (with the exception of B73A) have *C* factors of above 0.1. The S10A-E and T35 quaternaries (located in the Eastern Cape) have *C* factors ranging from 0.12-0.15 that is synonymous with grassland and scrub and bushland. However, the T35C quaternary has a slightly lower *C* factor of 0.09 that is likely influenced by a larger proportion of natural forest in the headwater basin. The A22B catchment in the dry North Western Cape has a *C* factor 0.17; the basin has the worst vegetation cover compared to the other study areas.

Soil erodibility (*K*) factor

There is little variation in erodibility across the study areas, with approximately 77% of the study areas falling within the moderate erodibility (0.25-0.5) range. All the selected study sites in the Eastern Cape fall in the moderate erodibility category, including A22B, J12G and H80A. Figure 5.26 shows the distribution of *K* across the study areas.

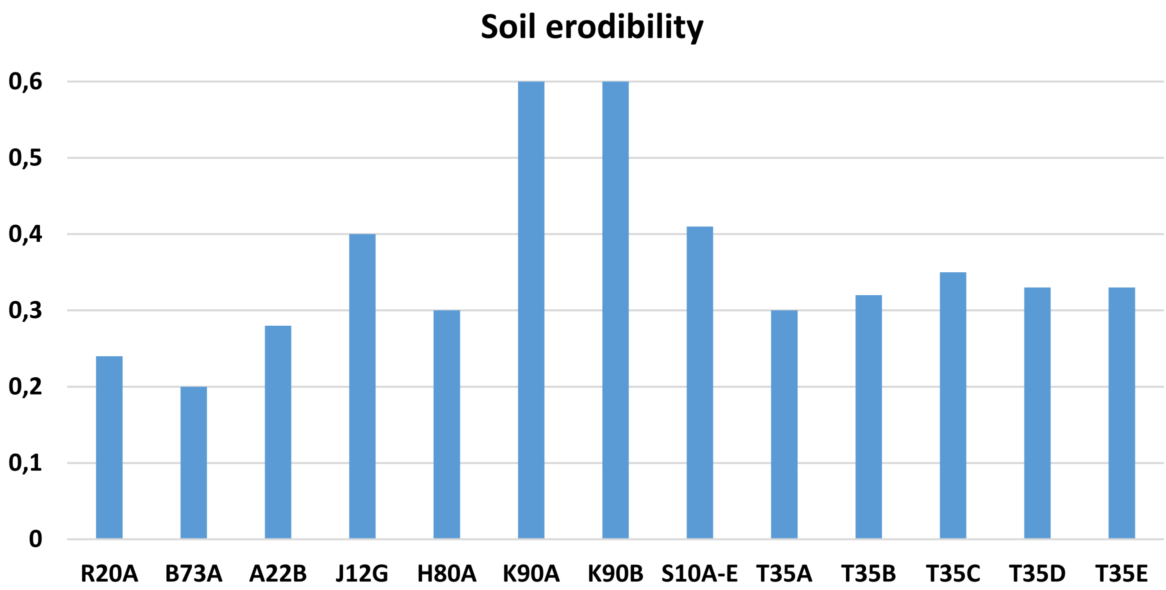

Figure 5.26 Distribution of the soil erodibility (*K*) factor for the selected study sites

Low erodibility values were estimated for quaternaries R20A and B73A that are located in the northeastern and southeastern parts of the country respectively. The highest erodibility values were estimated for the K90A-B quaternaries that are located in the southeastern areas and closer to the coast.

Management support practice (*P*) factor

The practice factor relates to the management activities implemented on agricultural lands to reduce soil loss from agricultural areas. Values closer to one indicate poor practice whereas values close to 0 indicate good practice. *P* values above 0.8 were applied to all study areas (Figure 5.27). The results show that close to 50% of the catchments have *P* factors above 0.95. The highest *P* value used is 0.99 for the J12G quaternary catchment located in the southeastern area of South Africa.

The *P* factor values used across the study catchments are high and not variable. However, lower *P* values were used in B73A and A22B of 0.8 and 0.88, respectively. Table 5.4 displays the list of catchments and their estimated parameter values.

5.6.2 Model outputs and analysis

Model outputs for Klaserie Dam (B73A)

The modelling of erosion within this catchment was driven by observed daily flows, and a period of complete daily flows from early 1960 to early 1970 was used. This catchment is characteristic of the extreme hydrological variability associated with arid catchments, as demonstrated by the significant peak flows (Figure 5.28). Periods of low to zero flows are interspersed by very high peak flows. The time series depicted in Figure 5.28 demonstrates this behavior noticeably for the period 1969-1972. This pattern is a result of rainfall characteristics of arid to semi-arid areas where long dry spells are accompanied by high intensity storms. The time series also shows a gradual increase in peak flows in the latter half of the period (1968 onwards). This reflects an increase in rainfall amount towards the end the decade after the 1964 drought (Masih *et al*., 2014).

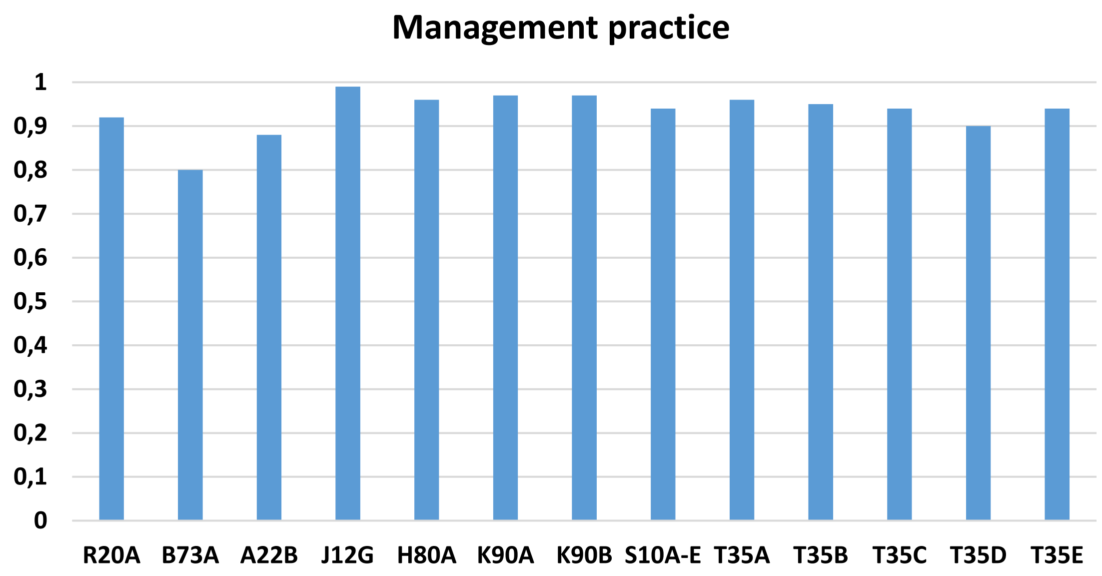

Figure 5.27 Distribution of the management practice (*P*) factor in the selected study sites

Table 5.4 Catchment erodibility parameters computed using GIS coverages

Catchment	Dam name	Size (km^2)	*K*	*LS*	*C*	*P*
R20A	Maden	30	0.24	7.7	0.01	0.92
B73A	Klaserie	136	0.2	9	0.04	0.8
A22B	Koster	187	0.28	1	0.17	0.88
J12G	Prinsriver	768	0.4	6.9	0.06	0.99
H80A	Duiwenhoks	150	0.3	9.7	0.05	0.96
K90A	Churchill	213	0.6	8	0.03	0.97
K90B	Churchill	149	0.6	6.4	0.03	0.97
S10A-E	Xonxa	1282	0.41	3.9	0.15	0.94
T35A	N/A	475	0.3	6.1	0.12	0.96
T35B	N/A	395	0.32	6.8	0.12	0.95
T35C	N/A	306	0.35	6.6	0.09	0.94
T35D	N/A	348	0.33	4.6	0.15	0.9
T35E	N/A	492	0.33	5.3	0.13	0.94

The model output for soil loss (Figure 5.28) shows a trend similar to that of the flow time series; therefore, it is evident that the model generates erosion events in response to surface flow events. Low flow events within this catchment subsequently result in low erosion events, whereas high peak flows (1971-1972) are accompanied by peak erosion events. This characterises the relationship between flow and erosion, where flow is the driver of erosion.

The analysis of simulated soil loss shows that an estimated 1,500 Kt of soil was lost from the 136 km^2 Klaserie Dam catchment over the 11-year time series. The simulated soil loss for the catchment is 9 t ha^{-1} year^{-1}. The Msadala *et al*. (2010) erosion risk study estimated that the erosion of this area would range between 13-26 t ha^{-1} year^{-1}.

The Klaserie Dam catchment is categorised as a low to moderate erosion zone by Msadala *et al*. (2010). Although the mean topography factor (*LS*) of this catchment is very high, it is affected by the extremely high Drakensberg escarpment slopes. The remaining catchment (50%) is located in the low slope zone, thereby explaining the low rate of erosion. The steep upper catchment, which is assumed to experience higher erosion, is well vegetated with low soil erodibility, thereby resulting in reduced soil loss. The B73A quaternary catchment is located in a relatively dry climate, and the infrequent and low runoff events lead to a low cumulative soil loss over the time series.

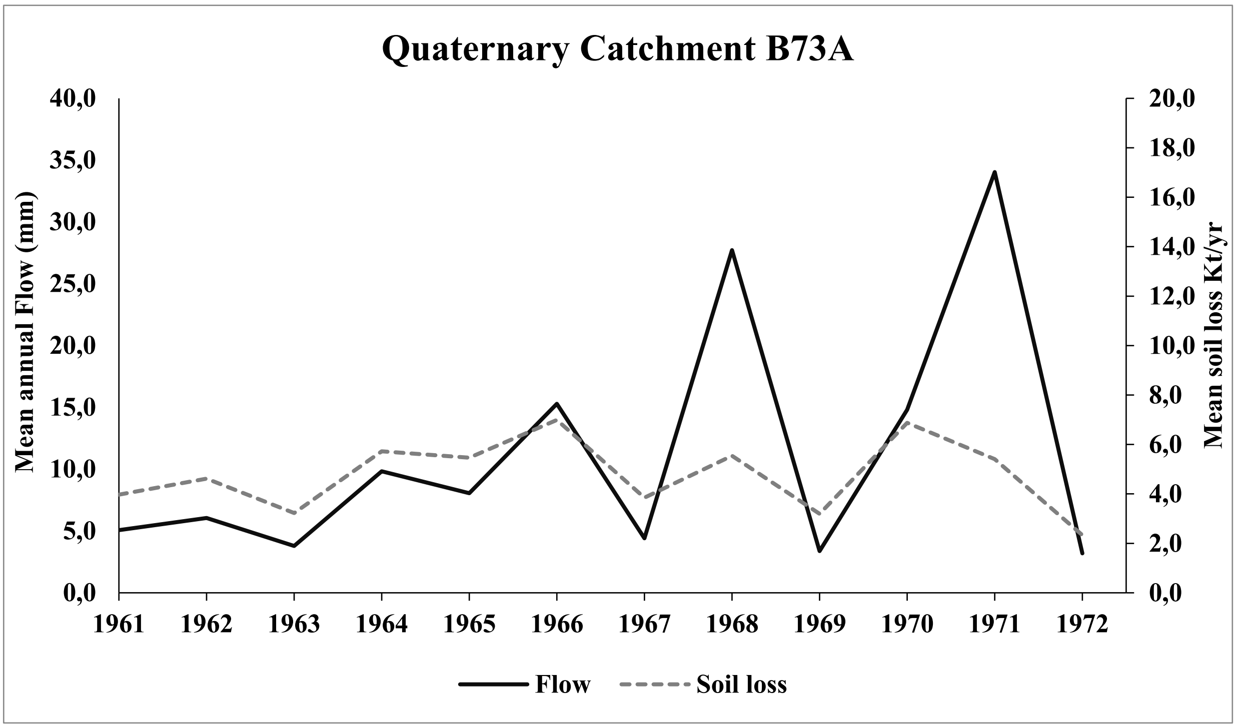

Figure 5.28 The model outputs in terms of surface flow and soil loss for the Klaserie Dam catchment in the Limpopo province, South Africa

Model outputs for Maden Dam (R20A)

A period of complete observed daily flow was used to drive the model estimates of erosion for this catchment, with flows for the period from early 1980 to late 2000 used.

The time series of daily flow for the Maden Dam catchment shows frequent peak flows over the study period; however, the beginning of either decade was characterised by low flows. The years between 1981-1983 and 1991-1993 (Figure 5.29) exhibit very low flows. This can be attributed to the historical droughts that occurred at the beginning of both decades (Masih *et al*., 2014). It is essential to note that the peak flows of the Maden Dam catchment are significantly lower than the peak flows of the other catchments used in the current study, such as the Klaserie Dam catchment.

The erosion time series shows a corresponding increase and decrease in erosion rate in response to flow rate (Figure 5.29). As a result of the lower peak flows, the early parts of each of the two represented decades contained the lowest erosion yields.

The simulated results show that the cumulative amount of soil lost to erosion in the Maden Dam catchment over the 21-year study period is 390 Kt, produced from the relatively tiny headwater catchment of 31 km^2. The simulated soil loss for the catchment is 6 t ha^{-1} year^{-1}. The result of this study falls slightly above the range of the estimate by Msadala *et al*. (2010)

for this region, which provided the most recent erosion estimation for South Africa. According to the estimate by Msadala *et al*. (2010), the soil loss from the catchment should range between 0-5 t ha^{-1} year^{-1}.

The Maden Dam catchment is characterised by steep slopes, although low soil erodibility and good vegetation cover reduce the rate of erosion. The Msadala *et al*. (2010) erosion risk map shows that the catchment is located in a very low to low erosion zone. The low soil loss estimated in the current study is likely associated with the good vegetation cover observed within the wider that part of the R20A quaternary catchment.

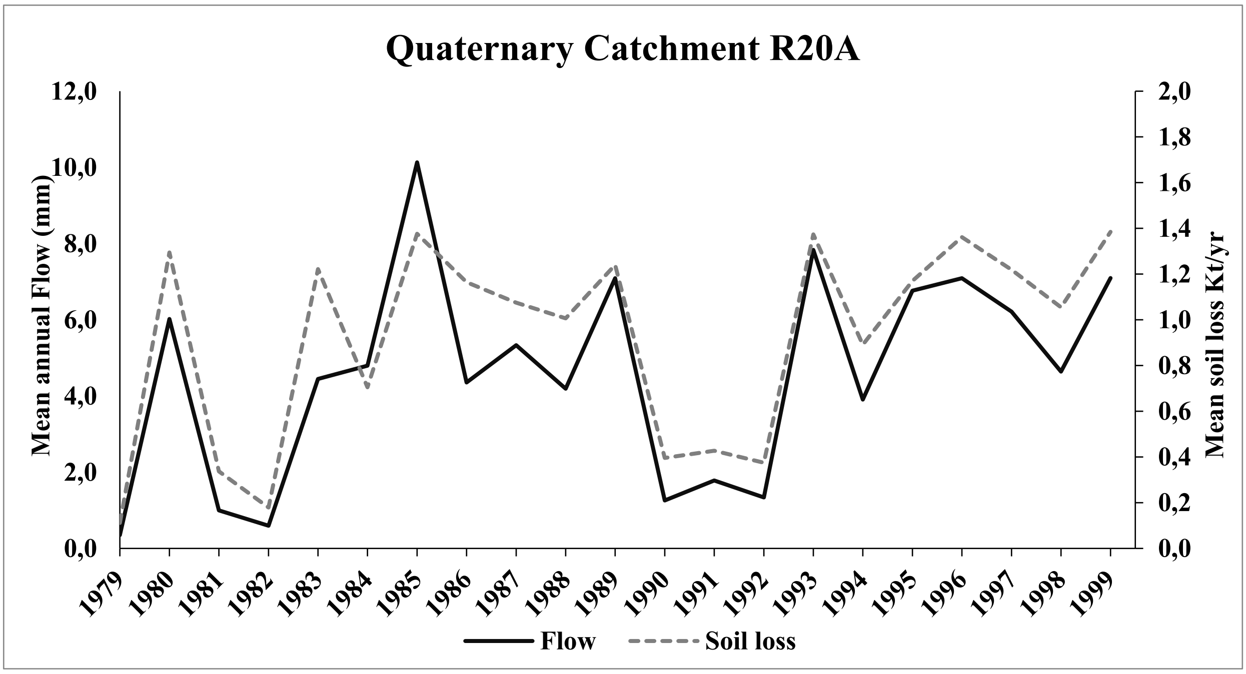

Figure 5.29 The model outputs in terms of surface flow and soil loss for the Maden Dam catchment (R20A) in the Eastern Cape, South Africa.

Model outputs for Koster Dam

The flows used to drive the sediment model for this catchment were a period of unbroken daily observed flows; therefore, the model outputs extend from the mid-1960s to early 2000.

The flow time series shows that the Koster Dam catchment is characterised by long dry spells typically associated with arid and semi-arid climates (Figure 5.30). Significantly high peak flows are evident for the years 1997 and 2000. Although low flows characterise the flow time series, severe dry periods are noted for 1967-1968, 1982-1984 and 1990-1994 (Masih *et al*., 2014).

The erosion output for the Koster Dam Catchment (Figure 5.30) shows increases and decreases in response to flows. This catchment generally exhibited lower erosion output compared to the other study areas of the current study. Cumulative erosion for the time series indicates that the Koster Dam catchment has considerably low erosion, and past erosion risk studies, such as that of Rooseboom (1992), have placed this catchment in a very low erosion zone.

The analysis of simulated soil loss shows that an estimated 650 Kt of soil was simulated as lost from the 187 km^2 Koster Dam catchment over the 34-year time series. The simulated soil loss for the time series is 1 t ha^{-1} year^{-1}. The Msadala *et al*. (2010) erosion risk study estimated that the soil loss in the catchment would range between 0-5 t ha^{-1} $year^{-1}$; therefore, the results of the simulations fall within the lower range of the Msadala *et al*. (2010) estimate.

The Koster Dam catchment is located in a region classified as experiencing very low erosion (Msadala *et al*., 2010). The low amount of erosion recorded in the catchment is likely a result of the interaction between multiple factors, including topography and soil erodibility. Although the vegetation cover is poor and is likely to contribute to soil loss, the soil erodibility and slope are very low, thereby reducing soil loss rates. The flow time series shows long dry spells accompanied by low peak flow events, indicating that that there is insufficient flow energy to drive rapid erosion across the A22B quaternary catchment.

Model outputs for the Xonxa Dam catchment (S10A-E)

Since no daily observed flow were available for this study area, monthly WR90 flows were used, disaggregated to daily using the method by Slaughter *et al*. (2015b); therefore, the flows used to drive the sediment simulations extend from 1920 to 1990.

The flow time series indicates that the Xonxa Dam catchment is characterised by high peak flows. Figure 5.31 shows that the peak flows for this catchment are higher than those observed in all the other catchments of the current study. The years 1924, 1944, 1972 and 1987 contain extreme peak flows > 200 mm. The flows indicate that periods of dryness were experienced between peak flows events, a pattern characteristic of the hydrological variability associated with semi-arid catchments. The high peak flows experienced throughout the time series are an important factor in the high erosion that is experienced in the study area.

The output of the erosion model shows that an estimated 600 × 10^6 tons of soil was lost from the 1,282 km^2 Xonxa Dam catchment over the 70-year time series. The simulated erosion for the catchment is 70 t ha^{-1} $year^{-1}$. The Msadala *et al*. (2010) erosion risk study estimates that erosion within the study would range between 60-150 t ha^{-1} $year^{-1}$; therefore, the erosion model simulated results are similar to the lower range of the Msadala *et al*. (2010) estimate.

The Xonxa Dam catchment is positioned in one of the highest erosion risk areas in the country, as shown by the erosion risk map of Msadala *et al*. (2010). The model output for the time series also shows extreme erosion events, particularly the years 1944, 1972 and 1987. Erosion for the year 1944 was simulated to exceed 600 Kt/day, an extreme case of erosion. A dam sedimentation study conducted by Msadala *et al*. (2010) found that the Xonxa Dam sedimentation rate is 888 tons km^{-2} $year^{-1}$, which is very severe given that the effective catchment area is > 1,000 km^2.

The Xonxa Dam catchment is located in a high erosion region. The catchment is characterised by steep slopes. The daily flow time series (Figure 5.31) shows very high peak flows, which correspond with high erosion events. The soil erodibility of the catchment is very high, whereas vegetation cover is relatively poor. The interactions between these erosion factors result in a high soil loss rate over the quaternaries S10A-E.

Model outputs for Churchill Dam (K90A−B)

Since an unbroken record of observed daily flows was not available for the catchment, the monthly WR90 flows were used, disaggregated to daily using the method by Slaughter *et al*. (2015). The flows used for simulations in this catchment extend from 1920 to 1990.

The average soil loss for the Churchill Dam catchment is estimated at approximately 20 t ha^{-1} $year^{-1}$. The estimate is within the range obtained by Le Roux *et al*. (2008) of 13-25 t ha^{-1} $year^{-1}$. The range relates to areas affected by moderate soil loss. The total simulated soil loss over the time series is 47 × 10^6 tons. The soil loss varies temporally in relation to variations in discharge over time. Periods of high discharge are characterised by high soil loss.

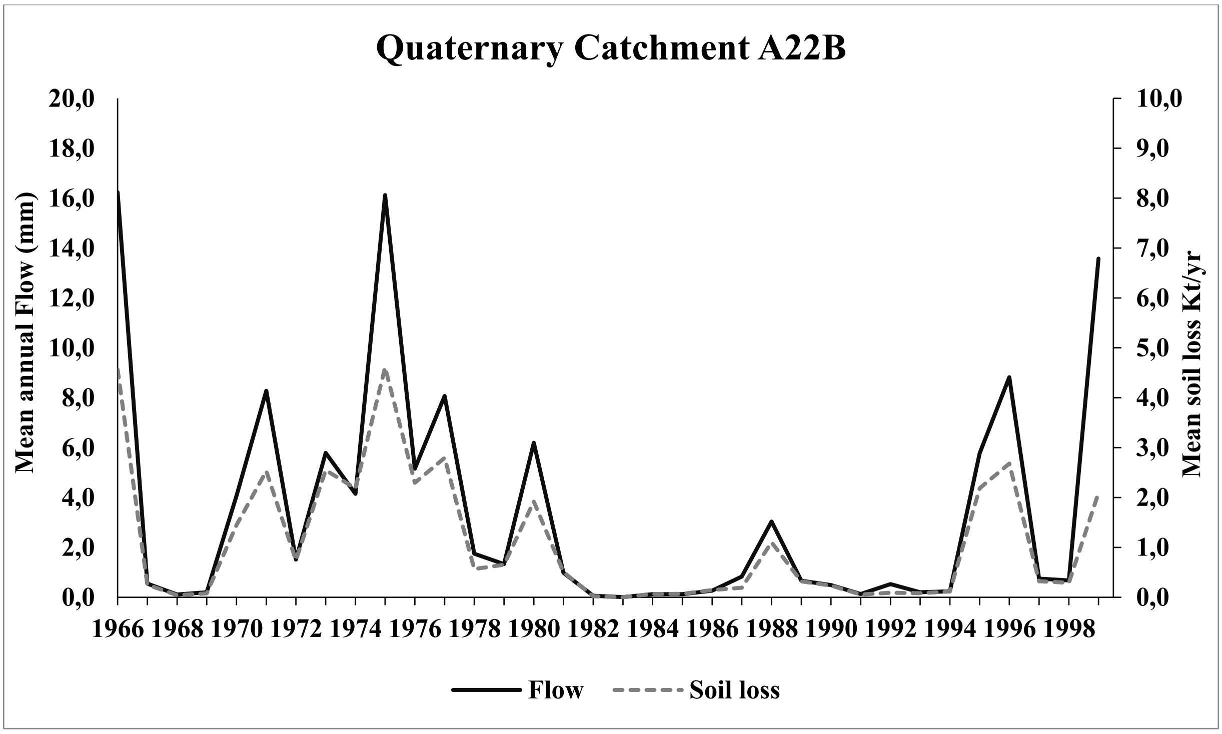

Figure 5.30 The model outputs in terms of surface flow and soil loss for the Koster Dam catchment (A22B) in the North West Province.

The Churchill Dam catchment is characterised by good vegetation. Whereas good vegetation cover reduces raindrop impact, encourages infiltration thus reducing runoff velocity, it is the highly erodible soils in the catchment that result in significant soil loss. The catchment however falls within the low to moderate soil loss category (Msadala *et al.,* 2010), and is influenced by the low runoff rate and good vegetation coverage.

Model outputs for T35A−E

Quaternary catchment T35A The simulation period for this catchment is from 1920-1990 and monthly WR90 flows disaggregated to daily using the method by Slaughter *et al*. (2015) were utilised to drive the model. The WR90 flows were used due to the lack of a continuous record of observed flows.

The simulated output of 166 × 10^6 tons was recorded from the catchment. The soil was lost from the 475-Km^2 over a 70-year time series. Approximately 50 t ha^{-1} $year^{-1}$ of soil is lost from the catchment. The output is within the range of previous estimates as Msadala *et al*. (2010) estimated that 26-60 t ha^{-1} $year^{-1}$ is lost from within the catchment. Although the range given by Msadala *et al*. (2010) is very wide and at a coarse scale, it gives a valuable indicator for us to see if our estimates are reasonable.

The simulated output indicates that the catchment has a high rate of soil loss (Figure 5.33). Msadala *et al*. (2010) places the catchment in a high to very high soil loss category. The catchment has poor vegetation cover; the cover factor of 1.2 indicates that the catchment is largely grassland that does not provide excellent protection against raindrop impact. The catchment also has one of the highest mean values of flow as compared to the other catchments used in the study, and this explains the high soil loss rate within the area.

Quaternary catchment T35B The simulated soil loss output for the catchment is 174 × 10^6 tons (Figure 5.34) .This value is cumulative daily time scale simulations over 70 years. The cumulative simulations equate to 63 t ha^{-1} $year^{-1}$ of soil that is lost from the 395-km^2 catchment. The result is slightly outside the 26-60 t ha^{-1} $year^{-1}$ estimated by Msadala *et al*. (2010). The result shows that the catchment is prone to high levels of soil loss.

The high soil loss in this catchment is attributed to the dominant grassland vegetation, which is sparse and degraded. Apart from the poor vegetation coverage, the catchment has the highest *LS* factor among T35 quaternaries and this largely influences the high soil loss simulation. The catchment is in the high to very high soil loss category (Msadala *et al*., 2010).

Quaternary catchment T35C The monthly WR90 flows disaggregated to daily using the method by Slaughter *et al*. (2015) were used to drive the model. The catchment has no gauging station; hence, there is no observed flow record available. The WR90 flow record used in the simulation is from 1920 to 1990.

The cumulative soil loss over the catchment is 128 × 10^6 tons (Figure 5.35). This was simulated over a 70-year time series. The annual soil loss rate is 60 t ha^{-1} $year^{-1}$.The simulated output falls within the range estimated by Msadala *et al*. (2010) of 26-60 t ha^{-1} $year^{-1}$ lost from the catchment. The catchment is also prone to soil loss similar to the other quaternaries selected from this region.

The T35C catchment has better vegetation coverage (C-factor 0.09) as compared to the other T35 catchments. However, the high output simulated for the catchment is attributed to the *LS* factor and soil erodibility factor (*K*) which is the highest among the T35 catchments. The reasonable vegetation coverage prevents the catchment from having the worst soil loss output among the T35 group of catchments.

Quaternary catchment T35D Since no daily observed flow were available for this study area, monthly WR90 flows were used, disaggregated to daily using the method by Slaughter *et al*. (2015b); therefore, the flows used to drive the sediment simulations extend from 1920 to 1990.

A cumulative 109 × 10^6 tons of soil was lost from the 348-km^2 study area (Figure 5.36). This amounts to 45 t ha^{-1} $year^{-1}$ of soil lost from the catchment. The simulated output falls within the range estimated by Msadala *et al*. (2010) of 26-60 t ha^{-1} $year^{-1}$ lost from the catchment.

The high soil loss output from the catchment is attributed to the poor vegetation cover. The catchment has a cover factor of 1.5 that is the highest among the group of T35 catchments. However, the catchment has the lowest *LS* and *P* factors among the T35 study catchments, and this reduces the soil loss significantly compared to headwater catchments T35A-C.

Quaternary catchment T35E The monthly WR90 flows were used, disaggregated to daily using the method by Slaughter *et al*. (2015). The flow period used within WR90 is from 1920-1990, and this is the simulation period for which the model was applied. The simulated results showed that the cumulative amount of soil lost due to erosion in the 492-km^2 T35E quaternary catchment is 137 × 10^6 tons over a 70-year period. The mean annual soil loss is 1.95 ×10^6 tons. This translates to approximately 40 t ha^{-1} $year^{-1}$ of soil that is lost from the catchment. The result of the current study falls within the range of the findings of Msadala *et al*. (2010) who estimated that 26-60 t ha^{-1} $year^{-1}$ is lost from the study area. Le Roux *et al*. (2014) estimated soil loss for the same area to be between 21-50 t ha^{-1} $year^{-1}$.

The rate of soil loss correlated well with runoff (Figure 5.32). High flows are typically accompanied by increased soil loss. The graph (Figure 5.32) shows the typical 'flashiness' associated with arid catchments where periods of dryness are followed by large storm events. This triggers rapid erosion, as displayed by the years 1976 and 1977. The model output for soil loss also shows the impact of low flows associated with droughts that affected South Africa. The severe drought period of 1980-1983 (Masih *et al*., 2014) was associated with low flows and reduced soil loss.

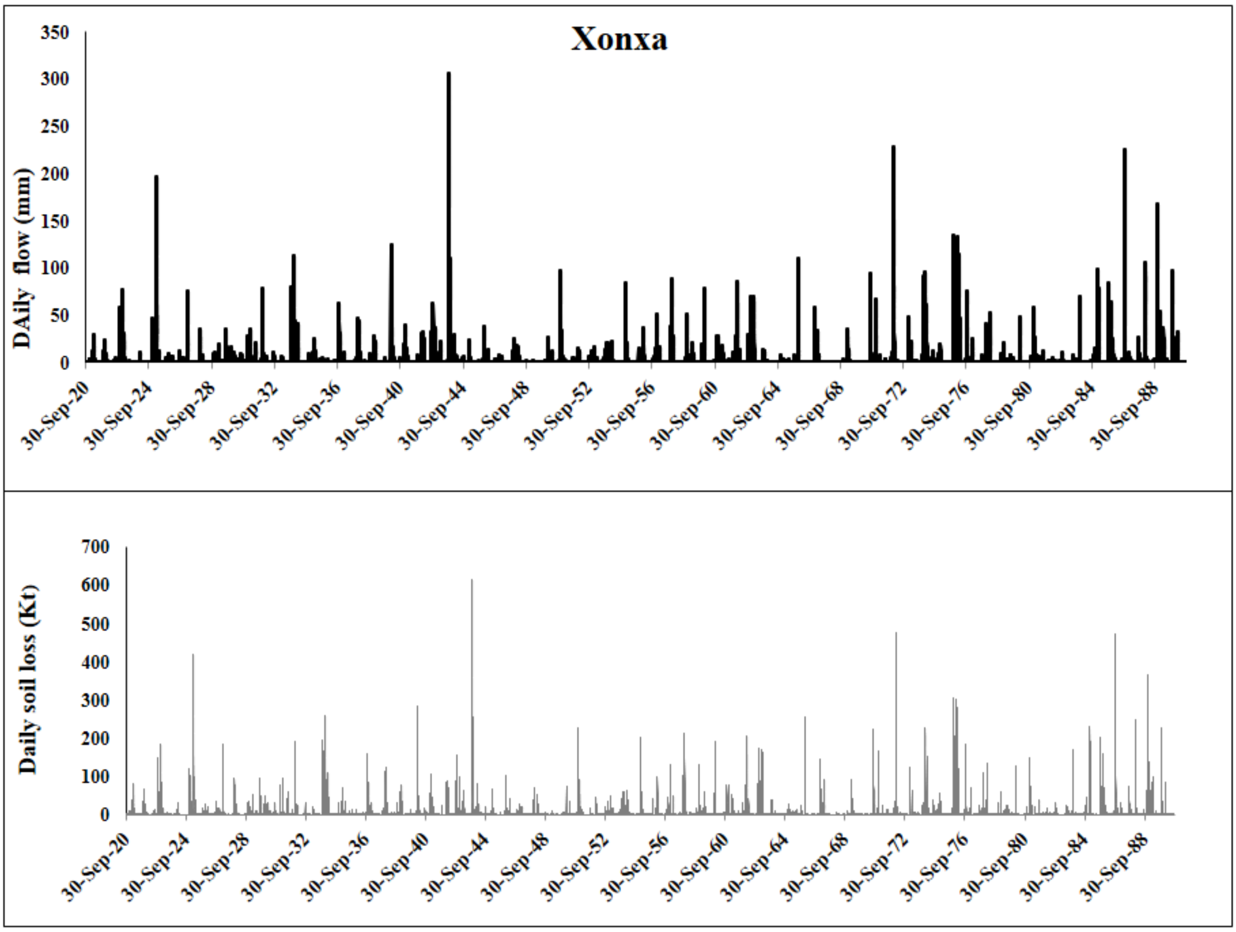

Figure 5.31 The model outputs in terms of surface flow and soil loss for the Xonxa Dam catchment in the Eastern Cape Province, South Africa.

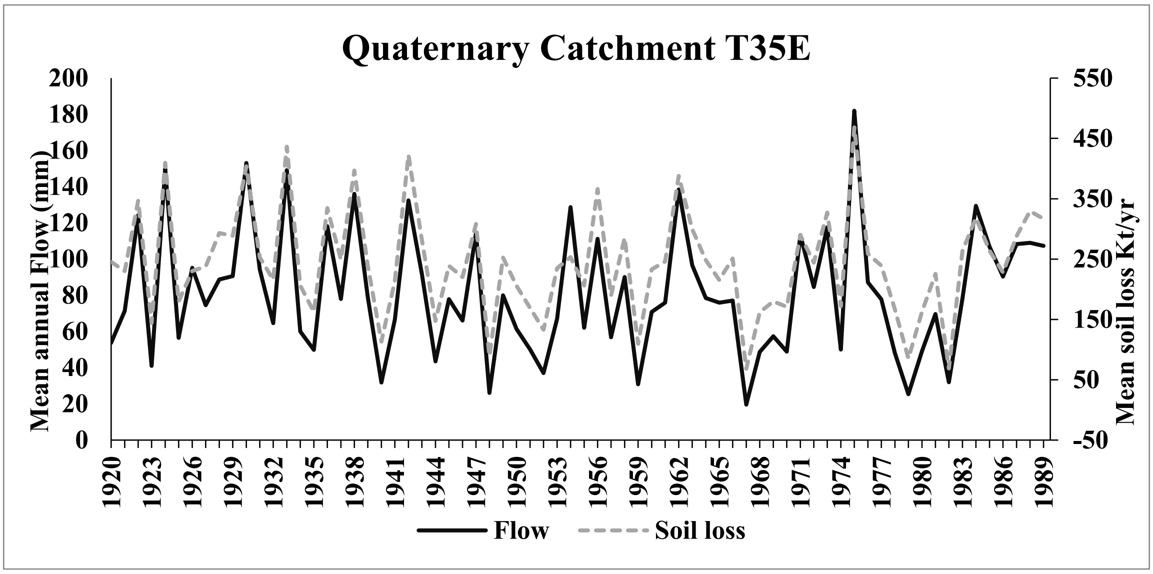

Figure 5.32 The model outputs in terms of surface flow and soil loss for the T35E catchment in the Eastern Cape Province, South Africa

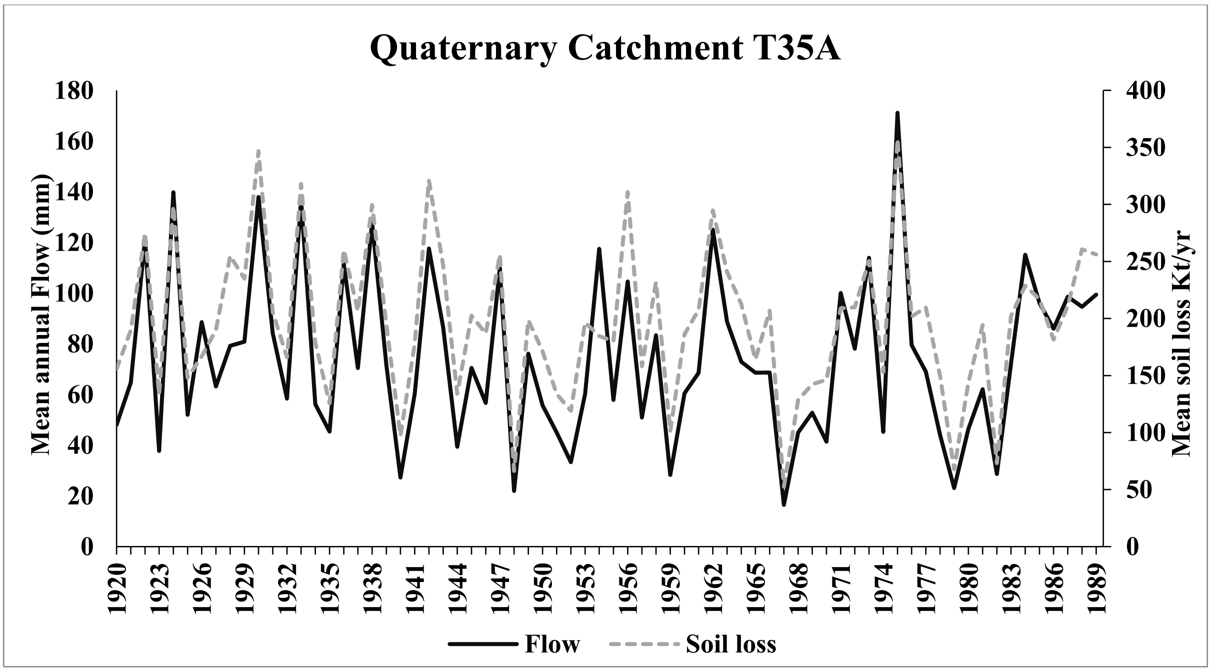

Figure 5.33 The model outputs in terms of surface flow and soil loss for the T35A catchment in the Eastern Cape Province, South Africa

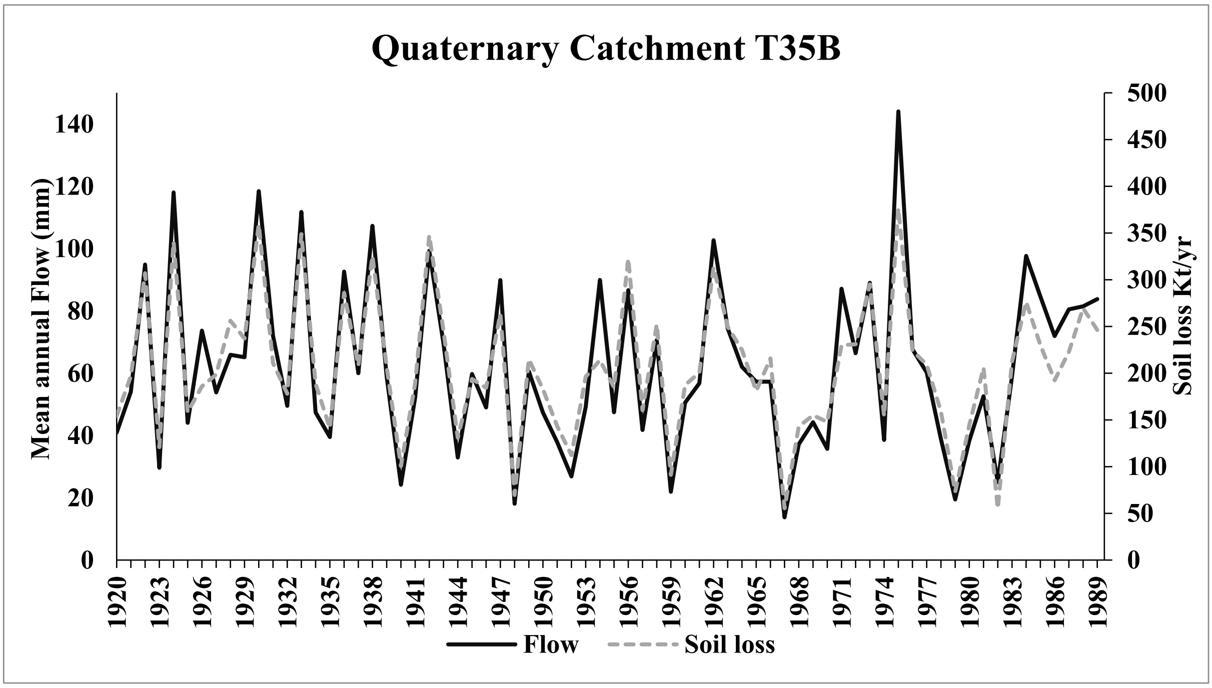

Figure 5.34 The model outputs in terms of surface flow and soil loss for the T35B catchment in the Eastern Cape Province, South Africa

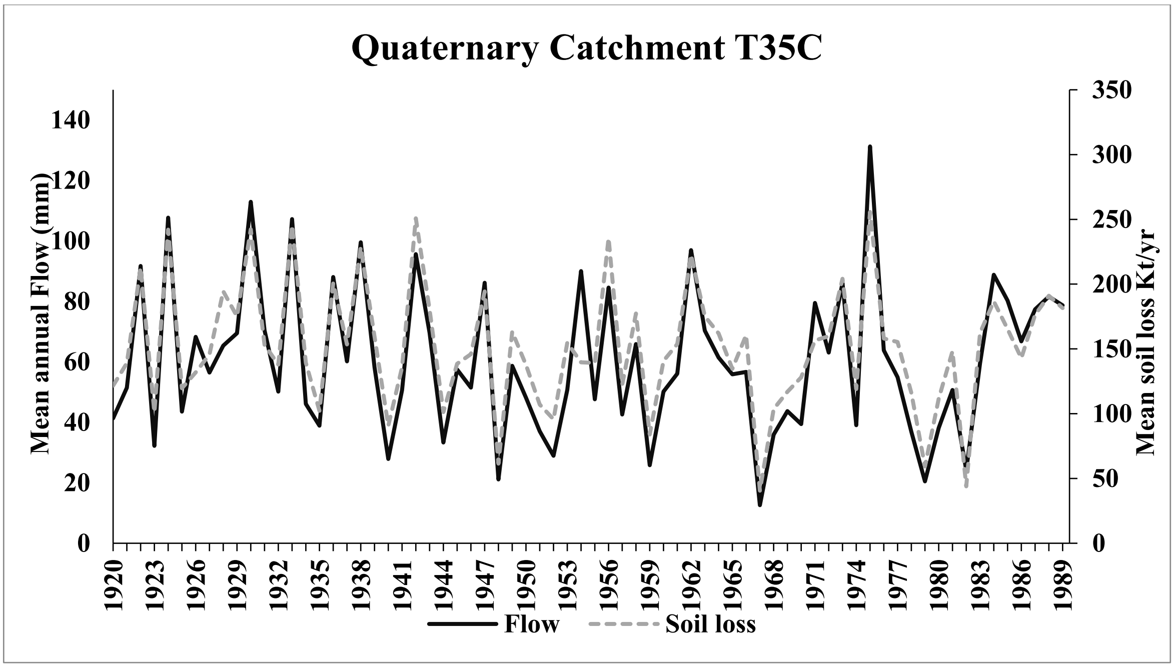

Figure 5.35 The model outputs in terms of surface flow and soil loss for the T35C catchment in the Eastern Cape Province, South Africa

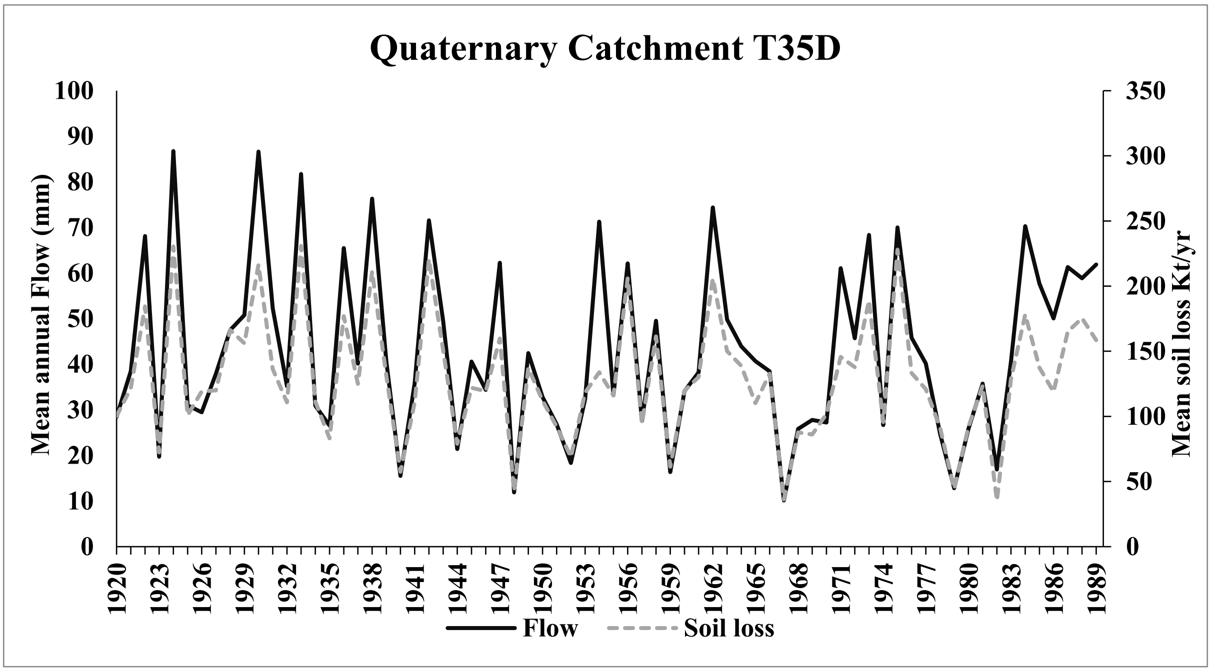

Figure 5.36 The model outputs in terms of surface flow and soil loss for the T35D catchment in the Eastern Cape Province, South Africa

Model outputs J12G

The WQSED Model was driven using a WR90 flow record from 1920-1990. The monthly flows were disaggregated to daily using the method by Slaughter *et al*. (2015).

The model estimated 3 t ha^{-1} $year^{-1}$ of soil lost from the catchment (Figure 5.37). A cumulative 16 × 10^6 tons of soil was lost from the 768-km^2 study area over the 70-year time series. The model simulation is lower than the previous estimates by Msadala *et al.* (2010) who estimated that 6-13 t ha^{-1} $year^{-1}$ of soil is lost from the catchment.

The J12G catchment is classified to be in a low erosion zone (Msadala *et al*., 2010). The erodibility parameters are marginally different from parameters recorded for high soil loss areas such as the T35 group of catchments, with the exception of the cover factor (0.06) which denotes good vegetation coverage. The low simulated soil loss rate is likely associated with low flow rate. The average flow rate of 0.12 $mm^{-1}\ s^{-1}$ is one of the lowest flow averages across all the catchments used in this study. Flow is the driver of the model; therefore, a catchment with low flows will be characterised by low soil loss output, even if other (erodibility) factors indicate potential for high erosion. Without sufficient flow energy, soil will not be dislodged and/or transported.

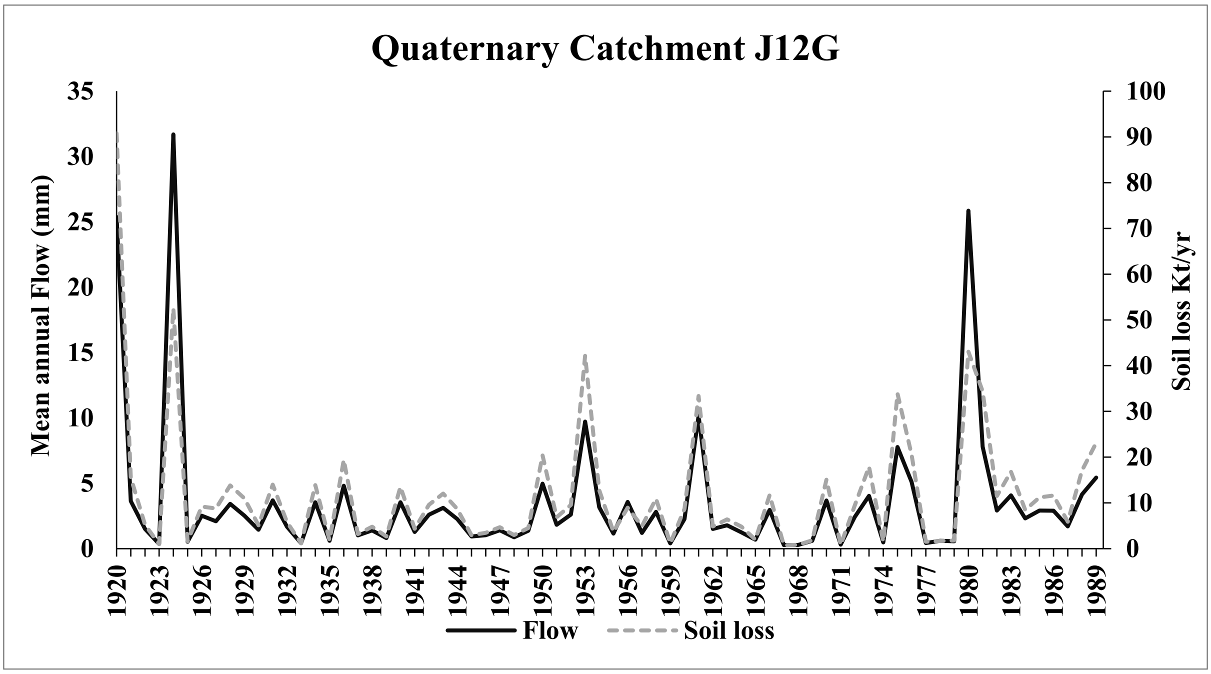

Figure 5.37 The model outputs in terms of surface flow and soil loss for the Prinsriver Dam catchment in the Western Cape Province, South Africa

Model outputs H80A

The monthly WR90 flows disaggregated to daily using the method by Slaughter *et al*. (2015) were used to drive the model. The flows used for simulations in this catchment extend from 1920 to 1990.

The simulated results show that the cumulative amount of soil lost to erosion in the Duiwenhoks Dam catchment over the 70-year study period is 25 × 10^6 (Figure 5.38). This equates to 24 t ha^{-1} $year^{-1}$ of soil that is lost from the catchment. The result of this study falls within the range of the estimate by Msadala *et al*. (2010) for this region, which provided the most recent erosion estimation for South Africa. According to the estimate by Msadala *et al*. (2010), the soil loss from the catchment over the time series should range between 13-26 t ha^{-1} $year^{-1}$; therefore, the result of the current study fell within the upper range of the estimate by Msadala *et al*. (2010)

The H80A quaternary catchment falls in a moderate erosion zone (Msadala *et al*., 2010). The catchment has the highest *LS* factor compared to all the other study areas. A high *LS* factor increases erosion rates (Morgan, 2005); however, the catchment has a very good vegetation coverage (*C* factor = 0.05). The good vegetation absorbs the effects of the high *LS* factor and eases the soil loss rate. The H80A catchment has a low average time series flow rate (0.7 $mm^{-1}\ s^{-1}$) compared to T35 catchments (> 1.5 $mm^{-1}\ s^{-1}$), and this partly contributes to lower soil loss rates.

5.6.3 Model outputs: sediment concentration

Four catchments were selected to analyse sediment concentration outputs by the model. These include A22B, T35E, B73A and R20A representing arid, semi-arid, semi-arid and temperate climatic regions respectively. The two semi-arid catchments are considered to cater for the Eastern Cape proposed site, which is to be constructed in a reportedly very high erosion area (Le Roux *et al.,* 2014). The model simulates sediment concentrations likely to be recorded at the outlets of the catchments. Sediment concentration duration curves were used analyse the time series outputs (Figure 5.39).

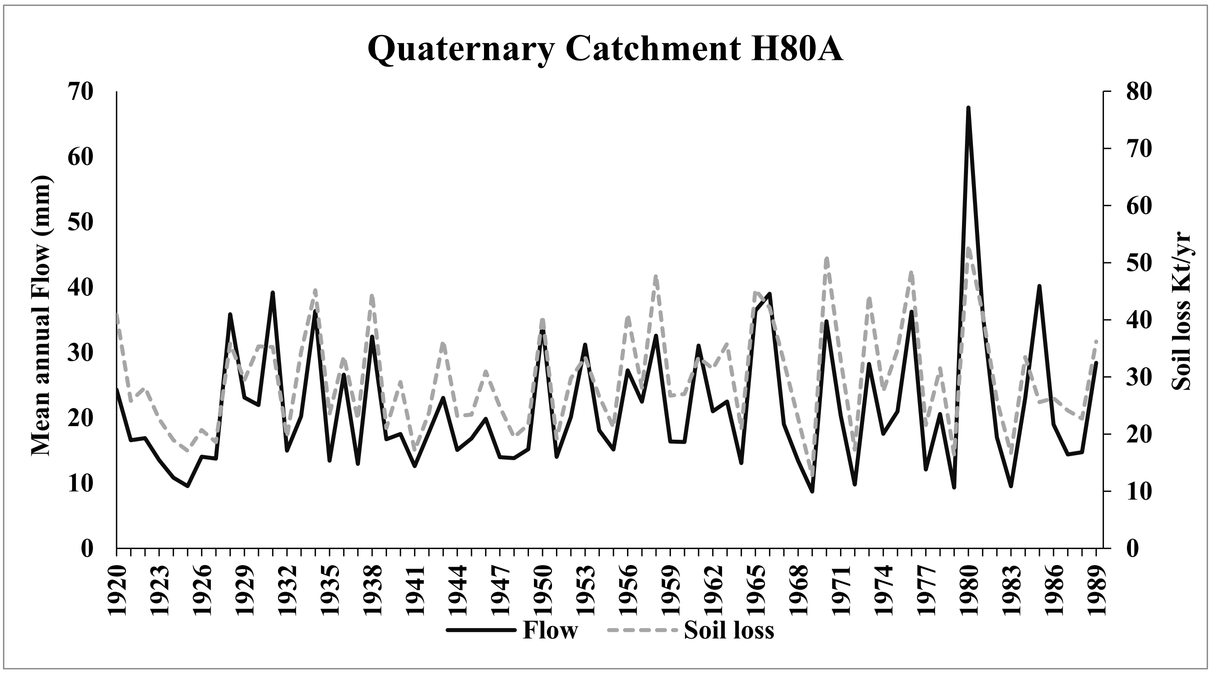

Figure 5.38 The model outputs in terms of surface flow and soil loss for the Duiwenhoks Dam catchment in the Western Cape Province, South Africa.

The model simulated low concentrations for the arid A22B catchment. The peak time-series concentration is 50 mg ℓ^{-1}. The curve shows that model simulations of sediment concentration are more than 1 mg ℓ^{-1} less than 10% of the time and below 0.1 mg ℓ^{-1} over 60% of the time. The model simulations of sediment concentration for the R20A quaternary catchment representing the temperate region show a much lower time series peak of 10 mg ℓ^{-1}. The simulations reflect concentrations above 1 mg ℓ^{-1} less than 5% of the time, whereas concentrations less than 0.1 mg ℓ^{-1} are reflected over 70% of the time series. Model simulations for the B73A catchment in the semi-arid zone show a high time series peak concentration of 477 mg ℓ^{-1}. Sediment concentrations above 1 mg ℓ^{-1} are reflected 50% of the time and 20% of the time for concentrations less than 0.1 mg ℓ^{-1}. Sediment sampling conducted in a nearby catchment observed a high of 3,000 mg ℓ^{-1}. The observed concentrations are five times higher than the model outputs. Model simulations for the T35E catchment showed the highest time series peak of 10,000 mg ℓ^{-1}. The simulations for the catchment also reflect concentrations of more than 1 mg ℓ^{-1} more than 90% of the time. Sampling conducted in a catchment relatively near to T35E (Bannatyne *et al.*, 2017) reported a high sediment concentration of 5,000 mg ℓ^{-1}. The model simulations are therefore two times higher than what has been observed in a separate catchment. It is however important to point out that sediment concentrations can vary immensely at spatial and temporal scales.

5.6.4 Sensitivity of model outputs to inputs

A statistical analysis was conducted using principle component analysis (PCA). The analysis sought to investigate the impact of inputs on the model outputs across catchments. The analysis is crucial in identifying the prominent drivers of soil loss in South African catchments. The results of the analysis (Figure 5.40) show that runoff (flow) is the major driver of soil loss. The correlation of flow to soil loss is very high (> 0.9). Apart from flow, the only other factor that correlates significantly with soil loss is the vegetation cover factor. The vegetation cover factor has a correlation of 0.6 to soil loss. All the other factors that include area, topography, management practice and soil erodibility have a correlation below 0.5. A correlation lower than 0.5 indicates a weak relationship and therefore lower impact on the soil loss outputs. Notably, soil erodibility and topography have a negative correlation with soil loss. The negative correlation indicates that among the study sites used in the study, most of those with high soil erodibility and topography values had low soil loss output. The analysis was undertaken using the inputs and outputs of all catchments in the study to identify trends in inputs and outputs.

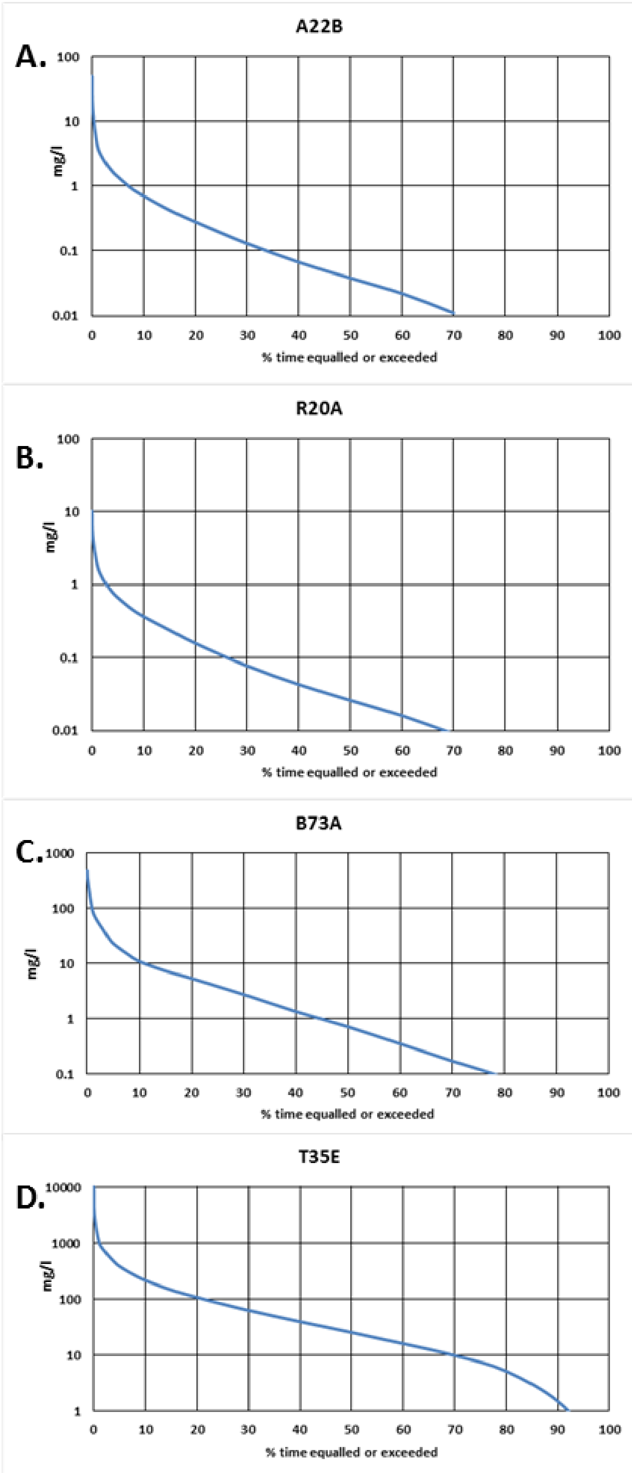

Figure 5.39 Sediment concentration duration curves representing varying climatic regions (A) A22B – semi arid (B) R20A – temperate (C) B73A − semi-arid and (D) T35E – proposed location for the Ntabelanga Dam

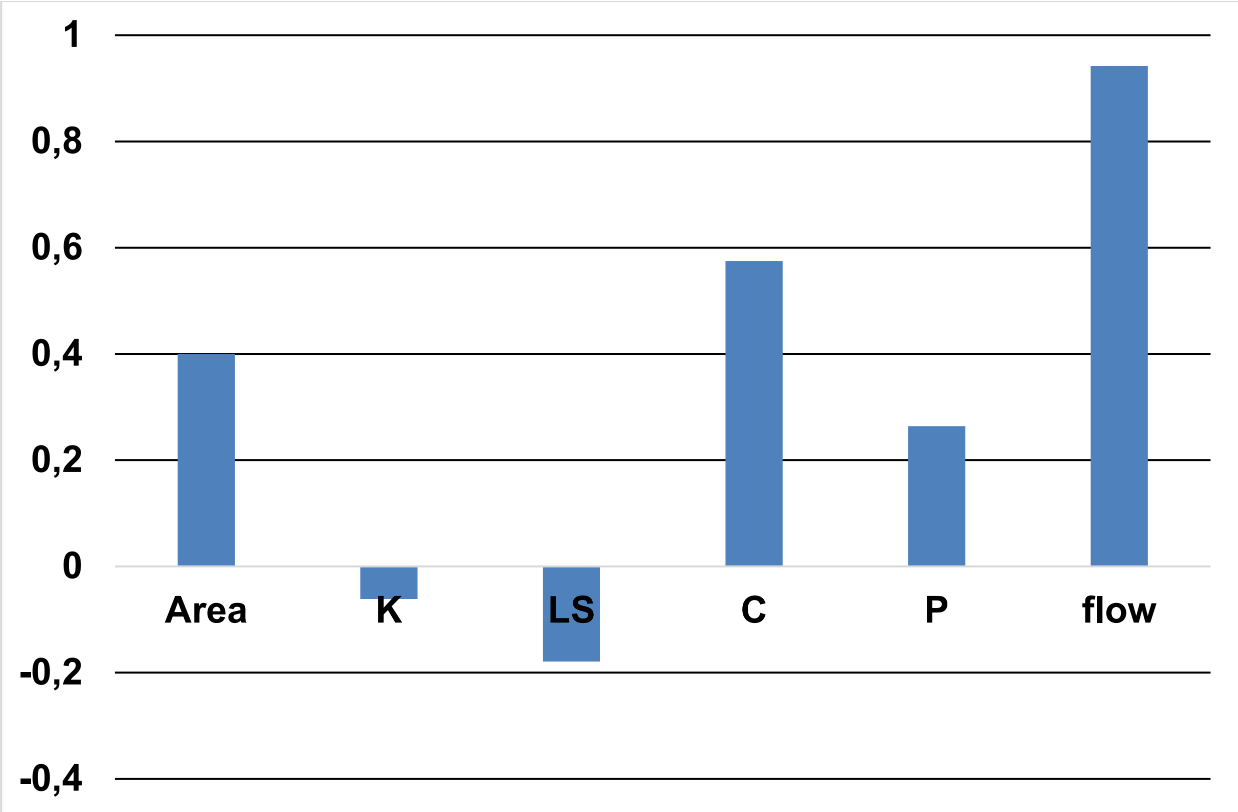

Figure 5.40 Correlation of the physical catchment parameters to simulated soil loss

The PCA tested the relationship of inputs and outputs across catchments. Although the analysis provides an important overview on the influence of parameter values on soil loss output, the scale at which it is applied does not suffice to explain model sensitivity to input parameter values. A deterministic sensitivity analysis was used to analyse model response to changes in parameter input values. The result of the sensitivity analysis summarised in Table 5.5, shows that the model was more sensitive to the parameter relating to vegetation cover (*C*) compared to the other parameters. The minimum and maximum ranges for the *C* parameter gave the lowest and highest model outputs, respectively. When all parameters were set to minimum values, model output associated with *C* (P_{min}) was > 75% lower compared to model outputs associated with the other parameters. The same trend was noted at the maximum parameter value where the outputs for *C* (P_{max}) were > 45% higher compared to the output for other parameters. The management support practice (*P*) parameter showed the least sensitivity in output.

5.6.5 Discussion

Model parameterisation

The use of readily-available geographic information system (GIS) datasets and the *a-priori* regionalisation procedure managed to yield parameter values that were consistent with physical properties of the various catchments under study. The parameter values could be related to catchment characteristics reported in the literature and observed in field observations and satellite imagery.

The distribution of the *LS* shows variations in topography across the selected sites. The Duiwenhoks Dam catchment has the highest *LS* factor (9.7) and this was attributed to it being located in a ravine; the steep slopes on either side of the catchment contribute to the *LS* distribution calculated for the catchment.

Table 5.5 Sensitivity of soil loss simulations (in Kilotons) to model input parameter values. The P_{min} & P_{max} correspond to the minimum and maximum values of the parameter, respectively

Parameters	Parameter Ranges		Soil Loss Output	
	Minimum	**Maximum**	P_{min}	P_{max}
Cover	0.003	0.5	3	530
Soil erodibility	0.03	0.7	12	290
Topography	1*	10*	25	260
Practice	0.1	1	14	140

*The *LS* values used were min and max values recorded in selected study areas; therefore, the *LS* factor can be higher or lower than stated above.

The Koster Dam Catchment located on a relatively flat plain has the lowest *LS* of 1. The T35 catchments located near Lesotho have high *LS* factor distributions; the Drakensburg range dominates this region, resulting in steep slopes. The *LS* factor for the selected catchments range from a low of 1 and a high of 9.7. It is essential to note that mean *LS* factor values are used as model inputs; therefore, much lower and higher values would be distributed spatially across a given catchment.

The distribution of the vegetation cover (*C*) factor does not show a lot of variation (Table 5.5). Approximately 50% of the study sites have a *C* factor of between 0.1 and 0.15, indicating the dominance of grassland in these areas. A dominance of grasslands in the *C* factor is consistent with the classification of Acocks (1988) and Mucina and Rutherford (2006) who highlight that approximately two thirds of South Africa is dominated by grassland and savannah grassland biomes. The *C* factor is largely influenced by the climatic zonation of respective catchments as climate correlates with vegetation coverage. The arid Koster Dam catchment has the highest *C* factor of 0.17. All the catchments in the semi-arid zones have a *C* factor ranging from 0.1-0.15 (indicating grassland) except for the Klaserie Dam catchment. The Klaserie is small, steep headwater catchment that receives up to 1,200 mm (Schulze *et al*., 2007) of rainfall due to the orographic effect. The Klaserie catchment contains good coverage of indigenous forest (NLC 2014) that influences its *C* factor. The catchments located in the southeastern humid and temperate regions such as the Maden and Prinsriver dam catchments have low *C* factors of below 0.05. The low *C* factor is a result of the good vegetation coverage in these areas. It was noted from field observations and from literature (Poesen *et al*., 2005), that the former Transkei region in the Eastern Cape (which includes T35A-E) is experiencing drastic vegetation loss because of overgrazing. It may be necessary to adjust the grassland *C* factor upwards to cater for degraded grassland scenarios.

The soil erodibility factor distribution (Table 5.5) shows that the majority (69%) of selected study sites have soils that are moderately erodible. *K* factors between 2.25-0.5 are classified as moderately erodible (Schulze and Lorentz, 1995). The Churchill Dam catchment has a high erodibility factor that is associated with the Podzolic (sandy) soils dominating that region. In an empirical study conducted in the T35 catchments, it was discovered that part of the catchment is covered by dispersive soil (Le Roux *et al*., 2014). Dispersive soils have a high infiltration rate and crumble and dissolve when exposed to water. The discovery means that our previous understanding of the soils of the area (Schulze, 2007) requires revision as *K* factor of the area may be higher.

The management practice (*P*) factor distribution (Table 5.5) shows that most of the study areas have high *P* factor values of > 0.8.The high *P* factor values indicate that there are poor management practices within the study areas. However, this is certainly not the case. In most of the catchments, agriculture constitutes a small percentage of the total area. Since non-agricultural land is assigned a *P* factor of 1 (indicating no management practice), weighting the *P* factor of all land used to obtain the mean catchment *P* factor results in a high *P* factor. The mean *P* factor effectively represents the parameter at a catchment scale; however, the mean value is misleading and fails to depict the actual status of the agricultural land.

Model outputs

The model results show that erosion is essentially driven by flows, and catchments with higher peak flows experience higher rates of erosion (Figure 5.41). A linear regression analysis of model output and flow yielded an R^2 of 0.88 (Figure 5.42). However, some of the catchments such as the T35A and T35E have lower soil loss rates but high flows. This can be attributed to other factors that influence erosion processes in catchments such as vegetation cover and slope. Flow is the most significant driver of erosion processes; however, soil loss results from an interaction of factors. A typical example of these interactions is that the size of a catchment affects the amount of sediment available in storage; however, this does not translate to increased erosion. This is exhibited by the Prinsriver Dam catchment (768 km^2), which has a lower soil loss rate compared to other catchments which are less than half its size. Notable also is that although steep-sloped catchments are expected to experience more erosion, steep slopes that are well-vegetated, such as those found in the Koster and Klaserie dam catchments, are protected from erosion. However, sensitivity analysis outputs show that flow and vegetation cover are the lead causal factors in soil loss.

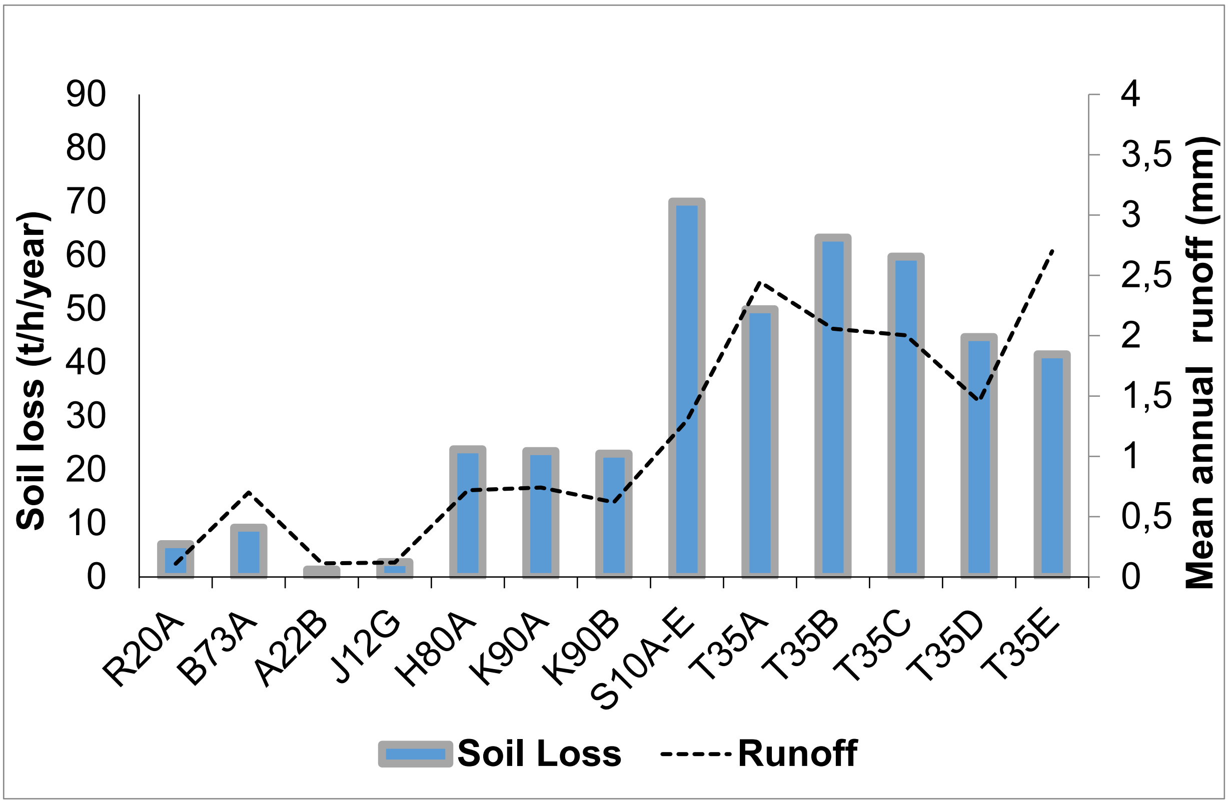

Figure 5.41 The relationship between mean annual runoff and annual soil loss for the selected study areas.

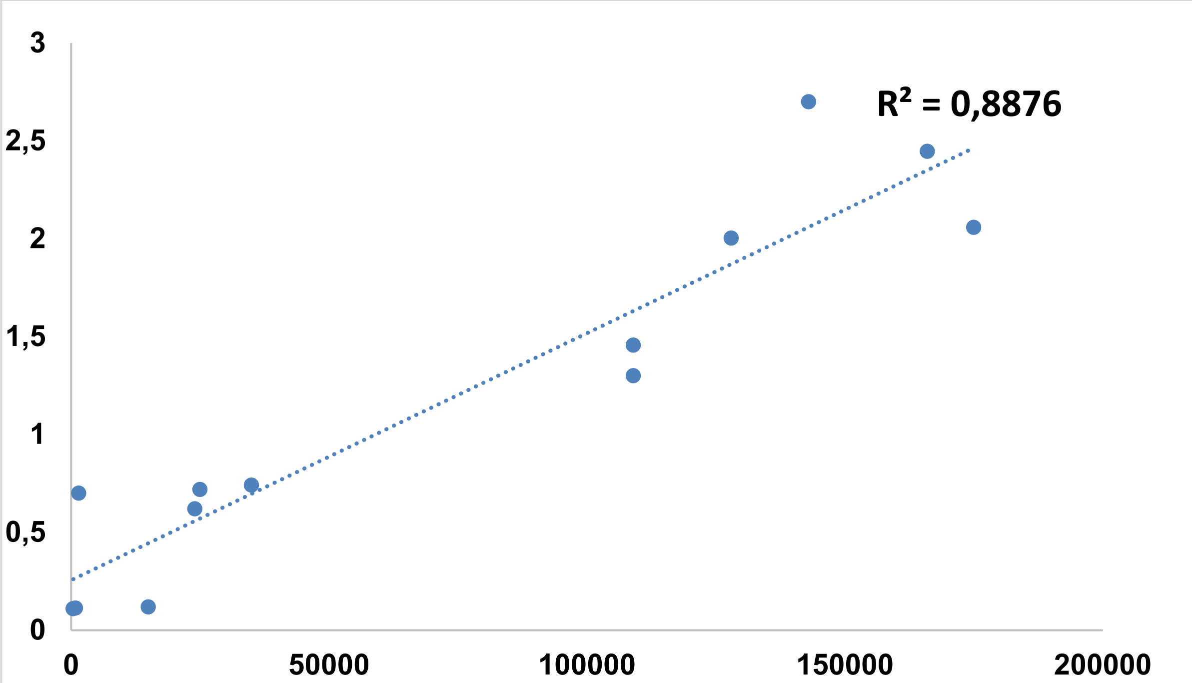

Figure 5.42 Linear correlations of soil loss and flow.

The model outputs for soil loss (Table 5.5) are consistent with soil loss estimates from previous studies. The outputs from the model fall within the range of soil loss estimates by Msadala *et al*. (2010), which is the most recent erosion study covering South Africa. The Msadala *et al*. (2010) sediment prediction for South Africa is a follow-up study to the Rooseboom (1992) study; however, the more recent study by Msadala *et al*. (2010) provides considerably higher estimates compared to the earlier study.

The results (Table 5.6) show that the catchments located in the Eastern Cape have the highest soil loss output. Le Roux *et al.* (2014) conducted an erosion modelling study in the Umzimvubu catchment in the Eastern Cape region and the results indicated a very high sediment yield of > 50 t ha^{-1} year^{-1} of soil loss. The high rates of soil loss in the region are attributed to massive gullying and the presence of dispersive soils that erode rapidly when exposed to rainwater (Le Roux *et al.,* 2014). Ongoing research by the department of environmental affairs in the Ntabelanga Dam site also suggests there may be ongoing erosion below the surface (known as piping), resulting in the surfaces suddenly collapsing into large gullies. The high soil loss rates in the Eastern Cape can also be attributed to human influence. Poor land management and overgrazing are destroying the vegetation cover, which are important factors contributing to soil loss (Poesen, 2005).

The temperate south eastern parts of the country which include the R20A and K90A-B catchments have much lower erosion rates compared to the semi-arid Eastern Cape catchments. The lower soil loss rates are attributed to the good vegetation coverage in the region (Table 5.6).

The sensitivity analysis (Table 5.5) shows that a low vegetation cover parameter (indicating good coverage) results in considerable decreases in soil loss. An experiment conducted by Hudson and Jackson (1959) proved that there is 99% less erosion on vegetated soil as compared to bare soil. This validates why catchments in the south east have > 45% lower erosion than catchments in the poorly-vegetated Eastern Cape. A study conducted by Rooseboom (1992) showed that the catchments in the temperate region experienced > 60% lower erosion as compared to the Eastern Cape. The parameterisation within the current study has managed to represent catchment conditions and the model outputs are consistent with the erosion trends that are reported by past studies for the country.

Table 5.6 Summary of model erosion outputs and estimates (*Kt*) by Msadala *et al*. (2010)

Name	(km^2)	Climate	Model estimates (tons h^{-1} yr^{-1})	Previous estimates (tons h^{-1} yr^{-1}) (Msadala *et al*., 2010)
R20A	30	Temperate	6	0-5
B73A	136	Semi-arid	9	13-26
A22B	187	Arid	1	0-5
J12G	768	Arid	3	6-13
H80A	150	Temperate	24	13-26
K90A	213	Temperate	23	13-26
K90B	149	Temperate	23	13-26
S10A-E	1282	semi-arid	70	60-150
T35A	475	semi-arid	50	26-60
T35B	395	semi-arid	63	26-60
T35C	306	semi-arid	60	26-60
T35D	348	semi-arid	45	26-60
T35E	492	semi-arid	42	26-60

The western part of South Africa is characterised by aridity (Schulze*,* 2007). The lack of precipitation also affects erosion and sediment transport. Rooseboom (1992) highlights that this region experiences on average 70% lower erosion as compared to the rest of South Africa. The model outputs of the catchment representing this region (A22B-Table 5.6) show that the catchment has the lowest erosion output compared to other selected study sites. The ability of the model to simulate erosion trends that have been reported in previous literature indicates the effectiveness of the parameterisation procedure employed to estimate model parameters.

5.7 Incorporation of WQSED into WQSAM

5.7.1 Introduction

The incorporation of WQSED into WQSAM is required from a water quality systems modelling perspective, as although it is sufficiently accurate to model sediment from individual subcatchments using natural incremental flow, once sediment enters the main stem of a river, flow is impacted through human use such as extractions and return flows as well as reservoirs. A certain velocity of flow is required to maintain sediment in suspension, and reservoirs can act as sediment traps. Therefore, to model the fate of sediment within a large catchment highly impacted by human use, there is no alternative but to drive the sediment modelling through flows generated by a systems (yield) model, rather than a hydrological model.

The broad approach taken within WQSAM is to model incremental inputs of sediment from individual subcatchments separately using WQSED. The simulations of daily sediment loads are then saved as time series in SPATSIM, from which they are read as input into WQSAM. Therefore, for conceptual understanding of erosion and sediment routing in individual subcatchments, please read the previous sections of the current chapter.

It is important to stress that since WQSED does not simulate bed load transport of sediment, WQSAM similarly ignores bed load transport and concentrates on the transport of suspended sediment.

5.7.2 Calculation of velocity, depth and river width with different flows

To calculate the transport of suspended sediment, WQSAM requires estimates of velocity (m s^{-1}), depth (m) and width (m) with different daily flows (m^3 s^{-1}). To calculate these, WQSAM makes certain assumptions about the channel shape, and also requires additional user input, i.e. the river channel maximum width (m) and slope. The assumptions of the channel shape are illustrated in Figure 5.43.

Within the sediment routing procedure of WQSAM, the model will first step through all the subcatchments (nodes) in the modelled system, and using the set parameters of $Width_{max}$ and *Slope*, will calculate width (*Width*), depth (*Depth*), flow (*Q*) and velocity (*Vel*) in one cm increments of depth until the maximum depth for the channel. These values are placed in an array in run-time memory, which effectively acts as a lookup table during the sediment routing.

$Width_{bed}$ is assumed to be 60% of $Width_{max}$. We need to calculate *Depth* at bankfull to determine the range of depths for the lookup table:

$Opp = (Width_{max} – (Width_{max} * 0.6))/2$ (Equation 5.12)

$Depth_{max} = 0.6 * ((Width_{max}/0.45)^{2.08})^{0.35}$ (Equation 5.13)

$Depth_{max}$ is the depth at bankfull and determines the range of depths for which *Q*, *Vel* and *Width* are calculated in one cm increments of *Depth*.

We need the angle α (Figure 5.43) in subsequent calculations:

$Hyp = (Opp^2 + Depth_{max}^2)^{0.5}$ (Pythagorean Theorem) (Equation 5.14)

$\alpha = \arcsin(Opp/Hyp)$ (Equation 5.15)

For each 1 cm increment of *Depth* from 1 to $Depth_{max}$:

$N = 0.1 – (\mathrm{Depth}/Depth_{max} * 0.06)$ (Equation 5.16)

Where *N* is Manning's N for an assumed range of 0.04 to 0.1, with 0.1 the value at the lowest depth and 0.04 the value at $Depth_{max}$.

To work out wetted perimeter and area with changes in depth:

$Hyp = Depth/\mathrm{Cos}(\alpha)$ (Equation 5.17)

$Opp = (Hyp^2 – Depth^2)^{0.5}$ (Equation 5.18)

$Wetted\_Perimeter = Hyp * 2 + Width_{max} * 0.6$ (Equation 5.19)

$Area = (Width_{max} * 0.6 * Depth) + (Depth * Opp)$ (Equation 5.20)

$Vel = ((\mathrm{Area/Wetted\_Perimeter})^{0.67} * Slope^{0.5})/N$ (Equation 5.21)

$Width = (Width_{max} * 0.6) + (Opp * 2)$ (Equation 5.22)

$Q = Area * Vel$ (Equation 5.23)

For each 1 cm increment of *Depth* from 1 cm to $Depth_{max}$, *Depth*, *Width*, *Vel* and *Q* are stored in a lookup table (runtime memory multi-dimensional array).

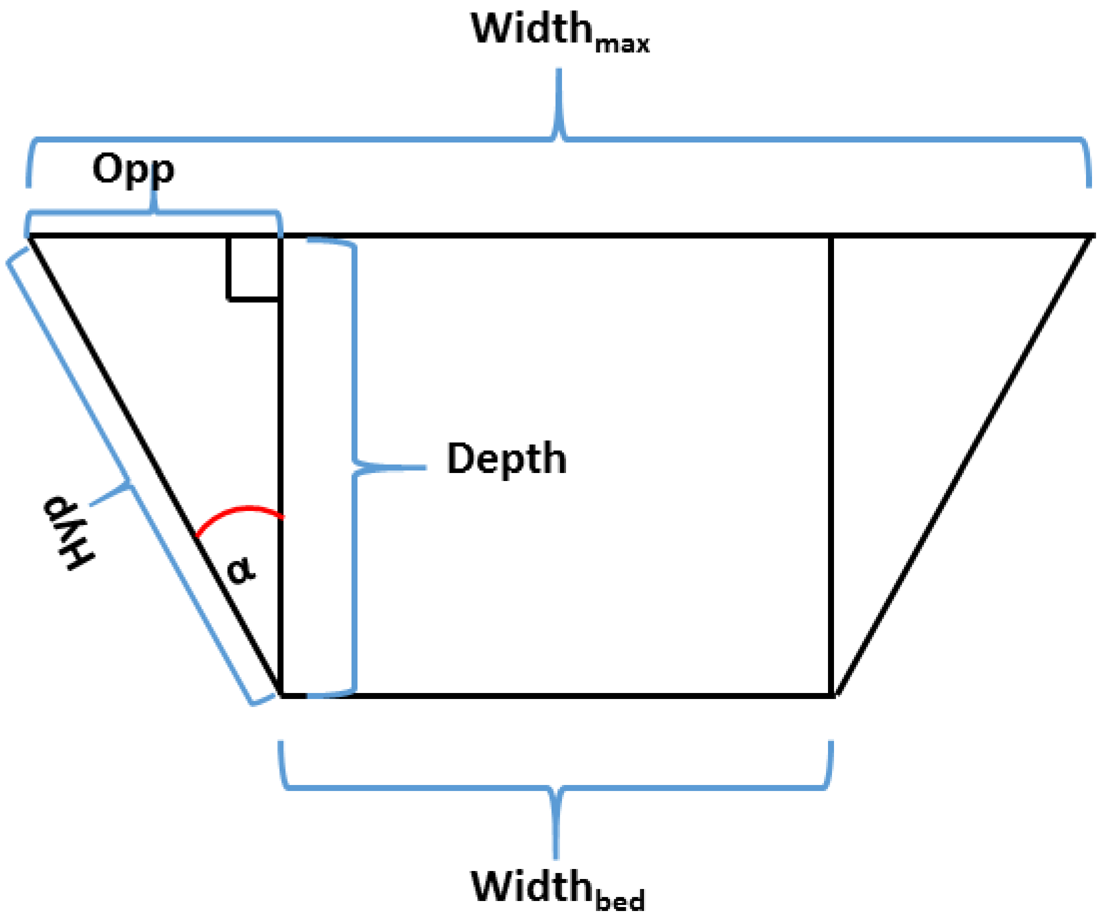

Figure 5.43 Conceptual representation of a river channel used to route sediment in the Water Quality Systems Assessment Model (WQSAM).

5.7.3 Calculation of suspended sediment

The approach adopted follows the method for suspended load transport for steady flow proposed by Van Rijn (1984).

$q_b = \alpha_s * \rho_s * Vel * d_{50} * M_e^{2.4} * (D^*)^{-0.6}$ (Equation 5.24)

$M_e = (Vel - Vel_{critical})/[(s - 1)gd_{50}]^{0.5}$ (Equation 5.25)

$D^* = d_{50}[(s - 1)g/v^2]^{0.33}$ (Equation 5.26)

$Vel_{critical} = a * (d_{50} * 10{,}000)^b$ (Equation 5.27)

$s = \rho_s/\rho_w$ (Equation 5.28)

q_b is suspended load transport (kg m^{-1}), α_s is assumed to be 0.012 (Van Rijn, 1984), ρ_s is the density of the sediment (kg m^{-3}) and is assumed to be 1,200 from an initial survey of the literature, d_{50} is the median particle size (m), which is set by the user, M_e is the mobility parameter, $Vel_{critical}$ is the critical depth-averaged velocity for initiation of motion (m s^{-1}), s is relative density, ρ_w is the density of water (kg m^{-3}), and is assumed to be 1,000, g is the acceleration of gravity (m s^{-2}), which is known to be 9.81, v is the kinematic viscosity coefficient (m^2 s^{-1}), which for water at 20°C is known to be 0.000001.

The values of *a* and *b* where calculated through linear regressions of the relationship between $Vel_{critical}$ and d_{50} given by Van Rijn (2012):

$a = 0.225 * Depth^{0.15}$ (Equation 5.29)

$b = 0.49 * Depth^{-0.02}$ (Equation 5.30)

For each day, WQSAM uses the cumulative flow ($m^3\ s^{-1}$) to obtain *Depth*, *Width* and *Vel* from the aforementioned lookup table in memory. Using the equations given above, the load of sediment that can be carried in suspension ($kg\ m^{-3}$) is calculated by multiplying q_b by *Width*. The loads of sediment entering the catchment from upstream are summed and the final load ($kg\ m^{-3}$) is compared to the load that can be carried in suspension. If the load entering the subcatchment is greater than what can be carried in suspension by the cumulative flow, the difference is deposited to the bed load. If the load entering the subcatchment is smaller than what can be carried in suspension by the cumulative load, the difference is taken from the bed load as it is assumed that some of the bed load enters suspension. The load in suspension is passed to the subcatchment downstream on a daily time step.

5.7.4 Settling of sediment in reservoirs

The settling of sediment in reservoirs is usually described using the theory of trap efficiency (e.g. Revel *et al*., 2013). However, estimates of trap efficiency are normally calculated on a yearly time step, which is of course not appropriate for a daily-time-step water quality model. The approach taken within WQSAM is to assume that sediment will settle with time:

$ISS_i = ISS_{i-1} - (K_{ISS} * ISS_{i-1})$ (Equation 5.31)

ISS is suspended sediment concentration ($mg\ \ell^{-1}$), K_{ISS} is the degradation coefficient for ISS (d^{-1}) and i is the time step. Of course, at each time step, *ISS* is updated through mass-balance for sediment entering a reservoir or leaving a reservoir through overflow or release flows.

CHAPTER 6. THE INCORPORATION OF A CHOLERA PREDICTION MODEL INTO WQSAM

6.1 Introduction

Advancements in medical care, nutrition and sanitation during recent history have eradicated or diminished many diseases that historically caused mass mortality amongst human populations. However, some of these diseases are resurging (Colwell, 1996). The most obvious underlying reason for this is the grinding poverty evident in many countries, due to the associated lack of safe sanitation, poor or insufficient nutrition, high population density, low education and lack of previous exposure, thereby allowing diseases to flourish (Colwell 1996; Griffith *et al*., 2006). However, there is not always a direct link between disease outbreaks and factors that traditionally have been thought to be causal, and increasingly, the environment has been linked to disease. Of particular relevance in this context is the changing climate.

Cholera is an ancient disease that has disappeared from most developed countries due to improvements in sanitation. However, the disease has re-emerged in several developing countries in recent decades (Bertuzzo *et al*., 2010), which has highlighted the relationship between cholera and environmental conditions (van den Bergh *et al*., 2008). The disease is caused by the bacterium *Vibrio cholerae*, which has been found to be naturally present in the environment. The bacterium colonises the small intestine of humans, and clinical manifestations of cholerae are due to the secretion of an exotoxin by the bacteria (du Preez *et al*., 2010). The infection typically has a very short incubation time of five hours to one day. The main symptom of cholera is the production of painless copious watery diarrhoea leading to sever dehydration, and even death if not treated (Jensen *et al*., 2006; van den Bergh *et al*., 2008)

Over 200 serogroups of *V. cholerae* have been reported, of which only two have been linked to epidemics, namely O1 and O139 (Lipp *et al*., 2002). This is supported by the fact that genes for the cholera toxin have rarely been found except in the two aforementioned serogroups. Historically before 1961, outbreaks were linked to the classical biotype of *V. cholerae* O1 (Lipp *et al*., 2002). However, the O1 El Tor strains had largely replaced the classical biotype by 1961 (Aslam *et al*., 2006). The O139 biotype first emerged as a threat in southeast India and the Bay of Bengal in 1992 (Gupta, 2005), and has not been reported anywhere else, and it has been hypothesised that this strain emerged through genetic exchange between other strains (Lipp *et al*., 2002).

Recent cases of cholera have been relatively well monitored; however, less attention has been given to the monitoring of *V. cholerae* (Collins, 2003). Although as a pathogen, cholera has been relatively well monitored and studied, recent outbreaks have offered a very unsatisfactory outcome, which casts doubts on how much we actually understand about the disease. *V. cholerae* and other Gram negative bacteria are able to enter a dormant stage, which has been termed viable but nonculturable (VBNC), which is utilised during unfavourable environmental conditions (Lipp *et al*., 2002). Using this adaptation allows bacteria to enter a state of dormancy which allows survival and persistence in a natural or host environment. This poses a problem for monitoring of *V. cholerae* as cells are unable to grow on conventional culture media.

6.1.1 A short history of cholera outbreaks

Although there is obviously a lack of written supporting history, it is thought that cholera may have existed in India as early as 400 BC (Underwood, 1974). Witten history exists on a devastating epidemic which occurred in the Lower Bengal in 1817 (Underwood, 1947). This pandemic was regarded as the first of seven within recorded history, and spread across India, extending as far as China and the Caspian Sea in Europe before receding. The second pandemic extended from approximately 1830 to 1850, affected various regions in Europe, North Africa and the Americas including Hungary, Germany, Russia, the United Kingdom, France, North America, Mexico and Egypt. The third pandemic occurred between the 1850 and 1860s and mainly affected Russia, but also spread to London, China, Japan and the Philippines. It was during this pandemic that John Snow made the now famous initial link between the spread of cholera and the water supply in a region of London. The fourth pandemic occurred between the late 1860s and the early 1870s, and began in the Bengal region and was spread by Muslim pilgrims to Mecca. Subsequently, the disease spread through the Middle East in Europe, Africa and North America. It was during an outbreak in London, using the previous knowledge by John Snow, that a particular water company was identified as the source of the disease, and quick action prevented further deaths. The fifth pandemic occurred between the early 1880s and the early 1890s, and affected Europe, the Americas, Asia and North Africa. By the sixth pandemic, recent advances in public health in Western Europe limited the impact of the disease; however, Russia was particularly hard hit. During this period, a distinct change in the impact of the disease was observed in Western Europe and North America due to improvements in public health and sanitation. Whereas previous pandemics resulted in the deaths of up to millions of people, the sixth pandemic was characterised by small outbreaks amongst travellers, who were quickly placed under quarantine in countries such as the United States.

By the 1920s, it was generally believed that cholera would not recur in pandemic form because of improvements to water supply and sanitation worldwide. However, what is now known as the seventh and current pandemic began in Indonesia, and by the early 1960s spread to India, Pakistan, the Soviet Union, Italy, North Africa and some parts of Asia. Interestingly, a new biovar or biotype of *V. cholera* is responsible for the current pandemic, namely the *V. cholera* O1 El Tor biotype. Cholera caused by this biotype is not as severe as that caused by the classical biotype.

6.1.2 A more detailed description of outbreaks in Southern Africa

Cholera outbreaks in South Africa are relatively recent, forming part of the latest (seventh) pandemic. Cholera surveillance programmes linked to mining first detected the *V. cholerae* bacteria for three Transvaal mines (Kustner and du Plessis, 1991). In 1978, three South Africans were found to be carriers after arriving back from overseas. The first case of locally contracted cholera was diagnosed in 1980 at NaNgwane (Kustner and du Plessis, 1991). Kustner and du Plessis mapped out cholera cases in South Africa between 1980 and 1987. The pandemic was confined to the eastern parts of the country, including the north eastern region incorporating what is now Gauteng, Mpumalanga and the Northern Province, eastern region incorporating KwaZulu-Natal and the south eastern, incorporating parts of the Eastern Cape. The pandemic appeared to start in the north east, bordering Mozambique. The *V. cholerae* strain was confirmed as O1 type El Tor. Between this period, the pandemic peaked between 1981-1982, with total confirmed cases of > 25,000. This period of cholera outbreak was preceded by a severe drought. From 1983 to 2000, the number of cases showed continual decline, falling to 37 cases between 1996-2000. A second peak starting during August of 2000 showed a massive number of cases within a span of just 13 months with > 80,000 cases, the vast majority in KwaZulu-Natal. The outbreaks of cholera since 2000 are outlined in the Epidemiological Comments publication by the Department of Health. Mentioned are the outbreak in Zimbabwe in 2008/2009 that spread into South Africa. In addition, an outbreak occurred in Mpumalanga Province from November 2008 to April 2009.

Le Roux *et al*. (2010) conducted a study of microbial water quality of the upper Olifants River, although the dates of the study are not specified. They found that most of the sites had high *Escherichia coli counts*, indicating high faecal contamination. Although *V. cholera* was widely detected, none of the strains were enterotoxigenic. Madoroba and Momba (2010) investigated the prevalence of *V. cholerae* in rivers within the Mpumalanga province, which as of 2009, has the highest prevalence of cholera cases in South Africa. Almost 600 Water samples were collected over a four month period from August to November 2009. Of these, 15 samples were positively identified to contain non-enterotoxigenic *V. cholerae* strains. Momba *et al*. (2006) conducted a study of microbial water quality of drinking water sources in Nkome in the Eastern Cape over a four month period (November 2001, January-March 2002). Surface and ground water samples were taken from various locations, including Lenge Dam, the Tyume, Sityi and Mnikini rivers and boreholes from various villages in the region. Their study found *Vibrio* species in borehole sources of two villages as well as in the Tyume River, and a total of 25% of groundwater samples were found to contain *V. cholerae*, indicating that groundwater can be a significant source of *V. cholerae* contamination. Nteme *et al*. (2014) investigated the occurrence and survival of *V. cholerae* in surface waters in and around the Msundizi, Umlazi and Isipongo rivers in KwaZulu-Natal between October 2012 and December 2013. Of a total of almost 700 river samples, almost 70% tested positive for non-toxigenic *V. cholerae*, indicating that the Msunduzi, Umlazi and Isipingo rivers are frequently contaminated with non-toxigenic *V. cholerae*.

However, South Africa has not experienced the highest number of cholera cases within southern Africa. Mozambique has over recent decades consistently reported the highest rate of cholera incidents globally, with over 87,000 cases from 1998 to 1999. In addition, a major cholera outbreak occurred in Zimbabwe from 2008 to 2009, with almost 100,000 cases and almost 4,000 deaths (Madoroba and Momba, 2010). This outbreak in Zimbabwe has been attributed to the deterioration in sanitary and health conditions in Zimbabwe over the past decades.

6.1.3 Relationship between cholera and the environment

John Snow was the first person to link the spread of cholera with water supply during one of the earlier pandemics of cholera in London. Prior to this, it was thought that the disease spread through person to person contact. It has since been established that cholera is caused by the *V. cholerae* bacterium, which appears to be a natural member of the coastal aquatic microbial community (Bertuzzo *et al*., 2010). In its natural environment, the bacterium appears to survive in association with chitinaceous zooplankton such as copepods and shellfish (Bertuzzo *et al*., 2010). The transmission of the *V. cholerae* to humans occurs either from the natural reservoir, termed primary transmission, or through V. cholerae contaminated human faecal matter entering the waterways during an epidemic, termed secondary transmission. Therefore, the environment has a great influence on the initial transmission as well as the subsequent spread of the disease. The pattern of cholera epidemics on spatial and temporal scales is linked to the ecology of *V. cholerae*, and how environmental variables affect the survival of the bacteria. The results of Investigations into the relationships between environmental variables and the occurrence of cholera have sometimes been contradictory, with relationships with particular environment variables appearing to change according to region or latitude

Relationships with meteorological variables

Seasonal patterns of cholera as well as longer-term patterns appear to be linked to meteorological variables such as air temperature and rainfall, and related variables such as sea surface temperature. For example, incidents of cholera showed an increase of 6.5% in association with a 1 mm d^{-1} increase in precipitation in the Bay of Bengal (de Magney *et al*., 2008). There is growing concern that the dynamics of many diseases, including cholera, are changing in response to changing global climate (Pascual *et al*., 2002). Although in the past it has been difficult to separate the effects of climate on disease dynamics from the effects of other factors, such as socioeconomic factors, the recent increase in the availability of climate data from remote sensing products has provided new opportunities to analyse the relationships between climate and disease. Despite this increase in data, the link between climate and cholera remains poorly understood (Pascual *et al*., 2002). Pascual *et al*. (2002) found that the coldest inhabited regions are generally spared from cholera, indicating that cold temperatures limit the spread of the disease.

Within the lower Bengal, considered to be the origin of cholera, the disease shows strong seasonality, with spikes during the spring and winter seasons and lower mortality during the monsoon rains and colder winter months (Bouma and Pascual, 2001). The effect of the El Niño-Southern Oscillation (ENSO) on the prevalence of cholera in various regions has been highlighted in various studies. In simple terms, the ENSO is a shift of pressure across the equatorial Pacific (Lipp *et al*., 2002). The El Niño phase refers to the shift of a zone of low pressure eastward, resulting in local changes including a drop in the easterly trade winds, a depression of the thermocline along the South American coast and a warming of the eastern Equatorial Pacific. During the La Nina event, the aforementioned trends are generally reversed. The ENSO is particularly important as the phenomenon has been linked to interannual shifts in global climate. Bouma and Pascual (2001) investigated the effects of seas surface temperature and the El Niño Southern Oscillation (ENSO) on incidents of cholera within the Bay of Bengal. They found that seasonality of cholera shows a bimodality with two peaks per year, with a rise in sea surface temperature corresponding with the spring peak of cholera, and that the effect of spring cholera is more pronounced within coastal regions. They also noted an influence of ENSO on both the interannual and seasonal dynamics of cholera. Pascual *et al*. (2000) has also investigated the link between the ENSO and cholera, and they noted the reappearance of cholera in Peru with the El Nino event of 1991-1992, as well as an association between diarrheal diseases in Peru and warmer temperatures associated with the El Nino event of 1997-1998. Their analysis of cholera and climate data in Bangladesh found the well-known seasonal variation of the disease in Bangladesh, but also identified an interannual variability with a dominant frequency occurring once every approximately four years, similar to that of the ENSO event, suggesting a role of ENSO in driving the dynamics of the disease. The role of ENSO in driving cholera dynamics relates to the changes in sea surface temperature (SST) (Pascual *et al*., 2002). In South Africa, cholera cases appear to be linked to regions of higher rainfall (> 600 mm), with outbreaks being most common in the wetter eastern and north eastern parts of the country (Kustner and du Plessis, 1991l).

Seasonality of cholera

Areas where cholera is endemic are areas in which the disease does not disappear after an outbreak, but reappears in successive waves over time. It is in these endemic areas where cholera shows distinct and remarkably regular seasonality (Lipp *et al*., 2002); however, the patterns of seasonality vary geographically. In addition, a study by Emch *et al*. (2008) found that seasonality is more pronounced at higher latitudes, whereas outbreaks do not follow a clear pattern at the equator. These patterns are described by Pascual *et al*. (2002) for different regions of the world. Within the coastal and surrounding regions of Bengal and parts of Madras, two annual seasons are evident, with a pronounced drop in cholera incidents over the monsoon. According to Pascual *et al*. (2002), this drop in incidents of cholera can perhaps be attributed to the drop in salinity associated with dilution resulting from the monsoon. In contrast, within the drier parts of the Indian subcontinent, cholera incidents appear to peak over the monsoon. Pascual *et al*. (2002) attributes this to increased flow resulting in increased transmission of the disease. A single peak in cholera incidents is typically seen in African and Latin American regions, with the epidemics associated with the summer months (Lipp *et al*., 2002; Pascual *et al*., 2002). In general, it appears that water temperature plays an important role in the seasonality of cholera.

Relationships with biotic variables

Some outbreaks of cholera have been associated with the consumption of seafood, such as an outbreak in Louisiana and Texas (Singleton *et al*., 1982). It has been hypothesised that shellfish may provide an effective environmental reservoir for *V. cholerae*, either through a nonspecific association or through a commensal relationship (Singleton *et al*., 1982). It has also been hypothesised that the enterotoxin of *V. cholerae* may play a role in sequestering Na+ from its commensal host, whereas in the human gut, the enterotoxin results in an efflux of Na^+ and other electrolytes from epithelial cells along with large quantities of water, thereby producing the classic cholera symptoms.

Other studies have highlighted the role of aquatic plants as temporary or long-term reservoirs of *V. cholerae*. It has been found that *V. cholerae* secrete an enzyme called mucinase that digests mucin in the environment (Emch), which is present in plant cell walls. Other studies have confirmed the association between V. cholerae and various aquatic plants such as water hyacinth, cyanobacteria and blue-green algae (Emch).

The *V. cholerae* 01 strain has been found to secrete an enzyme called chitinase (Emch), which digests chitin, a biological compound associated with the exoskeleton of chitinous fauna such as zooplankton (Emch *et al*., 2008).

A study by de Magny *et al*. (2008) found a significant correlation between coastal chlorophyll a and incidents of cholera in the northern Bay of Bengal.

A study by Nteme *et al*. (2014) of the prevalence of *V. cholerae* in surface waters of KwaZulu-Natal concluded that the environmental non-toxigenic *V. cholera* strains detected are well adapted to survive in the environment, likely through its ability to grown as a biofilm

The ability of *V. cholerae* to enter a dormant stage in response to unfavourable conditions is likely to be a key reason for the success of this bacterium as an opportunistic pathogen. This probably also explains the link between *V. cholerae* and zooplankton, which are able to survive unfavourable conditions through diapause (Codeco, 2001).

Relationship with socioeconomic factors

Socioeconomic factors mainly drive secondary transmission, and once the disease emerges, will determine whether the disease reaches epidemic proportions. These factors include contaminated drinking water, inadequate sanitation, inadequate medical interventions and treatment during outbreaks and the population density. The relationship between the secondary spread of cholera and socioeconomic factors explains why the disease has all but disappeared from developed countries, whereas epidemics reoccur in some developing regions, such as Africa and South America.

Relationship between cholera and the environment in South Africa

Mendelsohn and Dawson (2008) using data of the cholera epidemic that occurred in KwaZulu-Natal between 2000-2001 that resulted in over 100 000 cases of cholera, explored relationships between cholera incidents and various environmental variables, including sea surface temperature, sea surface height, chlorophyll a and precipitation. Within this epidemic, most cases (25%) occurred during February. The analysis found strong relationships between incidents of cholera and precipitation, sea surface temperature and coastal cholrophyll a, with lag times of two, zero and six months, respectively.

Socioeconomic factors in South Africa additionally increase the risk of secondary transmission of cholera, and the ultimate risk of full-blown cholera epidemics. Although great strides have been made in recent decades in providing the majority of the population with clean piped water for domestic use, other socio-economic risk factors remain in South Africa. Apart from the usual factors such as poverty and poor living conditions, many rivers in South Africa are compromised by poorly treated sewage effluent. A study by the CSIR of sewage effluent released from rural hospitals in KZN during the period 1998 to 2000 obtained positive tests for toxigenic *V. cholerae* from two hospitals, and in both cases, rural communities were drawing water from springs located nearby (Cottle and Deedat, 2002). The same study found that the sewage treatment plant had suffered breakdowns, had frequently run out of chemicals for treatment, and often untreated effluent had been released to nearby rivers. Also, it has been confirmed that the Umtata sewage works was the source of a subsequent cholera outbreak in the Eastern Cape.

The ability of *V. cholerae* to enter a dormant stage

V. cholerae, along with other Gram negative bacteria, are characterized by their ability to enter a dormant stage when environmental conditions are unfavourable, thereby allowing the bacteria to persist in the environment. Lipp *et al*., (2002) has termed this state within *V. cholerae* as 'viable but nonculturable' or VNC. This ability is believed to have played a major role in the success of *V. cholerae* as an opportunistic pathogen, and could in fact also explain the commensal relationship between *V. cholerae* and zooplankton, as zooplankton are known to enter a similar dormant state called diapause (Lipp *et al*., 2002).

6.1.4 Attempts to model cholera

A conceptual understanding of how *V. cholerae* spreads is required to develop a model. In addition, understanding environmental conditions conducive to the survival of V. *cholerae* is required. Although cholera is one of the most well-studied diseases, as cholera is an ancient disease, most studies and monitoring efforts have concentrated on the clinical aspects of cholera, and studies of cholera epidemics have monitored and analysed cases of cholera, whereas the temporal and spatial distributions of the bacterium *V. cholerae* have received relatively less attention. Since it has been shown that *V. cholerae* is a natural inhabitant of coastal estuarine systems, pathways of *V. cholerae* movement inland can be through waterways and river networks (Bertuzzo *et al*., 2010).The infection can spread from inland areas to surrounding areas as people get sick, and untreated waste water containing the bacteria enters waterways (Bertuzzo *et al*., 2010). The two aforementioned routes of transmission are termed primary transmission and secondary transmission, respectively.

The model by de Magny *et al*. (2005) simulated cholera infections within a population, and explicitly took into account the developed immunity of recovering individuals. The model by de Magny *et al*. (2005) divided the modelled human population into four classes: 1) infected individuals; 2) recovered individuals; 3) susceptible individuals and; 4) dead individuals. Jensen *et al*. (2006) created a model that considers the effect of bacteriophages on *V. cholerae*, and incorporates dynamics of both the infected population and the *V. cholerae* bacteria. Their model contains various model compartments including: 1) susceptible human individuals; 2) individuals infected with *V. cholerae*; 3 individuals infected with *V. cholerae* and phage; 4) individuals that are recovered/dead; 5) the reservoir of *V. cholerae* in the environment and; 6) the reservoir of phage.

Cedeco (2001) introduced a model to simulate the role of the *V. cholerae* reservoir, regions most likely to maintain endemic cholera and the prediction of human sickness from a cholera outbreak. In regards to the model compartment that simulates the fate of *V. cholerae* in the environment, their model incorporates factors to calculate the concentration of *V. cholerae* in water, a threshold parameter indicating the concentration of *V. cholerae* indicating a 50% chance of catching cholera if ingested, the growth rate of *V. cholerae* in the environment and the loss rate of *V. cholerae* in the environment.

Although many models have attempted to simulate the spread of cholera epidemics through surface waters, specifically demonstrating that the spread of cholera is driven by connectivity of the hydrological network, Mari *et al*. (2012) extended this conceptual understanding by considering the effect of mobility of the human population on the spread of the disease. Here, Mari *et al*. (2012) utilised the concept of 'gravity transmission', which considers the population sizes of communities and the distances between multiple communities.

Fleming *et al*. (2007) developed a cholera health risk prediction model for southern Africa using a fuzzy expert system and GIS, and was based on the assumption of the presence of endemic *V. cholerae* reservoirs in the environment, with environmental conditions triggering algal blooms, which in turn trigger the growth of *V. cholerae*. Their model also considers a threshold of *V. cholerae* concentration in the environment that may initiate primary transmission, after which the initiation of an epidemic through secondary transmission depends on socioeconomic conditions. Interestingly, their model assumed that the initiation of the rainy season, i.e. the first rains after the dry season, may flush salt into the rivers in sufficient loads to contribute to the salinity requirements of *V. cholerae*.

Bertuzzo *et al*. (2010) presented a spatially explicit model to account for the environmental matrix along which the *V. cholerae* bacteria can be transported. Their model operates on the assumption that since cholera transmission is mediated by water, direct contact between individuals is less important within disease transmission than spatial connectivity. Their model is therefore constructed as an oriented graph, consisting of nodes connected by edges, where the nodes represent reservoirs of the *V. cholerae* bacteria. Each node contains a human population, which release greatly increased loads of *V. cholerae* bacteria into a river once an epidemic begins. Their model considers two separate time scales: 1) the time for an epidemic to spread through the system and; 2) the time taken for the epidemic to run its coursed within a single community. The use of directed graphs with nodes and edges by Bertuzzo *et al*. (2010) is very similar to the systems approach taken by WQSAM (see Slaughter *et al*., 2015). Although Bertuzzo *et al*. (2010) present various alternative graph structures, optimal channel networks (OCNs) are the most similar to the underlying network structure used by the systems models that WQSAM communicates with (to obtain flow output).

6.2 Case study catchments and modelling approach

6.2.1 Case study catchment

In the current study, the Olifants River Catchment has been chosen as the initial case study catchment. There are various reasons for this approach. Firstly, the Olifants River Catchment has been modelled previously using WQSAM; therefore, much of the model setup and data are already in place. Secondly, the Olifants River Catchment has experienced cases of cholera outbreaks in the past (Kustner amd du Plessis, 1991), and although most cases have been reported in KwaZulu-Natal (Cottle and Deedat, 2002), since 2009, most cases have been reported in Mpumalanga, which incorporates the Olifants River Catchment. In addition, non-toxigenic *V. cholerae* bacteria has been detected in the Olifants River Catchment (Modoroba and Momba, 2010; Le Roux *et al*., 2010). Furthermore, the Olifants River Catchment borders and in fact extends into Mozambique, and Mozambique has repeatedly experienced cholera outbreaks in recent times. Mozambique has in fact over recent decades consistently reported the highest global rates of cholera incidents.

The present study will focus on the upper Olifants River Catchment, extending down to Loskop Dam (see Figure B2). The catchment originates from the east of Johannesburg, and is generally regarded as one of the most polluted rivers in South Africa (Balance *et al*., 2001; de Villiers and Mkwelo, 2009, van Vuuren, 2009). Water quality is compromised within the catchment by various anthropogenic activities including mining, petrochemical industries and diverse agriculture (Heath *et al*., 2010). Of relevance to the present study is that the microbial water quality of the Olifants River Catchment is also impacted by inadequately treated sewage effluent as well as runoff from informal settlements (van Vuuren, 2013).

6.2.2 Observed data

The available data relating to cholera in the Olifants River Catchment can be broadly divided into two groups: 1) Measures of *V. cholera*, either as presence/absence or concentration, and; 2) data on incidents of cholera for settlements within the catchment. Since this present study focuses on the fate of *V. cholerae* instream, data on human cholera cases would not be applicable. However, for the sake of discussion, the available data on cholera cases within the Olifants River Catchment is included.

Data on incidents of cholera within the Olifants River Catchment

Cottle and Deedat (2002) reports on the epidemic of 2000-2001. Although this epidemic mainly affected KwaZulu-Natal, Cottle and Deedat (2002) does give a breakdown of the incidents of cholera by province. Here, Mpumalanga is listed as recording 79 cases by 01 March 2001. A publication of the Epidemiological Comments by the South African Department of Health (Volume 2 Number 2, April-June 2009) provides a more detailed breakdown of cholera cases in South Africa in the period 2008-2009. Included in this report is a breakdown of daily cases of cholera from January to April 2009 in the Mpumalanga province (see Figure 6.1).

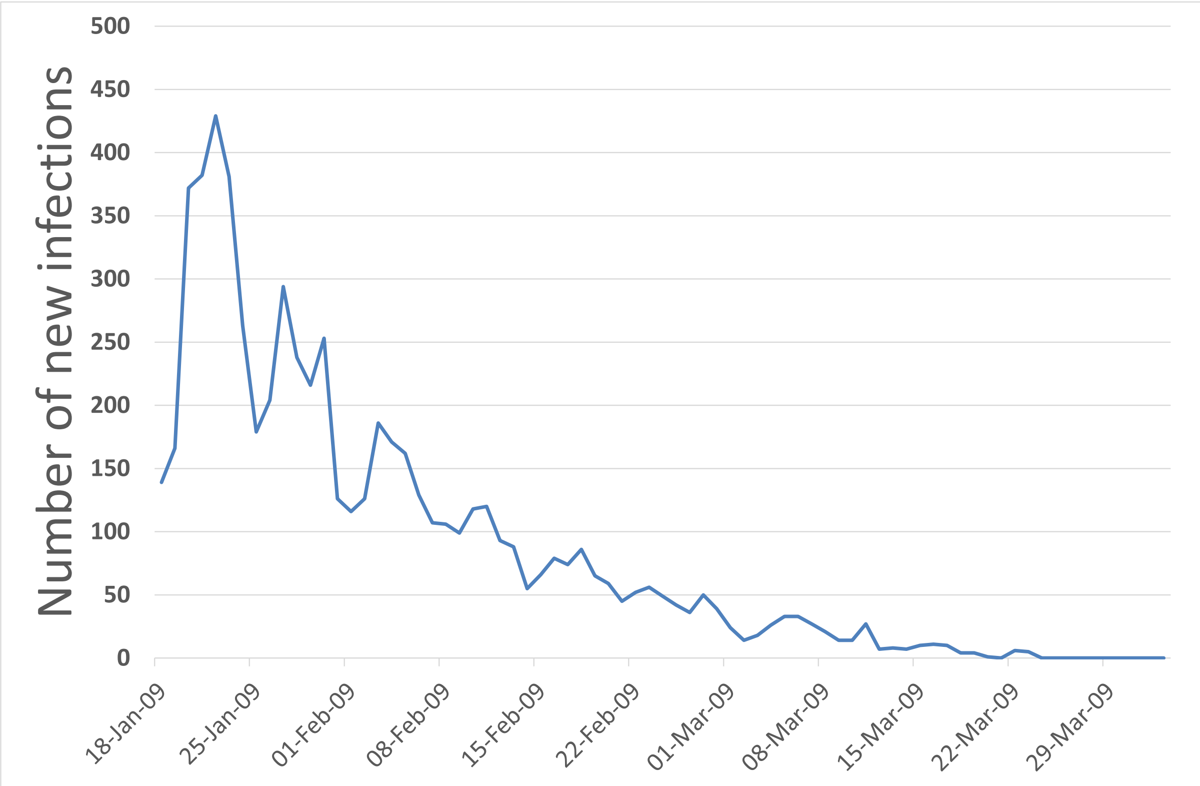

Figure 6.1 Daily breakdown of the cases of cholera that occurred in the Mpumalanga Province over the period January 2009 to March 2009. The data are sourced from the Epidemiological Comments by the South African Department of Health (Volume 2 Number 2, April-June 2009)

The report also provides a breakdown of total cases per sub-district in Mpumalanga, with Umjindi, Mbombela North, Mbombela South, Nkomanzi-Tonga, Nkomanzi-Shongwe, Thaba Chweu and Bushbuckridge experiencing cases numbering 88, 3 654, 345, 213, 207, 373 and 1901, respectively.

V. cholerae **presence/absence data within the Olifants River Catchment**

Le Roux *et al*. (2012) performed a study of microbial water quality of the upper Olifants River. The results of that study in regards to *V. cholerae* are summarised within Table 2.1. It is important to note that no toxigenic strains were detected within the study. Le Roux *et al*. (2012) indicated that positive results for *V. cholerae* were obtained downstream of WWTWs.

Madoroba and Momba (2010) similarly investigated for the prevalence of *V. cholerae* in Mpumalanga, with only one site falling within the upper Olifants River, and no positive results for *V. cholerae* were obtained for this site. Unfortunately, it appears that there is no concentration data for *V. cholerae* available for the Olifants Rivers.

6.2.3 Modelling approach

It was decided to only model the effect of environmental conditions on the survival and growth of *V. cholerae* in a river network, as the modelling of a cholera epidemic is not within the scope of a water quality model such as WQSAM. However, thresholds of *V. cholerae* concentration can serve as warnings of a high risk of transmission of the cholera disease into the human population within a catchment.

Due to the inherent directed graph structure of WQSAM, incorporating nodes (subcatchments) and edges (channels), the approach taken in the present study is similar to that presented by Bertuzzo *et al*. (2010), specifically the optimal channel network (OCN) type graph structure.

Survival and growth of the *V. cholerae* bacteria in the current study is modelled using the standard Optimal Model (Chapra, 1997) approach that has been extensively adopted within WQSAM, with factors affecting survival and growth selected from information available in the literature. In the current study, it is assumed that *V. cholerae* bacteria will enter a dormant state if values of any critical environmental variables move beyond certain specified thresholds. The transition back into an active state would then depend on the range of environmental variables affecting *V. cholerae* falling within the required ranges for the survival of the bacteria.

Factors considered for modelling instream V. cholerae concentration

The factors considered are: 1) water temperature (Madico *et al*., 1996; Mendelsohn and Dawson, 2008; Pascual *et al*., 2002; Singleton *et al*., 1982), thereby being able to simulate the seasonal patterns of cholera that show a spike during warmer months in South Africa; 2) salinity (Singleton *et al*., 1982), with specific salinity ranges being associated with the survival of *V. cholerae*, namely between 5 g ℓ^{-1} to 45 g ℓ^{-1}; 3) nutrients (Singleton *et al*., 1982), with a positive relationship between nutrient concentration and *V. cholerae* growth.

In the current study, nutrients are regarded to promote *V. cholerae* growth and survival. Since nutrients encompass a variety of chemical species, the present study uses dissolved organic matter (DOM) as a proxy for nutrients in general.

Model structure

The effect of temperature on *V. cholerae* growth rate is represented by Equations 6.1-6.3:

$K_{gT} = 0$ $(T \geq T_{max} \text{ or } T \leq T_{min})$ (Equation 6.1)

$K_{gT} = K_{g.opt} \times ((T-T_{min})/(T_{opt}-T_{min}))$ $(T_{min} \leq T \leq T_{opt})$ (Equation 6.2)

$K_{gT} = K_{g.opt} \times ((T_{max} - T)/(T_{max}-T_{opt}))$ $(T > T_{opt})$ (Equation 6.3)

Where K_{gT} is *V. cholerae* growth rate at temperature T, T_{max} is the maximum temperate, T_{opt} is the optimal temperature, T_{min} is the minimum temperature, and $K_{g.opt}$ is the optimal growth rate. Similar to the approach taken for algal growth in WQSAM, this approach assumes the Optimal Model (Chapra, 1997) for representing the effect of water temperature on growth.

The effect of salinity on *V. cholerae* growth rate is represented by Equations 6.4-6.6:

$K_{gS} = 0$ $(S \geq S_{max} \text{ or } S \leq S_{min})$ (Equation 6.4)

$K_{gS} = K_{g.T} \times ((S-S_{min})/(S_{opt}-S_{min}))$ $(S_{min} \leq S \leq S_{opt})$ (Equation 6.5)

$K_{gS} = K_{g.T} \times ((S_{max} - S)/(S_{max}-S_{opt}))$ $(S > S_{opt})$ (Equation 6.6)

Table 6.1 Presence/Absence data of non-toxigenic *Vibrio cholerae* within the upper Olifants River Catchment, South Africa. Data are sourced from le Roux *et al.* (2012)

Date	River Name	latitude	Longitude	Presence/absence
12-Nov-09	Wilge	-25.62153	28.99902	Not Detected
18-Jan-10				Not Detected
10-Mar-10				Not Detected
15-Jul-10				Not Detected
13-Sep-10				Not Detected
12-Nov-09	Klip	-25.62150	29.21253	Not Detected
12-Nov-09	Olifants	-25.62392	29.21685	Not Detected
12-Nov-09	Klein Olifants	-25.68073	29.30537	Not Detected
12-Nov-09	Groot Olifants	-25.68445	29.30042	Detected
12-Nov-09	Brugspruit	-25.85707	29.13565	Detected
18-Jan-10				Not Detected
10-Mar-10				Not Detected
15-Jul-10				Not Detected
13-Sep-10				Not Detected
12-Nov-09	Riverview	-25.84170	29.26633	Detected
18-Jan-10				Not Detected
10-Mar-10				Detected
15-Jul-10				Not Detected
13-Sep-10				Not Detected
12-Nov-09	Middleburg	-25.77093	29.48262	Detected
18-Jan-10				Detected
10-Mar-10				Detected
15-Jul-10				Detected
13-Sep-10				Detected
12-Nov-09	Klein Olifants	-25.87258	29.56964	Detected
18-Jan-10				Detected
10-Mar-10				Detected
15-Jul-10				Not Detected
13-Sep-10				Not Detected
12-Nov-09	Klein Olifants	-25.88297	29.64290	Detected
18-Jan-10				Detected
10-Mar-10				Detected
15-Jul-10				Not Detected
13-Sep-10				Not Detected
12-Nov-09	Koffiespruit	-25.99543	28.66347	Not Detected

Where K_{gS} is *V. cholerae* growth rate at salinity S, S_{max} is the maximum salinity, S_{opt} is the optimal salinity, S_{min} is the minimum salinity, and $K_{g.T}$ is the *V. cholerae* growth rate at temperature T. This approach similarly assumes the Optimal Model (Chapra, 1997), as there is both a minimum and maximum salinity below and above which *V. cholerae* growth is compromised, respectively.

The effect of nutrients, represented by DOM concentration, is represented by Equations 6.7-6.9:

$K_{gN} = 0$ ($DOM \leq DOM_{min}$) (Equation 6.7)

$K_{gN} = K_{g.S} \times ((DOM-DOM_{min})/(DOM_{opt}-DOM_{min}))$ ($P_{min} \leq P \leq P_{opt}$) (Equation 6.8)

$K_{gN} = K_{g.S}$ ($DOM > DOM_{opt}$) (Equation 6.9)

Where K_{gN} is *V. cholerae* growth rate at the nutrient concentration represented by DOM, DOM_{opt} is the optimum DOM concentration for *V. cholerae* growth, DOM_{min} is the minimum DOM concentration for *V. cholerae* growth, and $K_{g.S}$ is the *V. cholerae* growth rate at salinity S.

The growth rate is estimate in the aforementioned order (Equation 2.1-2.9), following which the change in *V. cholerae* concentration per time step is calculated:

$K_N = K_{qp}$

$$\frac{dC}{dT} = (k_g - k_0) \times C \qquad \text{(Equation 6.10)}$$

Where K_g is the final growth rate for *V. cholerae*, taken as the value of K_{gp} if the correct order of calculating the growth rate (Equation 2.1-2.9) is followed, K_0 is the decay rate of *V. cholerae* in the environment, and C is the concentration of *V. cholerae*. Therefore, if K_g is greater than K_0, a net increase in *V. cholerae* over time will occur, whereas the opposite will result in a net decrease in *V. cholerae* concentration. To simulate growth of *V. cholerae*, it is important to set $K_{g.opt} > K_0$ at the start of the model run.

The issue of whether V. cholerae is endemic, and the consequences for model structure

It has been hypothesised that *V. cholerae* is endemic to certain areas, and enters a state of dormancy when environmental conditions are not optimal. The modelling of endemic *V. cholerae* could be fairly simple: once the environmental variables simulated by the model (temperature, salinity and nutrients) enter ranges that facilitate *V. cholerae* growth, the model will automatically initiate the growth of *V. cholerae* from some minimal starting point concentration. However, *V. cholerae* may not be endemic to some regions, and may in fact be imported from other regions through the migration of an infected human individual. It is difficult to determine whether *V. cholerae* is endemic to certain regions, as the dormant stage is almost impossible to detect. Le Roux *et al* (2012), detected non-toxigenic strains of *V. cholerae* within certain sites of the upper Olifants River Catchment. However, past cholera epidemics in the region, such as that of the 2008 to 2009 epidemic in Mpumalanga, occurred because of an outbreak in Zimbabwe that spread into South Africa. The Olifants River Catchment also borders Mozambique, and many Mozambicans routinely cross the border into South Africa. Mozambique has been identified country with the highest incidents of cholera outbreaks in the world.

Therefore, although on one hand it may be justified to model *V. cholerae* in the Olifants River Catchment assuming that the bacteria is endemic to the catchment, it is equally, or perhaps more realistic to model *V. cholerae* in the catchment assuming that the bacteria is imported from outside the catchment. The model implementation of external import of *V. cholerae* into the catchment can be simulated by simply setting a *V. cholerae* concentration for WWTW sewage return flow and/or any of the signatures for the incremental flow fractions (surface water flow, interflow or ground water flow). Endemic *V. cholerae* growth can be simulated by allowing environmental conditions within the catchment to facilitate the initiation of *V. cholerae* growth.

6.3 Results and discussion

6.3.1 Scenarios investigated

From the literature, it appears that the occurrence of *V. cholerae* within a river network can occur from two origins: 1) from dormant endemic *V. cholerae* that begin to multiple and become active once environmental conditions become favourable and; 2) from faecal matter entering the river network once a cholera pandemic begins. As mentioned earlier, the environmental factors which determine whether instream *V. cholerae* experience growth include temperature, salinity and nutrients. In addition, *V. cholerae* have been linked to algal blooms. In regards to the input of *V. cholerae* into a river network when the bacteria is not endemic, this usually occurs through migration of an infected person into the catchment from outside of the catchment. Therefore, the present study investigated two broad scenarios: 1) the initiation of endemic *V. cholerae* bacterial growth without external input and; 2) input of *V. cholerae* bacterial growth as an external source.

6.3.2 Results

Growth of *V. cholerae* as an endemic bacteria strain linked to environmental conditions

From the literature, it appears that some data are available on variable ranges required for growth of *V. cholerae* for temperature and salinity (Singleton *et al*., 1982). The data appear to show that *V. cholerae* can tolerate a salinity of as much as 40 g ℓ^{-1}, as little as 5 g ℓ^{-1}, and appear to prefer salinities of around 25 g ℓ^{-1}. For temperature, it has been indicated that temperatures below 10ºC would not be conducive to *V. cholerae* growth. Although it has been indicated that *V. cholerae* require nutrients for growth, no actual concentration values have as yet been elucidated.

To investigate the scenario of endemic *V. cholerae* growth, a reach of the upper Olifants River was investigated without many WWTW return flows. The reach chosen was the catchment above and including the Middleburg Dam incorporating the B12A and B12B quaternary catchments. As an initial investigation, the following parameter values were chosen based on the literature: T_{max} = 35ºC, T_{min} = 10ºC, T_{opt} = 25ºC, S_{max} = 40 g ℓ^{-1}, S_{min} = 5 g ℓ^{-1}, S_{opt} = 25 g ℓ^{-1}.

Values of other parameters were set to reasonable initial values: K_g = 0.5, K_0 = 0.2, DOM_{min} = 0.5 mg ℓ^{-1}, DOM_{opt} = 1 mg ℓ^{-1}.

The results of model simulations for the Middleburg Dam are shown in Figure 6.2. Figure 6.2a shows that the water temperature within Middleburg Dam sometimes goes below the T_{min} value of 10ºC, and never reaches the T_{opt} value of 25ºC. Figure 6.2b shows that the salinity in the Middleburg Dam is most of the time well below the S_{min} value of 5 g ℓ^{-1}, although this value is exceeded once in the time series. Figure 6.2c shows that the DOM values are constantly above the DOM_{opt} value that was rather arbitrarily chosen for this scenario analysis. Figure 6.2c shows the model simulations of *V. cholerae* instream. Immediately obvious is the extremely low levels of bacterial cells simulated. Also evident is the relative spike in cells corresponding to the spike in salinity.

Growth of *V. cholerae* as an external input linked to WWTW effluent input

The second scenario investigated would be the fate of instream V. cholerae after external input through WWTW effluent. For this analysis, the reaches upstream of the Witbank Dam and incorporating Witbank Dam were investigated, because of the high number of WWTWs in this part of the catchment. This part of the catchment incorporates the quaternary catchments B11A-E. For this analysis, the same parameter values of the previous analysis were maintained; however, return flows linked to WWTWs were assigned *V. cholerae* signatures of 5 000 cells 100 mℓ$^{-1}$. This is a rather arbitrary value, and was chosen to merely investigate the trends evident with external input of *V. cholerae*. Figure 6.3 shows the results of simulations for this analysis. The temperature regime of Witbank Dam shows that the water temperature remains for the most part between T_{min} and T_{opt}, although the water temperature drops below T_{min} and rises marginally above T_{opt} during winter and summer, respectively (see Figure 6.3a). The salinity within the Witbank Dam was well below the S_{min} salinity required for *V. cholerae* growth over the entire modelled period (see Figure 6.3b). Figure 6.3c shows that even though environmental conditions within Witbank Dam are not conducive to the survival of *V. cholerae*, high inputs of the bacteria from the catchment can result in some persistence of *V. cholerae* in the dam.

6.3.3 Discussion

According to the available literature, it is obvious that the environmental conditions within the upper Olifants River Catchment are not optimal for the growth of *V. cholerae*. The simulations of endemic *V. cholerae* growth within the catchment upstream of Middleburg Dam showed that both temperature and salinity limit the growth of *V. cholerae* (Figure 6.2a and b). The water temperature in the dam falls below the optimum temperature value for *V. cholerae* growth most of the time, and often during winter falls below the minimum temperature for *V. cholerae* growth. The salinity environment within the upper Olifants River is not sufficiently saline for *V. cholerae* growth according to the data available in the literature. Within the Middleburg Dam, there is a single peak above the minimum salinity 5 g ℓ$^{-1}$ to induce V. cholerae growth of, whereas for the rest of the simulated period, the salinity fell way below this value. Interestingly, the simulation of V. cholerae in Middleburg Dam showed a relative peak corresponding with the salinity peak; however, overall *V. cholerae* simulations were of very low concentrations. The model therefore did not indicate that endemic *V. cholerae* would grow to any great extent in the upper Olifants River Catchment. Given that V. cholerae has been indicated to prefer salinities close to that of seawater (35 g ℓ$^{-1}$), this result is not surprising.

The investigation of *V. cholerae* fate with external input of *V. cholerae* through WWTW effluent indicated that even with large inputs of cells, the bacteria quickly degrade in the unfavourable environmental conditions, particularly in this case, the temperature (Figure 6.3a) and salinity (Figure 6.3b) of the Witbank Dam. However, a relatively large WWTW input of *V. cholerae* cells does have an impact downstream, as indicated in Figure 6.3c with the bacteria able to persist. Therefore, during a cholera epidemic, it is plausible that the river network could act as a conduit for cholera infections, despite environmental conditions for the survival of the bacteria being unfavourable.

Collins (2003) estimates that to contract cholera, a healthy individual would need to consume approximately 100 *V. cholerae* cells. At the highest simulated concentrations in the Witbank Dam, this would equate to about a litre of water, which is well within the bounds of possibility.

It must be remembered that due to a lack of observed data (the data by Le Roux *et al*. (2012) are merely *V. cholerae* presence/ absence data), the current investigation was more exploratory, rather than a rigorous model of *V. cholerae* fate instream of a river network. However, given more observed *V. cholerae* concentration data, the current study has demonstrated how simulated results could be of use. Future scenario modelling could indicate how changing temperatures and rising salinities could promote the growth of *V. cholerae* within a river catchment. In addition, with a sufficiently calibrated model (linked to the availability of observed data), the model simulations could give an indication of the risk of primary or secondary transmission of cholera, as this can be related to the concentration of *V. cholerae* cells instream.

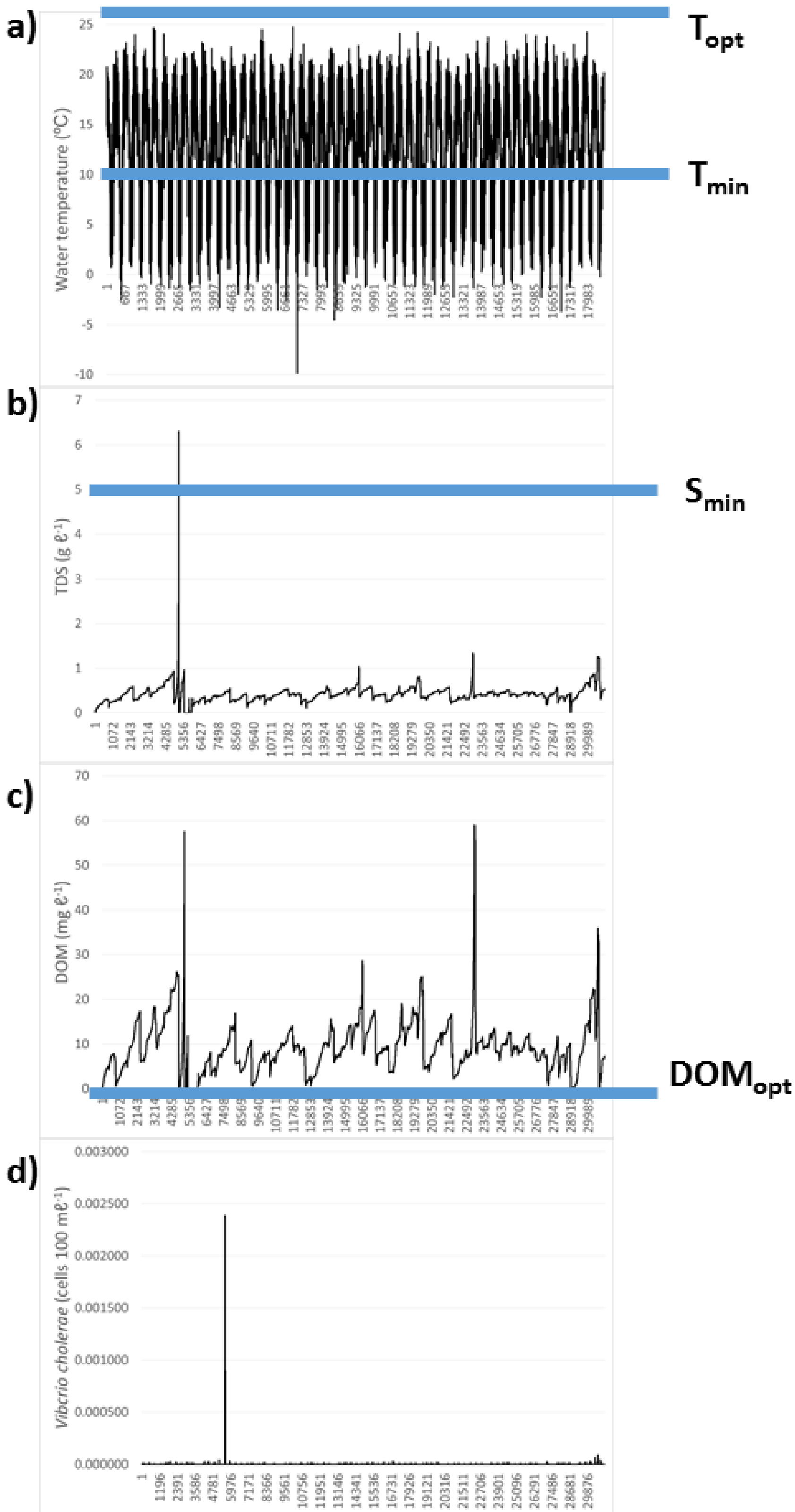

Figure 6.2 Results of modelling *Vibrio cholerae* as an endemic bacterial organism within the Middleburg Dam of the upper Olifants River Catchment. a) temperature; b) salinity; 3) nutrient (dissolved organic matter); d) instream *V. cholerae* concentration. X-axis: days since 1920.

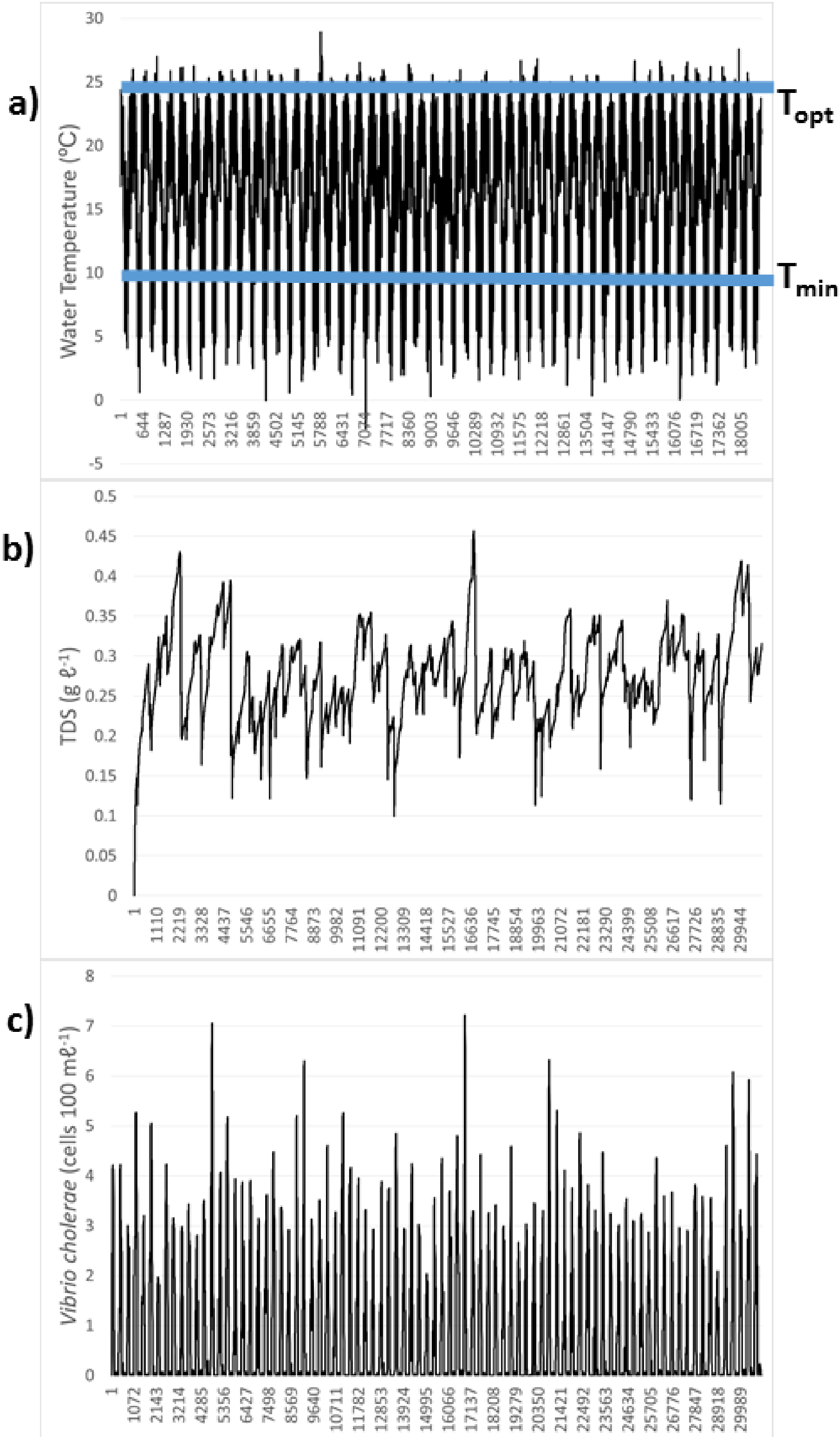

Figure 6.3 Results of modelling *Vibrio cholerae* as introduced through sewage effluent within the Witbank Dam of the upper Olifants River Catchment. a) temperature; b) salinity; 3) instream *V. cholerae* concentration. X-axis: days since 1920.

CHAPTER 7. CONCLUSIONS AND FUTURE DEVELOPMENT

7.1 Outcomes of the current project

The current project has shown that it is possible to develop a formal model for linking land use to non-point source inputs of nutrients. Although the method remains uncertain, it is an improvement on the massive uncertainty associated with calibrating the non-point source inputs of other existing water quality models.

The extension of WQSAM to simulate two important water quality variables, microbial water quality and sulphate (as indicative of acid mine drainage), was in particular successful. It was found that the modelling of *Escherichia coli* as a microbial indicator and sulphate could be achieved relatively simply but sufficiently accurately for management purposes.

Although the validation of simulations of algal and hyacinth growth within WQSAM by remote sensing data was limited, this needs to be weighed up against the inherent uncertainties within the remote sensing data. It can therefore be argued the indirect correlations obtained between WQSAM estimates of primary production within reservoirs and remote sensing estimates of primary production were reasonable.

The development and testing of the soil erosion and sediment transport model, WQSED, has been an extensive project in its own right. In particular, the model has been developed in conjunction with researchers working within the Ntabelanga catchment (T35A-E) through sharing of data and conceptual understanding. The project has revealed inherent scale-dependency problems within empirical estimates of soil erosion, such as the Modified Universal Soil Loss Equation (MUSLE). This project has shown that the WQSED model is able to general estimates of erosion that are within the range of previous estimates for South Africa.

At the initiation of the project, it was envisioned that a cholera prediction model could be relatively easily incorporated within WQSAM. This is because the survival in water of the bacteria that causes cholera, *Vibrio cholerae*, can be simulated in a relatively simple manner, similar to that of *E. coli*. This project has shown how this can be achieved within WQSAM, both conceptually and technically. However, it was found that although records of cholera cases are relatively well represented in the literature, studies of the bacteria, *V. cholerae*, and observed measures of the bacterial population, in particular the serotype causing cholera, are limited. Therefore, it was not possible to validate the implementation of *V. cholerae* survival in WQSAM or relate *V. cholerae* survival to cases of cholera outbreaks, and this study remained essentially an exploratory study.

7.2 Aspects of the model identified for further development

7.2.1 Soil erosion and sediment delivery model

This project has highlighted inherent scale-dependency issues within the MUSLE equation. An interrogation of the literature has revealed that this issue has been largely ignored in previous studies. Strategies for getting around this issue will need to be developed. In addition, the simulation of transport of sediment within the main river channel is related to the capacity of water to carry sediment, which is further related to water velocity. Although there is a preliminary implementation of this aspect, it is likely that further refinements will be required. Mr David Gwapedza, the Master’s student on this project, has been able to upgrade his project to a doctorate, and it is likely that these issues will form part of his extended project.

7.3 Scientific outputs of K5/2237 and K5/2448

7.3.1 Publications

Hughes, D.A. and Slaughter, A.R. (2015) Daily disaggregation of simulated monthly flows using different rainfall datasets in southern Africa. *Journal of Hydrology: Regional Studies* 4: 153-171.

Hughes, D.A. and Slaughter, A.R. (2016) Disaggregating the components of a monthly water resources system model to daily values for use with a water quality model. *Environmental Modelling and Software* 80: 122-131.

Slaughter, A.R. (2017) Simulating microbial water quality in data-scarce catchments: an update of the WQSAM model to simulate the fate of *Escherichia coli*. Water Resources Management. DOI 10.1007/s11269-017-1743-1. Available at: http://link.springer.com/article/10.1007/s11269-017-1743-1

Slaughter, A.R., Hughes, D.A., Retief, D.C.H. and Mantel, S.K. (2017) A management-oriented water quality model for data scarce catchments. *Environmental Modelling and Software* 97, 93-111.

Slaughter, A.R., Mantel, S.K. (2017) Land cover models to predict non-point nutrient inputs for selected biomes in South Africa. *Water SA* 43(3), 499-508.

Slaughter, A.R., Mantel, S.K. and Hughes, D.A. (2016) Water Quality Management in the Context of Future Climate and Development Changes: A South African Case Study. *Journal of Water and Climate Change*, jwc2016138.

Slaughter, A.R., Retief, D.C.H. and Hughes, D.A. (2015) A method to disaggregate monthly flows to daily using daily rainfall observations: model design and testing. *Hydrological Sciences Journal* 4(B): 153-171. http://www.tandfonline.com/doi/pdf/10.1080/02626667.2014.993987

7.3.2 Published conference proceedings

Slaughter, A.R. and Hughes, D.A. (2014) Investigating possible climate change and development effects on water quality within an arid catchment in South Africa: a comparison of two models. Proceedings of the 7th International Environmental Modelling and Software Society (iEMSs) biennial meeting, San Diego, USA 15-19 June 2014. http://www.iemss.org/sites/iemss2014/papers/iemss2014_submission_318.pdf

Slaughter, A.R. and Mantel S.K. (2016) The validation of algal growth processes in a water quality model using remote sensing data. Proceedings of the 8th International Environmental Modelling and Software Society (iEMSs) biennial meeting, Toulouse, France 10-14 July 2016. http://scholarsarchive.byu.edu/cgi/viewcontent.cgi?article=1374&context=iemssconference

Slaughter, A.R. and Mantel S.K. (2017) Water quality modelling of an impacted semi-arid catchment using flow data from the WEAP model. IAHS special issue “Water security and the food-water-energy nexus: drivers, responses and feedbacks at local to global scales”. Proceedings of the IAHS Scientific Assembly 2017, Port Elizabeth, South Africa, 10-14 July 2017. Proc. IAHS, 94, 1-9, 2017 https://doi.org/10.5194/piahs-94-1-2017

Slaughter, A.R., Hughes, D.A. and Mantel, S.K. (2012) The development of a Water Quality Systems Assessment Model (WQSAM) and its application to the Buffalo River Catchment, Eastern Cape, South Africa. Proceedings of the 6th International Environmental Modelling and Software Society (iEMSs) biennial meeting, Leipzig, Germany 1-5 July 2012. ISBN: 978-88-9035-742-8 http://www.iemss.org/sites/iemss2012//proceedings/I2_2_0497_Slaughter_et_al.pdf

REFERENCES

Acocks, J.P.H. (1988) Veld types of South Africa. 3nd edition. Mem. Bot. Surv. S. Afr. No. 57: 1-146.

Aksil, A. and Koldas, S. (2006) Acid mine drainage (AMD): causes, treatment and case studies. *Journal of Cleaner Production* 14, 1139-1145.

Albright, T.P., Moorhouse, T.G. and McNabb, T.J. (2004) The rise and fall of water hyacinth in Lake Victoria and the Kagera River basin, 1989-2001. Journal of Aquatic Plant Management 42: 73-84.

Arekhi, S., Shabani, A. and Rostamizad, G. (2012) Application of the modified universal soil loss equation (MUSLE) in prediction of sediment yield (Case study: Kengir Watershed, Iran). Arabian Journal of Geosciences 5(6): 1259-1267. http://doi.org/10.1007/s12517-010-0271-6

Aslam, M., Sultana, M., Nair, G.B., Sack, R.B., Sack, D.A., Siddique, A.K., Ali, A., Anwar Huq, A. and Colwell, R. R. (2006). Toxigenic Vibrio cholerae in the aquatic environment of Mathabaria, Bangladesh. Applied Environmental Microbiology 72 (4): 2849-2855.

Ayalew, G. (2015) Soil loss estimation using geographic information system in enfraz watershed for soil conservation planning in highlands of Ethiopia. International Journal of Agricultural Research, Innovation & Technology 5(2): 21-30.

Balance, A; Hill, L; Roux, D, Silberbauer, M. and Strydom, W. (2001). State of the Rivers Report: Crocodile, Sabie-Sand and Olifants River Systems. Resource Quality Services, DWAF, Pretoria, South Africa (www.csir.co.za/rhp).

Bannatyne, L.J., Rowntree, K.M., van der Waal, B.W. and Nyamela, N., 2017. Design and implementation of a citizen technician-based suspended sediment monitoring network: Lessons from the Tsitsa River catchment, South Africa. Water SA, 43(3), pp.365-377.

Beasley, D.B., Huggins, L.F. and Monke, E.J. (1980) ANSWERS: A model for watershed planning. Transactions of the American Society of Agricultural Engineers 23: 938-944.

Benson, T. (2014, June). Reynolds Number. In NASA Glenn Research Center. Retrieved from http://www.grc.nasa.gov/WWW/BGH/reynolds.html.

Bertuzzo, E., Casagrandi, R., Gatto, M., Rodriguez-Iturbe, I. and Rinaldo, A. (2010). On spatially explicit models of cholera epidemics. Journal of the Royal Society 7: 321-333.

Bevan, K. (2006) A manifesto for the equifinality thesis. *Journal of Hydrology* 320, 18-36.

Bicknell, B.R., Imhoff, J.C., Kittle, J.L., Jr., Donigian, A.S., Jr. and Johanson, R.C. (1997) Hydrological Simulation Program--Fortran, User's manual for version 11: U.S. Environmental Protection Agency, National Exposure Research Laboratory, Athens, Ga., EPA/600/R-97/080, 755 p.

Boardman, J. (2012) Soil erosion and land degradation. In P. Holmes, & M. Meadows (Eds.), Southern African Geomorphology: Recent trends and new directions. (pp. 307-328). Bloemfontein: SUN media.

Bouma, M.J. and Pascual, M. (2001). Seasonal and interannual cycles of endemic cholera in Bengal 1891-1940 in relation to climate and geography. Hydrobiologia 460: 147-156.

Bresciani, M., Stroppiana, D., Odermatt, D., Morabito, G. and Giardino, C. (2011) Assessing remotely sensed chlorophyll-a for the implementation of the Water Framework Directive in European perialpine lakes. Science of the Total Environment 409: 3083-3091.

Britz, T.J. and Sigge, G.O. (2012) Quantitative investigation into the link between irrigation water quality and food safety: Volumes 1-4.Water Research Commission report No. 1773/1/12. Water Research Commission, Pretoria, South Africa.

Bryson, L. (2015) An erosion and sediment delivery model for semi-arid catchments. Master's Thesis. Grahamstown: Rhodes University.

Candeias, C., Ávila, P.F., da Silva, E.F., Ferreira, A., Salgueiro, A.R. and Teixeira, J.P. (2013) Acid mine drainage from the Panasqueira mine and its influence on the Zêzere River (Central Portugal). *Journal of African Earth Science* 99(2), 705-712.

Carpenter, D.J. and Carpenter, S.M. (1983) Modeling inland water quality using Landsat data. Remote Sensing of Environment 13: 345-352.

Carstensen, J., Dah, K., Henriksen, P., Hjorth, M. and Josefson, A. (2011) Coastal Monitoring Programs. In: Treatise on Estuarine and Coastal Sciences. Vol. 7: Functioning of Ecosystems at the Land-Ocean Interface. Elsevier. Pp. 175-206.

Chapra, S. (1997). Surface water-quality modelling. The McGraw-Hill Companies, Inc.

Chawira, M., Dube, T. and Gumindoga W. (2013) Remote sensing based water quality monitoring in Chivero and Manyame lakes of Zimbabwe. Physics and Chemistry of the Earth 66: 38-44.

Cobbing, J.E. (2008) Institutional linkages and acid mine drainage: the case of the Western Basin in South Africa. Water Resources Development 24(3), 451-462.

Codeco, T.C. (2001). Endemic and epidemic dynamics of cholera: the role of the aquatic reservoir. MNC Infectious Diseases 1(1): 1471-2334.

Cole, T.M. and Wells, S.A. (2008) CE-QUAL-W2: A Two-Dimensional, Laterally Averaged, Hydrodynamic and Water Quality Model, Version 3.6. Department of Civil and Environmental Engineering, Portland State University, Portland, Oregon, USA.

Collins, A.E. (2003). Vulnerability to coastal cholera ecology. Social Science and Medicine 57: 1397-1407.

Collins, R. and Rutherford, K. (2004) Modelling bacterial water quality in streams draining pastoral land. *Water Research* 38, 700-712.

Colwell, R.R. (1996). Global climate and infectious diseases: the cholera paradigm. Science 274: 2025-2031.

Cottle, E. and Deedat, H. (2002). The cholera outbreak: a 2000-2002 case study of the source of the outbreak in the Madlebe Tribal Authority areas, uThungulu region, KwaZulu-Natal. Health Systems Trust.

Crone, T. (2004). The Basic Sediment Transport Equations Made Ridiculously Simple. In OCEAN/ESS 410 Marine Geology and Geophysics. Retrieved from http://www.ocean.washington.edu/courses/oc410/reading/sedtrans_2004.pdf

Czuba, J.A., Magirl, C.S., Czuba, C.R., Grossman, E.E., Curran, C.A., Gendaszek, A.S., & Dinicola, R.S. (2011). Comparability of Suspended-Sediment Concentration and Total Suspended Solids Data Sediment Load from Major Rivers into Puget Sound and its Adjacent Waters. USGS Fact Sheet 2011-3083. Tacoma, WA: U S Geological Survey.

De Magny, G.C., Murtugudde, R., Sapiano, M.R.P., Nizam, A., Brown, C.W., Busalacchi, A.J., Yunus, M., Nair, G.B., Gil, A.L., Lanata, C.F., Calkins, J., Manna, B., Rajendran, K., Bhattacharya, M.K, Huqj, A., Sack, R.B. and Colwell, R.R. (2008). Environmental signatures associated with cholera epidemics. PNAS 105(46): 17676-17681.

De Magny, G.C., Paroissin, C., Cazelles, B., de Lara, M., Delmas, J.F. and Guegan, J.F. (2005). Modeling environmental impacts of plankton reservoirs on cholera population dynamics. ESAIM: Proceedings 14: 156-173.

De Villiers, S. and Mkwelo, S.T (2009). Has monitoring failed the Olifants River, Mpumalanga? Water SA 35(5): 671-676.

Deksissa, T., Meirlaen, J., Ashton, P.J. and Vanrolleghem, P.A. (2004) Simplifying dynamic river water quality modelling: A case study of inorganic nitrogen dynamics in the Crocodile River (South Africa). Water Air Soil Poll. 155, 303-320.

Doerffer, R. and Schiller, H. (2008) MERIS Regional Coastal and Lake Case 2 Water Project – Atmospheric Correction ATBD, GKSS Research Center 21502 Geesthacht Version 1.0 18. May 2008.

Dollar, E.S.J. and Rowntree, K.M. (1995) Sediment sources, hydroclimatic trends and geomorphic response in a mountainous catchment, North Eastern Cape, South Africa, South African Geographical Journal 77(1): 21-32.

Du Preez, M., van der Merwe, M.R., Cumbana, A. and le Roux, W. (2010). A survey of Vibrio cholerae O1 and O139 in estuarine waters and sediments of Beira, Mozambique. Water SA 36(5): 615-620.

Dudal, R. (1981) An evaluation of conservation needs. In: Morgan RPC (ed) Soil conservation: problems and prospects. Wiley, New York.

DWAF (1995) Water Quality Situation Assessment of the Crocodile River Catchment, Eastern Transvaal: Water Quality Management Series, Volumes 1-9, Department of Water Affairs and Forestry, Pretoria.

DWAF (2004) State-of-rivers report buffalo river system. Rivers Report for the Eastern Cape: https://www.dwa.gov.za/default.aspx.
DWAF (2009) State-of-rivers report White-Kei River system. Rivers Report for the Eastern Cape: https://www.dwa.gov.za/default.aspx.
Edberg, S.C., Rice, E.W., Karlin, R.J. and Allen, M.J. (2000) *Escherichia coli*: the best biological drinking water indicator for public health protection. *Journal of Applied Microbiology* 88, 106-116.
Elwell, H.A. and Stocking, M.A. (1976). Vegetal cover to estimate soil erosion hazard in Rhodesia. Geoderma 15:61-70.
Emch, M., Feldacker, C., Islam, M.S. and Ali, M. (2008). Seasonality of cholera from 1974 to 2005: a review of global patterns. International Journal of Geographics 7(31): 1-13.
EPA. (2012) Channel Processes: Bedload Transport. In Water: Science & Technology. Retrieved from http://water.epa.gov/scitech/datait/tools/warsss/bedload.cfm.
ESRI (2006) Cumulative Effects Study Uses GIS to Assess the State of the River's Ecosystem, Predict Future Conditions and Distribute Data to Decision Makers. U.S. Army Corps of Engineers and Yellowstone River Conservation District Council. Retrieved March 15, 2012, from http://www.esri.com/library/casestudies/yellowstone.pdf.
ESRI (2008) Extending Enterprise GIS to Virginia Department of Forestry's Mobile Staff. Virginia Department of Forestry. Retrieved March 15, 2012, from http://www.esri.com/library/casestudies/virginia-dept-of-forestry.pdf.
Evans, R. (1980) Mechanisms of water erosion and their spatial and temporal controls: an empirical viewpoint MJ. Kirkby, R.P.C. Morgan (Eds.), Soil Erosion, Wiley, Chichester (1980), pp. 109-128.
Everitt, J.H., Richardson, A.J and Nixon, P.R. (1986) Canopy reflectance characteristics of succulent and nonsucculent rangeland plant species. Photogramm. Eng. Remote Sens. 52: 1891-1897.
Everitt, J.H., Yang, C., Escobar, D.E., Webster, C.F., Lonard, R.I. and Davis, M.R. (1999) Using remote sensing and spatial information technologies to detect and map aquatic macrophytes. Journal of Aquatic Plant Management 37: 71-80.
Ewen, J., Parkin, G. and O'Connell, P.E. (2000). SHETRAN: Distributed river basin flow and transport modelling system. Proceedings of the American Society of Civil Engineers, Journal of Hydrologic Engineering 5: 250-258.
Felip, M. and Catalan, J. (2000) The relationship between phytoplankton biovolume and chlorophyll in a deep oligotrophic lake: decoupling in their spatial and temporal maxima. J Plankton Res 22(1): 91-105.
Fink, J.C. (2005) The Effects of Urbanization on Baird Creek, Green Bay, Wisconsin. Master's Thesis. University of Wisconsin-Green Bay, Green Bay, Wisconsin.
Fleming, G., van der Merwe, M. and McFerren, G. (2007). Fuzzy expert systems and GIS for choler health risk prediction in southern Africa. Environmental Modelling and Software 22: 442-448.
Gallant, J.C., Dowling, T.I., Read, A.M., Wilson, N., Tickle, P. and Inskeep, C. (2011). Second SRTM derived digital elevation models user guide. Geoscience Australia, Canberra, 106.
Gao, P. (2008). Understanding watershed suspended sediment transport. Progress in Physical Geography 32(3): 243-263. http://doi.org/10.1177/0309133308094849
Gardiner, N. (2007) Trends in selected biomes, habitats and ecosystems: Inland waters. In: Sourcebook on Remote Sensing and Biodiversity Indicators. Editors Strand H., H. Robert, J. Stritthold, L. Miles, N. Horning, E. Fosnight, pp. 83-102. Secretariat of the Convention on Biological Diversity, Montreal, Technical Series no. 32. Available from http://cce.nasa.gov/pdfs/cbd-ts-32_sourcebook.pdf; downloaded on 14 April 2014.
Gibson, L., Newby, T., Makapela, L., Ramoela, A., Matthieu, R., Majozi, N., Jewitt, G. and Mengistu, M. (2015) Review on the status of remote sensing applications to water resource management. WRC Report No. KV 329/14, Water Research Commission, Pretoria, South Africa.

Gitelson, A.A., Dall'Olmo, G., Moses, W., Rundquist, D.C., Barrow, T., Fisher, T.R., Gurlin, D. and Holz, J. (2008) A simple semi-analytical model for remote estimation of chlorophyll-a in turbid waters: Validation. Remote Sensing of Environment 112: 3582-3593.

Gray, N.F. (1996) Field assessment of acid mine drainage contamination in surface and ground water. *Environmental Geology* 27, 358-361.

Gray, N.F. (1997) Environmental impact and remediation of acid mine drainage: a management problem. *Environmental Geology* 30 (1/2), 62-71.

Gray, N.F. (1998) Acid mine drainage composition and implications for its impact on lotic systems. *Water Research* 32(7), 2122-2134.

Griffith, D.C., Kelly-Hope, L.A. and Miller, M.A. (2006). Review of reported cholera outbreaks worldwide, 1995-2005. American Journal of Tropical Medicine and Hygiene 75(2): 973-977.

Gupta, S. (2005). Cholera pattern in children of Delhi. Letters to the Editor. Indian Pediatr. 42: 90.

Harrington Jr., J.A., Schiebe F.R. and Nix, J.F. (1992) Remote sensing of Lake Chicot, Arkansas: Monitoring suspended sediments, turbidity, and Secchi Depth with Landsat MSS data. Remote Sensing of the Environment 39: 15-27.

Heath, R., Coleman, T. and Engelbrecht, J. (2010) Water quality overview and literature review of the ecology of the Olifants River. WRC Report No. TT 452/10. Water Research Commission, Pretoria, South Africa.

Hickin, E.J. (1995) Hydraulic geometry and channel scour, Fraser River, British Columbia, Canada. In River Geomorphology, Hickin EJ (ed.). Wiley; Chichester.

Hicks, B.J., Stichbury, G.A., Brabyn, L.K., Allan, M.G. and Ashraf, S. (2013) Hindcasting water clarity from Landsat satellite images of unmonitored shallow lakes in the Waikato region, New Zealand. Environmental Monitoring and Assessment 185: 7245-7261.

Hipsey, M.R., Antenucci, J.P. and Brookes, J.D. (2008) A generic, process-based model of microbial pollution in aquatic systems. Water Resources Research 44, 1-26.

Hobbs, P. J. and Cobbing, J. E. (2007) A Hydrogeological Assessment of the Acid Mine Drainage Impacts in the West Rand Basin, Gauteng Province, Report No. CSIR/NRE/WR/ER/2007/0097/C (Pretoria: CSIR).

Hoffman, M.T. and Todd, S. (2000). A national review of land degradation in South Africa: The influence of biophysical and socio-economic factors. J. South. Afr. Stud. 26 (4): 743-758.

Horning, N. and DuBroff, N. (2004) Myths and misconceptions about remote sensing. Version 1.0. American Museum of Natural History, Center for Biodiversity and Conservation. Available from http://biodiversityinformatics.amnh.org. (accessed on 12 November 2015).

Hudson, N.W. (1981). Soil conservation, 2nd edn. Batsford, London.

Hudson, N.W. and Jackson, D.C. (1959) Results achieved in the measurement of erosion and runoff in Southern Rhodesia. Proceedings of the Third Inter-African Soils Conference. Dalaba: 575-83.

Hudson, N.W. and Jackson, D.C. (1959). Results achieved in the measurement of erosion and runoff in Southern Rhodesia. Proceedings of the Third Inter-African Soils Conference. Dalaba: 575-83.

Hughes, D.A. (1995). Monthly rainfall-runoff models applied to arid and semiarid catchments for water resource estimation purposes. Hydrological Sciences Journal 40(6): 751-769.

Hughes, D.A. (2008). Simulating the hydrology and total dissolved solids (TDS) of an ephemeral river in South Africa for environmental water requirement determinations. River Research and Applications 24: 1-11.

Hughes, D.A. and Slaughter, A.R. (2015) Daily disaggregation of simulated monthly flows using different rainfall datasets in southern Africa. Journal of Hydrology: Regional Studies 4: 153-171.

Hughes, D.A. Andersson, L., Wilk, J. and Savenije, H.H.G. (2006) Regional calibration of the Pitman model for the Okavango River. J. Hydrol. 331: 30-42.

Hughes, D.A., Hannart, P. and Watkins, D. (2003) Continuous baseflow separation from time series of daily and monthly streamflow data. *Water SA* 29(1), 43-48.

Hunter, P.D., Gilvear, D.J., Tyler, A.N., Willby, N.J., Kelly, A. (2010) Mapping macrophyte vegetation in shallow lakes using the compact airborne spectrographic imager (CASI). Aquat. Conxerv. 20: 717-727.

INTER-MINISTERIAL COMMITTEE (2010) Mine water management in the Witwatersrand Gold Fields with special emphasis on acid mine drainage. Report to the Inter-Ministerial Committee on Acid Mine Drainage. Department of Water Affairs, Pretoria.

Jain, M.K., Das, D. (2010) Estimation of Sediment Yield and Areas of Soil Erosion and Deposition for Watershed Prioritization using GIS and Remote Sensing. Water Resources Management 24: 2091-2112.

Jain, S.K., Tyagi J., Singh, V. (2010) Simulation of runoff and sediment yield for a Himalayan watershed using SWAT model. J Water Resource Protection 2: 267-281.

Jakeman, A.J., Hornberger, G.M. (1993) How much complexity is warranted in a rainfall-runoff model? Water Resources Research 29(8): 2637-2649.

Jang, C., Shin, Y., Kum, D., Kim, R., Yang, J. E., Kim, S. C., Jung, Y. (2015) Assessment of soil loss in South Korea based on land-cover type. Stochastic Environmental Research and Risk Assessment 29(8): 2127-2141. http://doi.org/10.1007/s00477-015-1027-3.

Jensen, M.A., Faruque, S.H., Mekalanos, J.J. and Levin, B.R. (2006). Modeling the role of bacteriophage in the control of cholera outbreaks. PNAS 103(12): 4652-4657.

Kapangaziwiri, E., Hughes, D.A., Tanner, J.L. and Slaughter, A. (2011) Resolving uncertainties in the source of low flows in South African rivers using conceptual and modelling studies. Conceptual and modelling studies of integrated groundwater, surface water and ecological systems, Proceedings of Symposium H01 held during IUGG 2011, Melbourne, Australia, July 2011. IAHS Publ. 345, 2011.

Kashefipour, S.M., Lin, B., Harris, E. and Falconer, R.A. (2002) Hydroenvironmental modelling for bathing water compliance of an estuarine basin. *Water Research* 36(7), 1854-1868.

Kasprzak, P., Padisak, J., Koschel, R., Krienitz, J., Gervais, F. (2008) Chlorophyll a concentration across a trophic gradient of lakes: An estimator of phytoplankton biomass? Limnologica 38: 327-338.

Kinnell, P.I. (2005) Why the universal soil loss equation and the revised version of it do not predict event erosion well. Hydrological Processes, 19: 851-854.

Kinnell, P.I.A. (2000) AGNPS-UM: applying the USLE-M within the agricultural nonpoint source pollution model. Environmental Modelling and Software 15, 331-341.

Kinsel, W.G. (1980) CREAMS: A field scale model for Chemicals, Runoff and Erosion, in Agricultural Management Systems. U.S. Department of Agriculture, Conservation Report no. 26, pp. 640.

Koponen, S., Ruiz-Verdu, A., Heege, T., Heblinski, J., Sorensen, K., Kallio, K., Pyhälahti, T., Doerffer, R., Brockman, C. and Peters, M. (2008) Development of MERIS Lake Water Algorithms: Validation Report. ESRIN Contract No. 20436/06/I-LG. Available from http://www.brockmann-consult.de/beam-wiki/display/LAKES/Validation+report; accessed on 10 December 2015.

Kusimi, J.M. and Attua E.M. (2008). Soil Erosion and Sediment Yield Modelling in the Pra River Basin of Ghana using the Revised Universal Soil Loss Equation (RUSLE) 7(2): 38-57.

Kustner, H.G.V. and du Plessis, G. (1991). The cholera epidemic in South Africa, 1980-1987. SAMJ 79: 539-544.

Roux, J.J., Barker, C.H., Weepener, H.L. and Berg, V. Den. (2014). Sediment yield modelling in the Umzimvubu River Catchment. Water Research Commission Report, WRC project K5/2243/1December 2014

Le Roux, J.J., Morgenthal, T. and Malherbe, J. (2008). Water erosion prediction at a national scale for South Africa. Water SA, 34(3), 305-314. Retrieved from http://www.wrc.org.za/Knowledge Hub Documents/Water SA Journals/Manuscripts/2008/03/WaterSA_2008_03_2243.pdf

Le Roux, J.J., Newby, T.S. and Sumner, P.D. (2007). Monitoring soil erosion in South Africa at a regional scale, review and recommendations. South African Journal of Science 103: 329-335.

Le Roux, J.J., Sumner, P.D., Lorentz, S.A. and Germishuyse, T. (2013). Connectivity aspects in sediment migration modelling using the Soil and Water Assessment Tool. Geosciences 3(1): 1-12.

Le Roux, W.J., Schaefer, L.M. and Genthe, B. (2012) Microbial water quality in the upper Olifants River catchment: implications for health. African Journal of Microbiology Research 6(36): 6580-6588.

Lipp, E.K., Huq, A. and Colwell, R.R. (2002). Effects of global climate on infectious disease: the cholera model. Clinical Microbiology Reviews 15(4): 757-770.
Low, A.B. and Rebelo, A.G. (1996). Vegetation of South Africa, Lesotho and Swaziland. DEAT, Pretoria. 85pp.
Luo, Y., Yang, S., Liu, X., Liu, C., Zhang, Y., Zhou, Q., Dong, G. (2016) Suitability of revision to MUSLE for estimating sediment yield in the Loess Plateau of China. Stochastic Environmental Research and Risk Assessment 30(1): 379-394. http://doi.org/10.1007/s00477-015-1131-4
Madico, G., Checkley, W., Gilman, R.H., Bravo, N., Cabrera, L., Calderon, M. and Caballos, A. (1996). Active surveillance for Vibrio cholerae O1 and vibriophages in sewage water as a potential tool to predict cholera outbreaks. Journal of Clinical Microbiology 34(12): 2968-2972.
Madoroba, E. and Momba, N.B. (2010). Prevalence of Vibrio cholerae in rivers of Mpumalanga province, South Africa as revealed by polyphasic characterization. African Journal of Biotechnology 9(43): 7925-7301.
Maillard, P and Santos, N.A.P. (2007) A spatial-statistical approach for modeling the effect of non-point source pollution on different water quality parameters in the Velhas river watershed – Brazil. *Journal of Environmental Management* 86 (1), 158-170.
Mancini, J.L. (1978) Numerical estimates of coliform mortality rates under various conditions. *Journal of Water Pollution Control* Federation 50 (11), 2477-2484.
Maree, J.P., Hlabela, P., Nengovhela, A.J., Geldenhuys, A.J., Mbhele, N., Nevhulaudzi, T., Waanders, F.B. (2004) Treatment of mine water for sulphate and metal Removal using barium sulphide. *Mine Water Environment* 23, 195-203.
Mari, L., Bertuzzo, E., Righetto, L., Casagrandi, R., Gatto, M., Rodriguez-Iturbe, I. and Rinalo, A. (2010). Modelling cholera epidemics: the role of waterways, human mobility and sanitation. Journal of the Royal Society Interface 9: 376-388.
Masih, I., Maskey, S., Mussá, F.E.F. and Trambauer, P. (2014). A review of droughts on the African continent: A geospatial and long-term perspective. Hydrology and Earth System Sciences 18(9): 3635-3649. http://doi.org/10.5194/hess-18-3635-2014
Matthews M.W., Bernard S. and Robertson, L. (2012) An algorithm for detecting trophic status (chlorophyll-a), cyanobacterial-dominance, surface scums and floating vegetation in inland and coastal waters. Remote Sensing of Environment 124: 637-652.
Matthews, M.W. (2011) A current review of empirical procedures of remote sensing in inland and near-coastal transitional waters. International Journal of Remote Sensing 32: 6855-6899.
Matthews, M.W. (2014) Eutrophication and cyanobacteria blooms in South African inland waters: 10 years of MERIS observations. Remote Sensing of Environment 155: 161-177. http://dx.doi.org/10.1016/j.rse.2014.08.010.
Matthews, M.W. and Bernard, S. (2013) Characterizing the absorption properties for remote sensing of three small optically-diverse South African reservoirs. Remote Sensing 5: 4370-4404.
Matthews, M.W. and Bernard, S. (2015) Eutrophication and cyanobacteria in South Africa's standing water bodies: A view from space. South African Journal of Science 111: 1-8. http://dx.doi.org/10.17159/sajs.2015/20140193.
Matthews, M.W. and Odermatt, D. (2015) Improved algorithm for routine monitoring of cyanobacteria and eutrophication in inland and near-coastal waters. Remote Sensing of Environment 156: 374-382.
Matthews, M.W., Bernard, S. and Winter, K. (2010) Remote sensing of cyanobacteria-dominant algal blooms and water quality parameters in Zeekoevlei, a small hypertrophic lake, using MERIS. Remote Sensing of Environment 114: 2070-2087.
McNally, W.H., & Mehta, A.J. (2004). Sediment Transport and Deposition in Estuaries (Sample Chapter). In Encyclopedia of Life Support Systems (EOLSS): Coastal Zones and Estuaries. Retrieved from http://www.eolss.net/sample-chapters/c09/E2-06-01-04.pdf
Mendelsohn, J. and Dawson, T. (2008). Climate and cholera in KwaZulu-Natal, South Africa: The role of environmental factors and implications for epidemic preparedness. International Journal of Hygiene and Environmental Health 211: 156-162.
Menon, P., Billen, G. and Servais, P. (2003) Mortality rates of autochthonous and fecal bacteria in natural aquatic ecosystems. *Water Research* 37, 4151-4158.

Merritt, W.S., Letcher, R.A. and Jakeman, A.J. (2003). A review of erosion and sediment transport models. Environmental Modelling and Software 18(8-9): 761-799. http://doi.org/10.1016/S1364-8152(03)00078-1

Mhangara, P. (2011). Land Use/Cover Change Modelling and Land Degradation Assessment in the Keiskamma Catchment Using Remote Sensing and GIS, (January), 200.

Middleton, B.J. and Bailey, A.K., (2008). Water Resources of South Africa, 2005 Study (WR2005). WRC Report No's. TT380 to 382/08 submitted by SRK Consulting, SSI Engineers and Environmental Consultants (Pty) Ltd., Knight Piesold, Arcus Gibb (Pty) Ltd., Ninham Shand Consulting Services, P D Naidoo & Associates, Umfula Wempilo Consulting on behalf of Water Research Commission, Gezina, South Africa.

Midgley, D.C., Pitman, W.V. and Middleton, B.J. (1994). Surface Water Resources of South Africa 1990. Pretoria: Water Research Commission.

Mishra, S.K., Tyagi, J.V., Singh, V.P. and Singh, R. (2006) SCS-CN-based modeling of sediment yield. J Hydrol 324: 301-322.

Missouri DNR. (2009). Chapter 3: Stream Discharge. In Introductory Level Volunteer Water Quality Monitoring T raining Notebook. Retrieved from http://www.dnr.mo.gov/env/wpp/vmqmp/level1-ch3.pdf

Momba, M.N.B., Malakate, V.K. and Theron, J. (2006). Abundance of pathogenic Escherichia coli, Salmonella, typhimurium and Vibrio cholerae in Nkonkobe drinking water sources. Journal of Water and Health 4(3): 289-296.

Moore, I.D. and Burch, G.J. (1986) Physical basis of the length-slope factor in the Universal Soil Loss Equation (USLE). Soil Sci. Soc. Amer. J. 50: 1294-1298.

Morgan, R.P. (2005). Soil Erosion and Conservation, Third edition. Oxford: Blackwell Science Ltd.

Morgan, R.P., Quinton, J.N., Smith, R.E., Govers, G., Poesen, J.W., Auerswald, K., Chisci, G., Torri, D. and Styczen, M.E. (1998). The European soil erosion model (EUROSEM): a process-based approach for predicting soil loss from fields and small catchments. Earth Surface Processes and Landforms 23: 527-544.

Morgan, R.P.C. (1974). Estimating regional variation in soil erosion hazard in Peninsular,

Morgan, R.P.C. (2005). Soil Erosion and Conservation, Third edition. Oxford: Blackwell Science Ltd.

Msadala, V., Gibson, I., Le Roux, J., Rooseboom, A. and Basson, G. (2010a) Sediment Yield Prediction for South Africa: 2010 Edition. WRC Report No. 1765/1/10, Water Research Commission, Pretoria, South Africa.

Msadala, V., Gibson, L., Le Roux, J., Rooseboom, A. and Basson, G. (2010b). Revised sediment yield maps for South Africa. The new sediment yield map for southern Africa, WRC Project K5/765.

Mucina, L. and Rutherford, M.C. (2006) The vegetation of South Africa, Lesotho and Swaziland. South African National Biodiversity Institute (SAMBI), Pretoria, South Africa.

Murphy, S. (2007). General Information on Solids. In City of Boulder: USGS Water Quality Monitoring. Retrieved from http://bcn.boulder.co.us/basin/data/NEW/info/TSS.html

NASA (2011) MODIS Surface Reflectance User's Guide. Version 1.3. Prepared by Vermote, E.F., Kotchenova, S.Y. and Ray, J.P. Available from http://modis.gsfc.nasa.gov/data/dataprod/mod09.php; accessed 18 November 2015.

NASA ARSET (2015) Fundamentals of remote sensing. Presentation available from Applied Remote Sensing Training (ARSET) http://arset.gsfc.nasa.gov/sites/default/files/users/S1_P4_RSbasics_final.pdf; accessed 5 October 2015.

Nash, J.E. and Sutcliffe, J.V. (1970) River flow forecasting through conceptual models. Part I – a discussion of principles. *Journal of Hydrology* 10, 282-290.

National Land Cover (NLC) (2014). 2014 South African National Land-Cover. Retrieved from Biodiversity GIS: http://bgis.sanbi.org/DEA_Landcover

Nearing, M.A. and Hairsine, P.B. (2011) The Future of Soil Erosion Modelling. In R. P. Morgan, & M. A. Nearing, Handbook of Erosion Modelling (pp. 387-397). Chichester: Wiley-Blackwell Publishers.

Nearing, M.A., Jetten, V., Baffaut, C., Cerdan, O., Couturier, A., Hernandez, M., Van Oost, K. (2005) Modeling response of soil erosion and runoff to changes in precipitation and cover. Catena 61 (2-3 SPEC. ISS.), 131-154. http://doi.org/10.1016/j.catena.2005.03.007.

Neitsch, S.L., Arnold, J.G., Kiniry, J.R. and Williams, J.R. (2005) Soil and Water Assessment Tool Theoretical Documentation, Version 2005, Springer, Berlin (2005)

Nteme, V.M., Potgieter, N., van Blerk, G.N. and Barnard, T.G. (2014). Investigating the occurrence and survival of Vibrio cholerae in selected surface water sources in the Kwazulu-Natal province of South Africa. Water Research Commission Report 2168/1/14. WRC, Pretoria, South Africa.

O'Keefe, J.H., van Ginkel, C.E., Hughes, D.A., Hill, T.R. and Ashton, P.J. (1996) A situation analysis of water quality in the catchment of the Buffalo River, Eastern Cape, with special emphasis on the impacts of low cost, high-density urban development on water quality. Water Research Commission Report No. 405/1/96, Water Research Commission, Pretoria, South Africa.

O'Reilly, J.E., Maritorena, S., Mitchell, B.G., Siegel, D.A., Carder, K.L., Garver, S.A., Kahru, M. and McClain, C. (1998) Ocean color chlorophyll algorithms for SeaWiFS. Journal of Geophysical Research 103: 24,937-24,953.

Oberholster, P.J., Myburgh, J.G., Ashton, P.J. and Botha, A.M. (2010) Responses of phytoplankton upon exposure to a mixture of acid mine drainage and high levels of nutrient pollution in Lake Loskop, South Africa. *Ecotoxicity and Environmental Safety* 73, 326-335.

Oelofse, S. (2008) Mine water pollution-acid mine decant, effluent and treatment: a consideration of key emerging issues that may impact the state of the environment. Report prepared for the Department of Environment and Tourism, Pretoria, South Africa. ISBN NO: 978-0-9814178-5-1

Olías, M., Nieto, J.M., Sarmiento, A.M., Cerón, J.C. and Cánovas, C.R. (2004) Seasonal water quality variations in a river affected by acid mine drainage: the Odiel River (South West Spain). *Science of the Total Environment* 333, 267-281.

Olmanson, L.G., Brezonik, P.L. and Bauer, M.E. (2011) Evaluation of medium to low resolution satellite imagery for regional lake water quality assessments. Water Resources Research 47: W09515, doi: 10.1029/2011WR011005.

Onywere, S.M., Mironga, J.M. and Simiyu, I. (2012) Use of remote sensing data in evaluating the extent of anthropogenic activities and their impact on lake Naivasha, Kenya. The Open Environmental Engineering Journal 5: 9-18. Available at http://www.benthamsciencepublisher.com/open/toenviej/articles/V005/9TOENVIEJ.pdf.

Palmer, S.C.J., Kutser, T. and Hunter, P.D. (2014) Remote sensing of inland waters: Challenges, progress and future directions. Remote Sensing of Environment 157: 1-8.

Parsons A.J. (2012) How useful are catchment sediment budgets? Progress in Physical Geography 36(1): 60-71 DOI: 10.1177/0309133311424591.

Pascual, M., Bouma, M.J. and Dobson, A.P. (2002). Cholera and climate: revisiting the quantitative evidence. Microbes and Infection 4: 237-245.

Pascual, M., Rodo, X., Ellner, S.P., Colwell, R. and Bouma, M.J. (2000). Cholera dynamics and El Nino-Southern Oscillation. Science 289: 1766-1769.

Pimentel, D. and Burgess, M. (2013). Soil Erosion Threatens Food Production. Agriculture 3(3): 443-463. http://doi.org/10.3390/agriculture3030443

Pitman, W.V. (1973) A Mathematical Model for Generating River Flows from Meteorological Data in South Africa. Report No. 2/73, Hydrological Research Unit, University of the Witwatersrand, Johannesburg, South Africa.

Poesen, J., Torri, D. and Vanwalleghem, T. (2005). Gully erosion: Procedures to adopt when modelling soil erosion. Handbook of Erosion Modelling pg. 361-86 edited by R. P. C. Morgan, Mark Nearing, John Wiley & Sons.

Poesen, J., Vanderkerckhove, L., Nachtergaele, J., Oostwoud Wijdenes, D., Verstraeten, G. and Wesemael, B. (2002). Gully erosion in dryland environments. In L. J. Bull, & M. J. Kirkby, Dryland Rivers: Hydrology and Geomorphology of Semi-Arid Channels (pp. 229-262). Chichester: John Wiley & Sons.

Politi, E., Rowan, J.S. and Cutler, M.E.J. (2015) Assessing the utility of geospatial technologies to investigate environmental change within lake systems. Science of the Total Environment, http://dx.doi.org/10.1016/j.scitotenv.2015.09.136 (accessed 3 December, 2015).
Pollard, S. and du Toit, D. (2011). Towards adaptive integrated water resources management in southern Africa: the role of self-organisation and multi-scale feedbacks for learning and responsiveness in the Letaba and Crocodile catchments. *Water Resource Management* 25(15), 4019-4035.
Randle, T.J., Yang, C.T. and Daraio, J. (2006). Erosion and sedimentation manual. U.S. Department of the Interior, Bureau of Reclamation, Technical Service Centre. Sedimentation and River Hydraulics Group Denver, Colorado.
Renard, K., Foster, G., Weesies, G., McCool, D. and Yoder, D. (1997) Predicting soil erosion by water: a guide to conservation planning with the Revised Universal Soil Loss Equation (RUSLE). Agricultural Handbook No. 703. http://doi.org/DC0-16-048938-5 65-100.
Revel, N.M.T.K., Ranasiri, L.P.G.R., Rathnayake, R.M.C.R.K. and Pathirana, K.P.P. (2013) Estimation of Sediment Trap Efficiency in Reservoirs – An Experimental Study. European International Journal of Science and Technology 2(10), 134-146.
Richter, G. and Negendank, J.F.W. (1977) Soil erosion processes and their measurement in the German area of the Moselle River. Earth Surface Processes 2: 261-78.
Ritchie, J. C., Schiebe, F. R., &McHenry, J. R. (1976). Remote sensing of suspended sediment in surface water. Photogrammetric Engineering and Remote Sensing 42: 1539-1545.
Rodrigueze, W., August, P.V., Wang, Y., Paul, J.E., Gold, A., Rubinstein, N. (2007) Empirical relationships between land use/cover and estuarine condition in the northeastern united states. *Landscape Ecology* 22, 403-417.
Rooseboom, A. (1992) Sediment transport in Rivers and Reservoirs – A South African Perspective. Water Research Commission Report No. 297/1/92, Water Research Commission, Pretoria, South Africa.
Rooseboom, A. and Lotriet, N.H. (1992) The new sediment yield map for southern Africa. Erosion and Sediment Transport Monitoring Programmes in River Basins (Proceedings of the Oslo Symposium). (210). http://doi.org/WRC Report No 297/2/92
Roux D.J., Badenhorst J.E., du Preez H.H. and Steyn G.J. (1994). Note on the Occurrence of Selected Trace Metals and Organic Compounds in Water, Sediment and Biota of the Crocodile River, Eastern Transvaal, South Africa, *Water SA*, 20(4), 333-340.
Sadeghi, S. H. R., Gholami, L., Khaledi Darvishan, a., & Saeidi, P. (2014). A review of the application of the MUSLE model worldwide. Hydrological Sciences Journal, 0(0), 1-11. http://doi.org/10.1080/02626667.2013.866239
Sadeghi, S.H.R. and Mizuyama, T. (2007). Applicability of the modified universal soil loss equation for prediction of sediment yield in khanmirza watershed, Iran. Hydrological Sciences Journal-Journal Des Sciences Hydrologiques 52(5), 1068-1075. http://doi.org/10.1623/hysj.52.5.1068
Sadeghi, S.H.R., Gholami, L., Khaledi Darvishan, A., & Saeidi, P. (2013) A review of the application of the MUSLE model worldwide. Hydrological Sciences Journal, 00(00), 1-11. http://doi.org/10.1080/02626667.2013.866239
Schmidt J., Elliott, S. and McKergow, L. (2008). Land-use impacts on catchment erosion for the Waitetuna catchment, New Zealand. In: Schmidt J, Cochrane T, Phillips C, Elliott S, Davies T, Basher L (Eds), Sediment dynamics in changing environments, IAHS Publication 325: 453-457.
Schulze, R. (1989). ACRU: background, concepts and theory. Report 35. Pietermaritzburg: Agricultural Research Unit, Department of Agricultural Engineering, University of Natal.
Schulze, R.E. & Lorentz, S.A. (1995) Chapter 16 of Hydrology and Agrohydrology, Department of Agricultural Engineering, University of Natal, Pietermaritzburg.
Schulze, R.E. (1995). Hydrology and Agrohydrology: A Text to Accompany the ACRU 3.00 Agrohydrological Modelling System. Water Research Commission, Pretoria, RSA, Report TT 69/9/95, pp 552.
Schulze, R.E. (2007) Climate change and the agricultural sector in South Africa: An assessment of findings in the new millennium. ACRUcons Report 55. School of Bio-resources and Environmental Hydrology Engineering, University of KwaZulu-Natal, Pietermaritzburg.

Servais, P., Billen, G., Goncalves, A. and Garcia-Armisen, T. (2007) Modelling microbial water quality in the Seine river drainage network: past, present and future situations. *Hydrological and Earth System Science* 11, 1581-1592.
Servir Global (2015) Algal bloom returns to Lake Atitlan, Guatemala. Available from https://www.servirglobal.net/Global/Articles/Article/1457/algal-bloom-returns-to-lake-atitlan--guatemala; accessed on 17 November 2015.
Simate, G.S., Ndlovu, S. (2014) Acid mine drainage: challenges and opportunities. *Journal of Environmental Chemical Engineering* 2, 1785-1803.
Singleton, F.L., Attwell, R., Jangi, S. and Colwell, R.R. (1982). Effects of temperature ad salinity on Vibrio cholerae growth. Applied and Environmental Microbiology 44(5): 1047-1058.
Slaughter, A.R. (2011). Modelling the relationship between flow and water quality in South African rivers. PHD Thesis. Grahamstown: Rhodes University.
Slaughter, A.R. (2017) Simulating microbial water quality in data-scarce catchments: an update of the WQSAM model to simulate the fate of Escherichia coli. Water Resources Management. DOI 10.1007/s11269-017-1743-1. Available at: http://link.springer.com/article/10.1007/s11269-017-1743-1.
Slaughter, A.R. and Mantel, S.K. (2015) The development of a diffuse source nutrient input model linked to land cover, to be integrated within the Water Quality Systems Assessment Model. Deliverable 1 of the Water Research Commission Project K5/2448. Water Research Commission, Pretoria, South Africa.
Slaughter, A.R., Hughes, D.A., Retief, H and Mantel, S.K. (2015a) *Development and application of a simple South African water quality model for management of rivers and reservoirs under current and future development and climate change scenarios*. Final report of Water Research Commission project K5/2237. Water Research Commission, Pretoria, South Africa.
Slaughter, A.R., Retief, D.C.H. and Hughes, D.A. (2015b) A method to disaggregate monthly flows to daily using daily rainfall observations: model design and testing. *Hydrological Sciences Journal* 4(B), 153-171. http://www.tandfonline.com/doi/pdf/10.1080/02626667.2014.993987
Smakhtin, V.U. and Masse, B. (2000). Continuous daily hydrograph simulation using duration curves of a precipitation index. Hydrological Processes 14: 1083-1100.
Sokolova, E., Pettersson, J.R., Bergstedt, O. and Hermansson, M. (2013) Hydrodynamic modelling of the microbial water quality in a drinking water source as input for risk reduction management. *Journal of Hydrology* 497, 15-23.
Southard, J. (2006). Introduction to Fluid Motions, Sediment Transport, and Current-Generated Sedimentary Structures, Course Textbook. In MIT Open Courseware: Massachusetts Institute of Technology. Retrieved from http://ocw.mit.edu/courses/earth-atmospheric-and-planetary-sciences/12-090-introduction-to-fluid-motions-sediment-transport-and-current-generated-sedimentary-structures-fall-2006
Sulebak, J. (2000). Applications of Digital Elevation Models. DYNAMAP Project Oslo, 1-11.
Tingting, L.V., Xiaoyu S., Dandan, Z., Zhenshan, X. and Jianming, G. (2008). Assessment of Soil Erosion Risk in Northern Thailand. Institute of Geographic Science and Natural Resources Research, CAS,100101 Beijing China – (lvtt.04b, sunxy.05b
Tripathi, M.P., Panda, R.K., Pradhan, S., Das, R.K. (2001) Estimation of sediment yield from a small watershed using MUSLE and GIS. J Inst Eng I 82:40-45
Tya, T.S.K and Oluwaseye, A.E. (2015). Evaluation of soil erodibility on the agricultural soil of the central zone of Adamawa state, Nigeria. Swift Journal of Research in Environmental Studies 1(3): 014-017 October, 2015. http://www.swiftjournals.org/sjres.
Underwood, E. (1947). The history of cholera in Great Britain. Proceedings of the Royal Society of Medicine 165: 1-8.
Van den Berg, E.C., Plarre, C., Van den Berg, H.M. and Thompson, M.W. 2008. The South African National Land-cover 2000. Agricultural Research Council-Institute for Soil, Climate and Water, Pretoria, South Africa (Report No. GW/A/2008/86).
Van den Bergh, F., Holloway, J.P., Pienaar, M., Koen, R., Elphinstone, C.D. and Woodborne, S. (2008). A comparison of various modelling approaches applied to cholera case data. Orion 24(1): 17-36.

Van Rijn, L.C. (1984). Sediment Transport, Part II: Suspended Load Transport. Journal of Hydraulic Engineering, ASCE 110(11).
Van Rijn, L.C. (2012). Principles of sediment transport in rivers, estuaries and coastal seas. Aqua Publications, Amsterdam, The Netherlands (WWW.AQUAPUBLICATIONS.NL).
Van Vuuren, L (2009) Experts unite to save abused river from extinction. The Water Wheel Jan/Feb: 14-17.
Van Vuuren, L (2013) Olifants – time to stand up for a river under siege. *The Water Wheel* May/June18-25.
Van Zyl, A.J. (2007) A knowledge gap analysis on multi-scale predictive ability for agriculturally derived sediments under South African conditions. Water Science and Technology 55(3): 107-114.
Venter, S.N., Lötter, A., Burke, L.M., le Roux, W.J. and du Preez, M. (2011) Management of the microbial water quality in catchments. Water Research Commission Report No. 1934/1/11, Water Research Commission, Pretoria, South Africa.
Wasson, R.J. (1994). Annual and decadal variation of sediment yield in Australia, and some global comparisons. IAHS-AISH Publication 224, 269.
Werdell, P.J. and Bailey, S.W. (2005) An improved in-situ bio-optical data set for ocean color algorithm development and satellite data product validation. Remote Sensing of Environment 98: 122-140.
Wheater, H.S., Jakeman, A.J., Beven, K.J. (1993). Progress and directions in rainfall-runoff modelling. In: Jakeman, A.J., Beck, M.B., McAleer, M.J. (Eds.), Modelling Change in Environmental Systems. John Wiley and Sons, Chichester, pp. 101-132.
Williams, J.R. (1975). Sediment yield prediction with universal equation using runoff energy factor. In Present and Prospective Technology for Predicting Sediment Yield and Sources (pp. 40: 244-254). Washington DC: USDA-ARS.
Williams, J.R. and Berndt, H.D. (1977) Sediment yield prediction based on watershed hydrology. Trans, Amer. Soc. Agr. Eng. 20: 1100-1104.
Wischmeier, W.H. (1962). Storms and soil conservation. J. Soil and water conserve 17: 55-59.
Wischmeier, W.H. and Smith, D.D. (1978). Predicting rainfall erosion losses. Agriculture Handbook No. 537, (537), 285-291. http://doi.org/10.1029/TR039i002p00285.
Wolka, K., Tadesse, H., Garedew, E., Yimer, F. (2015) Soil erosion risk assessment in the Chaleleka wetland watershed, Central Rift Valley of Ethiopia. Environmental Systems Research 4: 5. https://doi.org/10.1186/s40068-015-0030-5.
Woolhiser, D.A., Smith, R.E. and Goodrich, D.C. (1990). KINEROS, A Kinematic Runoff and Erosion Model: User Manual. U.S. Department of Agriculture, Agricultural Research Service, ARS-77, pp. 130.Xu, C. (2002). Textbook of Hydrologic Models (Vol. 72). Uppsala University Department of Earth Sciences Hydrology.
Xu, C. (2002) Textbook of Hydrologic Models. Uppsala University, Sweden.
Yang, X., Yu, B. and Xie, X. (2015). Predicting Changes of Rainfall Erosivity and Hillslope Erosion Risk Across Greater Sydney Region, Australia. International Journal of Geospatial and Environmental Research 2(1), Article 2.
Zaimes, G., & Emanuel, R. (2006). Stream Processes Part I: Basics. Arizona Watershed Stewardship Guide, Master Watershed Steward. Retrieved from https://cals.arizona.edu/watershedsteward/resources/docs/stream_processes.pdf
Zhu, M.Y. (2012) Soil erosion risk assessment with CORINE model: case study in the Danjiangkou Reservoir region, China. Stoch Environ Res Risk Assess 26: 813-822.

APPENDIX A. DATA FOR CHAPTER 3

Table A1 Description of the *Escherichia coli* data available for the sites on the Crocodile River

Gauge Name	Description	Yield Node	Coordinates		Record number	Dates		mean	min	max	SD
			Lat.	Lon.		from	to				
	DULLSTROOM – @ 540 ROAD BRIDGE ON CROCODILE RIVIER	EWR1	−25.41	30.11	24	2008	2010	140.74	0	1732	375.24
	ROODEWAL 117 JT – @ R36 ROAD BRIDGE ON KROKODILRIVIER U/S OF KWENA DAM	EWR2	−25.40	30.33	46	2008	2012	307.78	0	1732	469.24
	DOWNSTREAM OF KOMATIPOORT SEWAGE	EWR6	−25.42	31.96	25	2008	2011	345.92	0	2419	591.69
	KOMATIPOORT GOLF COURSE ON CROCODILE	EWR6	−25.44	31.97	122	2004	2010	412.45	3	3534	573.07
	DOWNSTREAM OF SHEBA COMMUNITY AT ROAD BRIDGE	EWR7	−25.68	31.17	25	2008	2011	627.76	0	2600	801.61
	UPSTREAM OF SHEBA COMMUNITY	EWR7	−25.71	31.17	27	2008	2010	360.59	0	3000	704.66
X2H087	X2H087Q01 BON ACCORD-DOWNSTREAM OF EUREKA	EWR7	−25.68	31.18	40	2006	2011	297.63	0	2419	621.80
	D/S OF WHITE RIVER WWTW AT HAIG WEIR	Haig_Weir	−25.30	31.06	23	2008	2011	653.83	0	2419	878.27
	UPSTREAM OF WHITE RIVER SEWAGE	Haig_Weir	-25.32	31.03	26	2008	2010	494.85	0	2419	867.93
	KLIPKOPJE 228 JT – @ ROAD BRIDGE ON WITRIVIER D/S OF KLIPKOPPIEDAM	Klipkoppie Dam	−25.22	31.01	23	2008	2011	104.43	0	1000	232.87
	LEEUSPRUIT 150 M U/S ASSMANG CHROME	X21F_1046	−25.73	30.22	16	2008	2010	99.69	0	1000	246.60

Table A1 Continued Description of the *Escherichia coli* data available for the sites on the Crocodile River

Gauge Name	Description	Yield Node	Coordinates		Record number	Dates		mean	min	max	SD
			Lat.	Lon.		from	to				
	U/S MACHADODORP S/W ON BRIDGE @ CARAVAN PARK ON ELANDSRIVIER	X21F_1046	−25.66	30.25	34	2008	2011	77.60	0	220	81.37
	LEEUSPRUIT AT BRIDGE 50 M D/S EMTHONJENI S/W	X21F_1100	−25.69	30.26	132	2004	2012	561.24	0	12100	1149.89
	LEEUSPRUIT D/S ASSMANG CHROME BRIDGE AT ENTRANCE TO SITE	X21F_1100	−25.72	30.24	28	2008	2010	128.33	0	1300	311.13
	D/S WATERVAL BOVEN S/W FROM FIVE BOOG BRIDGE ON ELANDSRIVIER	X21G-1037	−25.65	30.36	22	2009	2011	293.00	0	2800	617.57
	DOORNHOEK AT N4 BRIDGE D/S WATERVALBOVEN S/W ON ELANDSRIVIER	X21G-1037	−25.65	30.36	108	2004	2012	1026.7 0	0	12100	1775.86
	ELANDSRIVIER X21F TO X21K	X21G-1037	−25.64	30.34	30	2008	2010				
	AT HEMLOCK U/S SAPPI NGODWANA ON ELANDSRIVIER	X21J-1013	−25.60	30.58	26	2008	2011	103.54	0	1000	223.88
	AT LINDENAU 5 KM D/S SAPPI NGODWANA ON ELANDSRIVIER	X21K-997	−25.49	30.70	30	2008	2011	68.93	0	450	115.30
X2H015	X2H015Q01 AT LINDENAU ON ELANDSRIVIER	X21K-997	−25.49	30.70	9	2007	2009	115.50	7	700	236.57
	ELANDSHOOGTE 270 JT – @ ROAD BRIDGE, U/S OF ELANDSHOOGTE MINE ON HOUTBOSLOOP	X22A-913	−25.36	30.67	9	2008	2011	92.56	0	260	97.20
	SUDWALAASKRAAL 271 JT – @ ROAD BRIDGE ON HOUTBOSLOOP	X22A-913	−25.38	30.69	21	2008	2011	58.29	0	300	86.69
	RIVULETS – @ ROAD BRIDGE ON KROKODILRIVIER @ RIVULETS	X22B-2	−25.43	30.76	31	2008	2011	237.97	0	2419	539.14
X2H013	X2H013Q01 CROCODILE RIVER AT MONTROSE	X22B-987	−25.45	30.71	38	2007	2011	173.62	0	2419	395.91
	GLADDESPRUIT PAPPAS QUARY	X22C-1004	−25.46	30.95	25	2008	2011	296.68	0	2419	507.81

Gauge Name	Description	Yield Node	Coordinates		Record number	Dates		mean	min	max	SD
			Lat.	Lon.		from	to				
X2H092	X2H092Q01 BOSCHRAND MATAFFIN ROAD BRIDGE	X22C-946	−25.45	30.95	17	2008	2011	282.76	0	2419	582.21
	NELS RIVER ON BRONDAL ROAD	X22F-842	−25.34	30.88	20	2008	2011	97.55	0	420	124.58
	SAND RIVER ON BRONDAL ROAD	X22F-842	−25.33	30.94	21	2008	2011	2466.14	0	40000	8726.18
	BESTERSPRUIT UPSTREAM OFMMC DELTA	X22J-958	−25.46	30.97	22	2008	2011	20806.7	0	270000	67108.0
	DOORNHOEK AT N4 BRIDGE D/S WATERVALBOVEN S/W ON ELANDSRIVIER	X21G-1037	−25.65	30.36	108	2004	2012	1026.70	0	12100	1775.86
	ELANDSRIVIER X21F TO X21K	X21G-1037	−25.64	30.34	30	2008	2010				
	AT HEMLOCK U/S SAPPI NGODWANA ON ELANDSRIVIER	X21J-1013	−25.60	30.58	26	2008	2011	103.54	0	1000	223.88
	AT LINDENAU 5 KM D/S SAPPI NGODWANA ON ELANDSRIVIER	X21K-997	−25.49	30.70	30	2008	2011	68.93	0	450	115.30
X2H015	X2H015Q01 AT LINDENAU ON ELANDSRIVIER	X21K-997	−25.49	30.70	9	2007	2009	115.50	7	700	236.57
	ELANDSHOOGTE 270 JT – @ ROAD BRIDGE, U/S OF ELANDSHOOGTE MINE ON HOUTBOSLOOP	X22A−913	−25.36	30.67	9	2008	2011	92.56	0	260	97.20
	SUDWALAASKRAAL 271 JT – @ ROAD BRIDGE ON HOUTBOSLOOP	X22A-913	−25.38	30.69	21	2008	2011	58.29	0	300	86.69
	RIVULETS – @ ROAD BRIDGE ON KROKODILRIVIER @ RIVULETS	X22B-2	−25.43	30.76	31	2008	2011	237.97	0	2419	539.14
X2H013	X2H013Q01 CROCODILE RIVER AT MONTROSE	X22B-987	−25.45	30.71	38	2007	2011	173.62	0	2419	395.91
	GLADDESPRUIT PAPPAS QUARY	X22C-1004	−25.46	30.95	25	2008	2011	296.68	0	2419	507.81

Table A1 Continued Description of the *Escherichia coli* data available for the sites on the Crocodile River

Table A1 Continued Description of the *Escherichia coli* data available for the sites on the Crocodile River

Gauge Name	Description	Yield Node	Coordinates		Record number	Dates		mean	min	max	SD
			Lat.	Lon.		from	to				
X2H092	X2H092Q01 BOSCHRAND MATAFFIN ROAD BRIDGE	X22C-946	−25.45	30.95	17	2008	2011	282.76	0	2419	582.21
	NELS RIVER ON BRONDAL ROAD	X22F-842	−25.34	30.88	20	2008	2011	97.55	0	420	124.58
	SAND RIVER ON BRONDAL ROAD	X22F-842	−25.33	30.94	21	2008	2011	2466.14	0	40000	8726.18
	BESTERSPRUIT UPSTREAM OFMMC DELTA	X22J-958	−25.46	30.97	22	2008	2011	20806.70	0	270000	67108.00
X2H094	X2H094Q01 FRIEDENHEIM LION S CLUB IN CROCODILE RIVER	X22J-958	−25.46	31.01	24	2008	2010	422.33	0	4000	824.08
X2H095	X2H095 BOSCHRAND 283 JT – @ ROAD BRIDGE ON KROKODILRIVIER	X22J−993	−25.46	30.97	25	2008	2011	421.72	0	2000	598.62
	KANYAMAZANE D/S AT N4 BRIDGE KROKODILPOORT ON CROCODILE	X22K1	−25.50	31.18	148	2004	2012	806.14	0	4840	955.21
	KANYAMAZANE STREAM	X22K1	−25.48	31.17	27	2008	2011	4020.21	0	100000	18828.83
	KARINO BRIDGE IN CROCODILE RIVER	X22K1	−25.47	31.10	141	2004	2012	774.20	0	6050	1023.84
	NOORD KAAP RIVER FROM BRIDGE 200 M D/S NEW CONSORT MINE	X23B_1052	−25.67	31.09	26	2008	2011	325.69	0	2419	653.86
X2H080	X2H080Q01 SEGALLA-UPSTREAM OF CONSORT GOLD MINE	X23B-1052	−25.65	31.06	26	2008	2011	106.27	0	900	233.17
X2H082	X2H082Q01 DAISY KOPJE-NELSPRUIT/BARBERTON BRIDGE	X23F-1	−25.74	31.00	24	2008	2010	175.46	0	2419	494.37
X2H083	X2H083Q01 DIXIE-PUMP STATION	X23F-1120	−25.71	31.06	38	2007	2011	166.57	0	1660	327.86

Table A1 Continued Description of the *Escherichia coli* data available for the sites on the Crocodile River

Gauge Name	Description	Yield Node	Coordinates		Record number	Dates		mean	min	max	SD
			Lat.	Lon.		from	to				
X2H085	X2H085Q01 ITALIAN FARM UPSTREAM OF JOE S LUCK	X23G-1	−25.67	31.13	36	2006	2011	173.78	0	1986	383.09
X2H088	X2H088Q01 LOVEDALE-HONEYBIRD RAILWAY STATION	X23H-6	−25.65	31.24	35	2006	2010	310.36	0	2419	683.88
	UPSTREAM OF KABOKWENI SEWAGE	X24B-2	−25.31	31.18	24	2008	2010	275.42	0	2419	530.27
	DOWNSTREAM OF KABOKWENI SEWAGE	X24B-903	−25.30	31.18	23	2008	2011	162.70	0	1000	308.44
X2H048	X2H048Q01 CROCODILE RIVER AT MALELANE BRIDGE/KRUGER NAT PAR	X24D-994	−25.46	31.54	30	2007	2011	10011.00	0	300000	53824.12
	KRUGAR NATIONAL PARK − @ CROCODILE BRIDGE ON CROCODILE RIVER @ CROCODILE BRIDGE R/C	X24H-934	−25.36	31.89	20	2008	2011	125.45	0	1203	255.04

Table A2. Description of the effluent *Escherichia coli* data available for the sites on the Crocodile River

Description	Yield Model Node	Coordinates		Record number	Dates		mean	min	max	STD
		Lat.	Lon.		from	to				
BARBERTON SEWAGE EFFLUENT	X23F-1120	−25.75	31.04	18	2009	2010	765.2222	0	2419.00	957.49
EMTHONJENI SEWAGE	X21F-1100	−25.69	30.25	31	2008	2011	241.1667	0	2419.00	643.76
WATERVAL BOVEN SEWAGE	X21G-1037	−25.64	30.34	29	2008	2011	3745.593	0	62000.00	12529.49
MILLY'S SEWAGE	X21F-1046	−25.69	30.21	30	2008	2011	3952.893	0	37000.00	9429.97
WHITE RIVER SEWAGE EFFLUENT	Haig_Weir	−25.31	31.05	25	2008	2011	59344.88	0	520000.00	136232.66
KANYAMAZANE SEWAGE	X22K1	−25.49	31.17	27	2008	2011	75.7037	0	1000.00	222.54
KABOKWENI SEWAGE	X24B-2	−25.31	31.17	24	2008	2011	501.2083	0	8600.00	1758.21
KINGSTONVALE SEWAGE LEFT CHAMBER	X22J-958	−25.44	31.03	24	2008	2010	4172.88	0	100000.00	19970.58

APPENDIX B. STUDY SITES USED IN MULTIPLE CHAPTERS

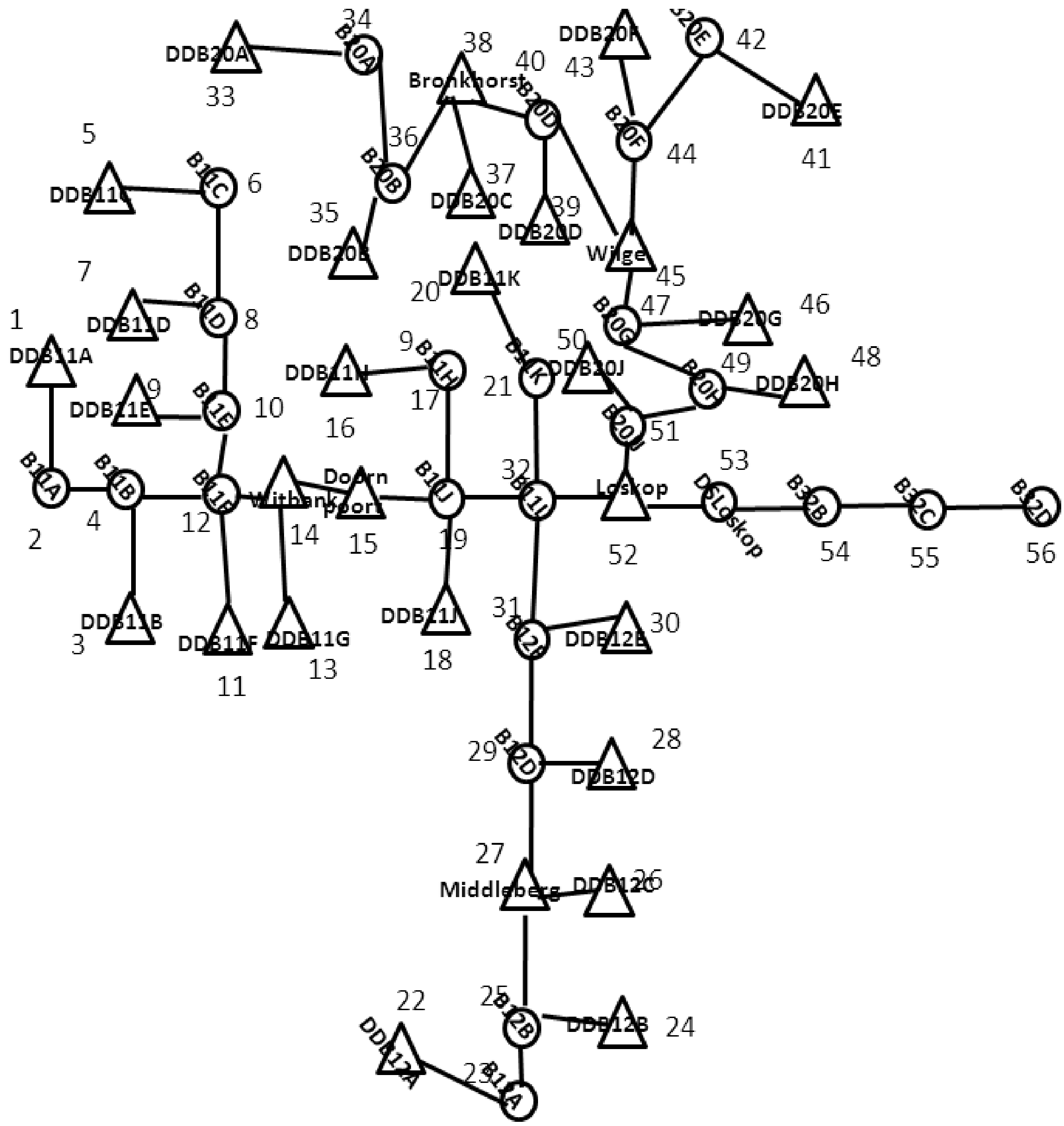

Figure B1 WReMP systems diagram of the upper Olifants River Catchment

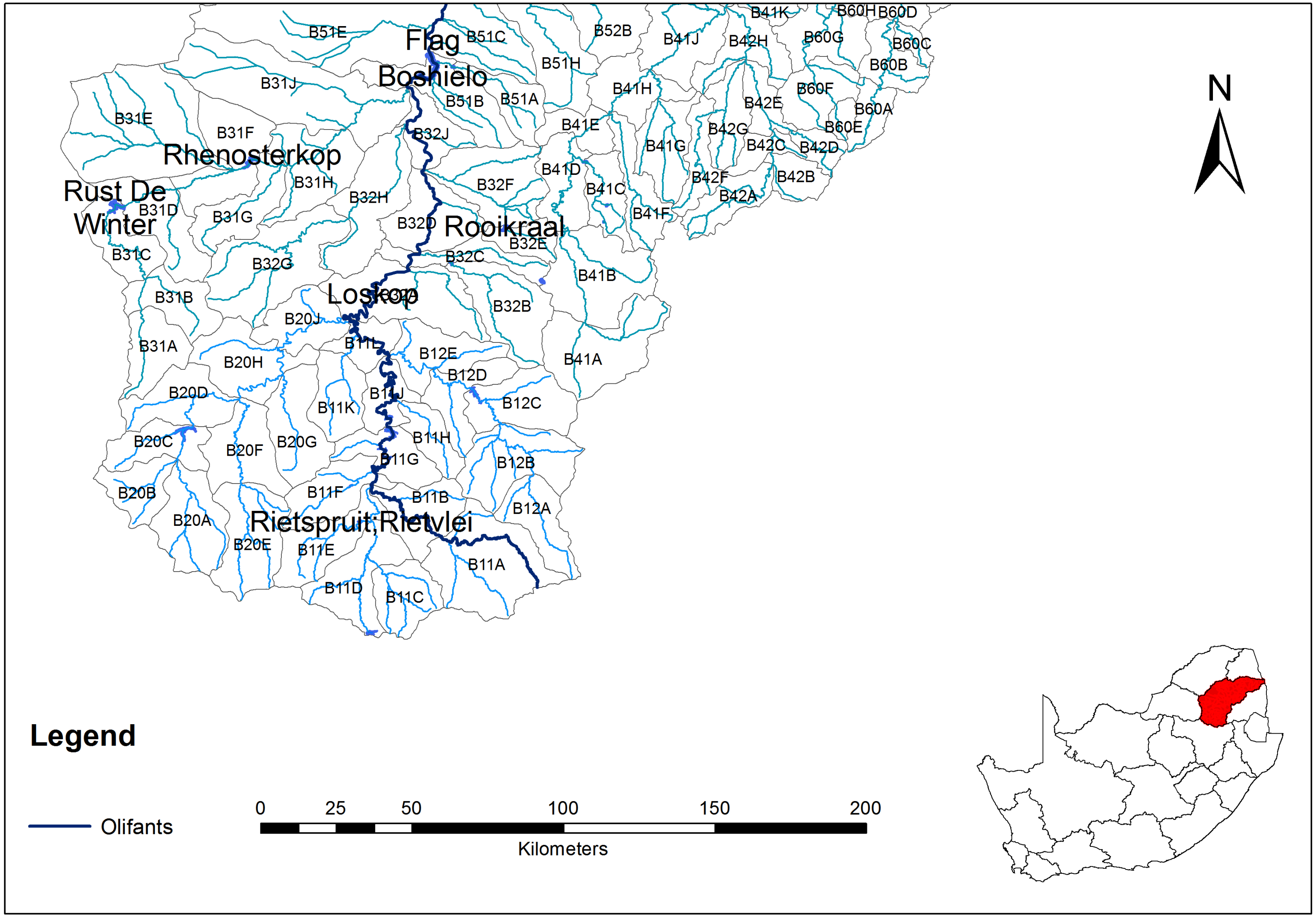

Figure B2 Map of the upper Olifants River Catchment showing quaternary catchments and major dams.

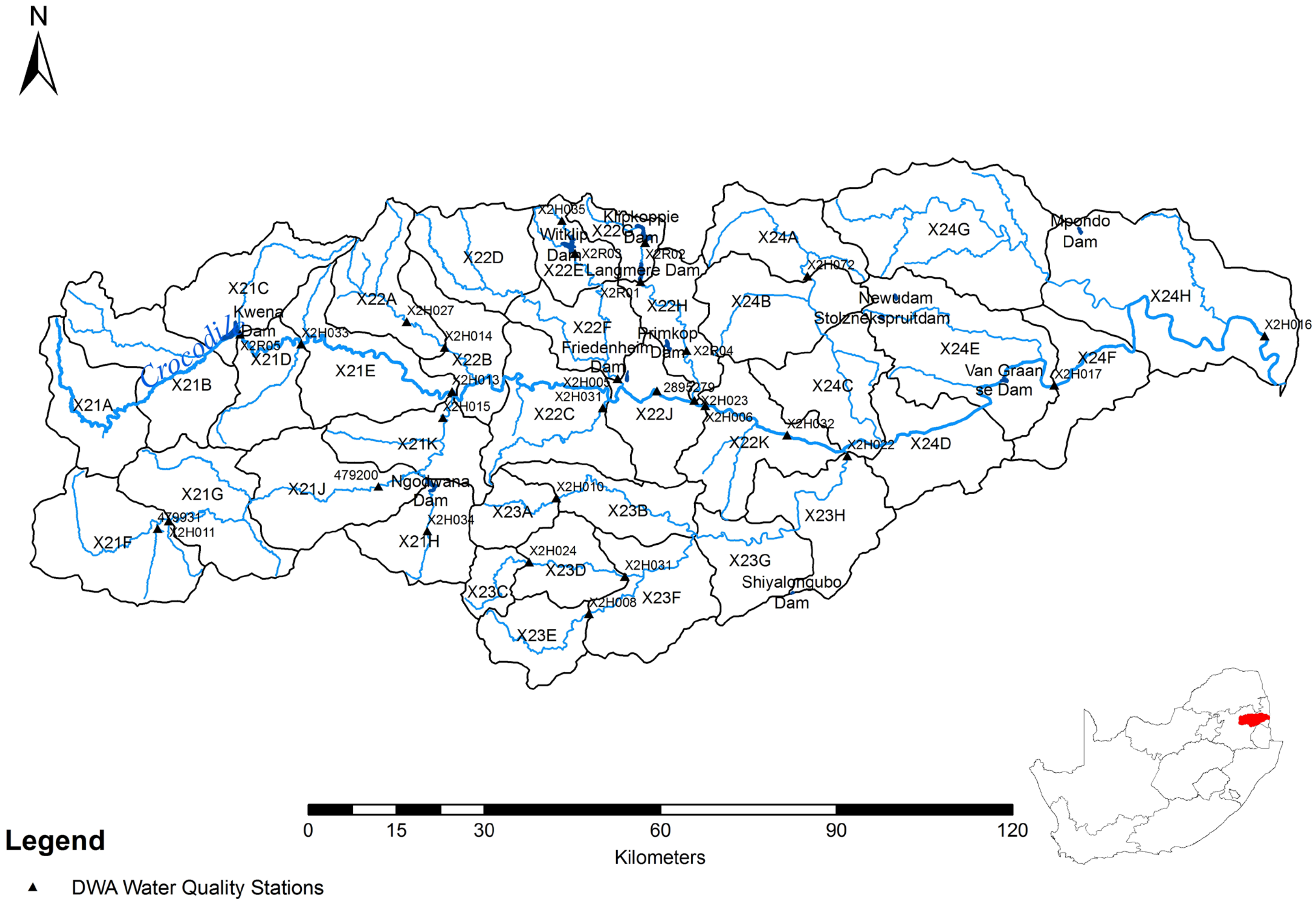

Figure B3 Map of the Crocodile River Catchment within the Mpumalanga province of South Africa, showing the location of the rivers, quaternary catchments and DWA gauging stations.

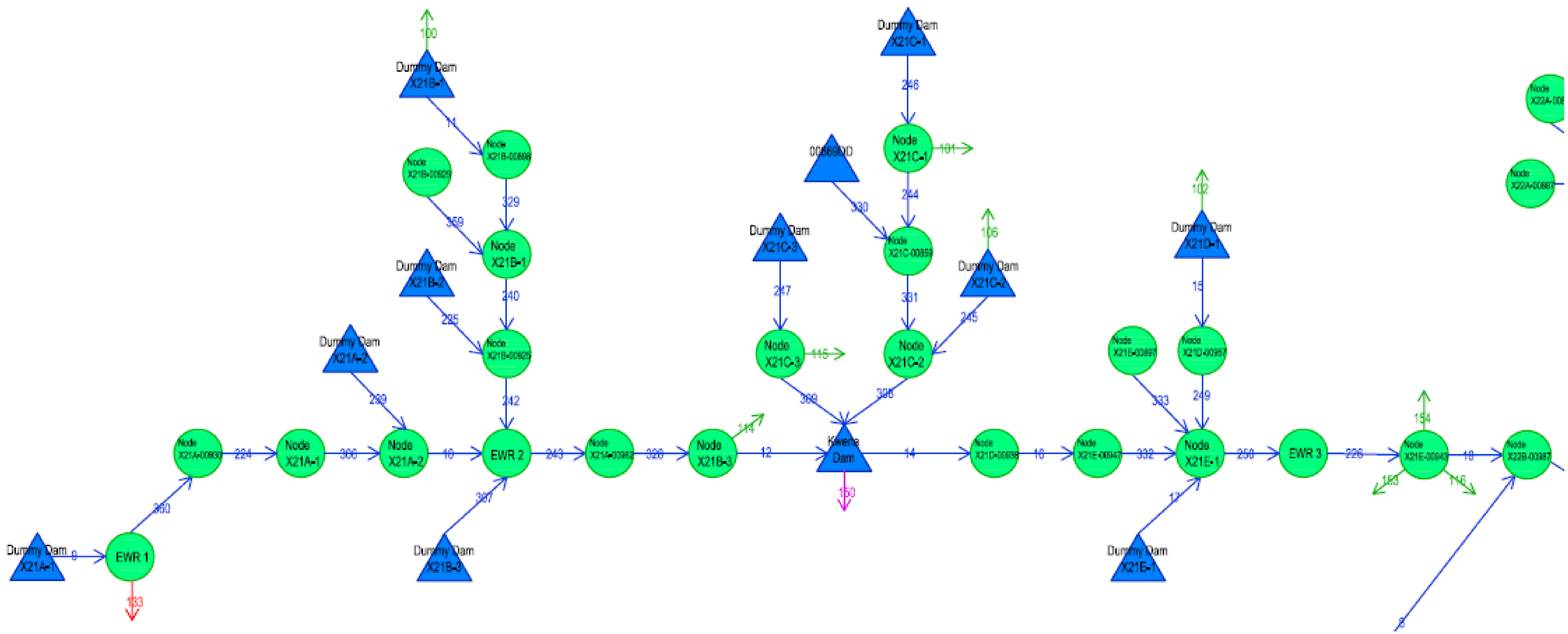

Figure B3 WReMP systems diagram for the Crocodile River Catchment

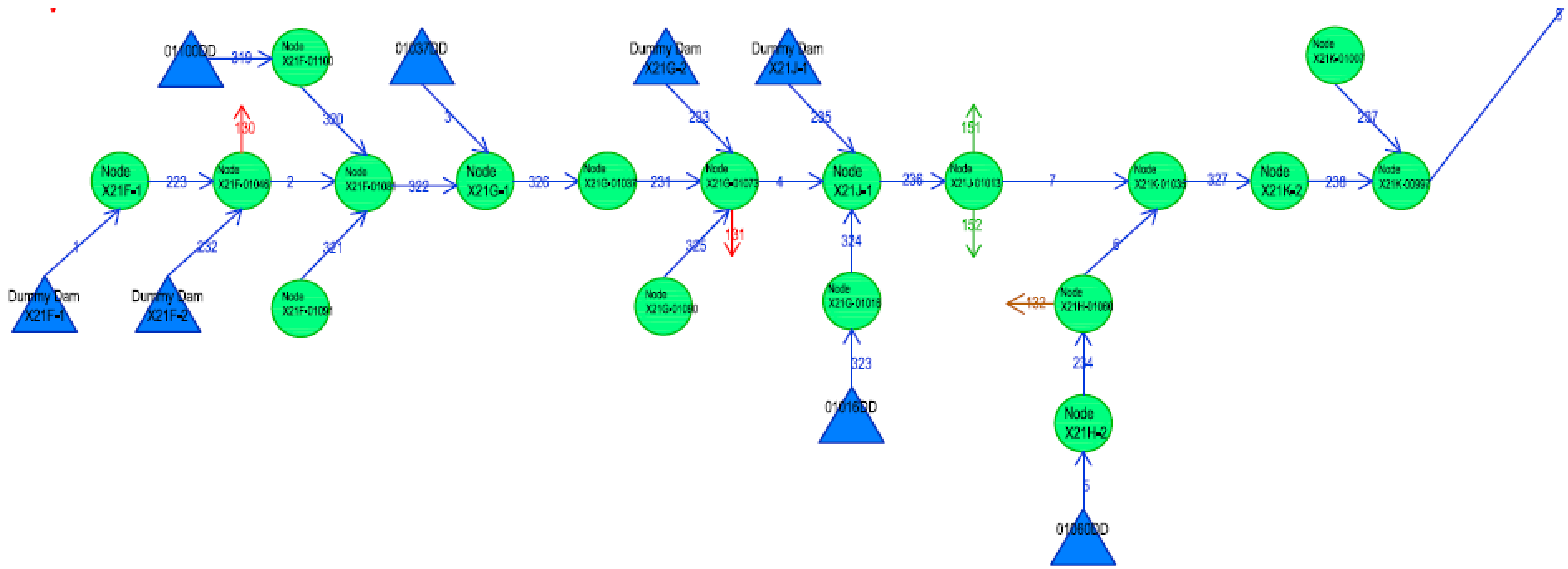

Figure B3 continued. WReMP systems diagram for the Crocodile River Catchment

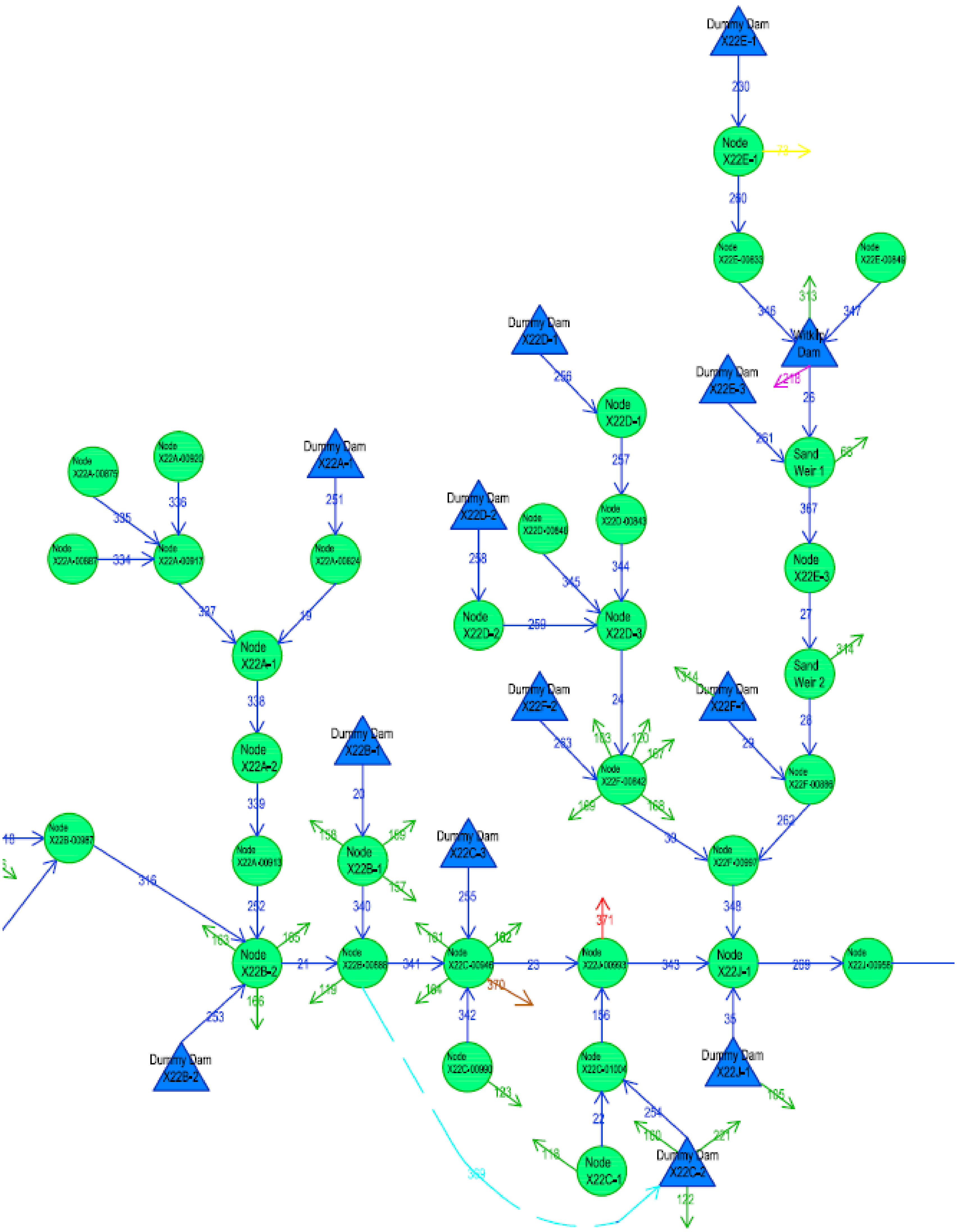

Figure B3 continued. WReMP systems diagram for the Crocodile River Catchment

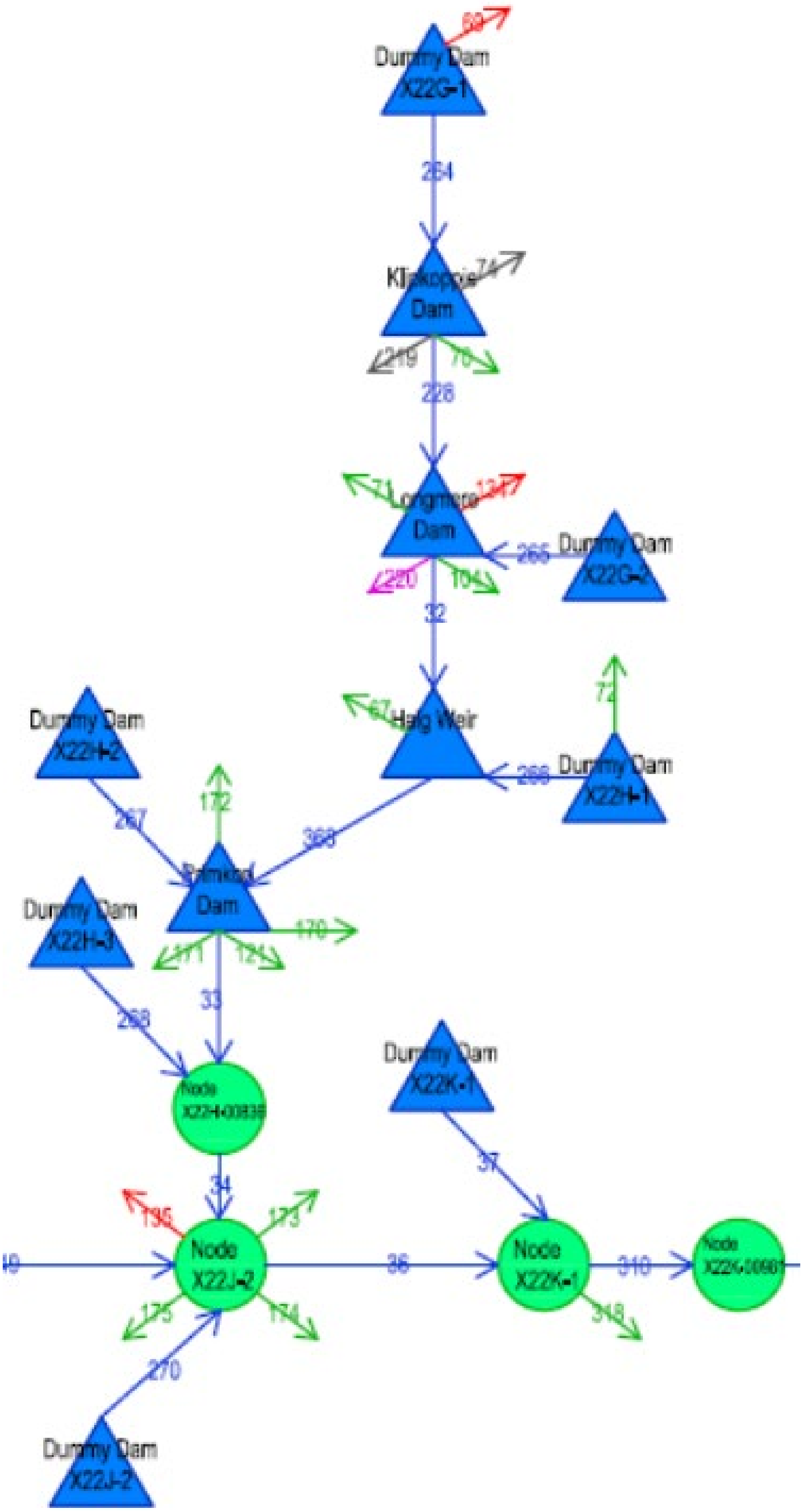

Figure B3 continued WReMP systems diagram for the Crocodile River Catchment

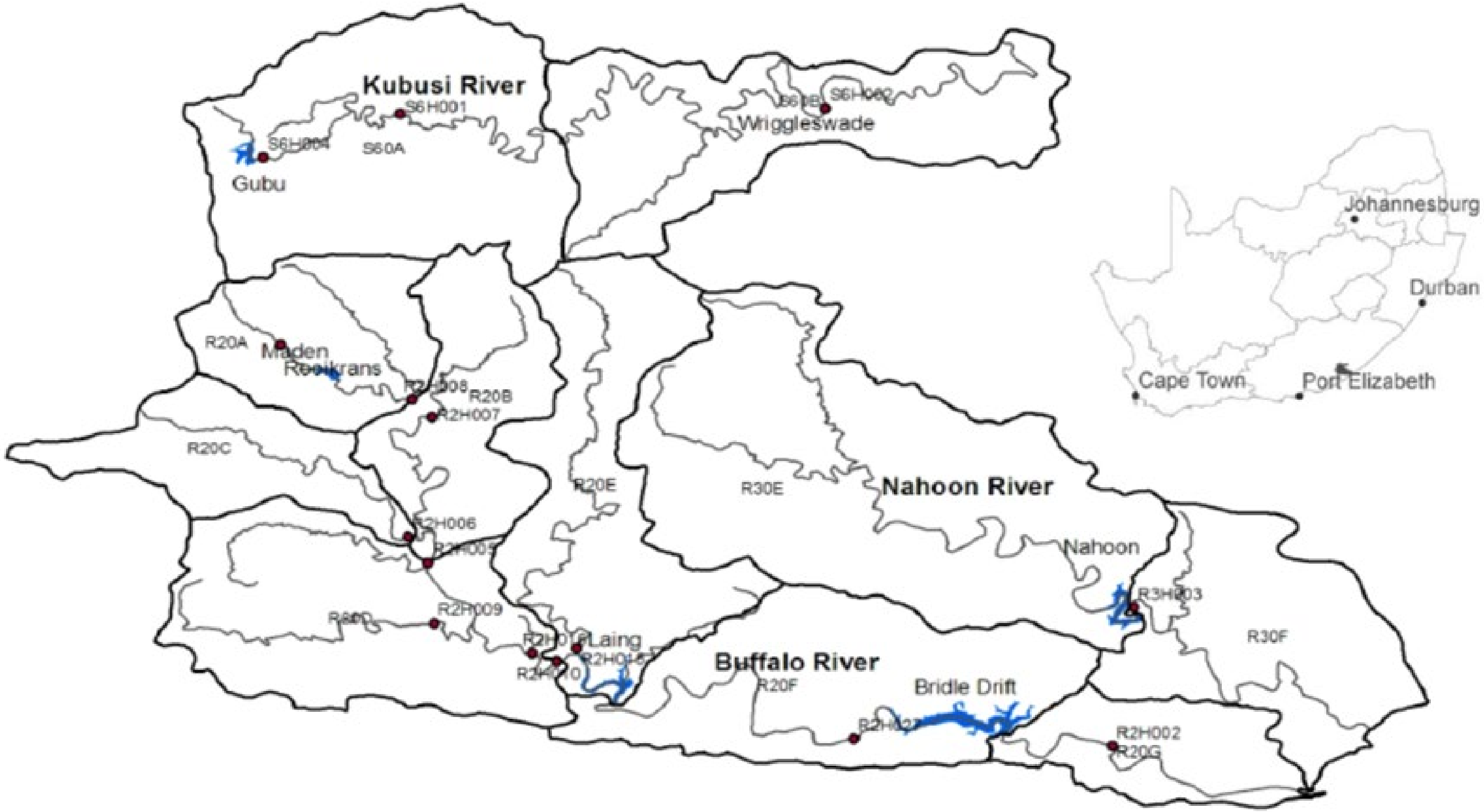

Figure B4 Map of the Buffalo, Nahoon and Kubusi River catchments in the Eastern Cape (Amatole System), showing the location of the rivers, dams, quaternary catchments and flow gauges. Laing Dam is visible within the middle Buffalo River Catchment.

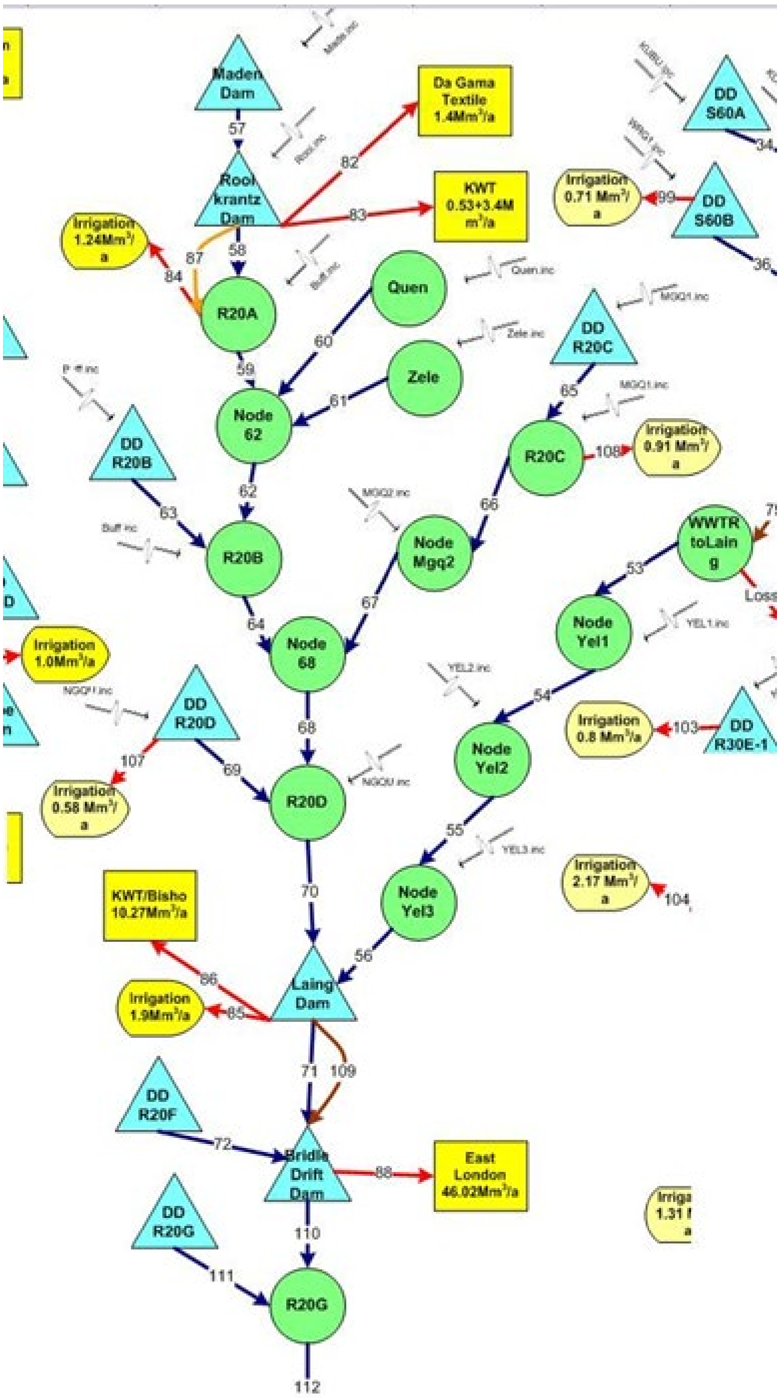

Figure B5 Segment of the WReMP yield model systems diagram for the Amatole System representing the Buffalo River Catchment.

APPENDIX C. MATHEMATICAL EQUATIONS USED IN THE SEDIMENT MODEL

Erosion estimation

Daily flows ($m^3\ s^{-1}$) are required for the erosion estimation. These can either be an unbroken time series of observed daily flow, daily flow estimated from a daily hydrological model such as the Agricultural Catchments Research Unit (ACRU) model (Schulze, 1989), or monthly flow simulated from a monthly hydrological model such as the Pitman model (Pitman, 1973) disaggregated to daily using a monthly-to-daily disaggregation routine (e.g. Slaughter *et al.*, 2015).

Daily flows are separated into surface and subsurface flow fractions, namely surface flow, interflow and groundwater flow, all in $m^3\ s^{-1}$, using the baseflow separation method by Hughes *et al.* (2003).

The catchment surface flow volume is calculated from surface flow ($Flow_s$):

$$Vsf = Flow_S \times 0.0036 \times 24, \quad \text{(Equation C1)}$$

where *Vsf* is the surface flow volume in million cubic meters (MCM) per day.

The storm duration associated with surface flow on each day is then calculated:

$$D = D_{Scale}(Vsf)^{DP} + D_{con}, \quad \text{(Equation C2)}$$

where *D* is the duration (hours), and D_{scale}, *DP* and D_{con} are the scaling, power and constant parameters for calculating the duration, respectively. All three runoff zones are assumed to have the same duration of runoff.

The peak discharge for each runoff zone is calculated assuming a double triangle-shaped hydrograph:

$$Q_{Hp} = \frac{2 \times Flow_S \times 24}{0.75 \times D}, \quad \text{(Equation C3)}$$

$$Q_{Mp} = \frac{2 \times Q_{Hp} \times 24}{0.75 \times D}, \quad \text{(Equation C4)}$$

$$Q_{Lp} = \frac{2 \times Q_{Mp} \times 24}{0.75 \times D}, \quad \text{(Equation C5)}$$

$$q_{Hp} = \left(\frac{Q_{Hp} \times 3.6}{A_H}\right), \quad \text{(Equation C6)}$$

$$q_{Mp} = \left(\frac{Q_{Mp} \times 3.6}{A_M}\right), \quad \text{(Equation C7)}$$

$$q_{Lp} = \left(\frac{Q_{Lp} \times 3.6}{A_L}\right), \quad \text{(Equation C8)}$$

where Q_{Hp}, Q_{Mp}, and Q_{Lp} are the peak runoff flows for the high, medium and low runoff zones, respectively (in $m^3\ s^{-1}$), A_H, A_M and A_L are the areas (km^2) of the high, middle and low runoff zones, respectively, and q_{Hp}, q_{Mp} and q_{Lp} are the peak runoff depths for the high, medium and low runoff zones, respectively (in $mm\ h^{-1}$).

The runoff depths for the high, medium and low runoff zones are then computed based on the assumption that the high runoff zone generates 75% more runoff than the moderate runoff zone, which in turn is assumed to generate 75% more than the low runoff zone:

$$Depth = \frac{Flow_S \times 86.4}{A_H}, \quad \text{(Equation C9)}$$

$$Depth_H = \frac{Depth}{H+\left(\frac{M}{1.75}\right)+\left(\frac{L}{3.0625}\right)}, \quad \text{(Equation C10)}$$

$$Depth_M = Depth_H/1.75, \quad \text{(Equation C11)}$$

$$Depth_L = Depth_H/3.0625, \quad \text{(Equation C12)}$$

where *Depth* is the runoff depth for the entire catchment (mm day^{-1}), *H*, *M* and *L* are the proportions of the entire catchment area falling within the high, medium and low runoff zones respectively, and $Depth_H$, $Depth_M$ and $Depth_L$ are the runoff depths (mm day^{-1}) for the high, medium and low runoff zones, respectively.

Daily sediment availability is calculated using the Modified Universal Soil Loss Equation (MUSLE) (Williams, 1975).

$$SA = R \times LS \times K \times C \times P \quad , \quad \text{(Equation C12)}$$

where *SA* is the daily sediment availability (tons ha^{-1}), *R* is the runoff factor, *C* is the cover factor, *LS* is the topography factor, *K* is the soil erodibility factor and *P* is the practice factor. Equation 5.24 would be run separately for each runoff zone, where *LS*, *K*, *C* and *P* would be related to the characteristics of the catchment area in a specific zone, and R would also be related to a specific runoff zone; therefore, for the high runoff zone for example:

$$R_H = 1.586 \times (Depth_H \times q_{Hp})^{0.56} \times A_H^{0.12}, \quad \text{(Equation C13)}$$

Erosion storage and transport estimation

The maximum storage capacity for each runoff zone as well as for the main channel is calculated by:

$$S_{max} = A \times p \times d, \quad \text{(Equation C14)}$$

where S_{max} is the maximum sediment storage capacity (kg) of the runoff zones or main channel, *A* is the area (m^2) of the runoff zone of the channel, *p* is the bulk density (kg m^{-2}) and *d* is the maximum depth (m) of the stored sediment.

The proportion of gully or channel storage in each runoff zone is then calculated:

$$C_{prop} = LnDD, \quad \text{(Equation C15)}$$

where C_{prop} (constrained between 0.1 and 0.8) is the proportion of the total storage in a runoff zone that is assumed to be represented by gully or channel storage and *DD* is the drainage density (km km^{-2}) of the channel features in that zone.

Sediment is added to the three slope storage zones during each time interval of the model:

$$SS(t) = SS(t-1) + S_{input}, \quad \text{(Equation C16)}$$

where $SS_{(t-1)}$ is the sediment storage at the end of the previous time interval, *SS(t)* is the new storage (before transport of other storages) and S_{input} is the sediment generated from the soil loss estimation procedure described in the previous section.

The output from each storage component is calculated using the peak surface runoff (q_{sed} mm h^{-1}) for that runoff zone relative to the maximum mean daily total flow depth (q_{max} mm h^{-1}) for the whole catchment (over the whole time series) and a threshold flow depth (q_t, mm h^{-1}), as well as a power function for the amount of sediment currently in storage relative to the maximum possible storage.

For the main channel storage, the peak runoff value is based on the total flow (not only surface runoff) depth during the day for the whole catchment. The maximum mean daily total flow depth is pre-calculated from the full time series of flow data input from the hydrological model.

If $q_{sed} > q_t$ then:

$$S_{out} = \frac{q_{sed} - q_t}{q_{max} - q_t} \times SS \times (SS / S_{max})^{pow} \qquad \text{(Equation C17)}$$

For the three slope sediment storage components, the $Cprop$ value (i.e. the proportion of total sediment storage for the runoff zone that is considered to be in channel features) is used to determine the destination of the sediment delivery. $S_{out} \times C_{prop}$ is added to the channel storage within the same runoff zone, whereas $S_{out} \times (1 - C_{prop})$ is added to the slope storage of the next runoff zone in the cascade. The outputs from the channel storages are directed to the next channel storage in the cascade, whereas all of the outputs from the lower runoff zone are directed to the main channel. The outputs from the main channel become the final sediment delivery for the total catchment.

Calculation of sediment transport in the main river channel

Calculation of velocity, depth and river width with different flows

To calculate the transport of suspended sediment, estimates of velocity (m s^{-1}), depth (m) and width (m) with different daily flows (m^3 s^{-1}) are required. To calculate these, certain assumptions about the channel shape are made, requiring additional user input, i.e. the river channel maximum width (m) and slope. The assumptions of the channel shape are illustrated in Figure C.1.

Within the sediment routing procedure, the model will first step through all the subcatchments (nodes) in the modelled system, and using the set parameters of $Width_{max}$ and *Slope*, will calculate width (*Width*), depth (*Depth*), flow (*Q*) and velocity (*Vel*) in one cm increments of depth until the maximum depth for the channel is reached. These values are placed in an array in run-time memory, which effectively acts as a lookup table during the sediment routing.

$Width_{bed}$ is assumed to be 60% of $Width_{max}$. We need to calculate *Depth* at bankfull to determine the range of depths for the lookup table:

$$Opp = (Width_{max} – (Width_{max} * 0.6))/2 \qquad \text{(Equation C18)}$$

$$Depth_{max} = 0.6 * ((Width_{max}/0.45)^{2.08})^{0.35} \qquad \text{(Equation C19)}$$

$Depth_{max}$ is the depth at bankfull and determines the range of depths for which *Q*, *Vel* and *Width* are calculated in one cm increments of *Depth*.

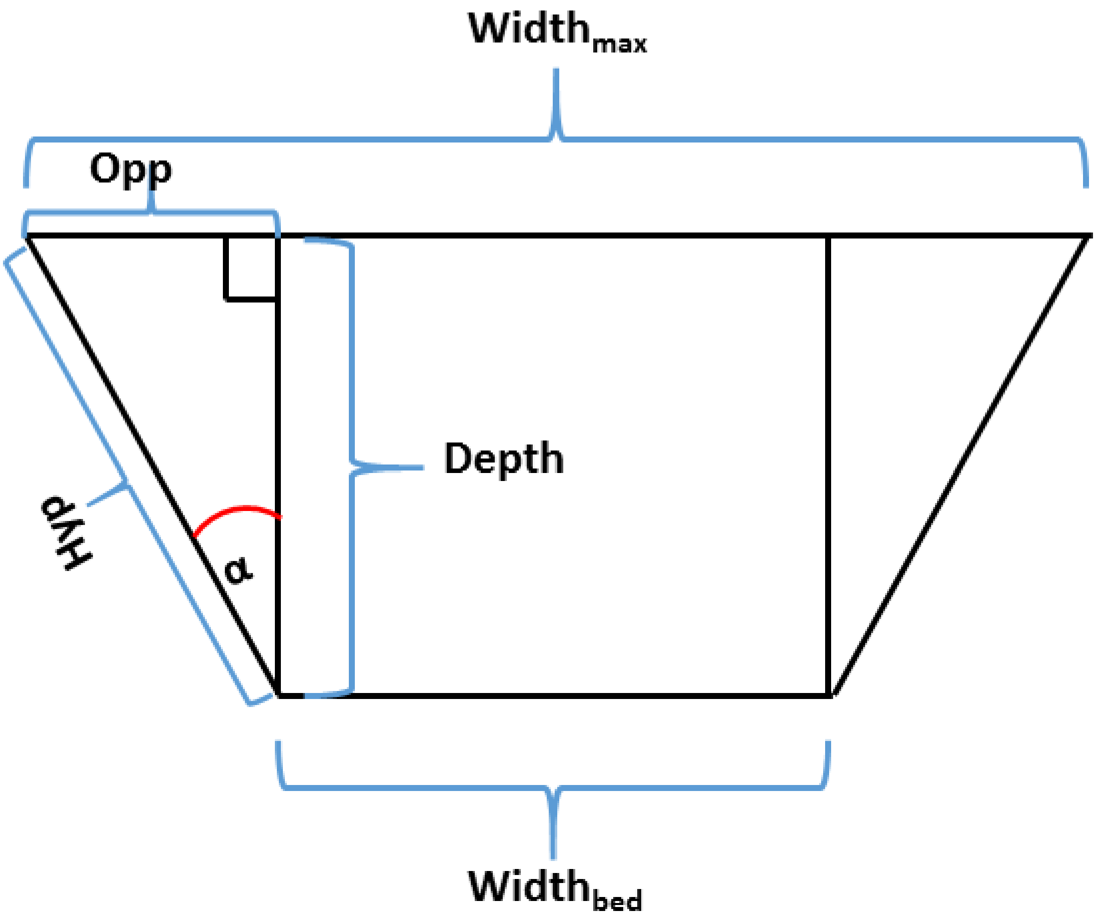

Figure C.1 Conceptual representation of a river channel used to route sediment

We need the angle α (Figure C.1) in subsequent calculations:

$Hyp = (Opp^2 + Depth_{max}^2)^{0.5}$ (Pythagorean Theorem) (Equation C20)

$\alpha = \arcsin(Opp/Hyp)$ (Equation C21)

For each 1 cm increment of *Depth* from 1 to $Depth_{max}$:

$N = 0.1 - (Depth/Depth_{max} * 0.06)$ (Equation C22)

Where N is Manning's N for an assumed range of 0.04 to 0.1, with 0.1 the value at the lowest depth and 0.04 the value at $Depth_{max}$.

To work out wetted perimeter and area with changes in depth:

$Hyp = Depth/\cos(\alpha)$ (Equation C23)

$Opp = (Hyp^2 - Depth^2)^{0.5}$ (Equation C24)

$Wetted\_Perimeter = Hyp * 2 + Width_{max} * 0.6$ (Equation C25)

$Area = (Width_{max} * 0.6 * Depth) + (Depth * Opp)$ (Equation C26)

$Vel = ((Area/Wetted\_Perimeter)^{0.67} * Slope^{0.5})/N$ (Equation C27)

$Width = (Width_{max} * 0.6) + (Opp * 2)$ (Equation C28)

$Q = Area * Vel$ (Equation C29)

For each 1 cm increment of *Depth* from 1 cm to $Depth_{max}$, *Depth*, *Width*, *Vel* and *Q* are stored in a lookup table (runtime memory multi-dimensional array).

Calculation of suspended sediment

The approach adopted follows the method for suspended load transport for steady flow proposed by Van Rijn (1984).

$q_b = \alpha_s * \rho_s * Vel * d_{50} * M_e^{2.4} * (D^*)^{-0.6}$ (Equation C30)

$M_e = (Vel - Vel_{critical})/[(s - 1)gd_{50}]^{0.5}$ (Equation C31)

$D^* = d_{50}[(s - 1)g/v^2]^{0.33}$ (Equation C32)

$Vel_{critical} = a * (d_{50} * 10{,}000)^b$ (Equation C33)

$s = \rho_s/\rho_w$ (Equation C34)

q_b is suspended load transport (kg m^{-1}), α_s is assumed to be 0.012 (Van Rijn, 1984), ρ_s is the density of the sediment (kg m^{-3}) and is assumed to be 1,200 from an initial survey of the literature, d_{50} is the median particle size (m), which is set by the user, M_e is the mobility parameter, $Vel_{critical}$ is the critical depth-averaged velocity for initiation of motion (m s^{-1}), s is relative density, ρ_w is the density of water (kg m^{-3}), and is assumed to be 1,000, g is the acceleration of gravity (m s^{-2}), which is known to be 9.81, v is the kinematic viscosity coefficient (m^2 s^{-1}), which for water at 20°C is known to be 0.000001.

The values of *a* and *b* where calculated through linear regressions of the relationship between $Vel_{critical}$ and d_{50} given by Van Rijn (2012):

$a = 0.225 * Depth^{0.15}$ (Equation C35)

$b = 0.49 * Depth^{-0.02}$ (Equation C36)

For each day, WQSAM uses the cumulative flow (m^3 s^{-1}) to obtain *Depth*, *Width* and *Vel* from the aforementioned lookup table in memory. Using the equations given above, the load of sediment that can be carried in suspension (kg m^{-3}) is calculated by multiplying q_b by *Width*. The loads of sediment entering the catchment from upstream are summed and the final load (kg m^{-3}) is compared to the load that can be carried in suspension. If the load entering the subcatchment is greater than what can be carried in suspension by the cumulative flow, the difference is deposited to the bed load. If the load entering the subcatchment is smaller than what can be carried in suspension by the cumulative load, the difference is taken from the bed load as it is assumed that some of the bed load enters suspension. The load in suspension is passed to the subcatchment downstream on a daily time step.